Department of Applied Chemistry

Calixarenes as Potential Ionophores for Thallium Ion-Selective Electrodes

Ryan Travis Chester

This thesis is presented for the Degree of
Doctor of Philosophy
of
Curtin University of Technology

June 2007

Declaration

To the best of my knowledge and belief this thesis contains no material previously published by any other person except where due acknowledgement has been made.

This thesis contains no material which has been accepted for the award of any other degree or diploma in any university.

Signature: …………………………..

Date: ………………………………..

Table of Contents

Abstract

The first part of this thesis reports the synthesis of five calixarene molecules and their incorporation into ISEs as thallium(I) selective ionophores for use in clinical and environmental analysis. Four calix[4]arene molecules were successfully synthesized. Two were isolated in the cone conformation with iso-propyl groups attached to the lower rim. The other two were in the 1,3-alternate conformation with allyl groups attached to the phenolic oxygen. The final calixarene synthesized was a calix[6]arene that was partially substituted with iso-propyl groups on the lower rim.

The parallel orientation of the aromatic rings was confirmed using single crystal X-ray structure determination. Nuclear Magnetic Resonance (NMR) complexation studies were conducted on the four calix[4]arene derivatives and showed that thallium binds within the aromatic cavity, and that the complexation/decomplexation kinetics and molecule flexibility are affected by the incorporated ion and the attached groups on the calixarene.

Once the binding characteristics of the synthesized calixarenes had been examined they were then incorporated into plasticized PVC together with an ion-exchanger to make ISEs capable of determining thallium activities in solutions. Three calixarenes were successfully incorporated into the membranes and produced Nernstian responses over the concentration range 10^{-2}-10^{-6} M $TlNO_3$. The lower detection limit of the above electrodes lies in the micro-molar range, which is a common characteristic of the experimental setup used. Since the electrodes behaved ideally with respect to thallium(I), it was then decided to test the complex formation constants and selectivities of the three ionophores. The complex formation constant (Log β_{ILn}) of two of the calixarene derivatives with thallium(I) were determined to be 6.44 and 5.85 respectively, through the use of the sandwich membrane technique. The selectivities were measured with a new protocol, whereby the electrode had not previously come into contact with the primary ion. This helps to remove ion fluxes of the primary ion and subsequent biased selectivity coefficient of highly discriminated ions. The three ionophores showed excellent selectivity against Zn^{2+}, Ca^{2+}, Ba^{2+},

Cu^{2+}, Cd^{2+} and Al^{3+}, and moderate selectivity against Pb^{2+}, Li^+, Na^+, H^+, K^+, NH_4^+ and Cs^+. Silver was the only common high interferent in all three ionophores tested.

As the detection limits of current thallium(I) ISEs in the literature would be insufficient in practical samples, attempts were made to lower the detection limits of the above ISEs with the application of relatively new experimental techniques. The lower detection limit of the three ISEs was successfully lowered by an order of magnitude from the original values through the use of an EDTA-buffered inner filling solution. The lowest achieved detection limit was obtained with the iso-propyl functionalized calix[4]arene, which reached a value of 8.32 nM (IUPAC definition).

The second part of the thesis investigated the incorporation of one of the calixarenes into a solid-contact ISE (SC-ISEs), which are seen as the future in this field due to their potential for miniaturisation and use in lab-on-a-chip applications. Four different solid-contact designs were tested to evaluate which was the best to pursue for future testing. The chosen calixarene was successfully incorporated into all four designs with Nernstian responses recorded in each case. The best response was recorded for an electrode which had a solid gold substrate, poly(3-octylthiophene) (POT) intermediate layer and a methyl methacrylate/decyl methacrylate (MMA-DMA) co-polymer membrane. This electrode exhibited a slope of 58.4 mV decade^{-1} and a lower detection limit of 30.2 nM. The other three solid-contact electrodes, which consisted of a graphite contact, a plasticised PVC membrane on a gold substrate, and a plasticized PVC membrane on a gold substrate with a polypyrrole intermediate layer, exhibited detection limits that were inferior to the MMA-DMA/POT SC-ISE.

Further tests were used to assess one of the main problems associated with SC-ISEs, being the presence of water layers of droplets between the membrane and the solid substrate. Potential tests, electrochemical impedance spectroscopy, small angle neutron scattering and the electrode's reactivity to changes in the concentration of dissolved oxygen were used to study water uptake and the concomitant formation of water layers in solid-contact ISEs. Water was confirmed at the surface of the membrane that consisted only of the membrane and gold substrate, but was not confirmed for the other three electrode designs.

Acknowledgements

The work conducted and presented in this thesis would not have been possible without the help and support of numerous people. Their contribution can not be measured nor forgotten.

Pejcic for the various help, both in and outside the lab. Mr Grant Cope for organizing chemicals and other laboratory supplies. Ms Jillian Brown and Claire Wrighton for their administrative assistance during my time at Curtin University. Special thanks go to Shandelle Bosenberg, Jonothon Morton who has been with me since first year of university and helped me throughout my PhD.

- I would like to thank my parents and family who have supported me throughout my studies. To my partner, Helen, her love and endless support throughout my research has allowed me to successfully complete my PhD. My deepest appreciation goes to her for putting up with the various ups and downs that have occurred throughout my work whilst sacrificing her time to support me in the crucial stages of my studies. To her I owe a great deal of gratitude.

1. Introduction

Analytical chemistry is a vital component of science and is responsible for the understanding and control of many processes throughout industry, research, medicine and environmental fields. The analysis of heavy metals in the environment has become extremely important due to their potential toxicity to both animal and plant life. Developments in the analytical field have been fuelled by the need for instruments with high accuracy, low limits of detection, fast analysis times, cheap purchase and operating costs and ease of use. Ion-selective electrodes (ISEs) have a long history, but form a minor yet developing field of analytical chemistry and have the potential to fill many of the above requirements. As is often the case in chemistry, disciplines overlap and this is no exception with ISEs. The following research combines the disciplines of organic, analytical and physical chemistry to develop a sensor capable of single species recognition, in a variety of samples. The aim of the project is to synthesize metal ion receptors based on the macrocyclic calixarene family and apply them as ionophores in ISEs.

1.1.   Calixarenes

Calixarenes are metacyclophanes, which are synthesized by the condensation reaction between phenols and formaldehyde [1, 2]. These unique and interesting molecules stem from phenol-formaldehyde chemistry, and the associated polymers, such as bakelite, which were studied in the late nineteenth and early twentieth centuries. It was not until the early nineteen forties that the possibility of cyclic structures was proposed after reactions between p-*tert*-butylphenol and formaldehyde were carried out. Over the following twenty years further investigation and discussion finally proved the formation of cyclic structures [2]. It was not until the late seventies and early eighties that C.D. Gutsche developed a synthetic procedure that ensured the production of tert-butylcalix[4]arene in a sufficient yield [3]. Today a vast range of synthetic procedures have been applied to the parent calixarene molecule to produce a diverse series of compounds capable of many uses. This

fascinating and versatile class of macromolecules is discussed in more detail in Chapter 2.

1.2.   Ion Selective Electrodes

Ion-selective electrodes are electrochemical sensors, which monitor changes in electromotive force (EMF) of a membrane against a reference electrode under virtually zero current conditions [4, 5]. The differences in EMF are idealistically a direct result of activity changes of a targeted ion, with no interference from other species in a sample solution. The significant advantage of ISEs over other analytical techniques is that they are simple to produce with minimal cost, consume no analyte during analysis and work reversibly. ISEs also have the advantage of analysing the free ion concentration, as opposed to the total ion concentration determined by techniques such as inductively coupled plasma-mass spectrometry (ICP-MS) and atomic absorption spectrometry (AAS).

ISEs have been known for almost a century with Cremer discovering in 1906 that a thin glass membrane was responsive towards the hydrogen ion [6]. With further refinements in the 1930's a pH electrode was developed and is still one of the most widely used analytical tools in modern chemistry. In the late 1930's, Tendeloo, Kolthoff and Sanders discovered that materials other than glass could selectively measure ions in aqueous environments [7-10].

The ISE field was relatively quiet until the early sixties when Pungor and Hollos-Rokosinyi developed a sensor based on AgI and paraffin for the determination of Ag^+ and I^- in solutions [11]. Over the following years, research was conducted on a vast range of materials from single crystal LaF_3 to liquid ion-exchanger and neutral carrier membranes [12-21]. One very important discovery was the excellent selectivity demonstrated by the antibiotic valinomycin towards potassium ions [22, 23]. Since the seventies the ISE field has expanded with many different research aspects being pursued.

ISEs can be characterized according to the ion-sensing matrix responsible for the sensor response and selectivity. The membranes in ISEs can be 1) crystalline in nature eg. a homogeneous mixture of LaF_3 or a heterogeneous mix of an electroactive species like CuS powder in an inert matrix of graphite, 2) non-crystalline in nature, with charged or neutral ion carriers distributed within a inert matrix eg. valinomycin in poly-vinyl chloride, 3) or as sensitised electrodes eg. an enzyme substrate electrode, or alternatively, a gas sensor electrode whereby a gas permeable membrane separates the sample solution from a solution containing an ISE [5].

At present the most widely used and researched matricies are those of liquid membranes with a rigid polymer support. The liquid or plasticiser and the supporting polymer, house the lipophilic ion and lipophilic ligand (ionophore), which are important to the selective and potentiometric response. The former is responsible for the membrane's permselectivity and Nernstian response while the latter is the membrane's ion recognition element capable of selectively binding the target ion species.

1.2.1. Components of Polymeric Ion-Selective Electrodes

Ion-selective electrodes consist of a range of components, with each contributing to the overall potential of the system. The primary component is the ion-sensing membrane, which contains several key elements needed for the production of potential differentials with selectivity. The vital components that make up an ion-sensing membrane are; polymer matrix, ionophore, plasticizer, lipophilic ion-exchanger and lipophilic salts. Each component is discussed in the following sections.

1.2.1.1. Polymer Matrix

The polymer is essentially the main support for the electroactive species i.e. ionophore and ion-exchanger, whilst giving the electrode mechanical stability and

flexibility. The polymer should act as an inert support and not perturb the electrode response; however low levels of impurities found in commercial polymers can act as ionic sites (see Chapter 4). The polymer can be varied to change the polarity, and also the adhesion properties in the case of solid contact electrodes. Poly(vinyl chloride) is the most widely used polymer but others like polyurethane, polyacrylates, poly(vinylidene chloride) and polysiloxanes are also used. Poly(vinyl chloride) was first used in 1970 for the construction of a calcium selective electrode [24].

1.2.1.2.　　　　Ionophore

The ionophore or ligand is the key component of the membrane. It accounts for the sensor's selectivity by only allowing a targeted ion to form relatively strong but reversible complexes with it. Ions other than the primary ion (interfering, or secondary ions) form weak to no complexes with the ionophore, and in turn reduce ion-exchange between the interfering and targeted ion. The complex formation constant of the ionophore should be several orders of magnitude greater for the primary ion over interfering ones, but not too large as the sensor will not function properly. If the binding of the primary ion is too strong then slow response times, and deviations in response slope, are likely due to the complexation/decomplexation process being kinetically too slow [25]. Many cryptands, which form highly stable complexes with certain ions, are often not utilized in ISEs due to the slow transfer rate [26]. Molecules utilised in ISEs should therefore consist of a balance between structural preorganisation and flexiblity, to minimize the overall free energy barrier between the complexed and free states whilst still maintaining fast kinetics [25, 27]. The rigid macrocycles known as spherands, Figure 1.1, form some of the most stable metal ion complexes known. For applications in ISEs, however, the kinetics of exchange are much too slow, which is a result of the rigidity of the structure. Hemispherands, Figure 1.2 (d), are more useful, combining half a rigid spherand structure with a more flexible component to improve the kinetics.
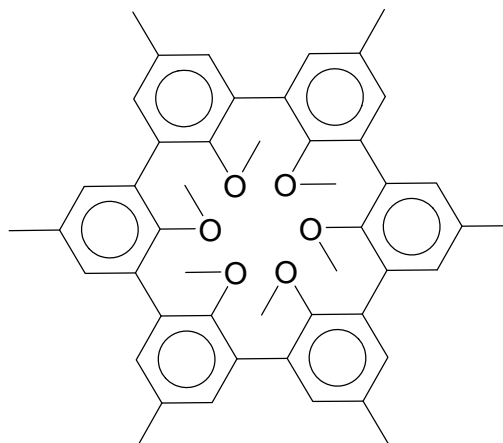
Figure 1.1: The structure of a common spherand.

Initially the membranes selectivity without ionophore is directly related to the sample ions hydration enthalpies [28]. Once the ionophore is incorporated into the membrane, its selectivity is directly related to the complex formation constant of the ionophore with various ions. Apart from the main binding site in the molecule the ionophore must also contain significantly large or numerous lipophilic groups in order for it to remain in the membrane phase and not leach out into the aqueous sample.

Ionophores can be either charged or neutral ion binding molecules. Charged ionophores or ion-exchangers were first tested in 1967 by Ross for the construction of a Ca^{2+} selective membrane [29]. The first neutral ionophore incorporated into membranes is the well-known antibiotic, valinomycin, which forms a 1:1 complex with K^+ ions [22, 23]. Since the initial discovery of this naturally occurring ionophore, a vast amount of research has been conducted into the synthesis of new and better ionophores for various elements.

A successful ionophore usually contains a hydrophilic cavity, which binds with the selected ion, and a hydrophobic surrounding allowing it to be evenly dispersed within the polymer matix. This is often achieved through the addition of non-polar groups around the polar cavity therefore shielding the charged cavity from the non-polar membrane [30]. Valinomycin, shown in Figure 1.2 (a), is able to wrap around the K^+ ion to form this cavity effect. The selectivity of ionophores is often

closely related to the size of the hydrophobic cavity and its ability to exclude certain ions.
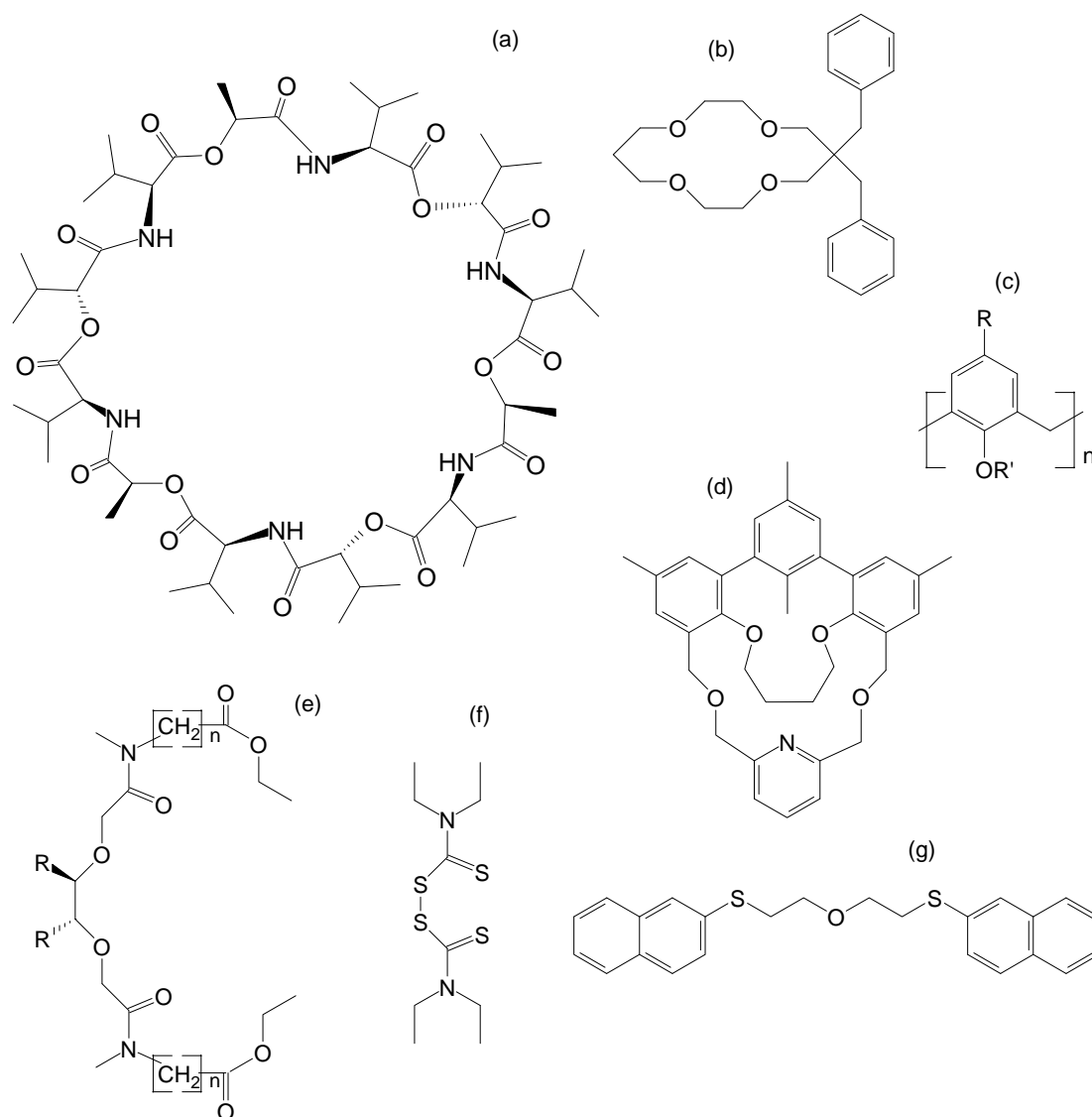
Figure 1.2. Molecular structures of some common ionophores: (a-d) cavity forming molecules, (e-g) acyclic molecules; a) Valinomycin, K^+-selective [31]; b) typical crown ether, 6,6-dibenzyl-14-crown-4, Li^+-selective [32]; c) calix[n]arene with various attached functionalities [33]; d) hemispherand, Na^+-selective [25]; e) ETH 1001, Ca^{2+}-selective [21]; f) dithiocarbamate, Cu^{2+}-selective [34]; g) bi-podand, Ag^+-selective [35].

The most highly selective ionophores are usually the ones with cavities of minimal size variations, allowing only ions of a particular size to complex with the binding

site. Ions larger than the cavity will be excluded from binding, whilst ions of small size will complex less readily as the distance between the binding sites and the ion is increased and the repulsion forces and energy required to bring the binding atoms closer together will be too great.

Crown ethers, Figure 1.2 (b), were perfect candidates for ionophores due to their numerous binding atoms and cavity forming ability. The large number of hard donor atoms improved the selectivity for alkali and alkaline earth metals over other ions. The selectivity could be tailored towards specific ions, by varying the macrocyclic ring size and/or the incorporation of different donor atoms like nitrogen and sulphur [31, 36-42].

Calixarenes have become one of the most utilized series of compounds incorporated into sensors as neutral ionophores [25, 43-46]. Their benefits in ionophore development are discussed further in the following chapters.

However, not all good ionophores are macrocyclic molecules that come equipped with an easily recognizable well-defined cavity. Acyclic ionophores (Figure 1.2 (e-g)) have also shown good to moderate selectivity in ISEs. These types of molecules utilize a predetermined geometrical conformation, also known as a "cleft" for their ion binding. The structure of these molecules enhances complexation by minimizing the free energy of the free-to-complexed ionophore transition [25, 47]. Similar to macrocyclic ionophores, additional functionalities can be added to enhance the binding characteristics, such as lipophilic tails and electron-density-withdrawing/donating groups [25]. Even though these ionophores are less rigid than most of the macrocycles, their flexibility allows the binding sites to be brought into an optimized binding conformation with minimal energy [25, 47]. As is the case with macrocycles, the selectivity of acyclic ligands is dictated by the nature of the binding atoms. A sub-group of acyclic molecules, podands, Figure 1.2 (e), can also provide higher selectivity/binding strength than more rigid cyclic ionophores as a result of flexibility and the "chelate effect" [25, 48]. The chelate effect is observed in podands due to the presence of multiple binding interactions that can wrap around a guest, and therefore stabilizing it more than a single complexation site present in many molecules. Both the macrocyclic and chelate effect are desirable in ionophores as

they would help to stabilise the host-guest system whilst still maintaining fast exchange kinetics.

The binding characteristics of ion-ligand interactions is discussed in more detail in Chapter 3.

1.2.1.3.   Plasticiser

The plasticiser is essential to increase the mobility of the membrane components if the glass transition temperature of the polymer is greater than room temperature [28]. The plasticiser reduces the viscosity of the membrane whilst still maintaining mechanical strength and allows the membrane components to be homogenously distributed within the polymer support. The chemical structures of some common plasticisers are shown in Figure 1.3. The structures of the plasticisers often contain highly lipophilic alkyl chains, aromatic rings, and adamantyl groups, which help prevent loss to the sample solution through leaching and also allow for high mobility and solubility.
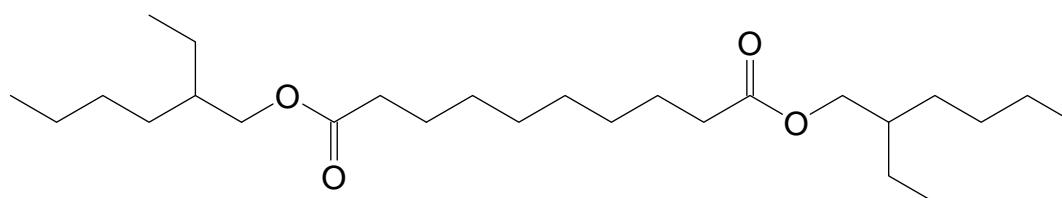
DOS
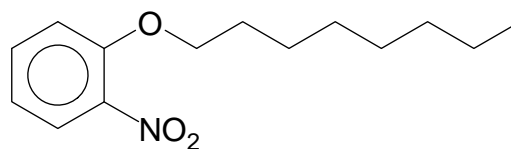
o-NOPE

Figure 1.3. Chemical structures of some common plasticisers: Bis-(2-ethylhexyl) sebacate (DOS), (apolar, $\varepsilon_t \sim 3.9$), 2-nitrophenyl octyl ether (o-NOPE) (polar, $\varepsilon_t \sim 23.9$),

Plasticisers should not contain functional groups that could act as ion binding sites and perturb the membrane response. However, the dielectric constant of plasticisers can influence the selectivity and detection limits of the ion-selective membranes [47]. High dielectric constant plasticisers were used to enhance the selectivity for divalent cations over monovalent cations of similar ionic radius [47, 49].

A disadvantage of commercially prepared plasticisers is that they often contain impurities that act as ionic sites in membranes. This is why a Nernstian response can be obtained with a membrane that contains absolutely no ionophore [28, 47]. This is discussed in more detail in Chapter 4.

1.2.1.4. Lipophilic Ion-Exchanger

The lipophilic ion-exchanger is a large salt that is incorporated into the neutral membrane to ensure its permselectivity, or Donan exclusion, by significantly reducing the coextraction of the measuring ions together with its counter-ion, into the membrane phase. The prevention of coextraction is required in order to obtain a theoretical Nernstian response. The lipophilic ion-exchanger ensures that there is a constant concentration of target ion in the membrane phase, which is significantly higher than the amount occurring through coextraction. As a result of the set concentration of ion-exchanger, the level of measuring ion within the membrane is sample independent.

The ion-exchanger consists of a lipophilic ion that is retained in the membrane, and an aqueous soluble inorganic counter-ion that can be exchange with the appropriate ions in the sample solution. For cation-selective membranes the ion-exchanger usually consists of a derivative of a tetraphenylborate and for anion-selective electrodes, incorporating tetraalkylammonium salts ensures permselectivity. The structure of the ion-exchanger can also play a minor role in the selectivity of an ion-selective membrane [50, 51].

In the case of charged ionophores, the Donan exclusion is achieved through the ionophore itself and therefore no additional sites are necessary. However the addition

of lipophilic sites does have the advantage of reducing the membranes bulk resistance, the response time after a sample activity change, and also has influences on the membrane's selectivity and lower detection limit [50-53]. The structure of common ion-exchanger molecules can be viewed in Appendix I

1.2.1.5. Lipophilic Salts

In addition to the lipophilic ion-exchanger that is required for a stable Nernstian response, alternative lipophilic salts can be added, which are not capable of ion exchange. These salts have the advantage of lowering the resistance of membranes without greatly affecting the primary ion response [54]. They can influence the selectivity by increasing the ionic-strength of the membrane [55]. An example of a lipophilic salt can be viewed in Appendix II.

1.3. Thallium

Thallium is element number 81 on the periodic table and occurs between mercury and lead, two other well known heavy metals. Even though thallium does not have the common stigma of other heavy metals, its toxicity is greater than most, including mercury, lead, cadmium, copper and zinc [56, 57]. It was first discovered in 1861 by Sir William Crookes and is widely dispersed throughout the environment in low concentrations [58-60]. It is mainly found in sulfur-containing ores like pyrite and sphalerite, and potassium minerals such as sylvite and pollucite, but is also found as an impurity in carnallites, zinc blende, silvine, micas, fedspars, lepidolite, braunite and others [56, 57, 59-62]. Thallium occurs in a vast range of minerals as a consequence of its interesting and unique chemical properties.

Concentrations in uncontaminated soils across a range of countries vary between 0.08 and 1.54 ppm with an average of 0.3 ppm, and in natural water samples below 0.2 ppb (0.98 nM) [56-58, 63-65].

Due to its high toxicity and low number of highly concentrated ores, thallium has only a few current uses. Initially thallium was used in a vast range of applications from treatment of syphilis, scalp ringworm and night sweats from tuberculosis to rodent and insecticide poison [57, 62]. Many of these initial uses were outlawed as a result of the large number of human poisonings. However thallium salts are still used as pesticides in developing nations and has resulted in accidental deaths [59]. Today, thallium is primarily used in the semiconductor industry, cardiac imaging and in the production of low-melting highly refractive glass [57, 59]. Other uses include research, sink-float mineral separation and in very low temperature thermometers as a thallium amalgam [59].

The use of thallium in these industries is not the major form of release into the environment. The major forms of anthropogenic release into the environment occur through the burning of fossil fuels especially coal, the roasting of minerals used in the cement industry and as a by-product in the refining of mainly zinc, cadmium and lead ores, but is also present in some gold, copper and uranium ores [56-58, 64, 66]. The mineral melnicovite, obtained from the postflotation waste of zinc-lead processing can contain thallium at levels of 5000 ppm [56]. Thallium from this mineral can easily be released through oxidation, and subsequently leaches into the surrounding water table and soils. Thallium salts are highly to moderately soluble, which allows them to be readily transported via aqueous routes [58].

High levels of thallium have been found in tap water (2.0 ppb, 10 nM) and in animal organs (liver and kidneys, 15-35 ppm) in areas of zinc-lead processing [56]. Thallium concentrations of 1-88 ppm have also been reported in rivers draining from metal mining areas [57, 58]. The U.S. Environmental Protection Agency (E.P.A.) has set the maximum tolerable level of thallium in drinking water at 2 ppb (~10 nM), but has set the desired level at 0.5 ppb (2.5 nM) [67]. Thallium salts have also been used in homicide cases, where the solid salt was added to drinking liquids to poison unsuspecting victims. As thallium salts are tasteless and odourless the victims were oblivious to the fact that what they were drinking contained a poison. Thallium is also highly bioconcentrated, which increases the concern of releasing this element into the environment where food sources are prevalent [68-70]. Trout in the Great Lakes in America have elevated levels of thallium as a result of human activities

around these areas, which could put people that eat significant amounts of fish at risk of thallium poisoning [58, 70].

Thallium occurs in two oxidation states 1+ and 3+ with the former being the most stable and therefore the most dominant in the environment [58]. However at high pH the element is usually oxidized to thallium(III), which is the most prevalent form in the Pacific ocean [57]. The dominance of the 1+ oxidation state, its similar ionic radi (144 pm) to that of alkali metals especially potassium (138 pm), and other similar chemical properties, is the reason for its high toxicity [31, 71]. It is easily transported into the body through the skin, breathing organs and digestive tract, where it is then distributed throughout the body, affecting areas such as the nervous system, potassium-containing cells and sulfur-containing enzymes [71]. Thallium causes peripheral polyneuritis leading to inflammation of the nerves and paralysis of the extremities, and damage to the kidney, liver and heart [66, 71, 72]. Thallium replaces potassium in cells as a consequence of their similar chemical properties, leading to inhibition of the K^+-Na^+-ATPase [71]. The estimated lethal dose for humans is 8-12 μg g^{-1} [71]. Symptoms of thallium poisoning include; muscle weakness, tremors, gastrointestinal irritation, acute ascending paralysis, vomiting, diarrhea, convulsions, hair loss, disturbed rhythm of heartbeat, pneumonia, respiratory failure and coma [71, 72].

A variety of techniques including UV-Vis spectrophotometry, spectrofluorimetry, atomic spectrometry, mass spectrometry, electrochemical and nuclear techniques have all been used to determine thallium in a variety of samples [60, 71, 73-75]. The electrochemical determination of thallium is the most widely used, and is usually carried out via stripping voltametry. ICP-MS is also used but is more costly than voltametry. Electrochemical methods offer the advantage of low cost, rapid response, simple operation and precise results [71].

1.4.   Ion-Selective Electrodes for Thallium Detection

The number of dedicated thallium(I) ISE papers in the literature over the past four decades is somewhat representative of its low use in today's society. However, due

to its toxicity, an analytical tool capable of screening for thallium(I) in various samples would be beneficial, especially in poisoning cases where the patients symptoms are often mistaken for other causes. The few compounds that have been tested for thallium(I) ISEs are very diverse in nature and have resulted in sensors with varying sensitivities and selectivities. The first examples of thallium(I) ISEs, made use of compounds including hetropoly acids in epoxy resins [76], bis(crown ethers) in PVC [77, 78], polycrystalline membranes [79], a thallium O,O'-didecyldithiophosphate ion-exchanger [80], salts of a water-insoluble basic dye [81] and a thallium(I) cyanotriphenyl borate or tetrakis(m-tri-fluoromethylphenyl)borate [82, 83]. Most of the above compounds showed selectivities that were poor for other heavy metals but good against alkali and alkaline earths or vice versa. The first series of compounds applied as thallium(I) ionophores were often reported elsewhere as ionophores for other ions [31, 84-86].

Since these initial compounds, the trend has focused on using improved organic receptor molecules incorporated in polymer membranes [87-96]. Since thallium possesses the properties of both hard metals and soft/heavy metals, compounds have ranged from crown-ethers, typical alkali ion ligands [96] to thia substituted macrocycles [95], which are known for their heavy metal affiliation [31, 89, 94, 95, 97, 98]. The compounds that consisted of crown-ethers usually suffered from alkali and alkaline earth interferences, and could not be used in many practical samples which normally comprise of relatively high concentrations of these ions [31, 96]. Better selectivities over the alkali and alkaline earth ions were observed with the range of thia-substituted compounds [94, 95]; however, these compounds can suffer from interferences from heavy metals, with most showing poor selectivity with silver. Other compounds such as a calix[4]pyrrole, indeno-pyran and a quinoline-carbonitrile compounds have also been reported and show good to moderate selectivity for most ions with the calix[4]pyrrole only suffering from a silver interference and the quinoline-carbonitrile suffering from a cesium interference [89, 92, 98].

A range of calixarene molecules have also been reported showing good to moderate selectivity of thallium(I) over other ions [73, 88, 91, 99]. However, the calixarene molecules discussed in the literature still suffer from significant interferences from at

least one ion, whether it be a hard alkali metal ion or a soft/heavy ion. The binding sites of the reported calixarenes, which will be discussed in more detail in Chapter 3, were shown to reside within the aromatic cavity. If the size of the cavity could be tailored further to accept only one ion, the selectivity could be improved over the previously studied molecules. The structures of organic molecules previously tested as thallium(I) ionophores are presented in Appendix III.

As well as improving selectivity, ISE design will also be addressed, so as to improve the detection limit of the device. This will be addressed in Chapters 4 and 5.

The research is separated into four chapters, starting with the synthesis of the ionophores, which leads into their characterisation, and then on to the incorporation of these ionophores in liquid-contact and solid-contact ISEs respectively. The work is summarised and concluded as a whole at the end of the thesis.

2. Synthesis, Characterisation and Applications of Calixarenes

2.1. Nomenclature and Structural Representation

The name 'calixarene' was originally used in 1975 to describe the cyclic array of one of the phenol-derived conformers, where all four aryl units are oriented in the same direction [1]. 'Calix' is derived from Latin, meaning vase, and 'arene' is used to describe the aryl units present. To incorporate the name to all oligomers of varying sizes, a bracketed number was inserted between the calix and arene parts, thereby specifying the number of aryl units. For example the cyclic tetramer obtained from p-*tert*-butylphenol is named p-*tert*-butylcalix[4]arene. Under nomenclature guidelines, this cyclic tetramer is named 5,11,17,23-tetra-*tert*-butyl-25,26,27,28-tetrahydroxycalix[4]arene and is generally only used in experimental sections [100, 101]. The shortened colloquial terminology is often used for simplicity in discussions and only describes the basic macrocyclic framework with any additional functionalities added as appendages. The different structural representations of p-*tert*-butylcalix[4]arene are shown in Figure 2.1.
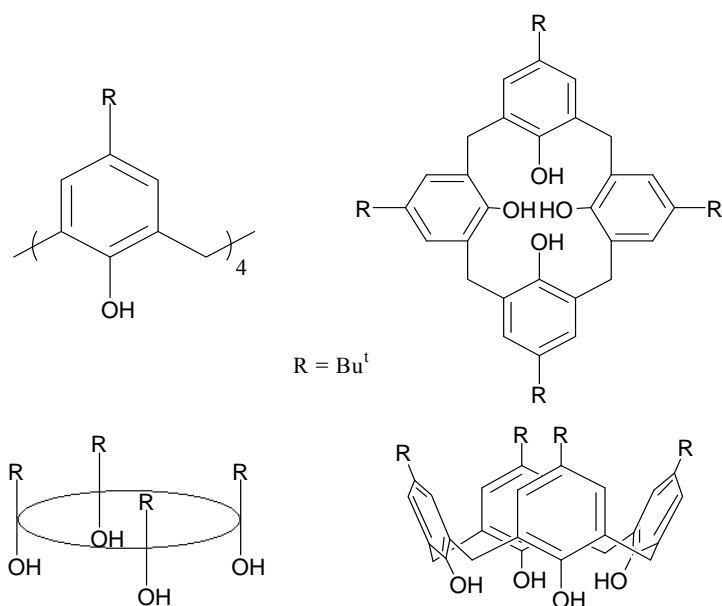
Figure 2.1: Structural representations of p-*tert*-butylcalix[4]arene.

Alternatively the phenolic oxygens are numbered one to four in order, so that any additional functional group can be labeled appropriately in the name. For example, if two of the hydrogens on opposite sides in the parent tetramer are substituted with propyl functionalities, the name would become 1,3-dipropyl-p-*tert*-butylcalix[4]arene.

2.2. Conformations of Calixarenes

Another important consideration for calixarene nomenclature is the conformations that these macrocycles can adopt. The various conformations are pivotal in the development of artificial receptors and the construction of supramolecular systems [101]. For the focus of this thesis and simplicity, only the cyclic tetramer will be discussed. Due to the flexibility of the methylene bridges, the cyclic tetramer exists as four principal conformers with each having a unique ^{1}H NMR pattern. These four conformers consist of different arrangements of the aryl units and can either be syn or anti to each other [101, 102]. The four conformers and their accepted terminology are shown in Figure 2.2. The different conformations are included in the name by indicating the conformation of the aryl units at the start, e.g. 1,3-alternate-p-*tert*-butylcalix[4]arene, which is shown in Figure 2.2, where R equals *t*-butyl. Proton NMR studies demonstrated that the tetramer preferentially exists in the cone conformation due to intramolecular hydrogen bonding of the phenolic hydrogens [100, 102]. It has been demonstrated that the hydrogen bonding can be weakened by a polar solvent such as pyridine, which enhances the rate of interconversion between cone and the other conformers [100]. Steric hindrance also plays an important role in determining the amount of conformational interconversion. The hydroxyl groups only experience a low amount of resistance when being brought through the center by the aryl groups rotating around the C-2/C-6 axis [102]. The conformational interconversion can be reduced by addition of bulky groups to the phenolic oxygen, increasing the resistance to being brought through the cavity, and therefore almost locking them into a stable conformer. Groups larger than ethyl in chain length result in the calixarene being locked into a set conformation [103]. The conformation can be determined through ^{1}H NMR spectroscopy, by examining the signals due to the

methylene protons: in the spectra, cone, partial cone, 1,2-alternate and 1,3-alternate appear as a pair of doublets, predominately two pairs of doublets, one singlet and a pair of doublets, and a singlet respectively [104]. The partial cone can also be represented in the spectra as a singlet and a pair of doublets making it difficult to differentiate from the 1,2-alternate.
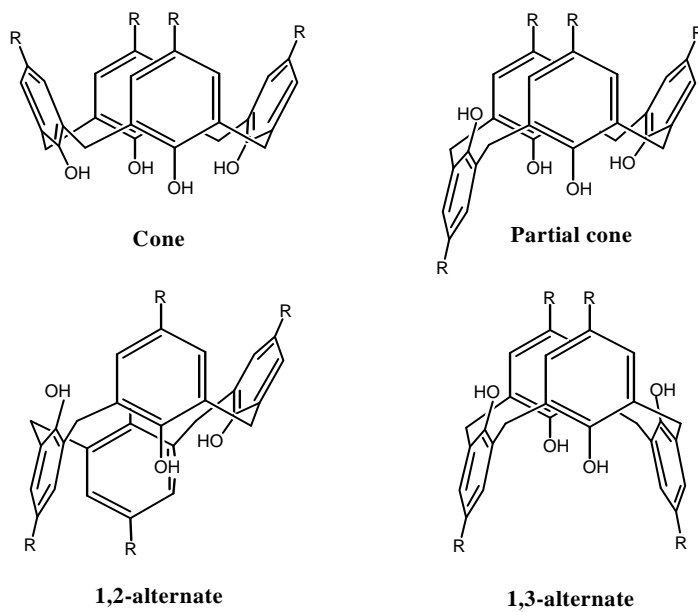
Figure 2.2: Conformations of calix[4]arne

2.3.   **Functionalising Calixarenes**

Once the parent calixarene has been synthesized, many alterations can be made to the basic macrocyclic structure. The initial calixarene structure can be divided into three sections, the upper or wide rim, the cavity and the lower or narrow rim. The upper rim of the structure is represented by the R functionality in the cone conformer in Figure 2.2. Additional functional groups can be added to the para position of the aromatic ring through simple processes such as electrophilic substitution or rearrangement reactions [101, 105]. The lower rim occurs at the phenolic hydrogens in the macrocycle, and can be altered to form ether and ester functionalities [106, 107]. The cavity occurs between the upper and lower rims and consists of the aromatic and the bridging methylene units, of which both can be modified [101, 108, 109]. Attaching functional groups to the upper and low rims introduces additional cavity forming areas, which can act as binding sites for a variety of guests.

The three different sections in the structure, allow for selective modification, fulfilling certain requirements of the desired outcome; such as tailoring the molecule to a specific cation to be used as an ionophore or attaching functional groups which allow it to be water soluble and act as a crystal growth inhibitor [31, 110, 111]. The ease of selective modification is one of the reasons for the vast array of calixarene derivatives and their popularity. Modifications can also be made to the attached functionalities to fine-tune the desired needs. Due to the vast range of chemical modifications in the literature and the scope of this thesis, only a selected few will be discussed.

Two of the earliest modifications made to calixarenes, and some of the most studied, are the esterification and etherfication at the lower rim. The esters were formed through reactions with acid halides and NaH or $AlCl_3$, or acid anhydrides and H_2SO_4 [102, 112]. Ethers are synthesized in a similar way to esters, and are achieved through the reaction of a suitable alkyl halide with NaH, or other bases. Even though the full substitution is the most popular, the extent can be varied as a result of changing the reaction conditions. The solvent, strengths of the base used, other functionalities on the calixarene, limiting the amounts of the esterifying/alkylating agent, and type of esterifying/alkylating agent all have an influence on the level of substitution [112-117]. This can become important when trying to lock the calixarene into a set conformation whilst attaching additional functional groups. Other methods of preparing ester and ether functionalized calixarenes can be found in the literature [101, 112, 117, 118].

One of the most basic alterations that can be made to the parent calixarenes is to remove the tertiary butyl group from the upper rim. This allows for the introduction of additional functional groups to the upper rim of the calixarene [1, 118-122]. Removal of the bulky tertiary butyl groups on the upper rim, offers guests a less hindered pathway to the aromatic cavity, which can lower the energy barrier between the free and complexed states [25, 112].

A novel way to modify calixarenes is by attaching bridging chains to either the lower or upper rim. The bridging chains can be either intramolecular or intermolecular, and

consist of a vast range of chemical compositions [112, 119, 123-125]. The bridging units can be as simple as crown ethers or complex like porphyrins, connected to the phenolic protons at different locations, and can bridge more than two calixarenes [125-127]. Apart from helping to lock the calixarene into a set conformation, bridging units also offer the potential of a set of very precise and well-organized binding sites. The cavity can be tailored to suit the size of the guest by altering the length of the bridge [112, 119].

Calixarenes can also be modified at the bridging methylene units, and the aromatic rings can also undergo chemical change [101, 109, 112]. The hydroxyl groups have also been substituted with hydrogen, nitrogen and sulfur moieties [101, 112, 128-132].

Over the past three decades many reactions have been developed to modify the calixarene in an assortment of ways. Only a few basic examples are listed above. It seems that the tailoring of these molecules is only limited by the researchers' imagination and the desired outcome.

2.4. Applications of Calixarenes

Calixarene scientists have sought interest from many fields since their development. Their popularity can be attributed to the several factors [133]:

a) Calixarenes can be synthesized easily in simple one-pot procedures, which allow for inexpensive large-scale production.
b) Calixarenes form a series of well defined cyclic oligomers, which can be tailored to suite the requirements of the various guests.
c) Chemical modification can be routinely performed, providing sites for a vast range of guests.

As a result of these properties, calixarenes have the potential for the development of a vast range of derivatives, with each being specially tailored to the needs of the desired application. Other important properties include their high melting points,

high thermal and chemical stability, their low solubility in many solvents and their low toxicity [1, 110-112, 133].

The apparent beneficial properties of calixarenes have driven research over a broad range of fields. Calixarenes have been used as catalysts, ion-separating agents, stabilizers, in the separation of neutral-organic-molecules, crystal growth modifiers and platforms in bioorganic and biomimetic chemistry, to name a few [134, 135].

The majority of calixarene uses incorporate some form of inclusion phenomena. In relation to ion-separating agents, calixarenes have been used for cesium recovery in nuclear wastes and uranium recovery from aqueous solutions, including sea water and extraction agents for americium, europium and platinum to name a few [100]. Calixarenes have been found to enhance the reaction of various systems through the binding of the involved cation, and subsequent anion solubilization and activating properties [133]. Applications such as stationary phases in gas and liquid chromatography, and bioanalytical sensors, have developed from the selective binding capabilities of various calixarenes with neutral organic molecules [133]. Calixarene applications in bio-organic and biomimetic chemistry also follow from molecular inclusion of organic molecules, but also includes ion binding/transport. The inclusion and binding characteristics of molecular species is discussed in more detail in Chapter 3.

One of the more common uses of calixarenes has been their use as host molecules in a range of chemical sensors.

2.5.   Calixarenes as Sensor Molecules

Calixarenes were originally thought to be appropriate molecules for enzyme mimetics and it was not long after this that they were incorporated into the field of metal ion recognition and subsequently analytical sensors. Investigation into the ion binding properties was brought about by the similar structural characteristics present in crown ethers and other macrocyclic ligands [136]. Researchers initially investigated the complexing capabilities of calixarenes with alkali and alkaline earth

cations. The ability to selectively complex metal ions by varying the cavity size and nature of the attached functional groups resulted in an increased interest in the ionophoric properties of calixarenes [43]. The first publication describing the use of calixarenes as ionophores in ion-selective electrodes for use in measuring sodium occurred in 1986 [137]. The initial series of calixarenes investigated were a range of ester and crown ethers used for the analysis of sodium and potassium. The focus in the early years was directed towards the alkali and alkaline earth metals due to their medical importance especially in blood analysis [112, 138].

A vast range of molecules, examples pictured in Figure 2.3, consisting of ester, ether, ketone, carboxylic acid, amide, crown ether and hemispherand derivatives of calix[4]arene in its cone conformation have been extensively studied [139, 140].
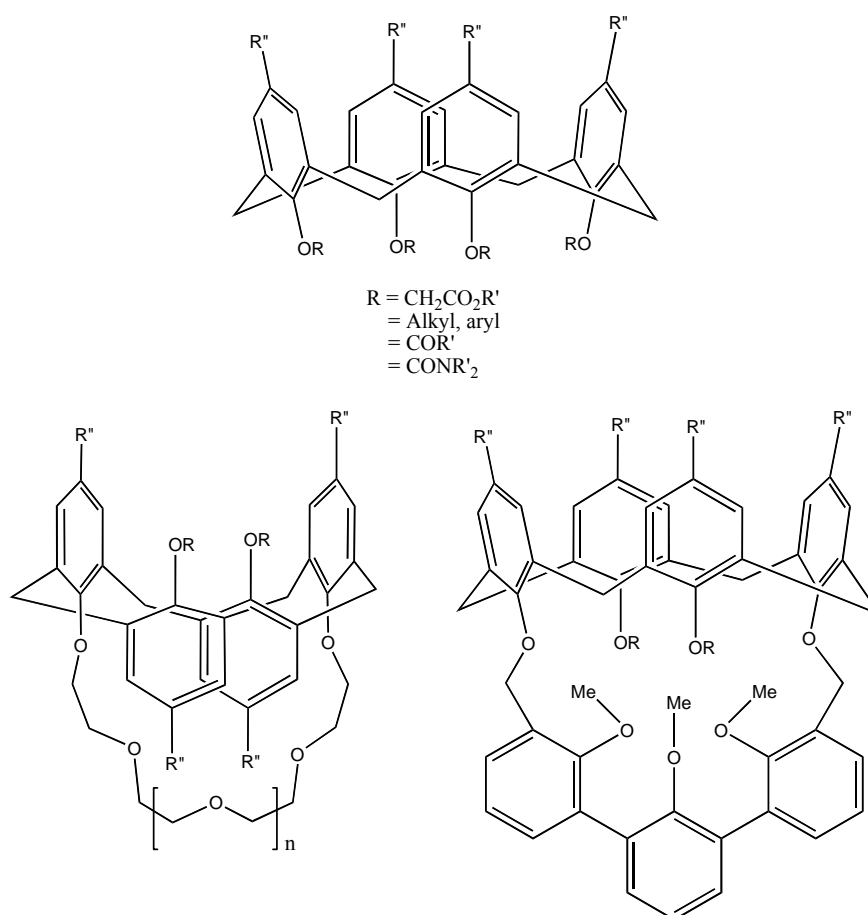
Figure 2.3: Several structures of some common calixarenes used as ionophores in chemical sensors [139]. R most commonly denotes *tert*-butyl or hydrogen.

Over the last decade, the trend has shifted from the alkali and alkaline earth metals to heavy metals. Initially, the limits of detection and selectivity of polymer based ISEs, were considered mediocre in the field of analytical chemistry, and subsequently lacked the requirements needed for monitoring of heavy metals in the environmental and clinical fields. The trend in ionophores towards heavy metals was followed in calixarenes with the inclusion of soft metal binding sites to the parent structure. Figure 2.4 shows some examples of some common calixarenes used as heavy metal ionophores.
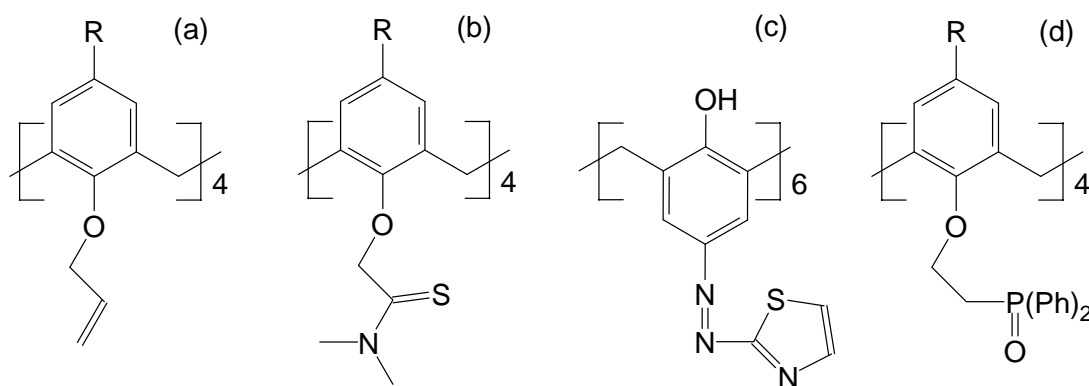
Figure 2.4: Structures of selected calixarenes used as ionophores in heavy metal ISEs. Targeted ions of the above ionophores are (a) Silver and thallium, (b) Lead and cadmium, (c) Mercury, (d) Lead.

The ionophores presented in Figure 2.4 only represent a small fraction of the total number of calixarenes dedicated to heavy metal binding. Far more elaborate functional groups have been attached to the parent calixarene, but consist of similar coordinating atoms [141-147]. Further structures of calixarenes used as heavy metal ionophores are presented in Appendix IV. The metal complexation of ions with calixarenes is presented in more detail in Chapter 3.

The use of calixarenes as ionophores has not been specifically limited to cations. Though not as popular, a range of anion selective calixarenes has also been developed [100, 148]. The popularity of anion receptor calixarenes can be put down to the unique properties of anions. The difficult properties of anions include a negative charge that is often delocalised over several atoms, together with their unique size and shape [100]. Anions are larger than cations and can exist as planar,

linear, spherical, tetrahedral and octahedral ions [100]. The binding of anions is also dictated more strongly by the pH and solvation effects than in the binding of cations. An example of an anion selective electrode, is the development of a monohydrogen phosphate receptor [148] that could be useful in the monitoring of phosphate levels in rivers and streams. To promote anion binding and subsequent transport through the membrane the parent calixarene requires specific modification to accommodate the negative charge. In the case above, the interaction between the anion and the calixarene is achieved through hydrogen bonding as well as electrostatic and dipole-dipole interactions [148].

Other processes such as redox couples have also been extensively studied and can be found in the literature [100, 149]. Analogues of calixarenes where the benzene rings are replaced with heterocycles have also been used as anion receptors in ISEs [150, 151]. A recent review by Matthews and Beer [149] covers a broad range of calixarenes that have the potential as anion sensors and demonstrates the increasing interest in this field.

Calixarenes fulfill many of the requirements of ionophores, which is why they have been extensively studied in the ISE field. As discussed in Section 2.3, the basic structure of calixarenes can be modified significantly to the desired needs of the measuring ion. The various modifications provide a significant list of potential binding sites with numerous variations. Ionophores have been developed with binding sites on both the upper and lower rims and within the cavity itself [99, 142, 152]. As a result of the calixarene's ability to undergo significant chemical modification, there is the potential for developing improved ionophores, to enhance the electrodes selectivity and sensitivity.

2.6.   Comments on the Synthetic Procedures

Calixarene (1)   R = *t*-butyl
Calixarene (2)   R = H

Calixarene (3)   R = *t*-butyl
Calixarene (4)   R = H
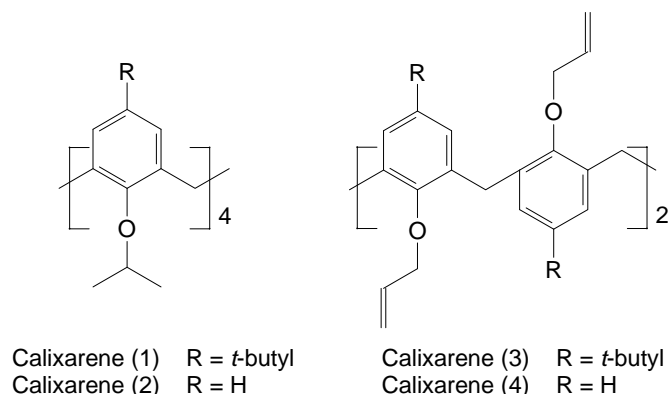
Figure 2.5: Structures of the four calix[4]arenes synthesised

The synthetic procedures of calixarenes (1) and (2) were adapted from a general alkylating technique described in Parker, which used sodium hydride, the starting calixarene and the alkylating agent [118]. For the synthesis of the isopropyl derivatives the direct alkylation method of Parker could not be precisely followed as elimination of 2-bromopropane is a competing reaction in the synthesis. The two competing reactions are shown in Figure 2.6.
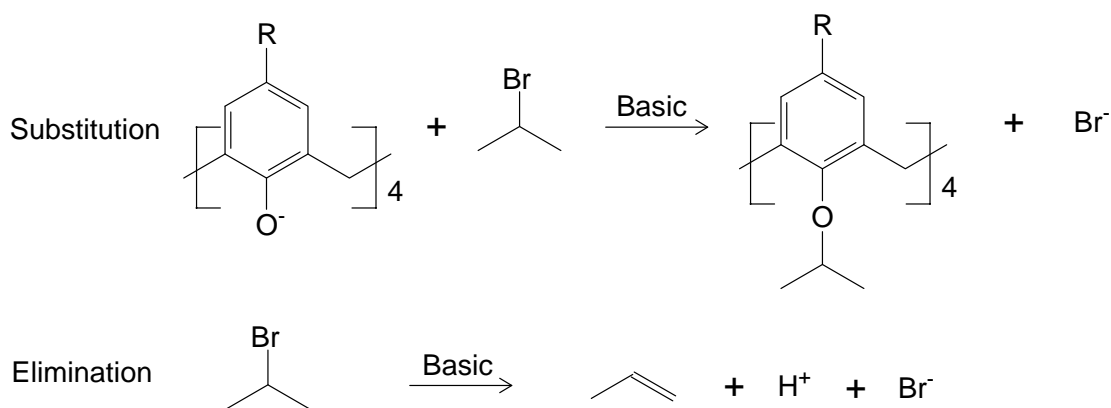
Figure 2.6: The two types of competing reactions occurring with the alkylating agent in the reaction vessel.

The desired product is a result of the nucleophilic substitution reaction, whereas propene is formed as a by-product of the elimination reaction. As a consequence of the type of alkylating agent used, it is difficult to promote one reaction over another, which is why a very large excess of the 2-bromopropane is used. Another reason for

the large excess is that even though the iso-propyl group is small, it is significantly bulky as a consequence of steric hindrance, and makes the full substitution on the lower rim very difficult. The reaction needs to be continuously pushed by the addition of both extra sodium hydride and 2-bromopropane, to force full substitution at the lower rim. Heating could not be used as this would promote the elimination reaction, which meant the reaction needed to be carried out at room temperature over an extended period of time. Imidazole is added to the reaction as a catalyst by helping remove the phenolic hydrogens off the calixarene. The structure was shown to exist in the cone conformer for both calixarenes (1) and (2) with the methylene hydrogens appearing as a pair of doublets in the NMR spectra. The peaks were sharp and well defined displaying that the structure had been locked into the cone conformer.

Through the surplus addition of sodium hydride and 2-bromopropane and a lengthy reaction time, the two isopropyl calixarenes (1) and (2) were successfully prepared in yields of 34 % and 30 % respectively. The other compounds in the reaction mixture are thought to be of the original calixarene and various levels of mono, di and tri substituted calixarenes which were not isolated.

Since this method was successful for the addition of iso-propyl groups to the two calix[4]arenes, it was adapted for the synthesis of the substituted calix[6]arene (5). Similar to the smaller analogues, the reaction was carried out in DMF with sodium hydride, imidazole and 2-bromopropane. The reaction was monitored by TLC and looked to be complete after 28 hours due to the formation of an extra spot with a retention time that was close to the solvent front compared to the initial calixarene which remained at the bottom of the TLC plate. As there was only one spot and not multiple spots it was thought that the reaction was complete and that there were no intermediate partially substituted molecules left in the reaction mixture, resulting in various spots on the TLC plate. It was thought that the reaction of the hexamer was going to proceed more rapidly as it has more flexibility than the tetramer and therefore less difficulty when trying to attach bulky groups at the lower rim. However the identification and characterisaiton of the compound found it to be only partially substituted with positions 3 and 6 still containing their phenolic hydrogens. This suggests that the first four iso-propyl groups were attached with relative ease

after only 28 hours. The last two positions like the tetramer may need extra force to attach since the lower rim is becoming crowded. This could be achieved by either increasing the reaction time or further additions of the sodium hydride and 2-bromopropane. The partially substituted calixarene was assigned with the isopropyl groups attached to the oxygen's at positions 37,38,40 and 41 instead of 37,38,39 and 40, as the ^{1}H-NMR spectra showed two peaks for the *tert*-butyl group hydrogens instead of three, which would be expected in the case of the later substitution. The yield was also lower than the first two derivatives suggesting that the reaction was stopped too early. In future, the reaction should be carried out on a similar time frame to the first two derivatives (1) and (2).

The synthesis of the two 1,3-alternate derivatives (calixarenes (3) and (4)) is vastly different to cone conformer calixarenes of (1) and (2). Sodium hydride is used as the base in the alkylation of the first two compounds, but cannot be used in preparing the 1,3-alternate derivatives. Cesium carbonate takes the place of sodium hydride as the base in the preparation, as the cesium cation exhibits a template effect in the calixarene, resulting in the 1,3-alternate conformer [153]. The calixarene is stirred for a significant period before the alkylating agent is added to ensure that all the compound has converted to the 1,3-alternate conformer. It is thought that the *tert*-butyl groups of the p-*tert*-butylcalix[4]arene (calixarene (a)) hinder the addition of the alkyl groups, which is why the procedure for calixarene (3) is performed in a two step process. The poor solubility of calixarene (a) in acetone could also prevent the direct route to the 1,3-alternate conformation as the alkylation reaction takes place one allyl unit at a time, which leads to better solubility, and eventually the calixarene is sufficiently soluble to enable cesium to exhibit its template effect on the structure.

It was noted, that in the preparation of calixarene (4), the reflux had to be vigorous otherwise the alkylation did not proceed. Heat can be used in this preparation as the elimination reaction is less significant. The 1,3-alternate conformation was confirmed through the NMR spectrum with only a singlet appearing for the methylene hydrogens. The structure was again locked into the 1,3-alternate conformer with a very sharp methylene hydrogen singlet appearing.

2.7.   Experimental

2.7.1.   Reagents

DMF refers to N,N-dimethylformamide. In all cases, the petroleum spirit used was 40-70°C grade. Dry acetone was obtained by drying over B_2O_3 for a minimum of two weeks prior to distillation. Sodium hydride was cleaned with petroleum spirits to remove oil. Imidazole was obtained from Merck, and used as supplied. Deutrated chloroform was obtained from Cambridge Isotope Laboratories Inc.. 2-Bromopropane and allyl bromide was obtained from Merck, and used in this form. Cesium and potassium carbonate were obtained from Aldrich.

2.7.2.   Instrumentation

Melting points were determined on a Reichert thermopan microscope equipped with a hot stage attachment. The instrument was calibrated prior to use with known standards.

All infrared spectra were obtained using a Bruker Vector 22 FTIR spectrophotometer. All samples were analysed by transmission mode using potassium bromide (KBr) as the supporting medium. Spectra were averaged over four scans in the 4000-450 cm^{-1} frequency range at 4 cm^{-1} resolution.

All nuclear magnetic resonance (NMR) spectra were obtained using a Varian Gemini 2000 NMR spectrometer. ^1H spectra were recorded at 200 MHz and ^{13}C at 50 MHz. All samples were dissolved in and referenced to residual chloroform in $CDCl_3$.

Thin layer chromatography (TLC) was performed on Merck silica gel 60 F_{245} aluminium backed sheets. The developed plates were viewed by short-wave ultra-violet light or by dilute ammonium molybdenate solution.

Flash chromatography was performed using Merck silica gel 60 grade (particle size 0.040-0.063 mm).

Combustion analysis was performed by Central Science Laboratories at the University of Tasmania, Australia.

Mass spectrometry was performed at the School of Biomedical, Biomolecular and Chemical Sciences at the University of Western Australia.

2.7.3.   Synthesis of the Thallium(I) Selective Calixarenes

2.7.3.1.   p-*tert*-Butylcailx[4]arene (a) and Calix[4]arene (b)

The synthesis of the p-*tert*-butylcalix[4]arene [154] was achieved according to the literature with a modification of using ethyl acetate in the workup procedure in place of chloroform. Calix[4]arene was prepared from p-*tert*-butylcalix[4]arene according to the literature with no modifications to the procedure [118]. The physical and spectroscopic data of both the p-*tert*-butylcalix[4]arene (a) and calix[4]arene (b) match the literature. The procedures for the two parent calixarenes are well established and result in products with good yield and high purity, therefore no changes or further comments need to be made.
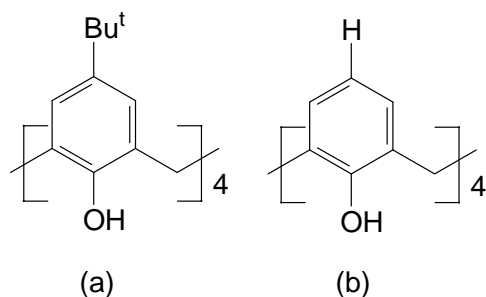
Figure 2.7: Structures of p-*tert*-butylcalix[4]arene (a) and calix[4]arene (b)

2.7.3.1.1.   5,11,17,23-Tetra-*tert*-butyl-25,26,27,28-tetra-isopropoxycalix[4]arene (1)
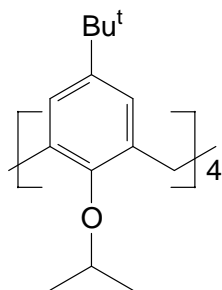
p-*tert*-Butylcalix[4]arene (a) (5.13 g, 7.7 mmol) was added to clean sodium hydride (2.96 g, 123 mmol) and imidazole (50 mg, 0.073 mmol) in dried DMF (125 mL) and stirred for 30 minutes under nitrogen. A large excess of 2-bromopropane (15.0 mL, 0.159 mol) was then added drop wise and stirred under nitrogen for 24 hours. Additional aliquots of 2-bromopropane (10 mL, 0.106 mol and 7.0 mL, 0.074 mol) were added to the reaction flask at 24-hour intervals. The reaction was quenched after 112 hours with the careful addition of methanol. Water was then added to precipitate the calixarene, which was then collected and washed with further proportions of water to yield the crude material. The crude calixarene was purified by flash chromatography (19:1 petroleum spirits: ethyl acetate) to yield a white powder (2.12 g, 34 %), m.p. 269.5°C.

IR: 2964.2 cm^{-1} (υ_{as} CH$_3$); 1602 & 1479 cm^{-1} (aromatic C=C); 1460 cm^{-1} (CH$_2$ scissor); 1364 cm^{-1} (δ_s CH$_3$); 1202 cm^{-1} (Ar-O-C antisym stretch); 1115 cm^{-1} (Ar-O-C sys stretch). **^{1}H NMR**: δ 1.09 [s, 36H, C(C$\underline{H}_3$)$_3$]; 1.40 [d, J = 6.2 Hz, 24H, (C$\underline{H}_3$)$_2$CH]; 3.06 [d, J = 12.1 Hz, 4H, Ar-C$\underline{H}_2$-Ar (equatorial)]; 3.99 [m, 4H, -C$\underline{H}$(CH$_3$)$_2$]; 4.51 [d, J = 12.1 Hz, 4H, Ar-C$\underline{H}_2$-Ar (axial)]; 6.81 [s, 8H, ArH]. **^{13}C NMR**: δ 23.56 (CH($\underline{C}$H$_3$)$_2$); 34.47 (C(CH$_3$)$_3$); 31.78, 32.23 (Ar-CH$_2$-Ar); 77.85 (O-$\underline{C}$H); 125.32, 135.26, 144.32, 152.14 (aromatic).

2.7.3.2.   25,26,27,28-Tetra-isopropoxycalix[4]arene (2)
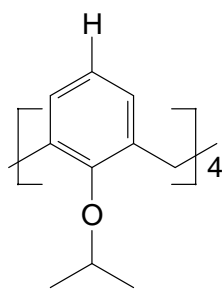
Calix[4]arene (b) (5.0 g, 11.8 mmol) was added to clean sodium hydride (8.0 g, 0.33 mol), imidazole (50 mg, 0.073 mmol) in DMF (60 mL) and stirred under nitrogen for 30 minutes. An excess of 2-bromopropane (30 mL, 0.318 mol) was then added drop wise to the reaction mixture with stirring. The reaction progress was monitored by thin layer chromatography (TLC) (1:1

petroleum spirits:toluene) and additional portions of sodium hydride and 2-bromopropane were administered when required (2 g, 0.08 mol and 15 mL, 0.159 mol at 48 and 120 hours respectively). The reaction was quenched after 160 hours with the careful addition of methanol to the mixture. Water was added to precipitate the calixarene, which was collected and washed with further aliquots of water. The product was purified by flash chromatography (1:1 petroleum spirits:toluene) to yield a white powder (2.13 g, 30.4 %) sublimation 268°C. Found: C 81.0; H 7.92 %, $C_{40}H_{48}O_4$, required: C 81.0 ; H 8.16 %.

IR: 2958 cm^{-1} (υ_{as} CH_3); 1654 & 1481 cm^{-1} (aromatic C=C); 1362 cm^{-1} (δ_s CH_3); 1200 cm^{-1} (Ar-O-C antisym stretch). **^{1}H NMR**: δ 1.37 [d, J = 5.86 Hz, 24H, C$\underline{H}_3$CH]; 3.08 [d, J = 12.4 Hz, 4H, Ar-C$\underline{H}_2$-Ar (eq)]; 4.47 [m, 4H, C$\underline{H}$(CH$_3$)$_2$]; 4.50 [d, J = 13.2 Hz, Ar-C$\underline{H}_2$-Ar (ax)]; 6.52 to 6.67 [m, 12H, Ar-H]. **^{13}C NMR**: δ 23.46 (CH($\underline{C}$H$_3$)$_2$); 31.79 (Ar-$\underline{C}$H$_2$-Ar); 77.32 (O$\underline{C}$H); 122.23, 128.65, 136.44, 154.92 (aromatic).

2.7.3.3.   1,3-alternate-5,11,17,23-Tetra-*tert*-butyl-25,26,27,28-tetra-alloxycalix[4]arene (3)
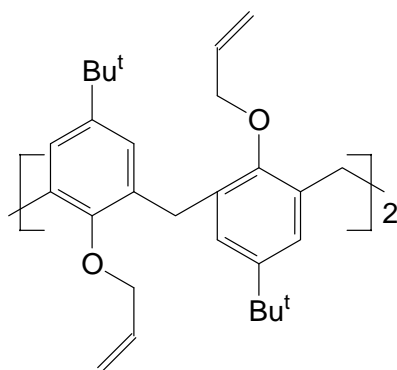
p-*tert*-Butylcalix[4]arene (a) (3.08 g, 4.6 mmol), allyl bromide (2 mL, 11.5 mmol) and potassium carbonate (10 g, 0.1 mol) was added to dry acetone (150 mL) and heated at reflux for 18 hours under nitrogen. The solution was then filtered and the residual solid washed with dichloromethane (2 x 15 mL). The solvent was then removed by reduced pressure distillation to yield the crude 1,3-di-allyl-p-*tert*-butylcalix[4]arene. The solid was collected washed with cold methanol (2 x 10 mL) and recrystallised from chloroform/methanol to yield the pure disubstituted derivative (1.93 g, 2.75 mmol, 60 %) m.p. 183-184°C. [Lit. 181-182°C, [155]]

The above compound (1.93 g, 2.75 mmol), was added to dry acetone (120 mL) containing a suspension of cesium carbonate (3 g, 15.5 mmol), and stirred for five

hours under nitrogen. Allyl bromide (3.0 mL, 33.9 mmol) was added and the reaction mixture heated to reflux for 72 hours under nitrogen. The solution was filtered and the solid washed with dichloromethane (2 x 15 mL). The solvent was removed by reduced pressure distillation to yield an oily residue. Methanol (30 mL) was added to the oily residue to precipitate the calixarene. The precipitate was collected and recrystallised with chloroform/methanol. The crude product was further purified by flash chromatography (500:80:1 petroleum spirits:toluene:ethyl acetate) to yield the 1,3-alternate tetra-allyl-p-*tert*-butylcalix[4]arene derivative as a white powder (0.92 g, 1.12 mmol, 41 %), m.p. 249-250°C [Lit. 248.2-248.7°C, [156]]

IR: 2962 cm^{-1} (υ_{as} CH$_3$); 2865 cm^{-1} (υ_s CH$_3$); 1648 cm^{-1} (allyl υC=C); 1599 & 1478 cm^{-1} (aromatic C=C); 1459 cm^{-1} (δ_{as} CH$_3$); 1420 cm^{-1} (allyl δCH in plane); 1361 cm^{-1} (δ_s CH$_3$); 1198 cm^{-1} (Ar-O-C antisym stretch); 1017 cm^{-1} (Ar-O-sym stretch); 991 & 922 cm^{-1} (allyl δCH oop). **^{1}H NMR**: δ 1.24 [s, 36H, C(C$\underline{H}_3$)$_3$]; 3.72 [s, 8H, Ar-C$\underline{H}_2$-Ar]; 3.91 [d, *J* = 5.1 Hz, 8H, O-C$\underline{H}_2$-CH=]; 4.88-4.91, 4.96-4.97 [2 m, 8H, C=C$\underline{H}_2$]; 5.56-5.73 [m, 4H, -C$\underline{H}$=CH$_2$]; 6.95 [s, 8H, ArH]. **^{13}C NMR**: δ 32.28, 34.55 (C($\underline{C}$H$_3$)$_3$ and $\underline{C}$H(CH$_3$)$_3$); 39.47 (Ar-$\underline{C}$H$_2$-Ar); 72.09 (O-$\underline{C}$H$_2$-); 115.97 127.59, 134.11, 135.96, 144.49, 154.73 (aromatic and CH=CH$_2$)

2.7.3.3.1. 1,3-alternate-25,26,27,28-Tetra-alloxycalix[4]arene (4)
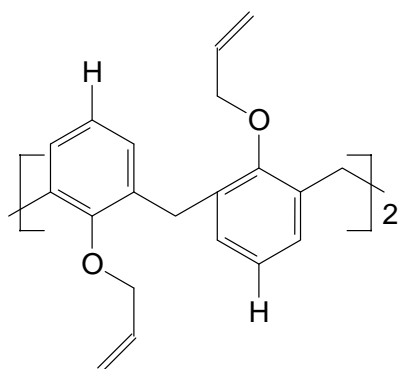
Calix[4]arene (b) (1.55 g, 3.67 mmol), was stirred with cesium carbonate (3.62 g, 18.8 mmol) in dry acetone (100 mL) under nitrogen for five hours. Allyl bromide (3 mL, 33.9 mmol) was then added to the reaction mixture, which was then heated to reflux for 72 hours under nitrogen. The solution was filtered and the solid was washed with dichloromethane (2 x 15 mL). The solvent was removed by reduced pressure distillation to yield an oily residue. Methanol (30 mL) was added to the oily residue to precipitate the crude calixarene derivative. The solid was recrystallised with chloroform/ethanol. Further purification was carried out via flash chromatography

(350:250:1:1 petroleum spirits:chloroform:glacial acetic acid:ethyl acetate). The product was again purified by recrystallisation, chloroform/methanol to yield the 1,3-alternate tetra-allylcalix[4]arene as a white powder (0.30 g, 0.52 mmol, 14 %) m.p. 177-178°C [Lit. 186.7-187.4°C, [156]]

IR: 2853 cm^{-1} (υ_s CH$_3$); 1647 cm^{-1} (allyl υC=C); 1601 & 1451 cm^{-1} (aromatic C=C); 1420 & 1319 cm^{-1} (allyl δCH in plane); 1361 cm^{-1} (δ_s CH$_3$); 1202 cm^{-1} (Ar-O-C antisym stretch); 1009 cm^{-1} (Ar-O-C sym stretch); 991 & 924 cm^{-1} (allyl δCH oop). **^{1}H NMR**: δ 3.6 [s, 8H, Ar-CH$_2$-Ar]; 4.15-4.19 [m, 8H, O-C$\underline{H}_2$-CH]; 5.12-5.13, 5.16-5.17, 5.21-5.21 [2m, 8H, -CH=C$\underline{H}_2$]; 5.83-5.99 [m, 4H, -C$\underline{H}$=CH$_2$]; 6.68 [t, J = 7.3 Hz, 4H, *para* Ar-H]; 6.99 [d, J = 7.3, 8H, *meta* Ar-H]. **^{13}C NMR**: δ 37.52 (Ar-CH$_2$-Ar); 72.24 (O-CH$_2$-); 116.58, 122.4, 131.67, 134.36, 134.67, 156.39 (aromatic and CH=CH$_2$).

2.7.3.4.   5,11,17,23,29,35-Hexa-*tert*-butyl-37,38,40,41-tetra-isopropoxycalix[6]arene (5)
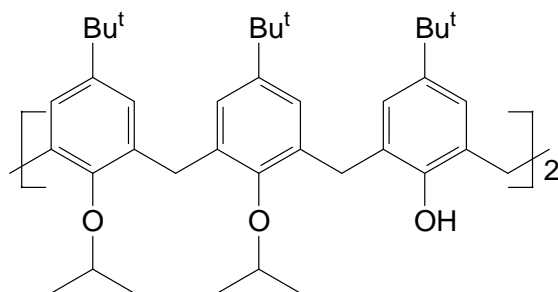
p-*tert*-Butylcalix[6]arene (1.0 g, 1.0 mmol) was added to clean sodium hydride (1.0 g, 41.7 mmol), imidazole (50 mg, 0.073 mmol) in DMF (50 mL) and stirred for 30 minutes under nitrogen. An excess of 2-bromopropane (20 mL, 0.212 mol) was then added dropwise to the reaction mixture under nitrogen with stirring. The reaction progress was monitored by TLC (19:1 petroleum spirits:ethyl acetate), whereby it was stopped after 28 hours. Excess 2-bromopropane was removed from the reaction mixture by reduced pressure distillation. The reaction mixture was poured into water to precipitate the calixarene. The precipitate was filtered and recrystallised from chloroform/methanol to yield the crude calixarene. The solid was further purified by flash chromatography (14:1 petroleum spirits:ethyl acetate) to yield the 1,2,4,5-tetra-isopropyl-p-*tert*-butylcalix[6]arene as a white powder (0.202 g,

0.17 mmol, 17 %) m.p. 226-227°C. Found: C, 80.8; H, 9.6 %. $C_{78}H_{108}O_6.H_2O$, requires: C, 80.0; H, 9.3 %.

^{1}H NMR: 1.07 [s, 36H, C(CH$_3$)$_3$], 1.17 [s, 18H, C(C$\underline{H}_3$)$_3$ unsubstituted], 1.71 [d, 24H, CH(C$\underline{H}_3$)$_2$], 3.87 [s, 12H, Ar-CH$_2$-AR], 4.29 (m, 4H, C$\underline{H}$(CH$_3$)$_2$), 6.952 (s, 8H, Ar-H), 7.10 (s, 4H, Ar-H unsubstituted)

FAB+ MS: m/z = 1140, Exact Mass $C_{78}H_{108}O_6$ = 1140.8

3. Crystallisation and Metal Complexes of Calixarenes

3.1. Introduction

The work put into synthesizing the large number of calixarene derivatives reported to date has been driven mainly by the wide variety of studies conducted on their inclusion phenomena [112]. The interaction between the calixarene host and a guest can occur through a variety of mechanisms including, hydrogen bonding, electrostatic and van der Waals attraction, and π-π and charge-transfer interactions [112]. The host/guest complex can be investigated using a wide variety of methods. In the case of metal complexation, extraction studies are often used. Although this does not produce a direct measure of the stability constant, such behaviour is directly relevant to a range of practical applications including ISEs. More fundamental thermodynamic studies are becoming more widespread, leading to a better understanding of calixarene metal complexation behaviour.

The structure of the host/guest complex can also be determined through a variety of techniques, with ^{1}H & ^{13}C NMR spectroscopy and X-ray crystallography being the most common. While single crystal X-ray structure determinations give a great deal of information about the host/guest complex in the solid-state, extrapolation to the solution phase must be done with great caution.

In most cases, the strength of binding by a host is not the only important factor. Applications also depend on the ability of the host to discriminate between different guests. Two such principals of host/guest binding, the *principle of preorganisation* and the *complementarity principle*, state that 'the smaller the changes in organisation of the host, guest and solvent required for complexation, the stronger the binding' [139], and 'to complex, hosts must have binding sites that cooperatively contact and attract the binding sites of guests without generating strong non bonded repulsion' [139] respectively. Experiments conducted on picrate salt extractions concluded that the complexing power of neutral organic receptors to cations proceeds via the following order, seen on the following page [157]:

Spherands > cryptaspherands > cryptands > hemispherands > coronands > crown ethers > podands

The above trend shows that the principle of preorganisation in the host is important when considering the design of receptors. The ability of calixarenes to selectively complex guests can be directly related to the two principles stated above. Additionally, for ion-selective electrodes, fast kinetics between the free and complexed states is also desirable, and the compound must not bind too strongly otherwise the sensor performs poorly. Calixarenes exhibit a semi-rigid cyclic array similar to that of spherands for calix-crowns and cryptands for calixarene-podands. These molecules exhibit minimal conformational change for binding, in addition to the vast range of binding functionalities available. However, calixarenes are more flexible than spherands which is typically a requirement for fast kinetics.

The cyclic array of calixarenes is beneficial in co-ordinating ions as their geometrical shape and attached functional groups can be arranged in a spherical fashion, which therefore reduces the energy required for complexation. The functional groups attached to the parent calixarene are already arranged peripherally about a central cavity, reducing the energy required for ion interactions. The size of the cavity and the binding properties of the atoms within the calixarene dictate the level of ion selectivity.

In addition to cation and anion binding, calixarenes also possess the ability to host a range of neutral organic molecules both internal and external to the cavity defined by the aromatic rings. While initial studies are often aimed to exploit this cavity as a mimitec for natural systems such as enzymes, such studies have not been widely successful.

3.2.   Inclusion of Neutral Organic Molecules

The first recognition of the inclusion of a neutral organic molecule in calixarenes in the solid state was reported in 1979 [158]. The X-ray crystal structure showed the

endo-cavity complex of p-*tert*-butylcalix[4]arene and toluene, with the methyl group directed into the aromatic cavity. Since then, a range of molecules including acetonitrile, methanol and methylene chloride have been shown to complex with the tetramer and its derivatives [112]. The strength of binding for neutral molecules is dictated by the kinds and number of simultaneous interactions, by the preorganisation of the host and solvation effects [159]. Furthermore, molecules can also act as hosts by packing together in such a way as to leave channels, cavities or layers in the crystal lattice whereby guests can be accommodated [160]. Amongst the vast range of known derivatives, calixarenes exhibit both *endo* and *exo* inclusions of neutral organic molecules, which have many potential benefits in a range of fields, such as molecular storage and separation, to drug transport [161-164]. Examples of *exo* and *endo* inclusion with calixarenes are shown in Figure 3.1.

Endo-cavity encapsulation of organic molecules have the potential for solution-phase applications, such as drug transport systems or nano-reactor vessels, whilst those with *exo*-cavity inclusion offer solid-state applications such as gas storage or purification systems [161, 163, 165, 166]. Research into supramolecular gas storage systems has been focused on metal-organic frameworks (MOFs), whereas organic crystals were believed to be of no use due to their typical close packing structures. While the study of MOFS continues to be of interest, organic lattices are now receiving attention as possible gas storage materials [167]. Over the past several years, p-*tert*-butylcalix[4]arene and calix[4]arene have been shown to entrap a range of small molecules, e.g. methane and its halogenated analogues, acetylene and hydrogen, within the crystal lattice [162, 163, 167-173]. The guest uptake and release of these two compounds and other similar derivatives is attributed to the weak van der Waals interactions between the molecular components [170].

(a)

(b)　　　　　　　　　　(c)

(d)
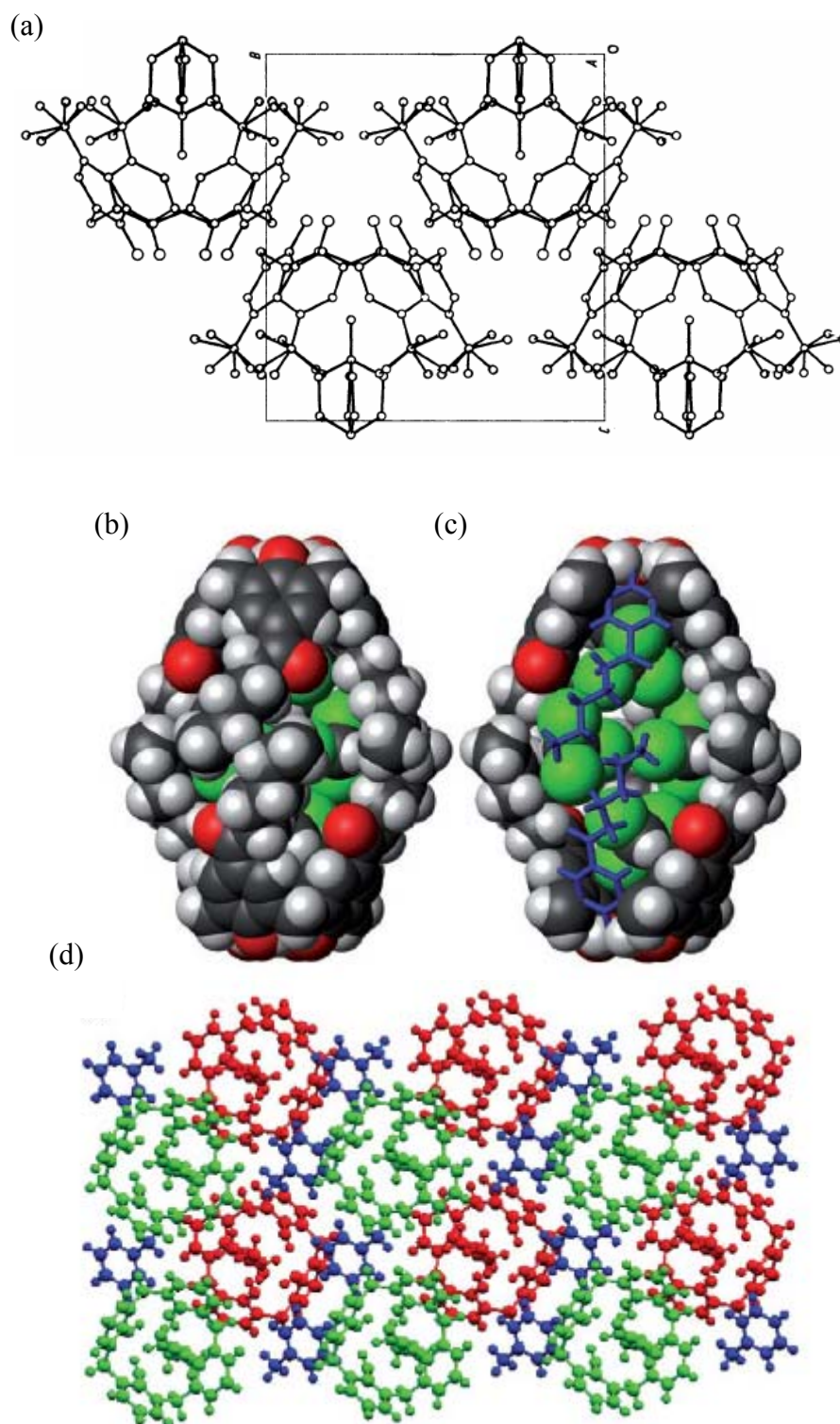
Figure 3.1: Crystal structures of various calixarenes, demonstrating guest inclusion within the aromatic cavity (a-c) and within the crystal lattice outside the cavity (red and green = calixarene layers, blue = toluene (d). Pictures taken from [158, 161, 164] respectively.

The most common forms of crystal packing for the p-*tert*-butylcalix[4]arene molecule with guests are *P*4/n for the 1:1 stoichiometry, where the guest resides partially within the cavity; and *P*4/nnc for the 2:1 interaction, where two calixarene molecules face each other to form a dimeric capsule which completely encloses the guest, see Figure 3.2 (a) and (b) respectively [173]. Upon desolvation, the crystal lattice can change to the space group *P*2$_1$/n which can occur through single-crystal-to-single-crystal phase transformations where the adjacent calixarene bilayers shift laterally by ca. 9 Å relative to one another [162, 172]. The resulting crystal lattice after full desolvation resembles that of the sublimed crystal, which is a slightly offset calixarene capsule or skewed capsule [162]. The various crystal structures of the p-*tert*-butylcalix[4]arene are shown in Figure 3.2.
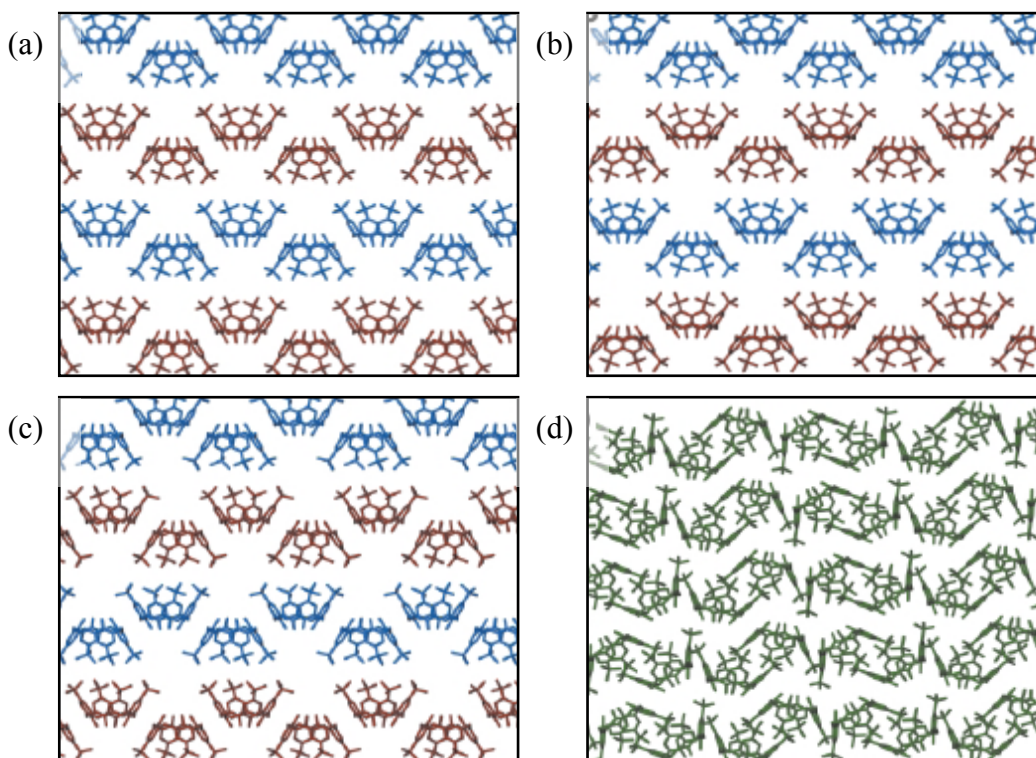
Figure 3.2: Different crystal packing of p-tert-butylcalix[4]arene: (a) with guest molecules (not shown) partially inserted in the calixarene cavity, host:guest ratio 1:1; (b) adjacent bilayers translated laterally relative to (a), after thermal loss of half the guest, such that facing calixarenes form dimeric capsules, host:guest ratio 2:1; (c) facing calixarenes are slightly offset and form skewed, unoccupied capsules obtained from sublimation; (d) A self-included dimer structure with no included guest. Pictures taken from [162]

In contrast to this, the crystal packing of the debutylated derivative occurs in the hexagonal space group $P6_3/m$ in both the solvated and desolvated forms [163]. The debutylated calix[4]arene molecule forms a cyclic trimer which packs together to form the hexagonal close-packed (hcp) arrangement, shown in Figure 3.3, which is only held together through relatively weak van der Waals interactions and not hydrogen bonding [163]. The 3-dimensional crystal lattice of the spherical trimers consists of two types of channels, the first (**a**) are not continuous and link solvent accessible voids of *ca.* 153 Å, and the second (**b**) that are continuous are constricted and this ensures that the bulk structure is non-porous [163]. Solvated forms of calix[4]arene with various halogenated small hydrocarbons, demonstrate that the guest resides within the lattice voids and is held there by weak van der Waals interactions with the host, see Figure 3.3 (b). The guests are highly disordered as a result of the loose fit and the presence of high crystallographic site symmetry [163]. One very important characteristic of this crystal packing with calix[4]arene is the guest molecules are retained within the lattice at elevated temperatures, even considerably past the guest's boiling point. For example carbon tetrachloride could be held within the crystal at temperatures up to 200°C [163]. The calix[4]arene molecule was shown to be a successful high temperature storage medium for a range of freons and methane. In a comparison to other compounds which have a hcp structure but do not hold guest at elevated temperatures, it was concluded that guests need to reside within type (**a**) channels if elevated temperatures are required. Only a handful of other compounds are known to possess similar crystal packing in both the solvated and desolvated form in addition to retaining the guest at elevated temperatures [165].

Zeolites are aluminosilicates compounds which have found widespread use in many industries based on guest inclusion principles, similar to the compounds above [174]. A significant amount of effort has been dedicated to the development of synthetic zeolites with tailored properties. Such materials are capable of selective guest inclusion and release without the collapse of the interconnected channels and cavities in the structure [174]. Most molecular crystal lattices are close-packed to maximize attractive intermolecular contacts and hence are not porous. The results discussed above suggest that derivatives of calixarenes may provide the necessary properties required to act as organic zeolites as a result of their unusual crystal lattice packing.
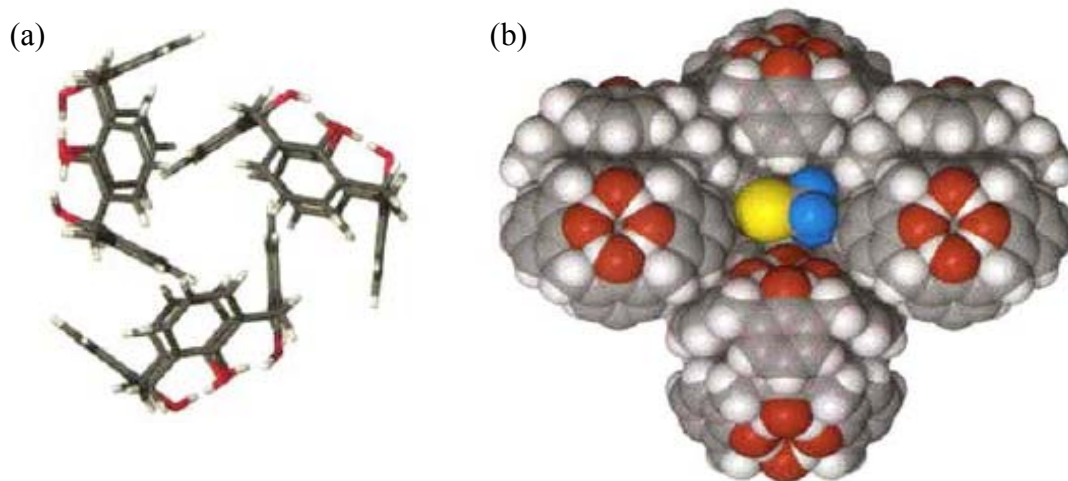
Figure 3.3: The sperical trimer of calix[4]arene (a) and the space-filling representation (b) of the interstitial void obtained with five units of the trimer (a). One (a) unit in the foreground has been removed to see the trapped guest of CF_3Br. Pictures from [163].

The host-guest chemistry experienced by calixarenes with neutral organic molecules maybe the cause of the competitive and uncontrolled membrane chemistry, which may prevent the detection limit of the ionophores tested in this work to be reduced below the values obtained in Chapter 4 Section 4.7.

3.3.   Selective Binding Sites of Calixarenes

3.3.1.   Metal Ion Complexes with Unsubstituted Calixarenes

Parent calixarenes offer very little in terms of significant binding sites for ion complexation. There are only two regions where ions can bind in the unsubstituted calixarene. Guest binding can occur at the aromatic cavity, both endo and exo, through π-interactions, and at the lower rim through the oxygens of the hydroxyl groups [112]. Interactions of metal binding to the oxygen at the lower rim have been proven through single crystal X-ray diffraction, and extraction studies [2, 112, 136, 175, 176].

Solution extraction studies demonstrated that the calixarene anion forms the complex with the metal ion, and this is only achieved through deprotonation of the phenolic hydrogens in a basic environment. Several metal complexes binding to the oxygen atoms of the unsubstituted parent calixarene have been synthesized and characterized [136, 176-178].

The second region available for binding in the unsubstituted calixarenes is the electron rich aromatic cavity, which provides binding sites for 'soft' cations like silver, cesium and thallium. The interaction between the cation and the π-electrons of an aromatic ring occur through several mechanisms, including the electrostatic attraction between the cation and the aromatic quadrupole moment, non-additive polarization effects, and dispersion interactions [179, 180].

The selectivity of the parent calixarenes is governed primarily by the size of the cavity and the conformation [2, 112]. As an example, NMR experiments on a tetramethoxy substituted p-*tert*-butylcalix[4]arene demonstrated that the sodium cation is exclusively complexed by the cone conformation whereas the 1,3-alternate or partial cone conformations preferentially complexes the cesium cation [2]. Theoretical calculations were used to demonstrate that the sodium bound in the cone conformation interacted with two oxygen atoms and two aromatic rings, whereas the cesium interacted with one oxygen atom and three aromatics [103]. However, the binding strength of cations with unsubstituted calixarenes is rather low, owing to the limited number and strength of binding atoms available [2]. With the addition of extra functional groups, the binding strength of calixarenes can be increased.

3.3.2. Metal Ion Complexes with Calixarenes Containing Oxygen Carrying Functionalities.

Some of the earliest calixarene derivatives synthesized were those containing ester, keto and acid functionalities. The addition of a greater number of potential binding atoms to the bottom of the original structure developed a second cavity for cation recognition and also enhanced the binding strength for the relevant ions. Following the Pearson concept of Hard-Soft-Acid-Base, where the hard acid (the electron

acceptor) is complexed by a hard base (the electron donor) and vice versa, the hard donor atom of oxygen, is suited to the small cations of high charge density like lithium, sodium and calcium [26]. The binding strength and selectivity is not only dictated by the size and conformation of the parent ring, but also on the additional groups attached to the complexing molecule [112]. Such instances include the stronger binding of a *tert*-butyl ester over an ethyl ester of the same structure and the increased selectivity for sodium over cesium when the *tert*-butyl group on the upper rim is present [112]. The selectivity with respect to the size of the macrocyclic ring was demonstrated with ester substituted tetramers, pentamers and hexamers all of which extracted alkali metal ions. The tetramer expressed sodium selectivity, and as the ring size increased, the selectivity shifted to the larger alkali metal cations [112].

Through the attachment of additional functional groups, the advantage of having a greater number of binding atoms soon became apparent, and it wasn't long before crown ethers were introduced as bridges across the calixarenes. As discussed previously, (see Section 3.1) the preorganisation of the binding site plays an important role in the complexing characteristics of the molecule and the attachment of crown ether linkages to the lower rim of the calixarene provides an excellent, well defined cavity for cation binding. Calixcrowns showed excellent selectivity for cesium [181], potassium [182] and sodium [183] by varying the size of the crown ether link attached to the lower rim of the molecule. A crown ether substituted calixarene was used to demonstrate that the conformation also plays an important role in the binding strength and selectivity. A 1,3-alternate calixcrown showed better binding strength for potassium than the cone and partial cone analogues, which is a result of the cation-π interaction exhibited in the 1,3-alternate conformer [184]. In the cone conformation, the potassium only binds to the available atoms of the crown ether and two phenolic oxygens demonstrating that the π-electron binding in the 1,3-alternate increases the stability of the complex [112]. This was also observed for a conformationally mobile calixcrown which preferentially adopted a 1,3-alternate state when complexing cesium. However, the locked conformations are more effective than the conformationally mobile molecules, as they are preorganised for binding [159, 185].

It is apparent that the size of the calixarene, conformation, additional groups and the cavity size of the attached functional groups all affect selectivity and binding strength. In addition to these factors, the nature of the binding atoms can be altered to manipulate the selectivity of the molecule. Sulfur, nitrogen and phosphorus atoms can be incorporated to change the binding characteristics.

3.3.3. Metal Ion Complexes with Calixarenes Containing Nitrogen, Sulfur and Phosphorus Functionalities

Since the binding ability of oxygen containing functional groups is usually associated with Group I and II cations, additional atoms need to be incorporated in the calixarene if other metal complexes are desired. Functional groups containing nitrogen such as amides, amines, azo, pyridyl and amino groups, to name a few, have been extensively studied for their ability to complex soft/heavy metals especially copper, silver, lead, mercury, cadmium and nickel [108, 112, 186]. However, tetramide derivatives also show good complexing ability to alkaline-earth ions which is attributed to the increased basicity of the carbonyl oxygen [2]. Other cations have been tested and found to complex with the various nitrogen containing groups, but are less commonly studied than the metals listed above.

Sulfur is another soft metal donor which can be incorporated into the calixarene molecule to form a range of soft/heavy metal sites. Often the sulfur atoms are incorporated in unison with a nitrogen atom to form thioamides, which further enhance the binding characteristics. The well known ionophore p-*tert*-butylcalix[4]arene-tetrakis(*N,N*-dimethylthioacetamide) contains both nitrogen and sulfur binding atoms and has shown to be a good receptor for lead and is commercially available [187]. The sulfur atom can also be incorporated as a sulfonyl group which has shown to bind well with mercury when presented as a sulfonyl carboxamide derivative [159]. Furthermore it has been demonstrated that by substituting the methylene bridges in the parent calixarene with epithio groups, the extractability of copper and silver increased significantly [108].

Phosphorus containing functional groups offer another type of binding site that can be added to calixarenes to change selectivity to a desired cation. Calix[n]arene phosphine oxide derivatives first reported in 1995 were initially tested as hosts for lanthanides and actinides and found analytical applications in the detection of europium [159]. Further investigations showed that the same compound exhibited high selectivity for calcium over magnesium and alkali metal ions in a plasticised PVC ISE [188]. By increasing the size of the calixarene from 4 to 6 aromatic units, the selectivity was changed from calcium being the most selective to lead [188]. The phosphine oxide calix[6]arene showed enhanced selectivity for lead over copper(II), cadmium and silver(I). This again demonstrates that the calixarene size is a very important influence on the metal binding properties of the molecule. By changing the attached atoms/groups to the phosphorus, the selectivity can again be tailored to different ions, for example by attaching (dialkoxyphosphoryl)alkyl groups on the lower rim results in selectivity for the alkali metal ions, noticeably lithium [189].

3.4. Coordinating Atoms Used for Thallium Complexes

As thallium expresses chemical properties of both Group I and heavy metals, binding can occur through a range of donor atoms [124]. Thallium is known to complex well with crown ethers, especially those that also bind well with potassium [96, 190]. However, good binding has also been observed with sulfur containing macrocycles, which typically bind heavy metals [94, 95]. The compounds that contain sulfur often contain oxygen as well, and single crystal X-ray studies have demonstrated that both the sulfur and oxygen can be coordinating atoms for thallium [89]. The crystalline complex of one of the thiaoxa macrocycles, as shown in Figure 3.4, demonstrates the thallium(I) atom binding to two oxygens and two sulfurs atoms which are close enough to lie within the sum of the van der Waals radii. Two other sulfur atoms in the macrocycle are reported to lie outside the bonding distance of the thallium atom and can therefore be considered only to interact weakly, if at all. The researchers also showed that the complex displayed a baseball-glove-like conformation which was the result of two aromatic units wrapping around the thallium(I) atom to offer π-electron binding sites [94]. This molecule shows that three very different binding moieties contribute to the complexation of thallium. The π-electron/thallium(I)

interaction is also observed in tetraalkylated calixarenes, where thallium was shown to complex in the aromatic cavity [88].
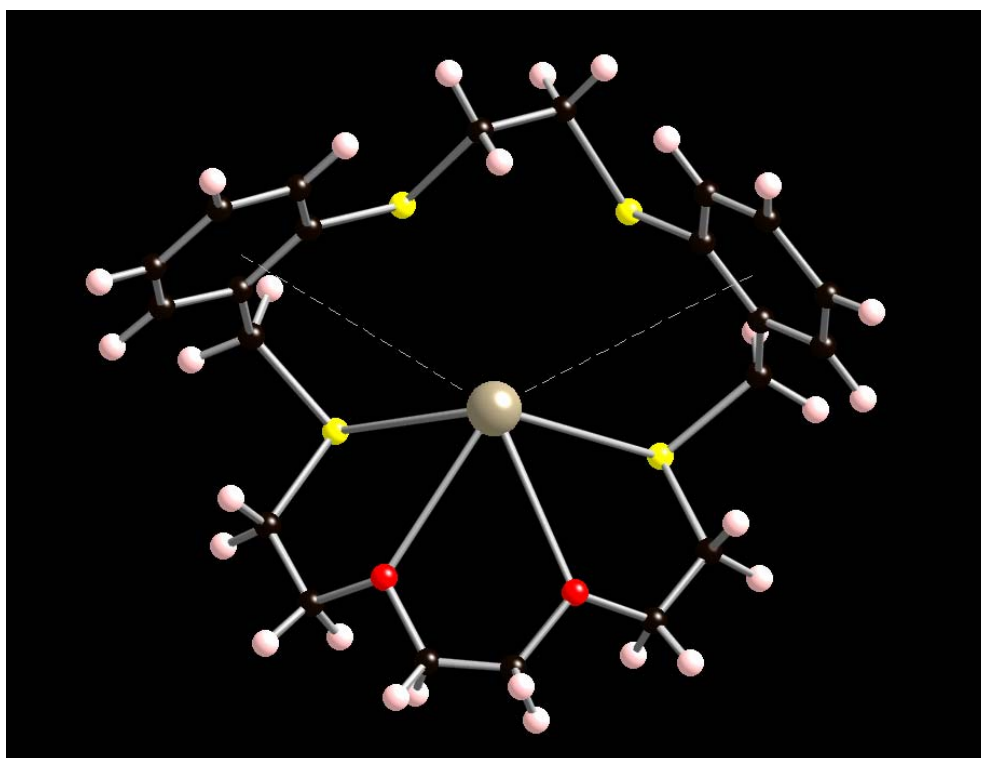
Figure 3.4: A crystal structure of a macrocycle/thallium(I) complex demonstrating the various coordinating atoms that can interact with thallium. [94]

A crystal structure of the thallium complex of a double calixarene, bridged at the lower rim showed that thallium(I) binds in the aromatic cavity of the two calixarenes, is shown in Figure 3.5 [124].

A disadvantage of the various binding characteristics of thallium(I) is that it makes it difficult to find molecules that are selective only to this ion. Compounds which contain oxygen atoms predictably have undesirable interferences from the alkali and alkaline earth metal ions, whereas those that contain sulfur, nitrogen and aromatic sites often exhibit interferences from heavy metals, especially silver. As a consequence, the selectivity towards thallium may not be improved by altering binding sites alone, and therefore a combination of size exclusion and binding sites may be the best method to achieve overall selectivity to thallium.
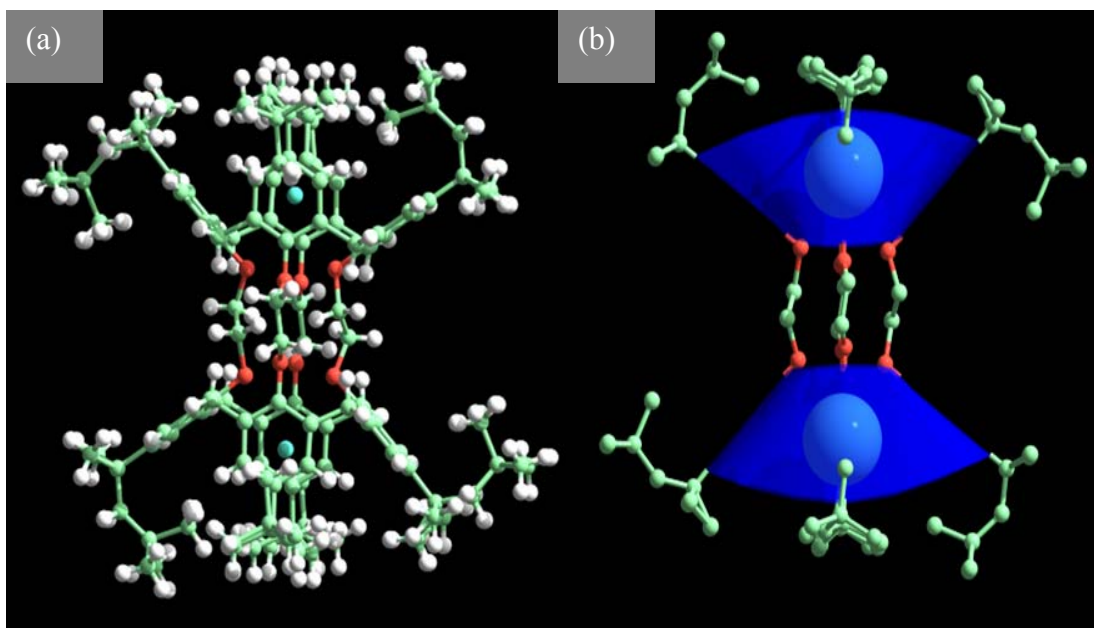
Figure 3.5: (a) A side on view of the calixarene/thallium complex, where two thallium ions are bound to the free π-electrons on either side of the molecule; (b) the calixarene aromatics are represented by ribbons showing thallium within the cavity. Carbon green; oxygen red; hydrogen white; thallium blue. [124]

The calixarenes synthesized, as described in Chapter 2, are expected to allow π-electrons of the aromatic units to interact with Tl^+ as reported for other calixarenes, and should enhance the selectivity by only allowing ions of a particular size to interact. Similar calixarenes reported by Kimura, K. et al. in association with the Curtin group, showed good thallium(I) selectivity over most ions; however, these calixarenes suffered from silver interferences [88]. The calixarenes reported in Chapter 2 were designed with the aim of enhancing the selectivity by reducing the size variation of allowed ions in the aromatic cavity by essentially pinching the aromatic units together, so two are parallel instead of being at an angle as found in the symmetrical cone confromation.

3.5.   Structures and Inclusion Phenomena of Calixarenes (1) to (4)

3.5.1.   Crystal Structures and Inclusion of Neutral Organic Molecules in Calixarenes (1) and (2)

Once the various calixarenes had been synthesized, diffraction quality crystals were grown from chloroform/methanol to firstly prove the structure and also determine their packing in the solid state. See Appendix V for details of the crystal and refinement data. The supramolecular arrays of calixarenes are interesting for a variety of reasons, such as gas adsorption, molecular separation and stabilization of reactive compounds [27, 174]. Calixarene (1) crystallizes from chloroform by the slow diffusion of methanol into the solvent and incorporates one $CHCl_3$ molecule per calixarene. The structure of the molecule is shown in Figure 3.6.
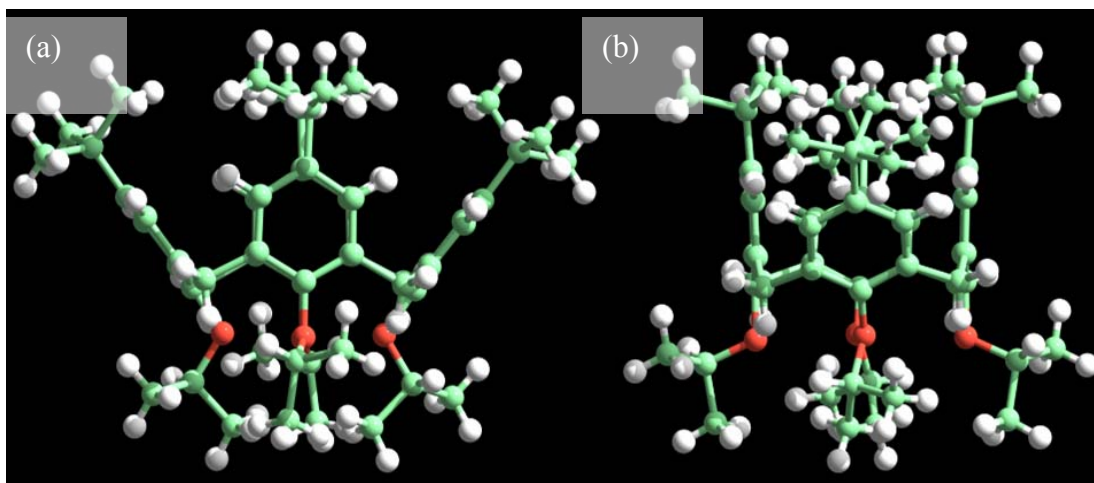
Figure 3.6: The molecular structure of calixarene (1). (a) view approximately perpendicular to the *quasi*-parallel aromatic rings. A 90° rotation (b) clearly showing the "pinched" cone conformation. The chloroform molecules were omitted for clarity.

The crystal structure of calixarene (1) shows the molecule in the cone conformer where two aromatic units are close to parallel with an interplanar angle of 3.22(7)° and the other two rings are at an angle 75.42(7)°. The "pinched" cone conformation is also observed in calixarene (2); see Figure 3.7. In this case, the upper rim C atoms of the pinched rings are closer together than the lower rim, with an interplanar angle

of -7.62(8)°. The increased distortion compared to calixarene (1) is presumably associated with the absence of the bulky *t*-butyl groups at the upper rim.
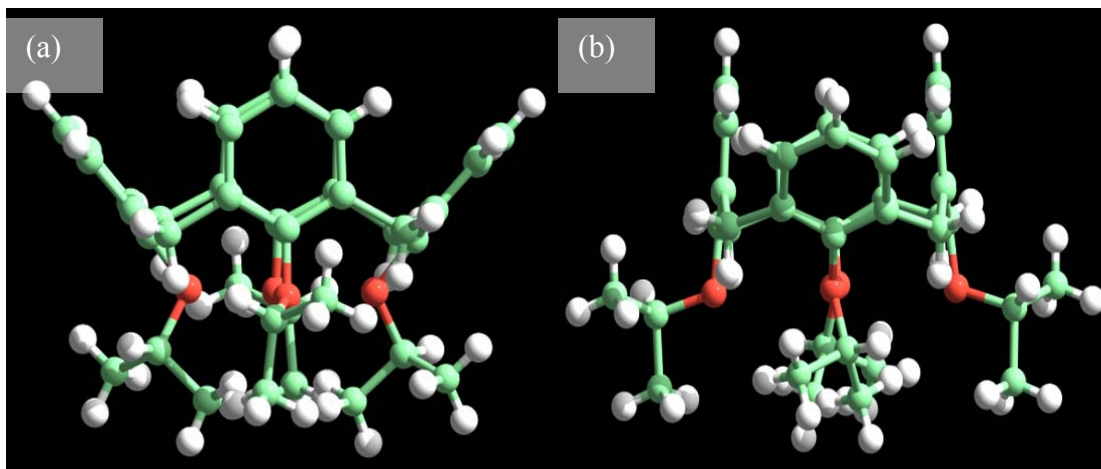
Figure 3.7: The molecular structure of calixarene (2). (a) view approximately perpendicular to the quasi-parallel aromatic rings. A 90° rotation (b) clearly showing the "pinched" cone conformation. The chloroform molecules were omitted for clarity.

The molecular solid-state structures confirmed that the isopropyl groups at the lower rim are sufficiently bulky to force the calixarene into a pinched cone conformation. Based on literature reports [88], the parallel disposition of the two "perpendicular" aromatic rings (see Figure 3.7 (b)) should help improve the selectivity observed when the ionophore is incorporated into ion-selective electrodes.

The crystal lattice of calixarene (1) with chloroform is shown in Figure 3.8 (note the chloroform molecule is disordered). It is interesting to note that the chloroform molecule is situated outside the aromatic cavity, but the structure still possesses a 1:1 stoichiometry. Inclusion compounds of the parent calixarene, p-*tert*-butylcalix[4]arene, usually only form 1:1 host:guest compounds when the guest is incorporated within the aromatic cavity and 2:1 compounds when guests are situated outside the cavity. Figure 3.8 (a) shows a view perpendicular to the *ab* plane with a single layer of molecules. The calixarene lower rims are all directed in the b direction. These layers are stacked in the c direction in an alternating "up-down" orientation, as shown in Figure 3.8 (b).
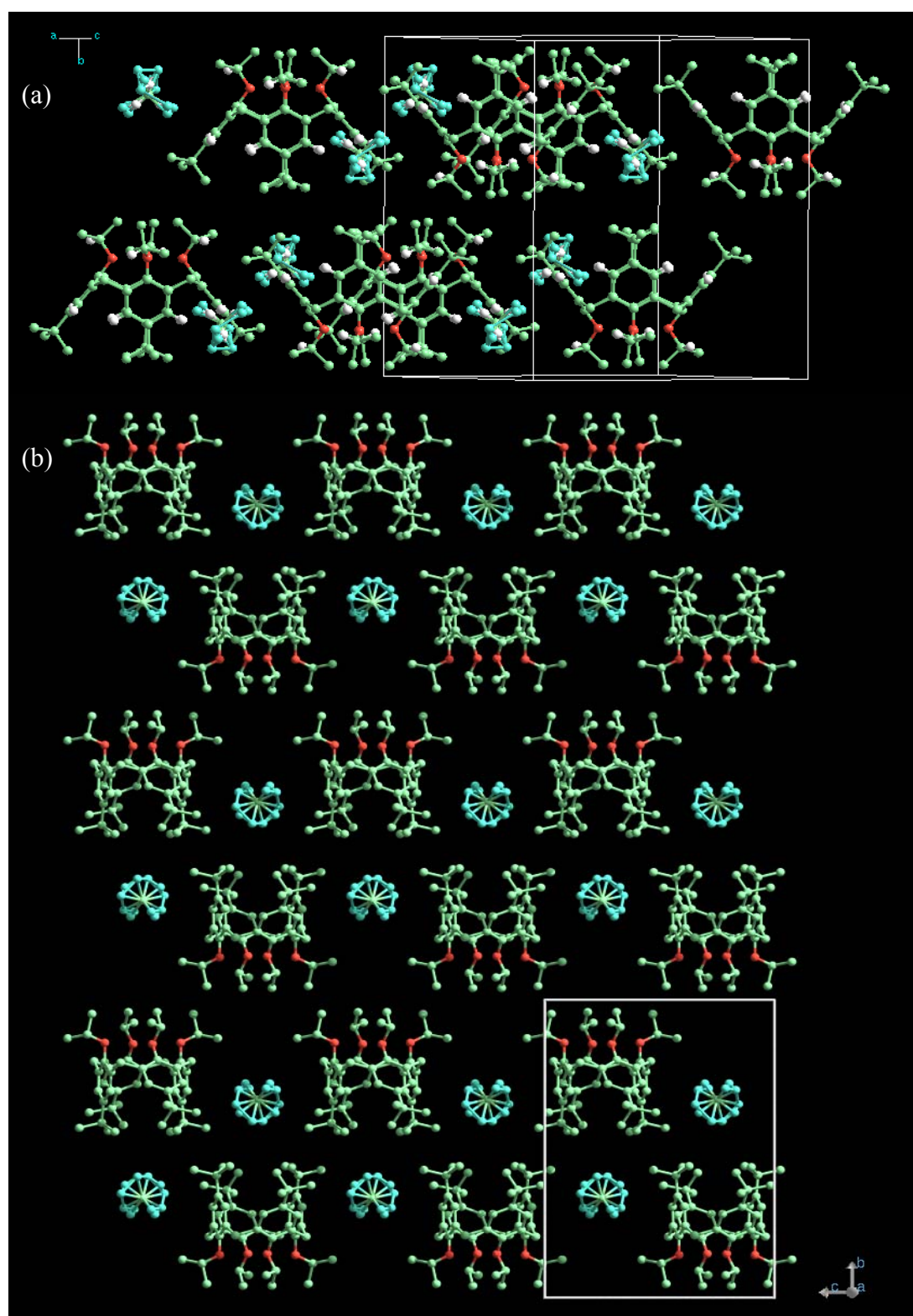
Figure 3.8: Crystal lattice packing of calixarene (1) with chloroform. Views are perpendicular to the *ab*-axis (a) and along the *a*-axis (b)

The crystal lattice of calixarene (2) is different to that of calixarene (1) when grown from the same solvent. The stoichiometry is different with a 1:2 chloroform:calixarene ratio and the structure has higher symmetry, (space group P_4/ncc). The key motif is shown in Figure 3.9 with lower rim to lower rim stacking of two calixarene molecules. The crystal structure is produced by columnar arrangement of these pairs, generated by a 2-fold screw axis in the c-direction (Figure 3.9 (b)).
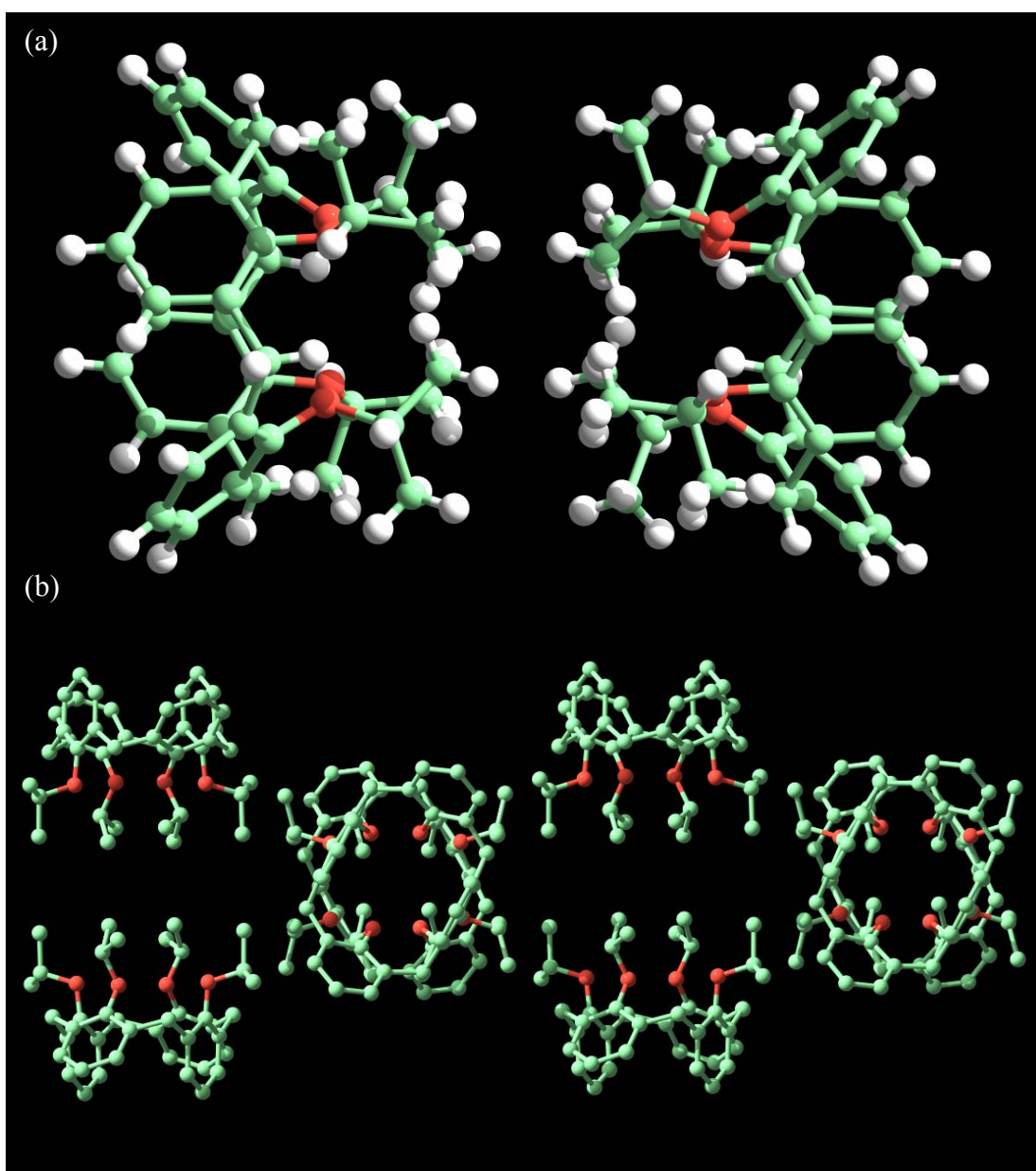
Figure 3.9: (a) The lower rim to lower rim stacking of calixarene 2, and the structure generated by 2-fold screw axis in the c-direction (b).

The resulting columns are interleaved, as shown in Figure 3.10, where each column has been designated by a single colour. The chloroform molecules reside in cavities with a volume of 133 Å^3 [191] between the stacked columns. A view along the *b*-axis shows the layered nature of the resulting structure (Figure 3.10 (b)), and the disposition of the solvent molecules relative to the layers.
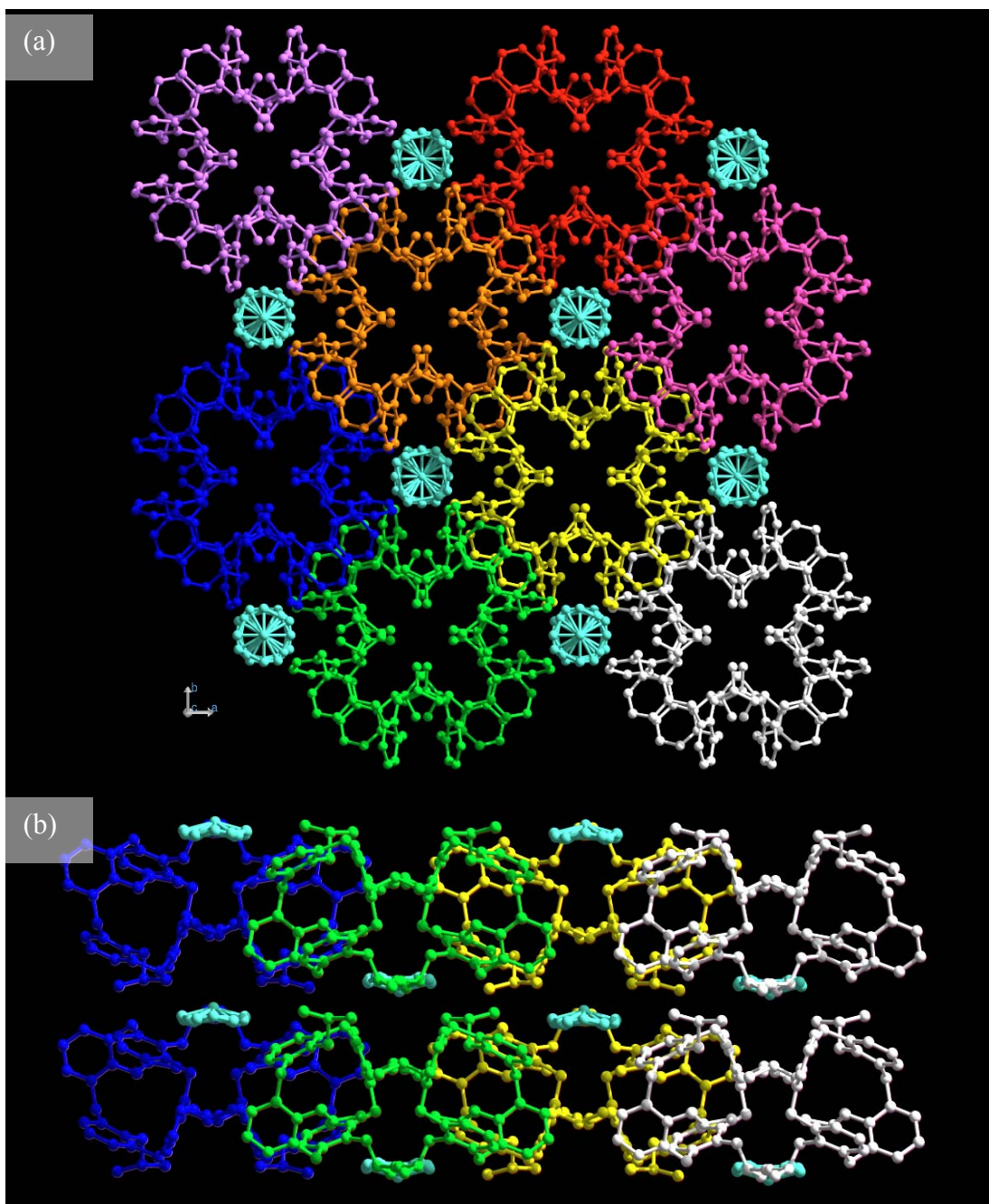
Figure 3.10: Crystal lattice packing of calixarene (2) with chloroform. (a) showing the interleaved columns along the c-axis, (b) side-on view looking along the b-axis, showing the layered nature of the structure.

When melting points were conducted on calixarene (2) it was discovered that the compound sublimed. Good quality crystals were then produced by sublimation at reduced pressure and submitted for structural determination. The crystal packing of the resulting solvent free structure is presented in Figure 3.11.
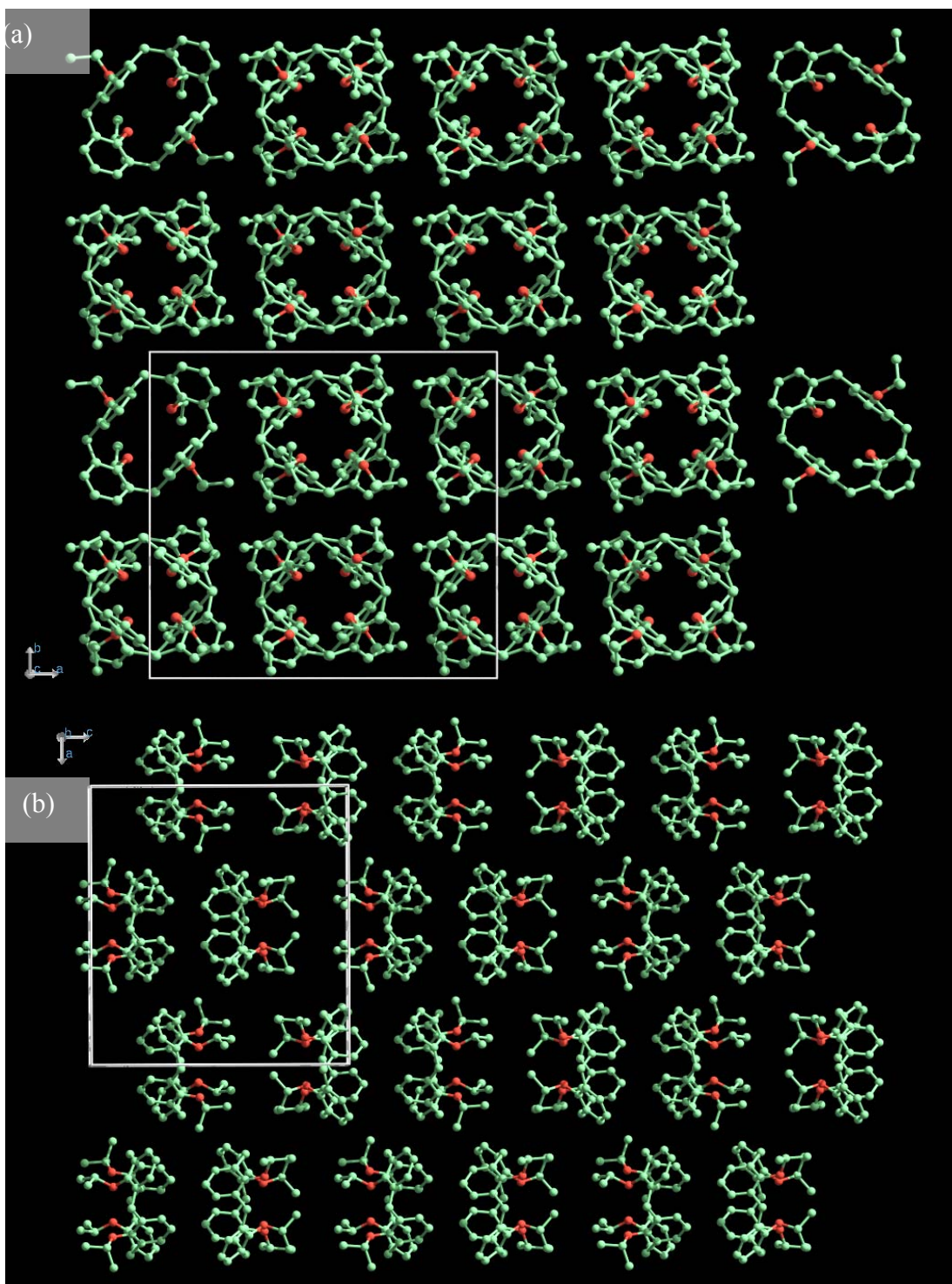
Figure 3.11: Crystal lattice packing of calixarene (2) without solvent. (a) looking along the c-axis, (b) looking along the b-axis, showing the offset layered structure.

The molecular conformation is similar to the solvated structure, although the pinching of the cone is even more extreme with the *quasi*-parallel aromatic rings having an interplanar angle of -19.43(14)°. In this case the calixarenes are packed in a columnar fashion, aligned along the axis of the calixarene cone. The orientation of the calixarene alternates up:down within the columns which are aligned with the *c*-axis (Figure 3.11 (a)). Figure 3.11 (b) displays the view down the *b*-axis, showing that the calixarene columns stack with an offset layered structure. A similar structure has been reported for the n-butyl substituted calix[4]arene [192].

Diffraction quality crystals of calixarene (1) could not be produced by sublimation, however, crystals grown from acetone showed no incorporation of the solvent within the lattice, which is displayed in Figure 3.12.
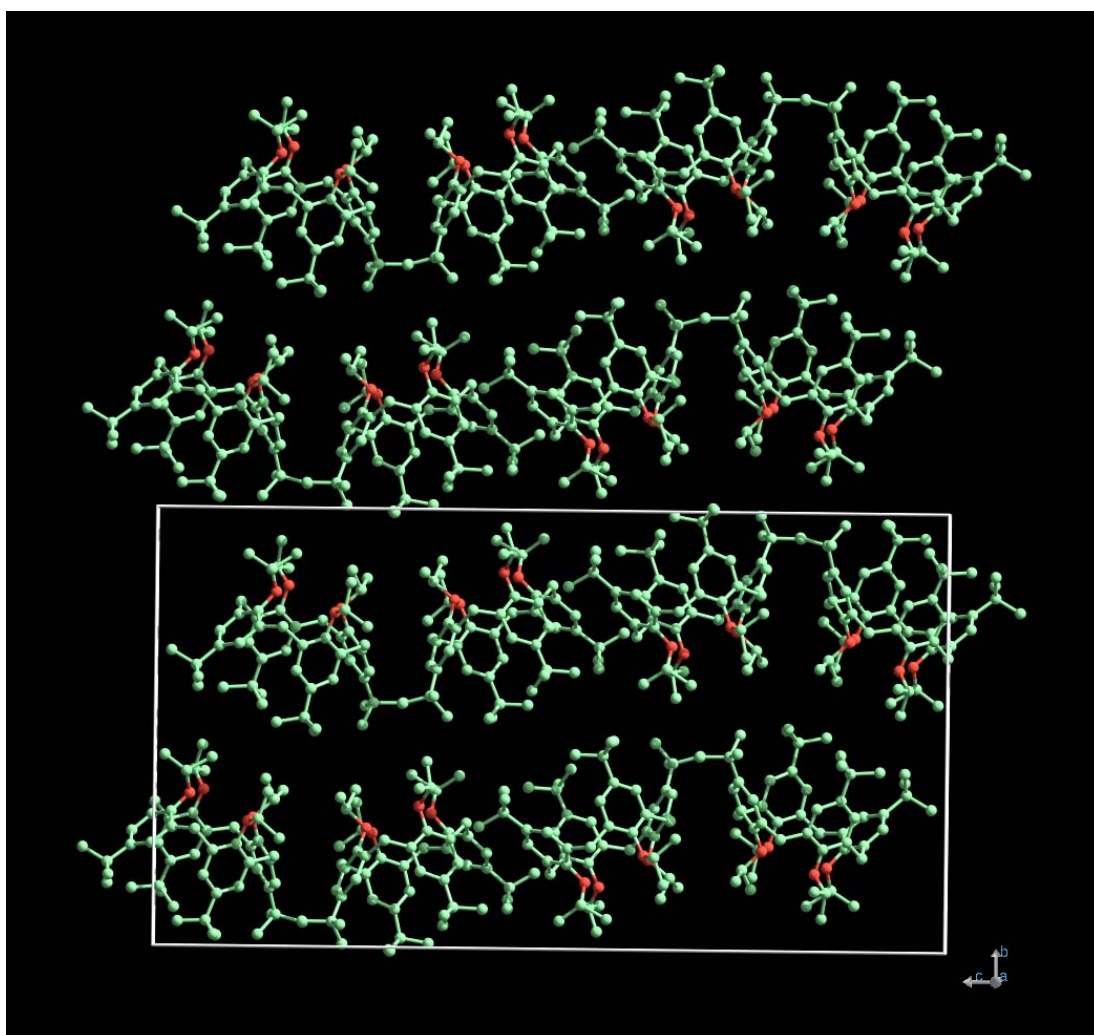
Figure 3.12: Crystal lattice packing of calixarene (1) without solvent.

As was the case with calixarene (2), the crystal packing of calixarene (1) without solvent is different to the solvated form. The structure is once again layered, this time in an undulating manner, along the *c*-axis. The calixarene molecules are paired along the layers with two up, two down. The asymmetric unit comprises of two inequivalent molecules, which are similar in terms of the molecular conformation and again adopt a pinched cone conformation, with the aligned aromatic rings at angles of 8.3(6) and 7.6(6)°.

These structural analyses show that calixarenes (1) and (2) retain the pinched cone structure regardless of the crystal packing, and the inclusion of solvent. There are subtle changes in the different structures, for example in terms of the angles between the aromatic rings, showing that the receptors have some flexibility, particularly in the debutylated calixarene (2).

3.5.2. Storage of Chloroform in Calixarenes (1) and (2)

When further analysis was carried out on the solvated crystals of calixarene (2), a very interesting property was discovered. The crystal lattice was able to retard the release of chloroform at elevated temperatures. The crystal was able to retain the chloroform molecule within the lattice up to temperatures of 125 °C, well above the liquid's boiling point of 61°C. The thermo-gravimetric trace is presented in Figure 3.13.

The onset of the chloroform release (T_{on}) occurs at 125 °C and produces a loss of 8.86 %, which is consistent with the molecular formula $C_{40.5}H_{48.5}Cl_{1.5}O_4$ obtained from the single crystal XRD and confirms the 2:1 calixarene:chloroform stoichiometry. The parameter (T_{on}-T_b) has been used as a measure of thermal stability of the host-guest system, where T_b is the normal boiling point of the guest [163]. The (T_{on}-T_b) of the calixarene (2)/chloroform system is 64 °C, which is much higher than the chloroform solvate of calixarene (1), which releases chloroform as soon as the crystals are removed from the solvent. The thermal stability of the calixarene (2) solvate is not as high as that of calix[4]arene with various volatile freons and halogenated compounds [163]. Calixarene (2), however, includes the

solvent in channels in the structure, whereas the more stable calix[4]arene system incorporates the guest in isolated voids [163].
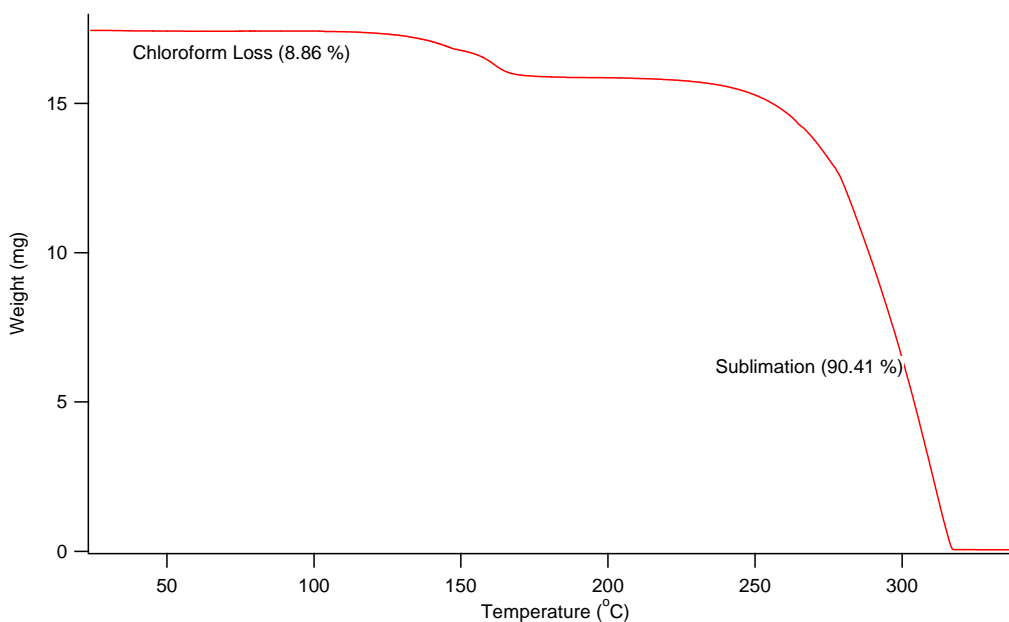
Figure 3.13: TGA-DTA trace of the solvated form of calixarene (2) showing the loss of chloroform at elevated temperatures.

Thermally desolvated crystals of calixarene (2) were exposed to chloroform vapours and then analysed by TGA, which again showed the same loss associated with the release of chloroform. This demonstrates that the solvation/desolvation process is reversible and suggests that the compound could be used as a storage medium for volatile solvent molecules. The chloroform molecules presumably diffuse through the channels in the structure, although a space filling representation suggests that the channels are quite restricted between the chloroform containing voids (see Figure 3.14). In a recent article, it was proposed that channels are not required for a guest to diffuse through the lattice, with thermal motion within the crystal sufficient to make windows of opportunity for molecules to enter the appropriate sites [174]. Hence, it is not unreasonable to suggest that the chloroform molecules are able to diffuse along the restricted channels in the structure reported here.
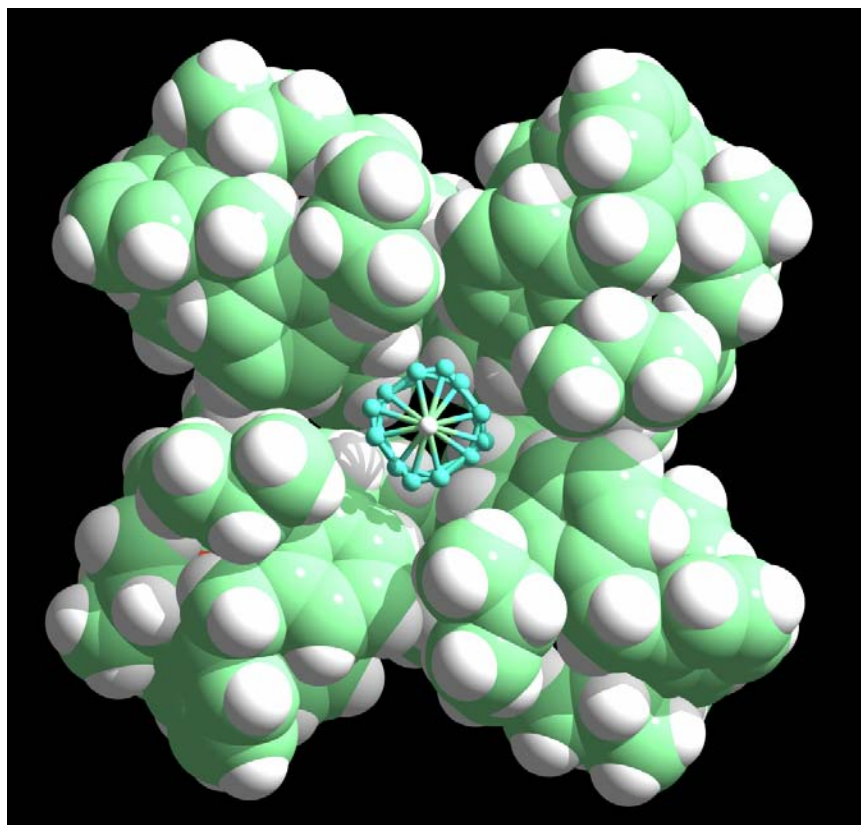
Figure 3.14: Space filling representation of the crystal structure of calixarene (2) showing the restricted channels between the voids containing chloroform.

When sublimed crystals of calixarene (2) (solvent free) were subjected to the same chloroform vapour system, the crystals absorbed chloroform to the extent that the dissolution of the crystals occurred. This suggests that the thermally desolvated and sublimed crystals of calixarene (2) have different structures. It seems likely that the thermally desolvated crystals retain their original structure allowing chloroform to be readily readsorbed. Unfortunately, the crystal quality was degraded by the desolvation process, such that analysis by single crystal XRD was not possible.

3.5.3. Crystal Structure of Calixarene (4)

Crystals of calixarene (4) were grown by Lobler [156]. The molecular structure of calixarene (4) is presented in Figure 3.15. The crystal structure confirms the 1,3-alternate conformation and shows that the aromatic rings are essentially parallel to each other (the relevant interplanar angles range between 4 – 9 °) suggesting a limited size range of ions would be able to access the π-basic cavity.
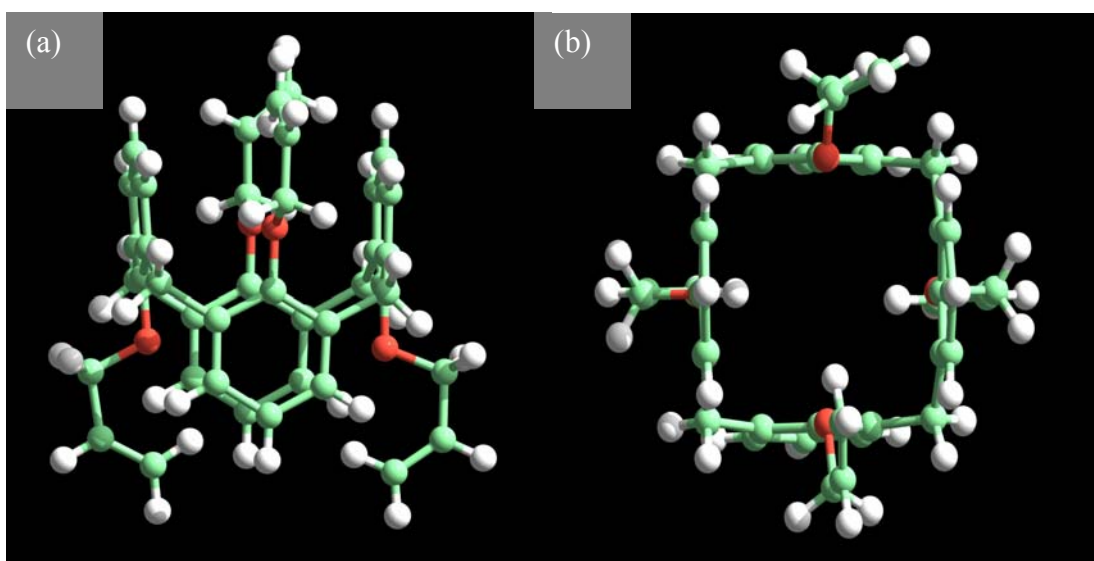
Figure 3.15: Molecular structure of calixarene (4). (a) side-on view showing the 1,3-alternate conformation (b) looking through the cavity demonstrating the parallel nature of the aromatic rings.

3.6. Metal Complexation Studies of the Synthesised Calixarenes

Even though two of the synthesized calixarenes exhibited some very unique and interesting properties with neutral organic molecules, the primary goal of the research was to incorporate these molecules as ionophores in ion-selective electrodes. In anticipation of this outcome, it was decided to explore the metal binding characteristics of the synthesized calixarenes prior to application in ISEs. Techniques such as NMR, solvent extraction and crystallography can be used to determine various binding characteristics.

3.6.1. Metal Binding Properties of Calixarenes (1) and (2)

NMR is a useful technique to evaluate the interaction of organic molecules with potential guest species. Calixarenes (1) and (2) were dissolved in deuterated chloroform then mixed with thallium picrate. Initial tests on calixarene (1) showed various ^{1}H peak shifts upon addition of the thallium picrate to the solution. All peaks showed a downfield shift which is indicative of cation binding resulting from

electrons being drawn towards the metal binding site. Since it is assumed that the cation will exert the same shielding/deshielding effect on all atoms in the molecule, one is able to suggest possible binding sites, as the cation will have more of an affect around the point of binding than in other areas of the molecule. Large chemical shifts are observed for hydrogens which are closest to the binding site while peaks with small shifts are relatively unaffected by the presence of the cation. The addition of thallium picrate to calixarene (1) resulted in not only the evolution of new shifted peaks, but splitting of certain peaks within the spectra (see Figure 3.16). The thallium(I) cation appears to have an effect on the symmetry of the compound as the conformation changes to accommodate the guest. The single aromatic peak at 6.81 ppm separates to what looks like a doublet for the complexed molecule. It is more likely that the doublet is in fact two singlets which have eventuated from the "pinching" of the aromatic ring in the complex. The calixarene structure in the absence of a guest is highly mobile on the NMR time scale and the associated singular peaks observed for the aromatic pinching is an average of the exchange between two pinched states. This can be pictured as a "breathing" effect where at one stage two aromatic rings are parallel to each other and the other two are reclined, and at another point in time the opposite is observed. When a guest is incorporated into the centre of the aromatic cavity, the "breathing" effect is slowed relative to the NMR time scale and the initial averaged signal is now observed as two peaks for the pinched and angled aromatics. The splitting of the peaks for the guest-free calixarenes could possibly be observed with lower temperature NMR. The peak splitting was also observed in the NMR complexation study conducted on the bridged calixarene presented in Figure 3.5, whereby the C_{2v} symmetry of the parent ligand is lowered slightly [124].

Other peaks which have split are the equatorial methylene hydrogens from a doublet to two doublets, which overlap to what looks like a triplet. The remaining peaks look to be relatively unaffected with regards to splitting upon complexation, which may be attributed to the flexibility and mobility of the isopropyl groups.
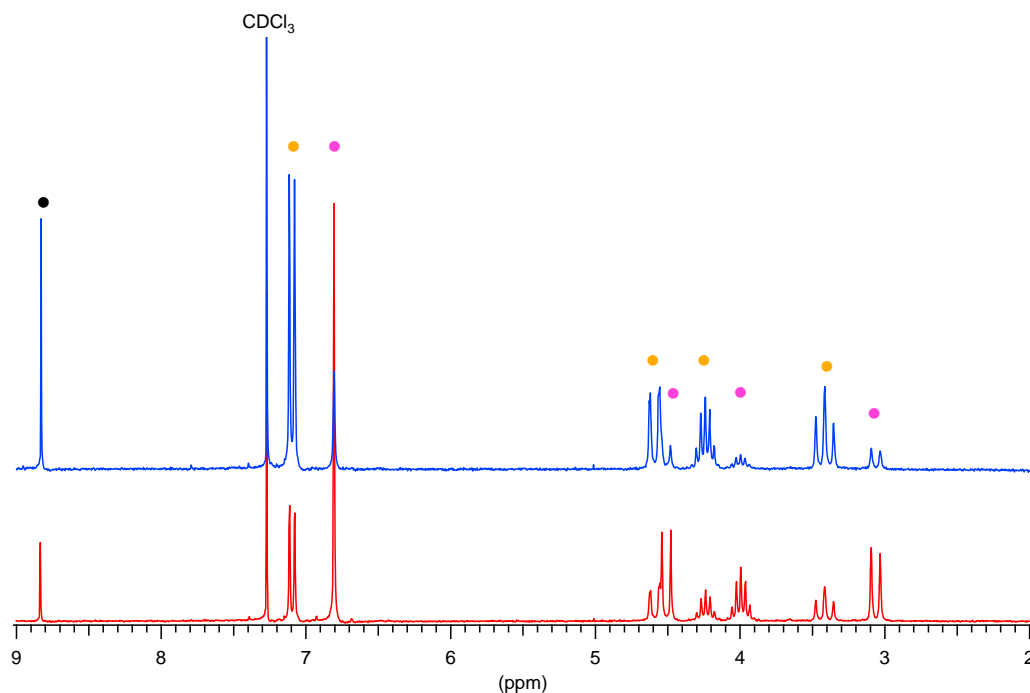
Figure 3.16: ^{1}H NMR spectra of Calixarene (1) with different amounts of thallium picrate salt added to the original calixarene in CDCl$_3$. Bottom only partial complexation, top almost full complexation. • Free ligand peaks • Complex peaks • Picrate peak

The magnitude of the changes of chemical induced shifts is shown in Figure 3.17. The largest chemical shift is observed for the methylene equatorial hydrogen with a chemical shift of 0.36 ppm. The next largest shift occurs with the aromatic hydrogens which suggests that the thallium(I) ion is binding at the phenolic end of the aromatic cavity close to both the methylene and aromatic hydrogens. The lack of chemical shift for any of the methyl groups supports this hypothesis. The NMR study conducted on the bridged calixarene by Matthews S., et. al. showed that the thallium(I) ion binds within the aromatic cavity and not in the oxygen rich calixarene bridge, which was shown to be the site for potassium binding [124].

The formation of new peaks, as opposed to a gradual peak shift for the complexed calixarene, indicates that the rate of exchange between the free and complexed states is relatively slow on the NMR timescale. The two spectra presented in Figure 3.16 were obtained by shaking solid thallium picrate with the calixarene/CDCl$_3$ solution for twelve hours (bottom) and upon the further addition of more thallium picrate

(top). The disappearance of the free ligand peak in the top spectra suggests that a relatively strong complex is formed.
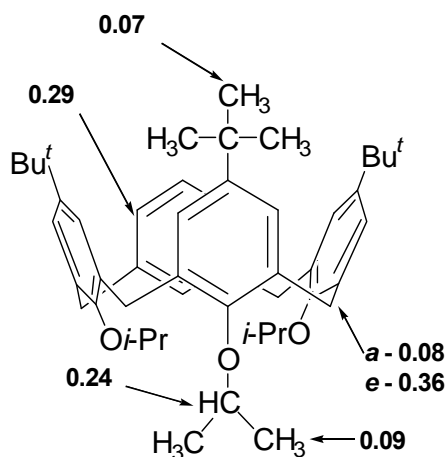
Figure 3.17: Changes in chemical shift ($\Delta\delta$) of compound (1) with thallium(I) picrate. Solvent $CDCl_3/CD_3OD$

Since it is well known that silver interferes with similar derivatives to calixarene (1), it was decided to test the complexing properties of this compound with silver picrate. The NMR spectra of the silver/calixarene (1) complex is displayed in Figure 3.18. The ^{1}H NMR spectra of the Ag/calixarene (1) complex is substantially different to that of the thallium(I) complex. First there appears to be no peak splitting, with the aromatic hydrogen peak remaining as a singlet and the equatorial peak as a doublet. This suggests that silver exerts less of an effect on the aromatic rings, which allow the calixarene molecule to retain its flexibility on the NMR time scale and therefore only express averaged peaks. Silver is a smaller ion than thallium (115 pm as opposed to 153 pm) which may prevent it from binding to the aromatic rings with the strength that thallium does [193]. The silver ion may also complex lower in the cavity as it is smaller. In cyclophanes, silver is known not to complex in the centre of the benzene rings, but on edge of the π-basic cavity, suggesting interaction with only certain C=C bonds [184]. The magnitude of the peak shifts are also different to the thallium complex, which may suggest a weaker interaction with the relevant binding atoms. Both the peaks associated with the aromatic and equatorial methylene hydrogens are shifted less in the silver complex than the thallium complex, whilst that of the single iso-propyl hydrogen, is shifted slightly more, further suggesting the lower position of the silver ion in the aromatic cavity. The size of the picrate peak indicates the extent of extraction, and gives some indication of the binding strength

of the calixarene with thallium as opposed to silver. When an excess of silver picrate is exposed to the calixarene solution, only a minute fraction is incorporated, leaving a large percentage of residual free ligand.
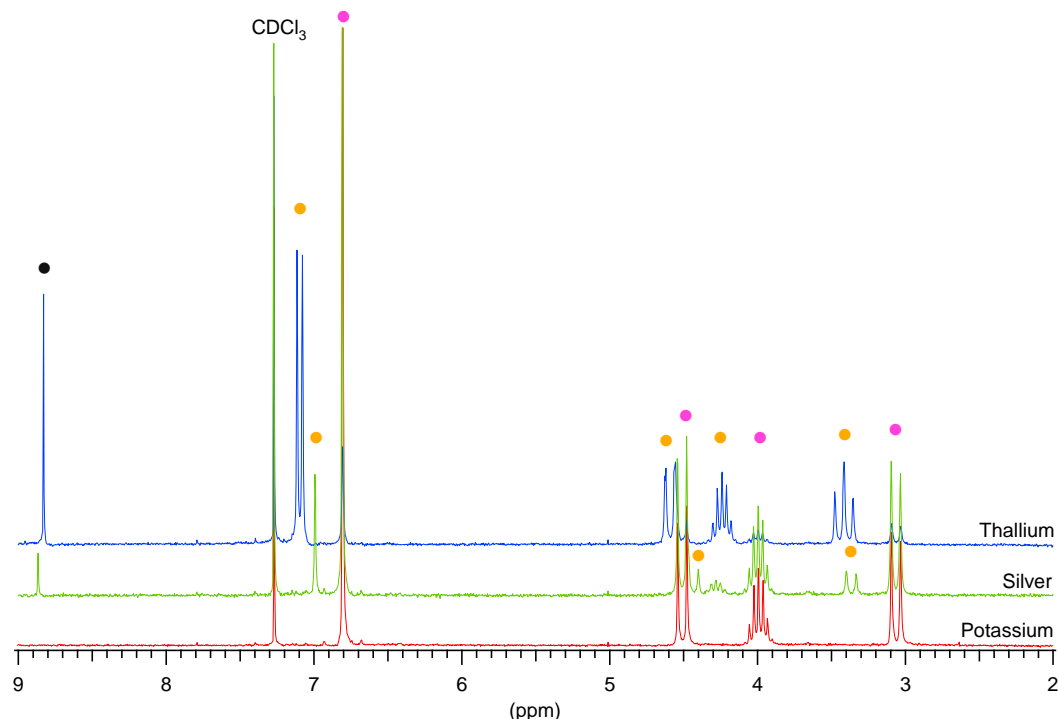
Figure 3.18: ^{1}H NMR patterns of calixarene (1) in CDCl$_3$ with added solid thallium, silver and potassium picrate. ● Free ligand peaks ● Complex peaks ● Picrate peak

Complexation of calixarene (1) was also tested with potassium, which is known to have some similar chemical properties to thallium. In this case, no picrate salt was extracted into the calixarene (1) solution, indicating that the potassium-calixarene interaction is not strong enough to overcome the lattice energy of the potassium picrate salt.

NMR complexation studies were also carried out on calixarene (2) to determine the effect of the *tert*-butyl group on the upper rim of calixarene (1). As was the case with calixarene (1), the addition of thallium(I) picrate to calixarene (2) resulted in the downfield shift of peaks. Both the free ligand and complex peaks of calixarene (2) are presented in Figure 3.19.
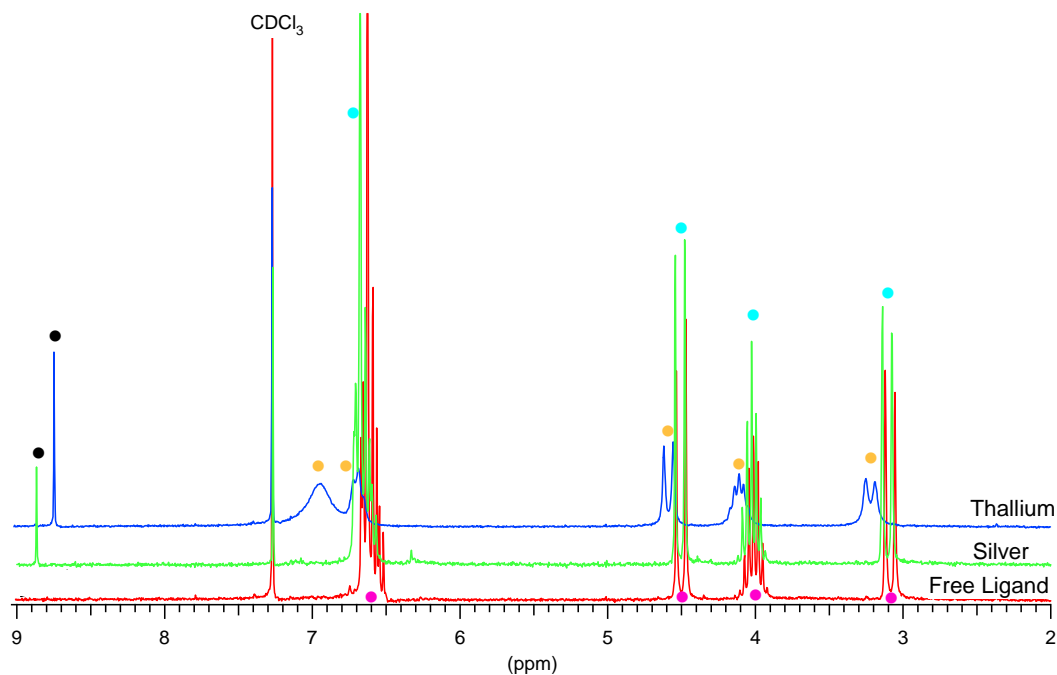
Figure 3.19: ^{1}H NMR spectra of calixarene (2) in CDCl$_3$ with solid thallium and silver picrate. • Free ligand peaks, • Thallium complex peaks, • Silver complex peaks, • Picrate peaks.

As was the case for calixarene (1), calixarene (2) only shows a slight difference between the free and complexed peaks when silver picrate is added to the solution. Significant peak shifts are only observed for the aromatic and equatorial methylene hydrogens suggesting a relatively weak complex with silver which binds within the aromatic cavity. The lower intensity of the picrate peak compared to the other peaks also suggests that the extraction of silver is poor with calixarene (2).

When thallium(I) picrate is added to calixarene (2), the peaks shift with the amount of thallium being added suggesting a fast rate of exchange between the free ligand and complex relative to the NMR timescale. Peak broadening was observed; however, this signalled that thallium complexation is having an impact on the conformational flexibility of the molecule. Thus, an NMR titration can be carried out to determine stability constants and the binding site. The NMR titration of calixarene (2) with incremental additions of thallium(I) picrate is displayed in Figure 3.20.
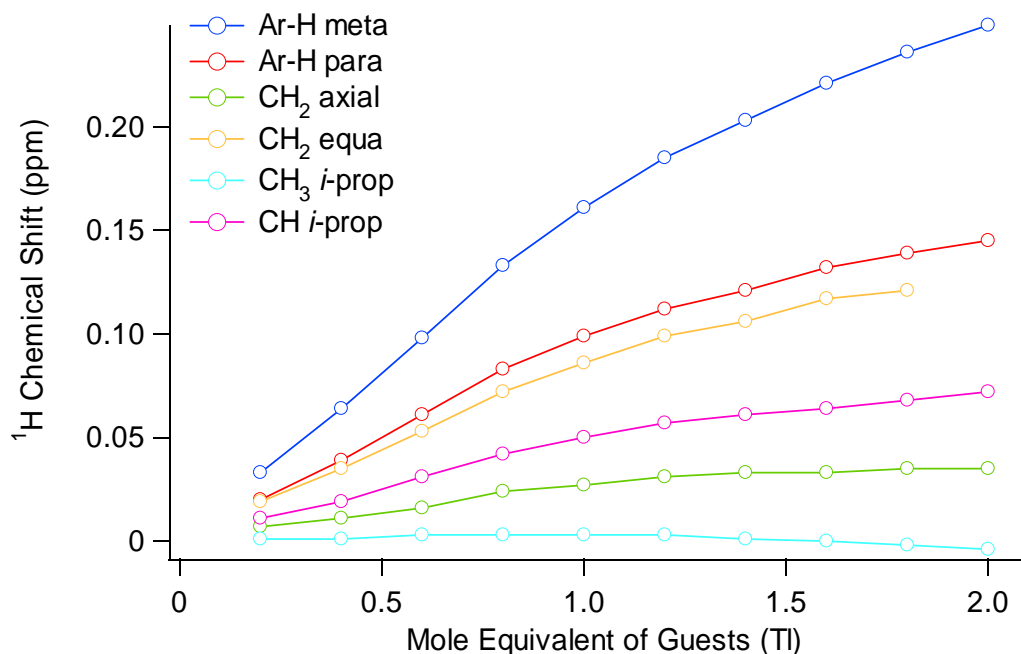
Figure 3.20: ^{1}H NMR titration of calixarene (2) with 0.2 molar equivalent additions of thallium(I) picrate. Ar = Aromatic, axial and equi = the axial and equatorial methylene hydrogens respectively, *i*-prop = isopropyl. Solvent CDCl$_3$/CD$_3$OD

The largest shifts were again observed for the aromatic hydrogens further supporting the cavity mode of binding. The gradual increase and the fact that the chemical shift never reaches its limiting value $\Delta\delta_{max}$, is suggestive of a small association constant [194]. Unfortunately, precipitation was observed towards the end of the titration which prevents an accurate determination of the stability constant with NMR spectroscopy.

3.6.2. Metal Binding Properties of Calixarene (3) and (4)

The studies of receptors 1 and 2, in the cone conformation showed that thallium complexation reduced the conformational flexibility of the calixarenes. A comparison with receptors in the 1,3-alternate conformation was of interest since these systems are conformationally less mobile and should be more preorganised for metal cation binding. Calixarene (3) was previously tested by Lobler, with a range of metal picrates and large chemical shifts were observed for the methylene and aromatic hydrogens [156].

An advantage of the 1,3-alternate calixarenes is that they are soluble in acetone which allows a single solvent to be used in the complexation studies. Since calixarene (3) had previously been tested with metal picrates in a mixed solvent system, it was decided to only test calixarene (4) with the single solvent. A similar result to calixarene (2) was observed with a gradual downfield peak movement as incremental amounts of thallium(I) triflate were added. The gradual downfield shift again demonstrates the fast exchange kinetics on the NMR time scale. The NMR titration of calixarene (4) with thallium(I) triflate is shown in Figure 3.21.
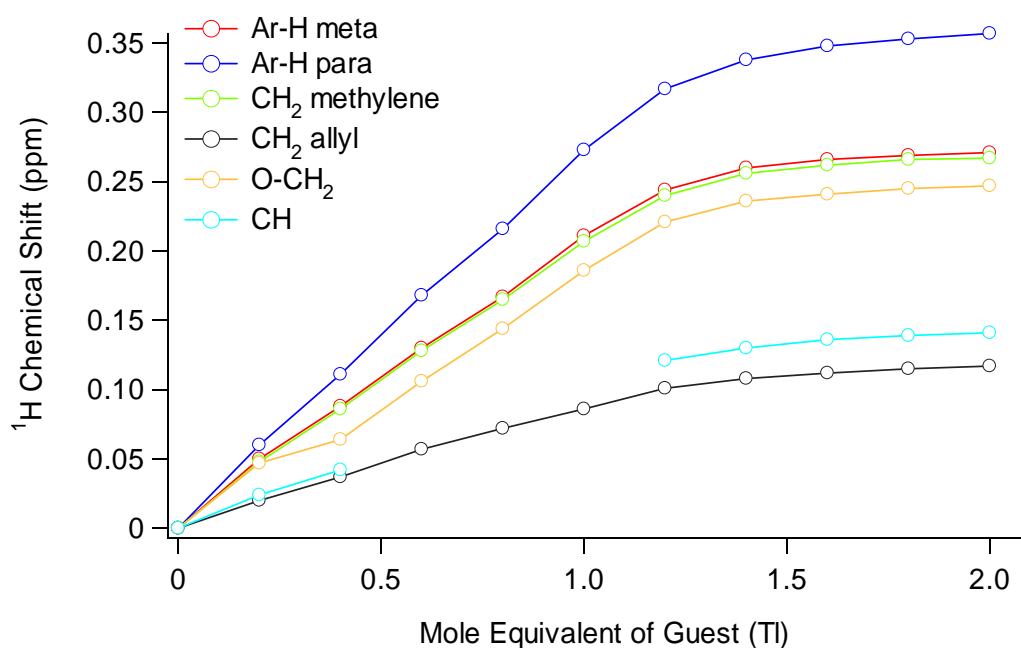
Figure 3.21: 1H NMR titration of calixarene (4) with 0.2 molar equivalent additions of thallium(I) triflate. Ar = aromatic, CH_2 methylene = the aromatic bridging units, CH2 ally = the end group on the allyl, CH = the hydrogen on the middle carbon of the allyl and O-CH2 = the start of the allyl chain. Solvent CD_3COCD_3

The largest shifts with the 1,3-alternate calixarene are again associated with the aromatic hydrogens, further supporting the aromatic cavity mode of binding. The flattening of the curve at higher concentrations of guest, suggests a relatively stable complex with $\Delta\delta_{max}$ almost being reached [194]. Another indication of a relatively stable complex is the formation of crystals soon after the addition of 1 equivalent of thallium, which is most likely to be the complex since it crystallizes from a single solvent system where both host and guest are soluble.

A NMR titration was also carried out with potassium triflate to assess the potential for competitive binding of potassium. The largest peak shift was again observed for the aromatic para hydrogens; however, the chemical shift was only in the order of 0.04 ppm after one mole equivalent of potassium was added. This suggests a weak complex is formed with potassium, indicating that this host should be selective for thallium over potassium.

Since the NMR titration produced a precipitate of the complex, it was decided to attempt the growth of diffraction quality crystals to prove the mode of binding. Diffraction quality crystals of the complex were grown and a diffraction pattern was collected; however, a solution for the diffraction data is yet to be obtained. The formation of a thallium(I) complex with calixarene (4) was supported through laser-ablation ICP to measure thallium in the crystal. While not quantitative, the levels observed were consistent with the presence of a stoichiometric amount of thallium, rather than surface adsorption. The diffraction data also confirmed the presence of a heavy metal ion in the crystal.

One important difference between the 1,3-alternate calixarenes and the cone conformer is the potential to have two binding sites in the one molecule. Thus, it was necessary to test the stoichiometry of the calixarene (4)/thallium triflate complex, which becomes important in calculations for characterizing ISE behaviour. A NMR continuous variations method, or Job's plot, was conducted with calixarene (4) and thallium(I) triflate, but with very dilute solutions to prevent the complex precipitating out. The Job's plot for calixarene (4) with thallium triflate is displayed in Figure 3.22.
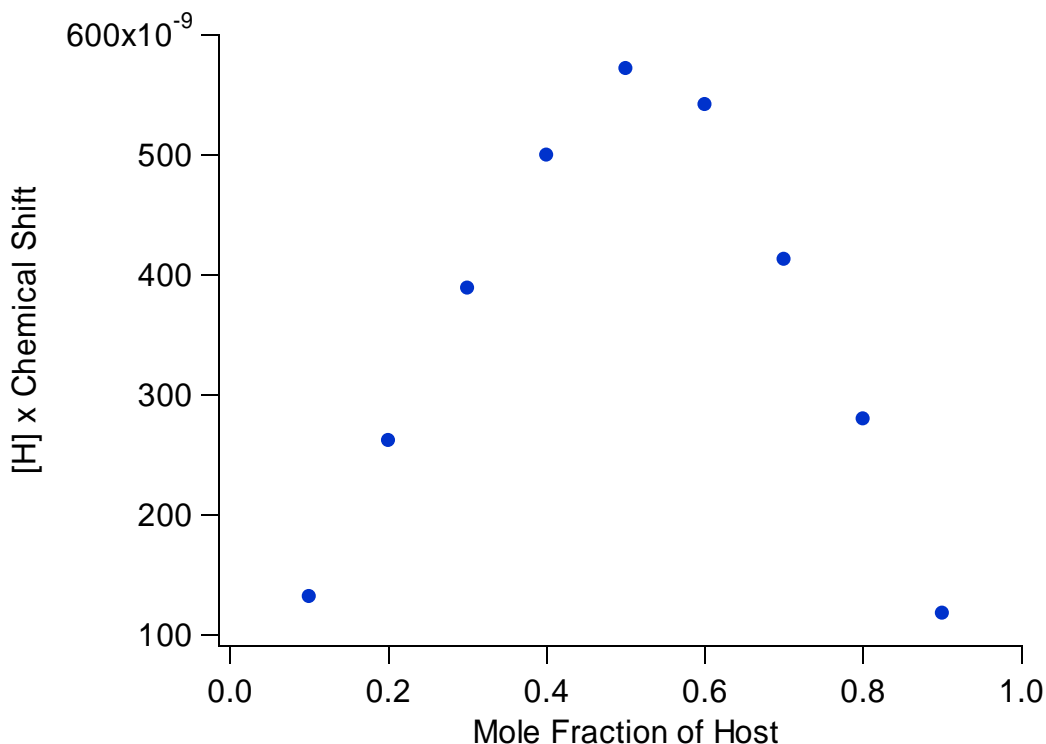
Figure 3.22: NMR Job's plot of calixarene (4) with thallium triflate showing a 1:1 complex. Solvent CD_3COCD_3

The curve maximum occurs at 0.5 mole fraction of host, which is indicative of a 1:1 complex stoichiometry, demonstrating that only one side of the calixarene molecule is able to complex with thallium(I) at any one time. The two binding sites may be too close together to fit more than one thallium(I) ion as the repulsion of two positive ions becomes too great. The bridged calixarene displayed in Figure 3.5 is able to complex two thallium(I) ions as the two binding sites are separated by a large four atom chain (two oxygens and two carbons), which is enough to prevent the electrostatic repulsion forces of two positively charged ions. However, it should be pointed out that, 1,3-alternate calixarenes have been shown to complex two ions in the one molecule [195]. A di-potassium complex of a tetraamide substituted calixarene in the 1,3-alternate conformation illustrates that it is possible for the 1,3-alternate to incorporate two ions at the same time. The n-propyl 1,3-alternate calix[4]arene has been shown to form only a 1:1 complex with Ag^+, consistent with the results for Tl^+ found here [184].

3.7. Experimental

3.7.1. Instrumental

All TGA-DTA data were recorded on a TA Instruments, SDT 2960 Simultaneous DSC-TGA instrument. Samples were placed into platinum crucibles and heated at a rate of 1°C per minute, up to 350°C.

All nuclear magnetic resonance (NMR) spectra were obtained using a Varian Gemini 200 NMR spectrometer. ^{1}H spectra were recorded at 200 MHz and all samples were dissolved in either deuterated chloroform ($CDCl_3$) or acetone (CD_3COCD_3) and referenced to their associated peaks.

Single crystal XRD was carried out by Alan White and Brian Skelton at the School of Biomedical, Biomolecular and Chemical Sciences, The University of Western Australia.

3.7.2. Reagents

Deutrated chloroform was obtained from Cambridge Isotope Laboratories Inc. Deutrated methanol and acetone was obtained from Merck and Aldrich, respectively. Metal picrates were prepared from picric acid and the relavent metal oxide. Picric acid was added to a slurry of metal oxide in water. Once reacted, water was added to the slurry (400 mL), and the remaining solid filtered off. Water was then removed via reduced pressure distillation to yield the crude solid. The solid was then recrystallised twice from water to yield the metal picrate.

Thallium triflate and potassium triflate were prepared from triflic acid and the relevant metal carbonate. Equivalent moles of triflic acid (0.19 mL, 2.15 mmol, and 0.61 mL, 6.89 mmol) were added to the Tl_2CO_3 (0.5 g, 1.07 mmol) and K_2CO_3 (0.5 g, 3.62 mmol), respectively; water (1 mL) was then added to the reaction mixture. The water was allowed to evaporate, and methanol was added and the remaining

solid filtered off. The solid thallium triflate was precipitated from methanol by the addition of ether. The white solid was recrystallised from methanol/ether to yield the pure thallium triflate (0.43 g, 1.22 mmol, 57.0 %). Potsssium triflate (0.50 g, 2.66 mmol, 36.8 %) was prepared via the same method.

3.7.3.   Crystal growth

Solvated crystals of calixarenes (1) and (2) were grown from chloroform through the slow diffusion of methanol into the chloroform solution. Solvent free crystals of calixarene (2) were obtained by sublimation at 270°C under reduced pressure with a cold finger apparatus. Solvent free crystals of calixarene (1) were obtained by growing from acetone with the slow diffusion of methanol.

3.7.4.   Solid Phase NMR Extractions

Solid picrate extractions were conducted by dissolving the calixarene in $CDCl_3$, then adding the solid metal picrate and shaking. Prior to analysis, any remaining solid was filtered and removed.

3.7.5.   NMR Complexation Studies

NMR titrations

Calixarene (2)
Thallium picrate in CD_3OD (0.5 mL, 4.09 mM,) was added in incremental amounts (25 µL, 81.8 nmol) to a $CDCl_3$:CD_3OD (1:1) mixed solvent solution (1 mL) of calixarene (2) (0.5 mM, 0.5 µ mol).

Calixarene (4)

Thallium triflate in CD_3COCD_3 (0.5 mL, 0.49 M) was added in incremental amounts (20 µL, 19.5 m mol) to a CD_3COCD_3 solution containing calixarene (4) (1.5 mL, 32.6 mM, 49 µ mol)

Potassium triflate in CD_3COCD_3 (0.5 mL, 0.5 M) was added in incremental amounts (20 µL, 0.01 m mol) to a CD_3COCD_3 solution containing calixarene (4) (1.5 mL, 29.8 mM, 44.7 µ mol)

Job's Plot

Stock solutions of thallium triflate (0.0178 g, 50.3 µ mol) in CD_3COCD_3 (10 mL) and calixarene (4) (0.029 g, 50.1 µ mol) in CD_3COCD_3 were prepared. Aliquots of the above stock solutions were added together in different proportions to always produce a total mole value of 3.77 µ mol in 1.5 mL of CD_3COCD_3.

4. Ion-Selective Electrodes Incorporating Calixarenes for Thallium(I) Detection

4.1. Response Mechanism of Ion-Selective Electrodes

The basic setup of an ion-selective electrode measuring station is presented in Figure 4.1, and consists of two galvanic half-cells that are connected to a potential measuring device [5]. One of the half-cells consists of a reference electrode maintained in a reference electrolyte, the other is that of the ion-selective electrode. The ion-selective electrode can consist of either an ion-selective membrane with an internal reference system (Ag/AgCl, conventional setup), or a conducting substrate coated with the ion-selective membrane (solid-state electrodes) [5].
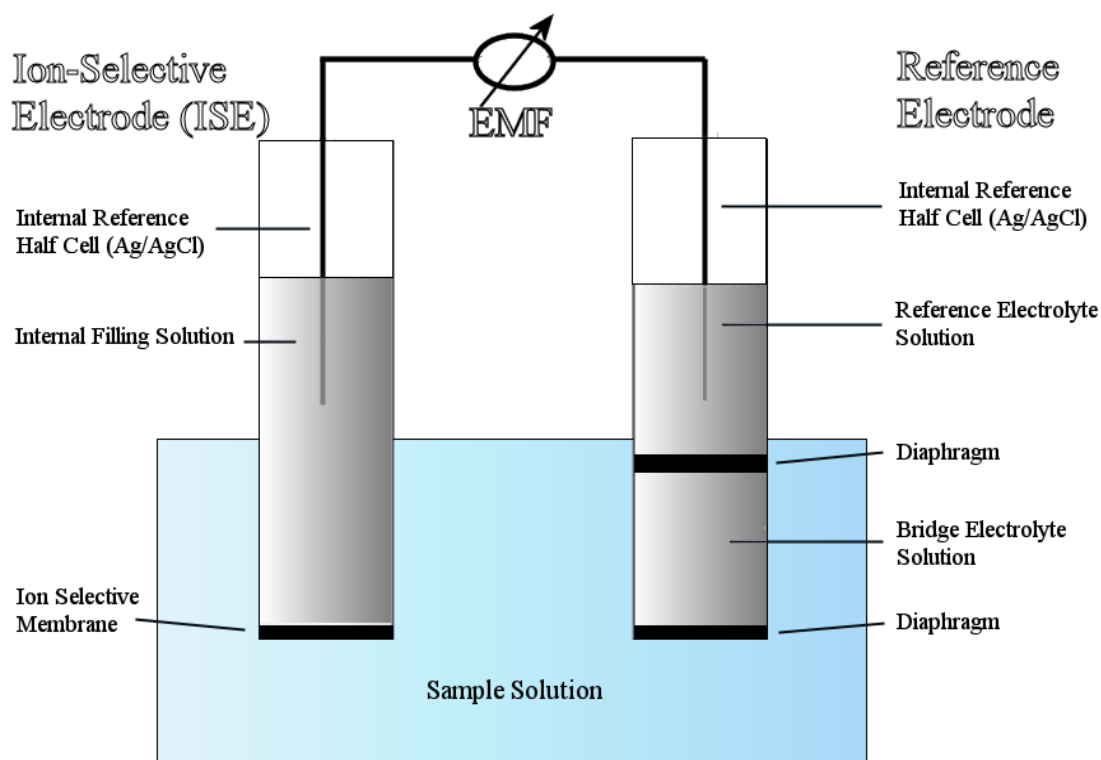
Figure 4.1: Schematic diagram of a conventional ion-selective membrane, measuring cell.

The electrochemical cell can be represented as follows:

Ag|AgCl | KCl 3 M | bridge electrolyte | sample | membrane | inner ref. solution | AgCl|Ag

The electromotive force (EMF) or total potential difference across the electrochemical cell, measured under zero current, is the sum of a series of local potentials at various interfaces across the two-electrode cell. The potential difference across the electrodes can be expressed as follows:

$$EMF = E_{const} + E_m + E_{lj}$$

<div align="right">Equation 4.1</div>

The majority of the individual local potentials are sample independent, and can therefore be termed constant under standard measuring conditions, E_{const} in Equation 4.1. The liquid junction potential, E_{lj}, arises from the different mobilities of ions at the phase boundary between the sample and the bridge electrolyte of the reference electrode. The contribution that the liquid junction potential has on the total EMF can be kept minimal or at least constant if a high concentration (1 M) of equitransferent bridge electrolyte, such as KNO_3, NH_4NO_3 or $LiCH_3COO$ is used in the reference electrode. Alternatively E_{lj} can be kept minimal by using solutions with a constant ionic strength. The liquid junction contribution of the system can be calculated using the Henderson equation [5, 196].

$$E_{D,ref} \cong -\frac{RT}{F} \frac{\sum_I z_I u_I (a_{I,S} - a_{I,ref})}{\sum_I z_I^2 u_I (a_{I,S} - a_{I,ref})} \ln \frac{\sum_I z_I^2 u_I a_{I,ref}}{\sum_I z_I^2 u_I a_{I,S}}$$

<div align="right">Equation 4.2</div>

where,

R   is the universal gas constant (8.314 J K^{-1} mol^{-1})

T   is the absolute temperature (K)

F   Faraday constant (96487 C mol^{-1})

z_I is the change of ion I

u_I is the absolute mobility of ion I (cm^2 mol s^{-1} J^{-1})

a_I the activity of the ion I in the sample (S) and in the bridge electrolyte solution of the reference electrode (ref).

The membrane potential (E_m) in Equation 4.1 consists of potential contributions from various sources within the working electrode. Potentials arise at the two phase boundaries on either side of the membrane, and also from ion diffusion within the membrane. The membrane potential can be expressed as follows:

$$E_m = E_{i,PB} + E_{s,PB} + E_d$$

<div align="right">Equation 4.3</div>

Of the two phase boundaries, one occurs at the interface between the inner reference solution and the ion-sensing membrane (ISM) ($E_{i,PB}$), and the other occurs at the interface between the ISM and the sample solution ($E_{s,PB}$). The potential contribution from the inner phase boundary is said to be constant, as the ion concentration in the inner reference solution is fixed and ideally sample independent.

The diffusion potential within the membrane can contribute towards the overall potential if substantial concentration gradients of ions with different mobilities are present within the membrane. In most cases, the contribution is insignificant and often neglected in potential readings as membranes with Nernstian behavior contain an even distribution of oppositely charged primary and lipophilic ions due to the homogeneously distributed lipophilic ion-exchanger and ionophore [47, 197, 198]. An experiment established by Pungor [199], showed that the response time of various electrodes was in the order of 20 ms, which coincides with the time required for an ion to travel across the adhering layer on the electrode, and therefore suggesting that the diffusion process in the membrane is significantly slower than the potential-determining process. Since there was a very low equilibration time, ion-diffusion across the membrane influencing the potential was dismissed. Even in the situation where more than one ion is present in the membrane, the ionophore complexes with it thus rendering the mobilities equivalent. Equation 4.3 can therefore be simplified to:

$$E_M = E_{M,const} + E_{S,PB}$$

<div align="right">Equation 4.4</div>

where,

$E_{M,const}$ =   the sum of inner phase boundary potential at the membrane/inner reference solution interface and the diffusion potential within the membrane.

$E_{S,PB}$ =   the phase boundary potential at the sample/membrane interface.

The phase boundary potential arises from the charge separation that occurs across the sample/membrane interface as a result of the non-uniform distribution of ionic species on either side of the interface, which is shown schematically in Figure 4.2.
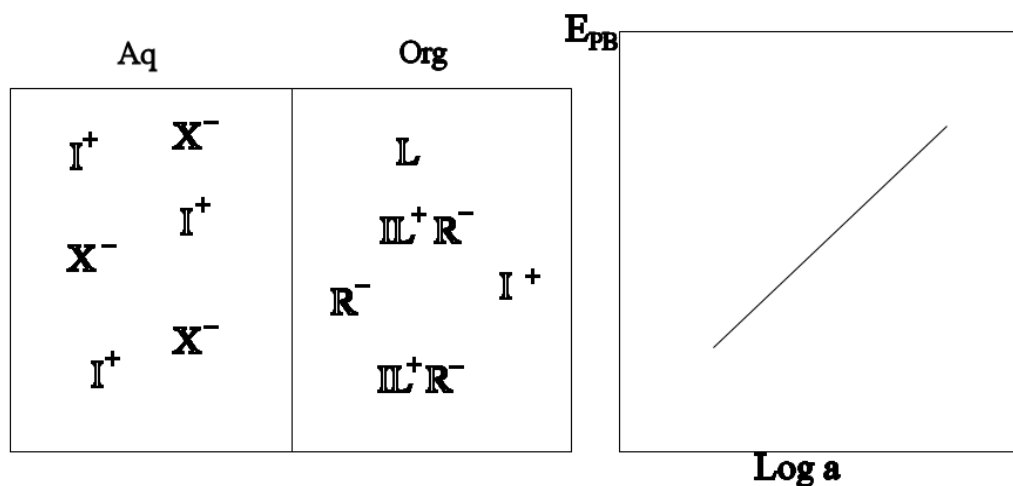
Figure 4.2: Schematic representation of the phase boundary potential, shown for a monovalent ion (I$^+$), whereby the potential is determined by the free energies of transfer and activities of the ion in the aqueous and membrane phases. A Nernstian response slope (shown on right) is observed when the concentration/activity of I$^+$ in the membrane phase is constant and independent of the aqueous sample. [200]

Considering chemical and electrical contributions, the electrochemical potential ($\overline{\mu}$) for the primary ion (I) in the sample (S) and membrane (M) phases can be formulated as:

$$\overline{\mu} = \mu_I + z_I F\Phi = \mu_I^{\circ} + RT\ln a_I + z_I F\Phi \qquad \text{Equation 4.5}$$

where,

μ   chemical potential (μ° under standard conditions) (J mol^{-1})

a_I is the activity of the uncomplexed ion I (mol L^{-1})

z_I the charge of the ion (I)

Φ   electric potential (V)

F   is Faraday's constant

At thermodynamic equilibrium, the electrochemical potentials of the membrane ($\bar{\mu}_M$) and the sample ($\bar{\mu}_S$) for the ion (I) are equal.

$$\mu_{I,S}^{\circ} + RT \ln a_{I,S} + z_I F \Phi_S = \mu_{I,M}^{\circ} + RT \ln a_{I,M} + z_I F \Phi_M \quad \text{Equation 4.6}$$

Which can be simplified to obtain the phase boundary potential,

$$E_{S,PB} = \Phi_M - \Phi_S = \left(\frac{\mu_{I,S}^{\circ} - \mu_{I,M}^{\circ}}{z_I F}\right) + \left(\frac{RT}{z_I F}\right) \ln\left(\frac{a_{I,S}}{a_{I,M}}\right) \qquad \text{Equation 4.7}$$

The free energy difference $\mu_{I,S}^{\circ} - \mu_{I,M}^{\circ}$ across the membrane is dictated by the lipophilicity and can be expressed as.

$$k_I = \frac{1}{RT} \exp^{(\mu_{I,S}^{\circ} - \mu_{I,M}^{\circ})} \qquad \text{Equation 4.8}$$

If the activity of the ion in the membrane phases ($a_{I,M}$) is regarded as sample independent and constant, then Equations 4.7 and 4.4 can be simplified to the well known Nernstian equation:

$$E_m = E^0 + \frac{RT}{z_I F} \ln a_{I,S} \qquad \text{Equation 4.9}$$

where E^0 is the sum of all the constant potentials in the membrane. The electrode potential of a measuring cell can then be defined by combining Equations 4.1 and 4.9 to obtain the following expression:

$$E_I = EMF - E_{lj} = E_I^0 + s_I \log a_{I,S}$$

Equation 4.10

where,

$$s_I = \frac{RT}{z_I F} \ln 10$$

Equation 4.11

and is identical to the Nernstian slope of the linear region of the response graph, which is ($59.16/z_I$ mV/decade at 25°C). The intercept E_I^0 in Equation 4.10 is a standard potential (constant) if the liquid-junction potential is insignificant or zero.

$$E_I^0 = E^0 + E_{lj} - s_I \log a_{I,S} \cong \quad \text{constant}$$

Equation 4.12

There are several models used to describe the potential generated in the ISE cells. Of these, the phase boundary potential model is the simplest, and assumes thermodynamic equlibrium between the membrane and solution phases [200, 201]. It allows for easy explanation of the response function with simple thermodynamic parameters. An alternate model (membrane-surface or space-charge) describes the potential arising from a charge separation at the surface of the membrane/solution interface, whereby the primary ions chemisorbs onto the membrane surface making it charged, leaving the counter ion in solution [199, 201]. Other more complex models such as the Nernst-Planck-Poisson and the extended Plank model describe the potential occurring at the membrane interfaces (phase boundary potentials) and within the membrane (diffusion potentials) [202-204]. The different models can be used to describe the membranes response, selectivities and detection limits. However the various models can be somewhat contradictory and have resulted in numerous discussions and experiments supporting their cases. Of the various models, the phase

boundary model is simple, widely applicable and explains the vast majority of experimental results [201].

4.1.1. Selectivity

One of the most important characteristics of ISEs is their preference to primary or measuring ions (I) over secondary or interfering ions (J). The relative selectivity that a membrane exhibits is one of the underlying factors that determine its usefulness in practical samples. Ideally, the membrane is sensitive to primary ions only and obeys the well-known Nernstian equation (Equation 4.9). However, in practice, the membrane only obeys this behaviour in a limited concentration range and outside this the potential is influenced by the presence of other ions. The affinity of one ion over another in the membrane phase can be related to the equilibrium constants of the primary and interfering ion exchange reactions (i.e., K_I and K_J respectively) between the membrane and aqueous phases, which can be explained as follows:

$$K_{I,J} = \frac{((k_J)^{z_J})^{\frac{z_I}{z_J}}}{k_I}$$

Equation 4.13

where,

$$k_I = \frac{1}{RT} e^{(\mu_{I,S}^\circ - \mu_{I,M}^\circ)}$$

Equation 4.14

The ion-exchange between the two uncomplexed ions in the solution and membrane phases can be viewed in Figure 4.3.
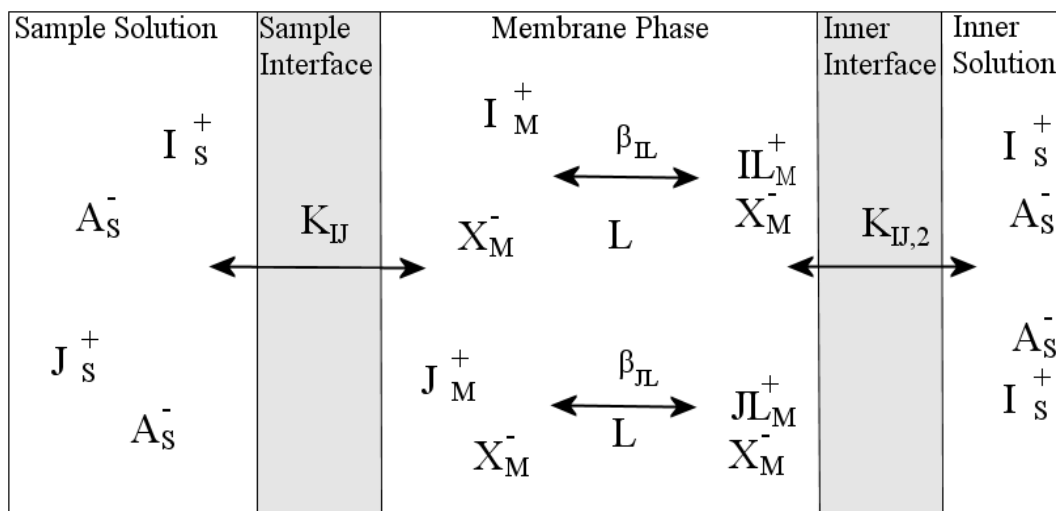
Figure 4.3: Schematic representation of the equilibria established between the membrane and solution phases for a primary (I) and interfering ion (J). The terms L and X^- represent the ionophore and lipophilic ion-exchanger respectively; β_{IL} and β_{JL} are the complex formation constants of the complexes IL^+ and JL^+. K_{IJ} is the interfering and primary ions equilibrium constants between the sample and membrane phases. $K_{IJ,2}$ is the equilibrium constant between the inner solution and the membrane. $K_{IJ,2}$ is the same as K_{IJ} but the exchange on this side of the membrane should be kept to a minimum.

The selectivity can be expressed as a coefficient ($K_{I,J}^{pot}$) and used to determine the concentration of primary ion where the interfering ion influences the electrode response. In the separate solution method, the selectivity coefficient can be calculated from the intercepts ($E_I^0 \& E_J^0$) of the linear regions of the calibration graphs of both the primary and interfering ions measured independently (see Figure 4.4). The following equations can be used to calculate the selectivity coefficients.

$$\log K_{I,J}^{pot} = \frac{(E_J^\circ - E_I^\circ)}{s_I}$$

<div align="right">Equation 4.15</div>

Or

$$\log K_{I,J}^{pot} = \frac{(E_J^\circ - E_I^\circ)}{s_I} + \log a_I(I) - \frac{z_I}{z_J}\log a_J(J)$$

<div align="right">Equation 4.16</div>

where $a_I(I)$ and $a_J(J)$ are the activities of the primary and interfering ions in separate solutions, producing the potentials E_I and E_J respectively. A graphical representation of the selectivity determinations is presented in Figure 4.4.
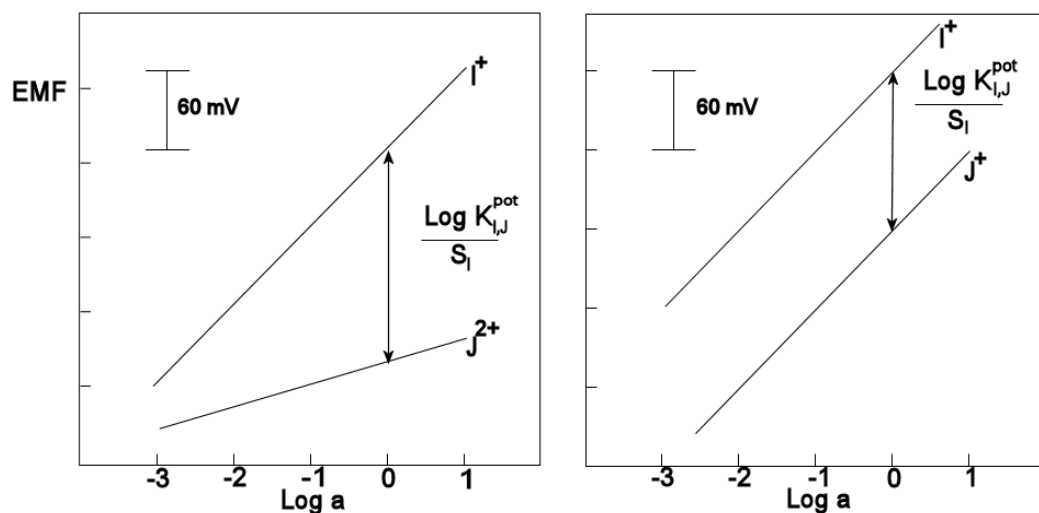
Figure 4.4: Determination of selectivity coefficients via the separate solution method. $K_{I,J}^{pot}$ is calculated by the difference in potential of the two individual linear response functions, at log activity of zero, divided by the ideal Nernstian slope of the primary ion.

Unbiased selectivity coefficients can be calculated via this method only if the membrane experiences Nernstian behaviour to both the primary and interfering ions over the calibration range [183, 205]. This can be achieved by conducting the calibration plots with membranes that have not previously been exposed to the primary ion, and only exposed to the interfering ions in increasing order of selectivity (most discriminated to the least discriminated). Membranes that have been exposed to the primary ion prior to the interfering ion, only exhibit Nernstian responses for low discriminatory ions. For highly discriminated ions, the response is perturbed due to ion fluxes, resulting in biases in their coefficient calculations. The effect of ion-fluxes is discussed in more detail in the following sections.

Solutions that contain two or more ionic species of the same charge may produce a response that is different to that of the individual primary ion. The response of the

mixed ionic solution (E_{IJ}) can be estimated according to the semi-empirical Nikolsky-Eisenman formulism [5, 47]:

$$E_{IJ} = E_I^\circ + s_I \log\{a_I(IJ) + \sum_{J \neq I} K_{I,J}^{pot}(a_J(IJ))^{\frac{z_I}{z_J}}\} \qquad \text{Equation 4.17}$$

where,

   a_I activity of the primary ion in the sample solution (mol L^{-1})

   a_J activity of the interfering ions in the sample solution (mol L^{-1})

Here the activity term in the Nernstian Equation 4.9 has been extended to include the sum of activities, weighted accordingly to the selectivity coefficients of each ionic species. However this equation does suffer from only providing correct results if ions of similar charge are in solution. The Nikolsky-Eisenman equation fails to predict the response observed for solutions containing ions of differing charge in the non-linear response range of the ISE.

To overcome the limitations of the Nikolsky-Eisenman equation the activity term from Equation 4.9 has been extended to accommodate ions of various charges. Equation 4.18 can be used to determine the potentiometric response of solutions that contain any number of ions with differing charge. The full derivation of Equation 4.18 is presented in the literature [206].

$$E = E_I^\circ + \frac{RT}{F} \ln\left[\frac{1}{2}\sum_{i(1)} K_{I,i(1)}^{pot\ \frac{1}{z_I}} a_{i(1),S} + \sqrt{\left(\frac{1}{2}\sum_{i(1)} K_{I,i(1)}^{pot\ \frac{1}{z_I}} a_{i(1),S}\right)^2 + \sum_{i(2)} K_{I,i(2)}^{pot\ \frac{2}{z_I}} a_{i(2),S}}\right]$$

Equation 4.18

where $i(1)$ and $i(2)$ indicate the monovalent and divalent primary or interfering ion respectively, and by definition $K_{I,I}^{pot} = 1$.

4.1.2. Detection Limits

One of the most important aspects of any analytical technique is its limit of detection. In the case of ISEs, the limits of detection occur when the observed potential differs significantly to that of the expected value obtained from the linear region of the response function. ISEs have both upper and lower limits of detection, at high and low activities respectively. According to IUPAC. recommendations [207], the limits of detection are predicted from the interception of the extrapolated linear regions on the calibration curve, which is presented in Figure 4.5 (a).

As a result of new experimental procedures leading to super-Nernst responses, a second definition of the detection limit has been proposed [208]. According to this new definition, the limit of detection occurs at the activity when the response deviates by (RT/z_IF) ln 2 from the linear Nernstian region (Figure 4.5 (b)). The limits of detection are almost identical for electrodes behaving ideally according to the Nernstian equation. For a monovalent ion, the EMF is not allowed to deviate more than 17.8 mV at 25 ºC away from the linear region of the graph. The new definition can also be used to predict the optimum experimental setup for low detection limit electrodes. By inserting (RT/z_IF) ln 2 into the appropriate equations, one can determine the optimum concentration of primary ion in the inner filling solution for a given sample, which will be discussed later in the chapter.

The upper detection limit is a result of the membrane losing its permselectivity (Donnan failure), due to the coextraction of the primary ion together with its counter ion into the membrane. The deviation away from the ideal Nernst response is a result of the activity of the membrane ($a_{I,M}$) increasing together with that of the sample ($a_{I,S}$), which leads to a smaller than expected difference in EMF because under ideal Nernst behaviour the membrane activity is kept constant. The effect of changing the membrane activity can be calculated in Equation 4.7 and 4.10. [32, 209-211].
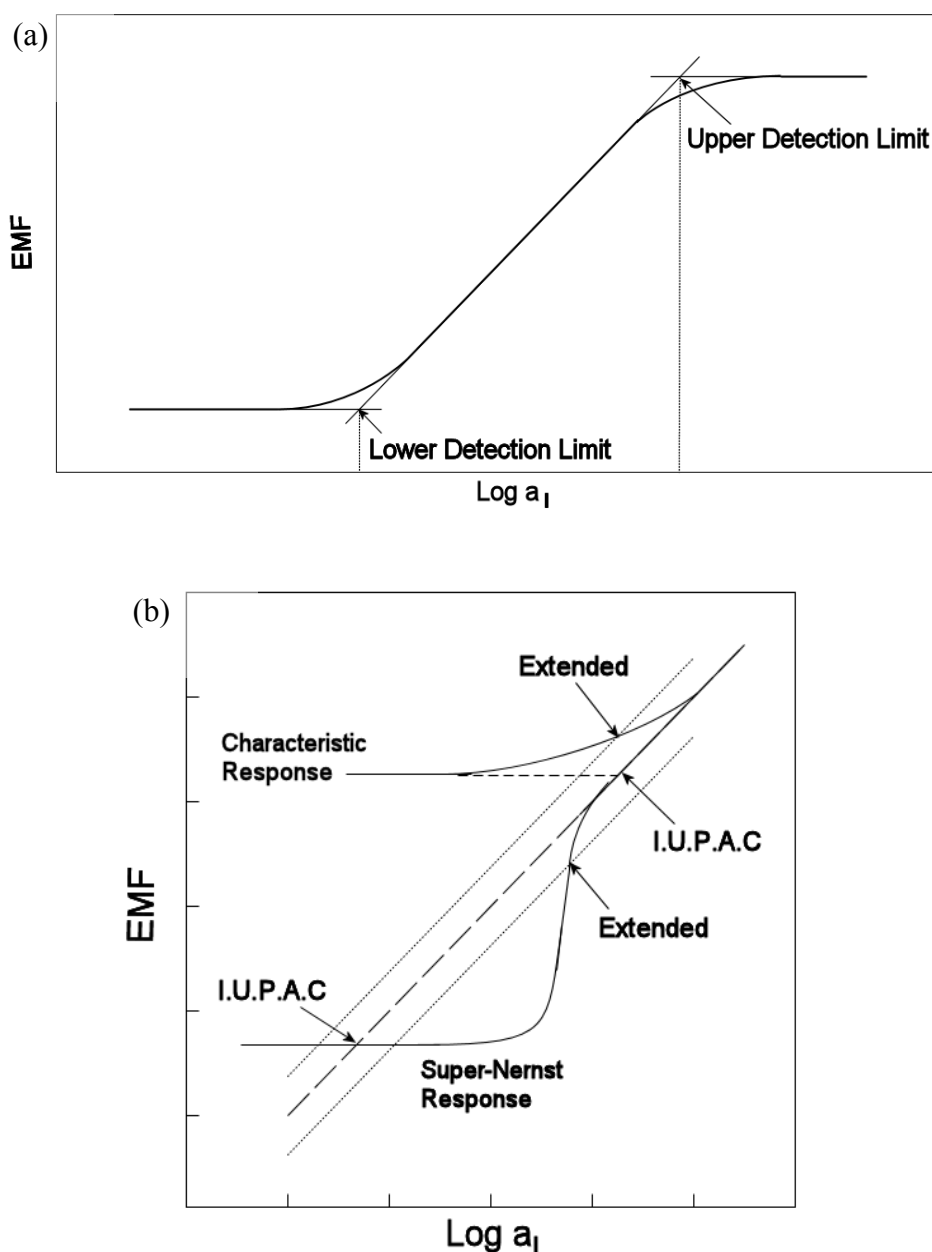
Figure 4.5: The upper and lower detection limits of a standard ISE calibration plot according to the IUPAC. recommendations (a), and the new extended definition (b) [208], which is required for determining detection limits where a super-Nernst step is observed. Figure (b) shows the response of two electrodes, which deviate away from the ideal Nernst behaviour and their apparent limits of detection according to the IUPAC. recommendations [207] and the new extended definition (dotted line). [201]

The lower detection limit can eventuate from two processes, but differ to that responsible for the upper detection limit. The lower detection limit can be caused by

the presence of an interferent or competing ion, if its concentration in the solution is significantly high, or by the presence of significant ion-fluxes. The detection limit resulting from the first effect is related to the Nikolsky Equation 4.17, and can be calculated via:

$$a_I(DL) = K_{I,J}^{pot} a_J^{\left(\frac{z_I}{z_J}\right)}$$

Equation 4.19

It is apparent from Equation 4.19 that the better the selectivity of the primary ion over an interferent the lower the detection limit. Ionophores with poor selectivities will experience higher limits of detection over highly selective ones. The calculations performed using Equation 4.19 are based on a static membrane process and are only relevant for concentrations above 10^{-6}-10^{-7} M, due to the presence of ion fluxes below these concentrations perturbing the response. To incorporate the ion fluxes present in membranes, a different approach is required to calculate the expected detection limits. A dynamic model is used to explain the non-idealistic scenario occurring in membranes where ion-fluxes are prevalent. The outward flux of ions from the membrane into the sample solution, or Nernst diffusion layer, is discussed in more detail in the next section.

4.2. Bias in Responses as a Result of Zero-Current Ion Fluxes

One of the most important developments for ion-selective electrodes in the past decade has been the reduction of detection limits and improved selectivity coefficients as a result of addressing the problem of zero-current ion fluxes. Prior to this, the low detection limits of ISEs were thought to lie in the micromolar range, and selectivity coefficients no lower than 10^{-2}-10^{-4} and 10^{-4}-10^{-5} were reported for divalent/monovalent and divalent/divalent ions respectively [212, 213]. These values were thought to be mediocre in the field of analytical chemistry and resulted in the general consensus that ISEs had little practical applications, especially in the field of heavy metal determination in environmental and clinical fields [4, 214].

It was not until researchers alluded to the fact that an optical selective sensor and a potentiometric ISE based on the same ionophore had differing limits of detection by many orders of magnitude, that the limit of detection for potentiometric sensors was considered to be at elevated levels [215-217]. In one paper, a lead-selective bulk optode based on a neutral carrier was able to reach a detection limit of 5x 10^{-9} M, significantly lower than that obtained from an ISE [215]. Lower limits of detection were discovered when an ion-buffering agent was added to the sample solution to keep the activity of the primary ion under control [218]. At the time, the mechanism behind these improvements was not explicitly understood and only recently has the problem been pinpointed.

The biases in results were associated to the release of primary ions from the membrane into the sensed surface layer or Nernst diffusion layer [212, 213, 219, 220]. As a consequence, the concentration in the sensed Nernst layer could be significantly higher than that in the bulk sample. Traditionally, the experimental setup of ISEs consisted of an inner filling solution of a highly concentrated primary ion as a chloride salt, typically in the order of 10^{-3}-10^{-1} M. The chloride counter ion is required for the correct thermodynamic workings of the Ag/AgCl reference electrode. This high concentration in the inner compartment causes the release of primary ions from the membrane into the electrodes surface layer at a concentration of ~10^{-6} M, even in very dilute solutions or solutions containing no analyte at all. This constant leaching of primary ions from the membrane therefore biases the limit of detection of conventional ISEs, as seen in Figure 4.6. The leaching of primary ions also perturbs the response of highly discriminated interfering ions. The selectivity coefficient of an interferent may be better by many orders of magnitude, due to the sensor responding to the leached primary ion only, and not the interfering ion itself.
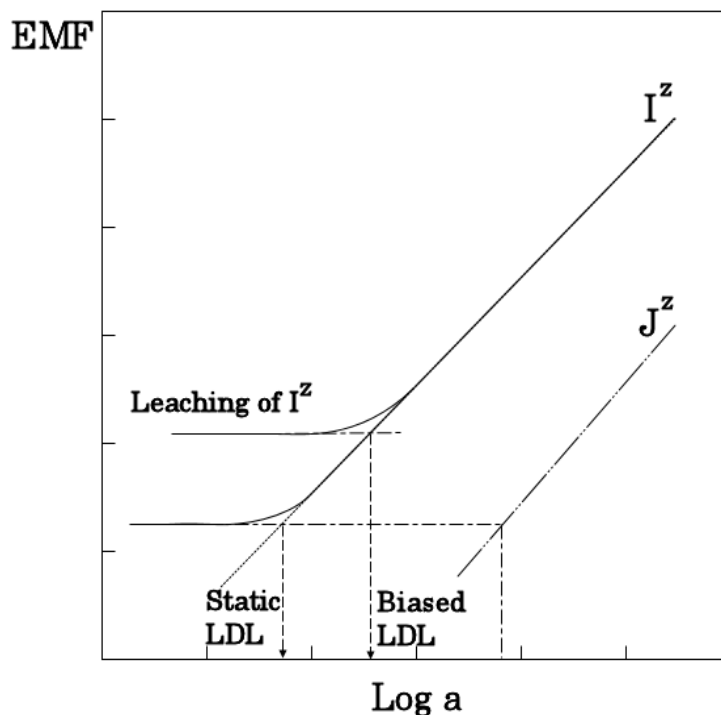
Figure 4.6: The optimum detection limit (static) determined by the selectivity of the interferent, and the biased lower detection limit as a consequence of primary ions being released into the sample solution. [221]

It has been proven that concentration gradients still exist in ISEs membranes even though measurements are conducted under zero-current conditions [222]. A schematic representation of concentration gradients within the membrane is presented in Figure 4.7

There are several processes responsible for the leaching of primary ions from the membrane into the sample solution. The several processes are: primary ion leaching together with the ion-exchanger; co-extraction; ion-exchange; and diffusion. The leaching of the primary ion together with the ion-exchanger is a simple partitioning process and can be avoided with the use of highly lipophilic molecules which prefer to be in the hydrophobic membrane [214, 223]. The ion-exchanger leaching can also be prevented through the use of strongly complexing ionophores [53]. The highly lipophilic ion-exchangers are commercially available and consist of large tetraphenylborate derivatives or tetraalkylammonium salts. Structures of the various ion-exchangers are presented in Appendix I.

(a)

Ideal Membrane System

(b)

Near DL Membrane System
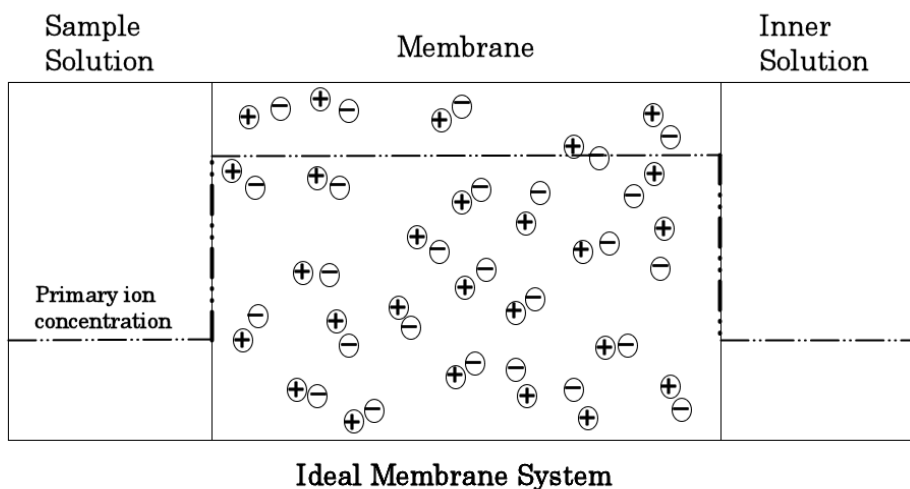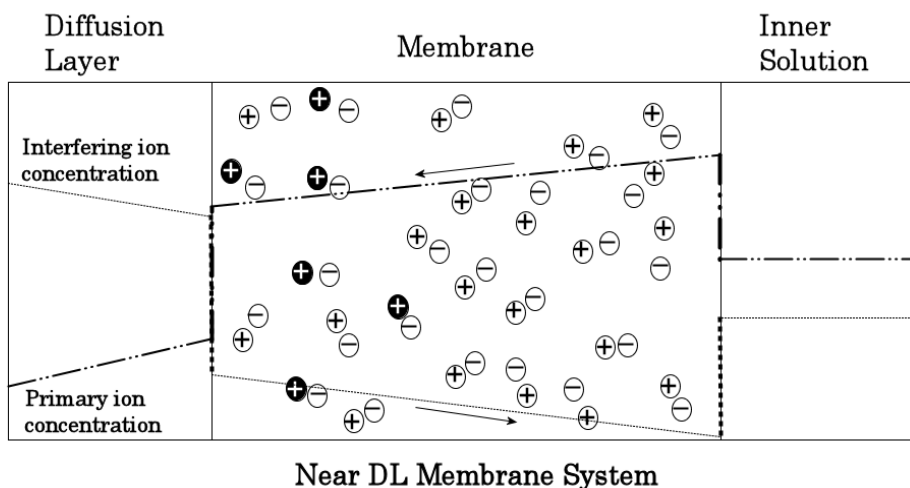
Figure 4.7. Schematic representations of concentration gradients within the membrane at equilibrium (a) and in the presence of zero-current ion fluxes, which influence the lower detection limit (b). Clear spheres with positive signs represent the primary ions, whilst those with negatives represent the constant concentration of ionic sites and the dark spheres represent the secondary/interfering ions. [4]

Co-extraction

Co-extraction is the process whereby the primary ion together with its counter ion is extracted from the aqueous phase of the electrode into the membrane phase [47, 187, 208].
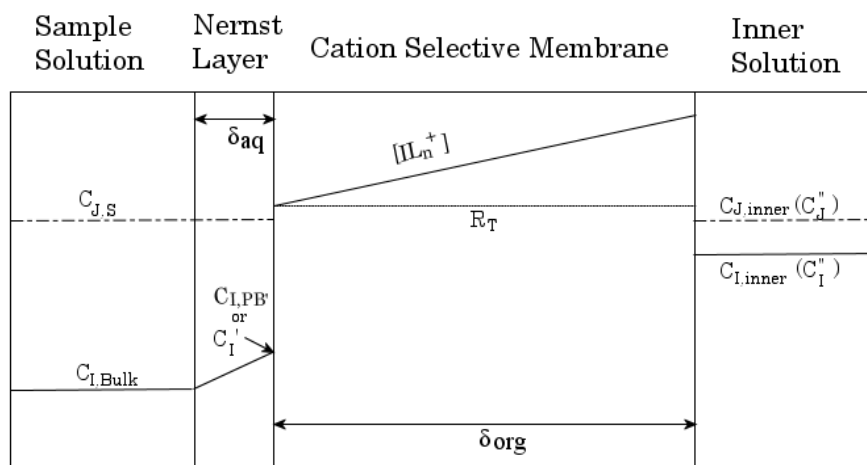
Figure 4.8: Cross-section schematic of a membrane showing the process of co-extraction with a primary ion (I^+) that forms a 1:1 complex with the ionophore. [223, 224]

This extraction of ions into the membrane leads to an increased concentration of ions on one side of the membrane, which results in a flux of ions in the opposite direction away from the co-extraction side of the membrane. If the co-extraction occurs at the inner side of the membrane, an ion flux would be established towards the sample side of the membrane and subsequently be released into the sample phase. The release of the ion from the membrane into the sample increases the concentration of that ion in the diffusion layer ($c_{I,PB'}$), thereby perturbing it from the bulk concentration ($c_{I,PB'} > c_{I,Bulk}$), as demonstrated in Figure 4.8 [187, 208, 224].

The co-extraction of an ion together with its counter ion, can be described by the following equilibria [209]:

$$\frac{z_I}{-z_X} X^{z_X}(S) + I^{z_I}(S) \Leftrightarrow \frac{z_I}{-z_X} X^{z_X}(M) + I^{z_I}(M) \qquad \text{Equation 4.20}$$
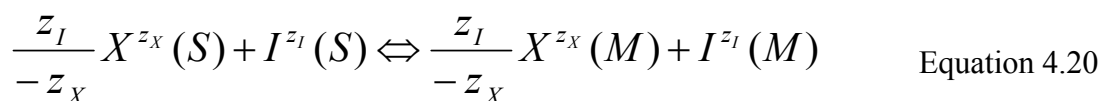
where (S) and (M) denote the species in the aqueous and membrane phases respectively. The distribution of ions across two phases can be defined by the coextraction constant (K_{IX}) [209].

$$K_{IX} = \frac{k_I}{(k_X)^{\frac{z_I}{z_X}}} = \frac{[I^{z_I}]}{a_{I,S}} \left(\frac{[X^{z_X}]}{a_{X,S}} \right)^{-\frac{z_I}{z_X}}$$

<div align="right">Equation 4.21</div>

The thermodynamic equilibrium process (K_{coex}) can be calculated for a membrane containing ionophore which complexes the primary ion, via;

$$K_{coex} = \beta_{IL_n} \frac{k_I}{(k_x)^{\frac{z_I}{z_X}}} = \frac{[IL_n^{z_I}]}{a_{I,S}[L]^n} \left(\frac{[X^{z_X}]}{a_{X,S}} \right)^{-\frac{z_I}{z_X}}$$

<div align="right">Equation 4.22</div>

where k_x is defined in complete analogy to k_I in Equation 4.8, X is the counter ion of the measuring ion I, $[IL_n^{z_I}]$ is the primary ion complex, L is the ionophore and β_{IL_n} is the complex formation constant of the primary ion with the ionophore. The process occurring at the upper detection limit is a direct consequence of co-extraction and can be used to estimate the apparent co-extraction constant. More detail on the influence of co-extraction on the theoretical response of ISEs can be found in the literature [187, 208, 209, 224, 225].

Ion-exchange

Ion-exchange occurs when the primary ion is released from the membrane into the aqueous phases together with a simultaneous incorporation of interfering ion of the same charge, from the aqueous phases into the membrane phase [208].
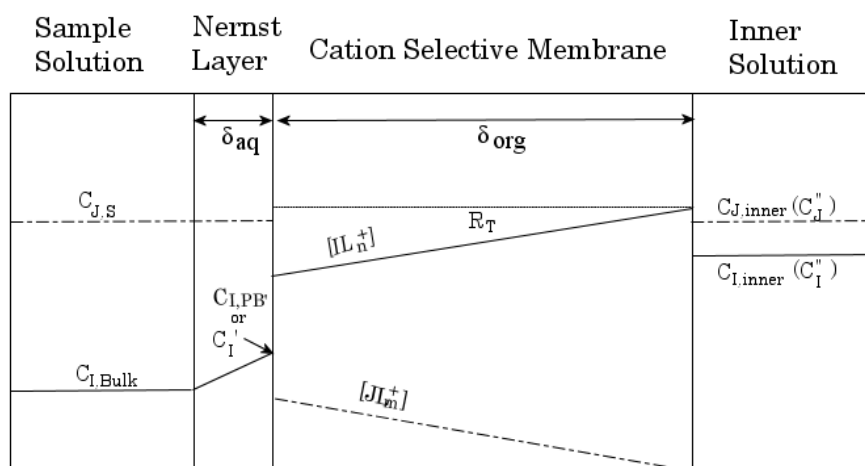
Figure 4.9: A cross-sectional schematic of a membrane showing ion-exchange of the primary ion (I$^+$) with an interfering one (J$^+$) at the sample side and the inner reference side. [223, 224]

Similar to the process of co-extraction, a concentration gradient is established within the membrane, which results in the movement of ions and subsequent increase in the concentration of primary ion in the sensed Nernst layer (see Figure 4.9).

The equilibrium process can be explained as follows:

$$\frac{z_I}{z_J} J^{z_J}(S) + I^{z_I}(M) \Leftrightarrow \frac{z_I}{z_J} J^{z_J}(M) + I^{z_I}(S)$$
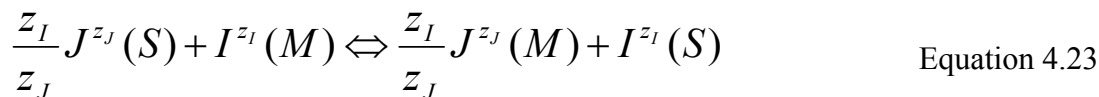
Equation 4.23

The equilibrium constant (K$_{IJ}$) can then be calculated according to

$$K_{IJ} = \left(\frac{a_{I,S}}{[I^{z_I}]}\right)\left(\frac{[J^{z_J}]}{a_{J,S}}\right)^{\frac{z_I}{z_J}}$$

Equation 4.24

Taking into account the complexation between the ions and the ionophore within the membrane, the ion-exchange equilibrium constant (K$_{exch}$) can be calculated via; [208]

$$K_{exch} = K_{IJ} \frac{(\beta_{JL_m})^{z_I/z_J}}{\beta_{IL_n}} = \frac{a_{I,S}}{a_{J,S}} \frac{[JL_m^{z_J}]^{z_I/z_J}}{[IL_n^{z_I}]} \frac{[L]^n}{[L]^{nz_I/z_J}}$$

Equation 4.25

Diffusion

The mass transfer of ions in an electrochemical cell can result from either a difference in the electrochemical potential $\bar{\mu}$, through diffusion or migration, or by hydrodynamic processes accountable for convection through processes such as stirring. The Nernst-Plank equation can be used to describe the ion transport in an electrochemical cell at constant temperature and pressure.

$$J_i(x) = -\underbrace{D_i \frac{\partial c_i(x)}{\partial x}}_{\text{diffusion}} - \underbrace{\frac{z_i F}{RT} D_i c_i \frac{\partial \phi(x)}{\partial x}}_{\text{migration}} + \underbrace{c_i v(x)}_{\text{convection}}$$

Equation 4.26

where,

$J_i(x)$ is the flux of the species i per unit area in the x-coordinate (mol cm^{-2}s^{-1})

c_i concentration of species i (mol cm^{-3})

x is a space coordinate measure perpendicular to the section (cm)

D_i the diffusion coefficient of the species i (cm^{2}s^{-1})

$\phi(x)$ is the electrical potential in the x-coordinate

$v(x)$ is the hydrodynamic velocity along the x-coordinate (cm s^{-1})

If the migration and convection terms in Equation 4.26 are neglected, the Nernst-Plank equation can be simplified to Fick's first law of diffusion [223]. Concentrations are used here for simplicity by implying that all activity coefficients are set to unity.

$$-J_i(x) = D_i \frac{\partial c_i(x)}{\partial x}$$

Equation 4.27

Equation 4.27 relates to the number of moles of ionic species i that pass through a unit area in a set time. The differential of Equation 4.27 has the solution,

$$J_i = -D_i \frac{\Delta c_i}{\Delta x}$$

Equation 4.28

in a system at steady state, at equilibrium, where D_i is the diffusion coefficient in $(cm^2 s^{-1})$ and ($\Delta c_i / \Delta x$) is the concentration gradient of the species i. A steady state means that the concentration of species i at a defined point is not time dependent.

Considering that the law of mass conservation requires the fluxes in each phase to be equal, it follows from Equation 4.28 that

$$\left(c_i' - c_{i,Bulk}\right)\frac{D_{i,aq}}{\delta_{aq}} = \left([IL^+]'' - [IL^+]'\right)\frac{D_{IL,m}}{\delta_m}$$

Equation 4.29

where δ_{aq} and δ_m represent the thickness of the Nernstian layer of the sample and of the membrane respectively (see Figures 4.8 and 4.9 [208]). The fluxes of the interfering ion in each phase are also calculated using Equation 4.29, by inserting the appropriate interfering ion concentrations in place of the primary ion. Also for zero-current conditions, the law of charge conservation states there is no net charge transfer.

$$\sum_i z_i J_i(x) = 0$$

Equation 4.30

Considering the charge and mass conservations laws (Equations 4.30 and 4.29 respectively), Equation 4.28 can be used to predict the influence ion fluxes have on ISEs, assuming ionic species in the sample bulk ($c_{i,Bulk}$) and inner membrane boundary layer (($IL^+)''$) are constant [208].

By considering the mass balance of the ionophore and the charge balance of the membrane, Equations 4.31 and 4.32 respectively, and Equation 4.25, the ion-complex concentrations, $[IL_n^{z_I}]$ and $[JL_m^{z_J}]$, at the phase boundaries on either side of

the membrane can be calculated, if the activities of the ions I and J at the aqueous phase boundary are known.

$$[L] = L_T - n[IL_n^{z_I}] - m[JL_m^{z_J}]$$

Equation 4.31

$$R_T = z_I[IL_n^{z_I}] + z_J[JL_m^{z_J}]$$

Equation 4.32

where R_T is the total concentration of ion-exchanger in the membrane. The above series of equations together with the process of co-extraction for a system of $z_I = z_J$ and n = m = 1, have been solved [208]. For other cases there is no analytical solution and the problem needs to be solved numerically.

An alternate series of equations based on thermodynamic principles have been established to describe the processes occurring in a dynamic system and can be used to calculate the limits of detection in samples based on ion selectivities. This allows the ISE response to be modeled much more easily, which makes it unnecessary to solve the above system of equations. To keep the dynamic model simple and avoid use of excessive parameters a few assumptions have been proposed, which have been reported previously [208, 220, 225].

- The ionic phase-transfer reactions are significantly faster than the corresponding diffusion process rendering the sample-membrane phase boundary at local equilibrium.
- The lipophilic ionic sites are distributed homogeneously across the membrane.
- The complexes in the membrane are significantly strong therefore avoiding fluxes of uncomplexed ions.
- The system is always at steady state resulting in linear concentration profiles.
- The ionic concentration of each species in the inner filling solution is constant. This is brought about through the use of buffers or high concentrations.

- The diffusion coefficients are constant in each phase and are equal for all species within the membrane.
- The concentration of uncomplexed ionophore is constant. This is achievable through having a higher ionophore concentration compared to the ion-exchanger.

The above assumptions allow for careful derivation of equations based on the phase boundary potential model incorporating ion-exchange and coextraction equilibria. However, the limits of detection estimated through these equations are often more optimistic than values obtained experimentally. This is a consequence of the various assumptions made in the derivation of the equations. The new formalisms are discussed in the following section.

4.3. Reducing Detection Limits and Selectivities Through Minimizing Zero-Current Ion Fluxes.

Since the discovery of lower detection limit ISEs, a significant proportion of work has been dedicated to the optimization of these sensors through various measures.

Considering Equation 4.29, the concentration difference at both sides of the membrane ($[IL^+]'' - [IL^+]'$) and Nernst diffusion layer $\left(c_I' - c_{I,Bulk}\right)$ for the primary ion are directly related to the diffusion coefficients in each phase and to the thickness of the concentration gradient in each layer.

$$\frac{c_I' - c_{I,Bulk}}{[IL_n^{z_I}]'' - [IL_n^{z_I}]'} = \frac{\Delta c_{I,aq}}{\Delta c_{I,m}} = \frac{D_{I,m}\delta_{aq}}{D_{I,aq}\delta_m} = q \qquad \text{Equation 4.33}$$

Diffusion coefficients of cations in an aqueous media are in the order of 10^{-6}-10^{-5} cm^{2}s^{-1} [187], whilst those in the membrane phase for ion-ionophore complexes are lower at 10^{-8} cm^{2}s^{-1} [222, 226-228]. Even though the diffusion coefficients for water are higher than the membrane, the significant concentration of lipophilic ionic sites (in the order of 5 mmol kg^{-1}) and subsequently the measuring

ion concentrations in the membrane, along with the movement of ions in the membrane phase ($\Delta c_{I,M} D_{I,M}$), can be somewhat higher than the aqueous movement ($\Delta c_{I,S} D_{I,S}$) in dilute samples. As a consequence, the slow uptake or release of ions from the membrane is counter balanced by the high concentration of ions, which therefore perturb the Nernst diffusion layer, even though the diffusion coefficient in water is somewhat higher.

Through rearrangement of Equation 4.33, the phase boundary concentration can be determined.

$$c_I' = c_{I,Bulk} + q([IL_n^{z_I}]'' - [IL_n^{z_I}]')$$

<div align="right">Equation 4.34</div>

The concentration at the phase boundary is determined by the sample's bulk concentration and the biases caused by the leaching process. At high bulk concentrations, the biases caused by the second term of Equation 4.34 are negligible. The high bulk concentration is one of the reasons internal filling solutions consisting of highly concentrated salts is employed in the traditional setup. When the bulk concentration is low, the second term has more of an influence and according to Equation 4.34, two things can be done to reduce the influence of the second term. Both the q and ($[IL_n^{z_I}]'' - [IL_n^{z_I}]'$) factors can be altered to reduce the influence of the bias.

The value of q can be determined via Equation 4.35 and can be altered through a number of ways which are discussed below.

$$q = \frac{D_{org}\delta_{aq}}{D_{aq}\delta_{org}}$$

<div align="right">Equation 4.35</div>

Altering the material properties of the membrane and therefore reducing the ionic diffusion coefficients (D_{org}) can reduce the value of q. This can be achieved by increasing the content of PVC [187] or utilizing alternative polymers [229, 230]. The ionophore may also be chemically bound to the polymer backbone reducing fluxes

[230-232]. Lipophilic particles have also been incorporated in membranes to reduce the uptake of ions by the membrane [233].

Varying the thickness of the diffusion layers can also change the value of q. Decreasing the thickness of the aqueous Nernst diffusion layer through vigorous stirring [187], flow through cells [187], rotating electrodes [234, 235] or a wall-jet system [236] have all improved the lower detection limit. The thickness of the membrane can also be increased to aid in detection limits, but comes at a cost of increasing response times [187].

Alternatively, the variance in the ion-ionophore complex concentrations at either side of the membrane should be minimised, or kept at the same value. The reduction in the concentration gradient, $[IL_n^{z_I}]'' - [IL_n^{z_I}]'$ across the membrane can be achieved through reducing the total concentration of ionic sites in the membrane (see Figure 4.10 (b)), or by partially exchanging the primary ion at the inner side of the membrane with an interfering ion (see Figure 4.10 (c)).

Reducing the total number of ionic sites decreases the maximum difference between the two sides of the membrane, therefore lowering the concentration gradient ($[IL_n^{z_I}]'' - [IL_n^{z_I}]'$), and subsequent release of primary ions into the Nernst diffusion layer [52].
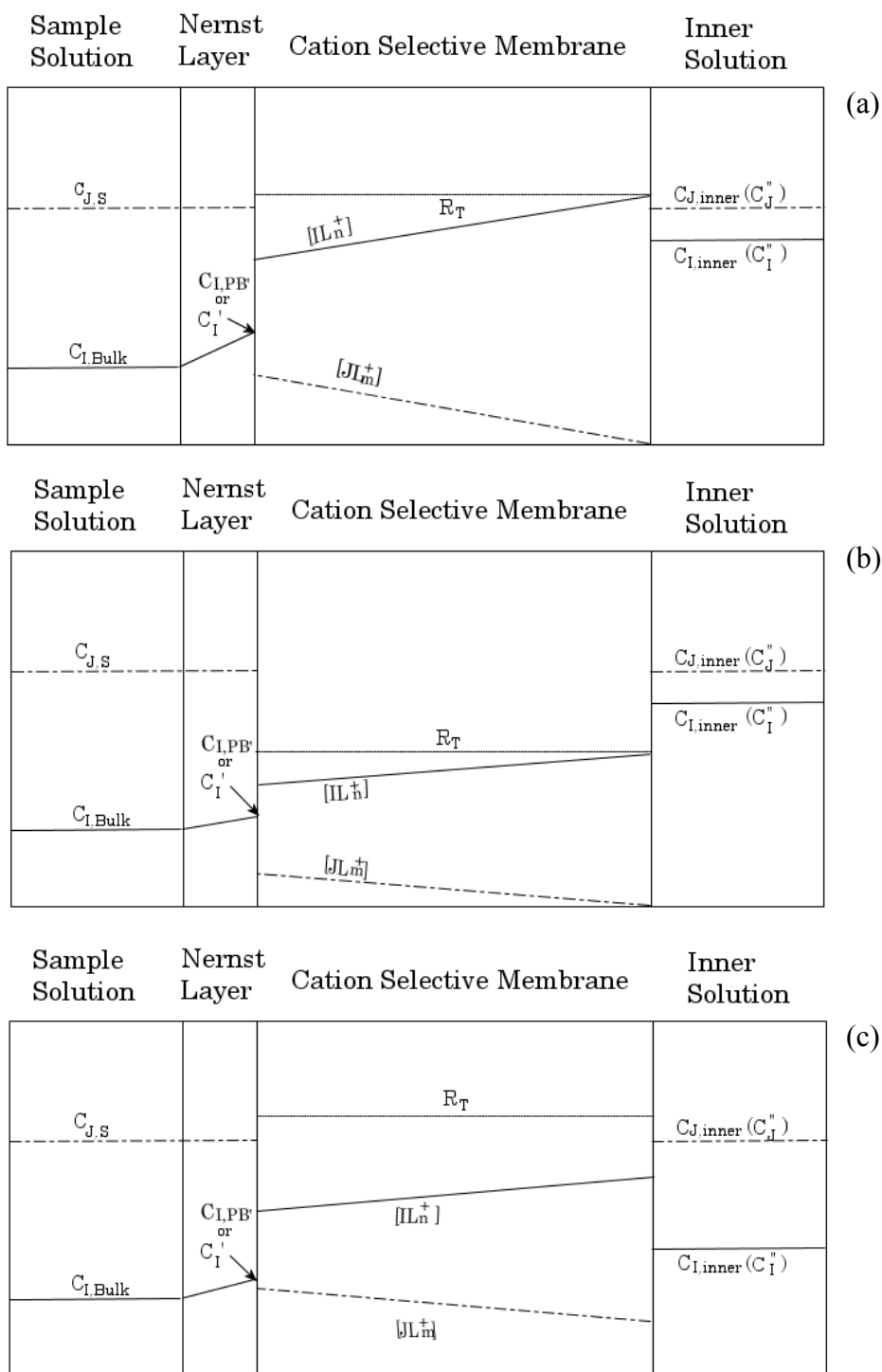
Figure 4.10: Concentration profiles of an ISE membrane showing the gradients of relevant species occurring in membranes with two different concentrations of ionic sites (a) and (b), and as a result of partial exchange on the inner side of the membrane (c). [208]

The concentration gradients in Figure 4.10 (c) are achieved by varying the concentration of primary and interfering ions allowing for a level of exchange based on their selectivities in the membrane. The inner solution can be optimized so that the concentration of complexes on either side of the membrane are equal ($[IL_n^{z_I}]'' \cong [IL_n^{z_I}]'$) and zero ion fluxes result. This will prevent the release of ionic species into the sample as the system experiences little or no movement of ions. The inner filling solution should consist of an interfering ionic species capable of partially exchanging with the primary ion in the membrane. The level of exchange between the membrane and aqueous phases can be calculated by knowing the concentrations and selectivities of the various ions. The optimal level of exchange occurs when both sides of the membrane have equal concentrations of ion complexes.

An electrochemical alternative to adjusting the inner filling solution of an ISE to obtain a minimal concentration gradient, is to apply a few nanoamperes of galvanostatic current through the cell [237, 238]. The flux of ions is controlled through the application of a small current, which prevents the release of primary ions into the sample and allows detection limits down to picomolar levels [237]. A hypothetical concentration profile where currents are used to control the ion fluxes is shown in Figure 4.11. In this scenario, the current is assigned a negative value when the diffusion of ions is directed towards the inner filling solution, and positive when it is directed towards the sample solution [237]. It is also assumed that the applied current does not affect the Nernstian equilibrium at the membrane/sample interface.
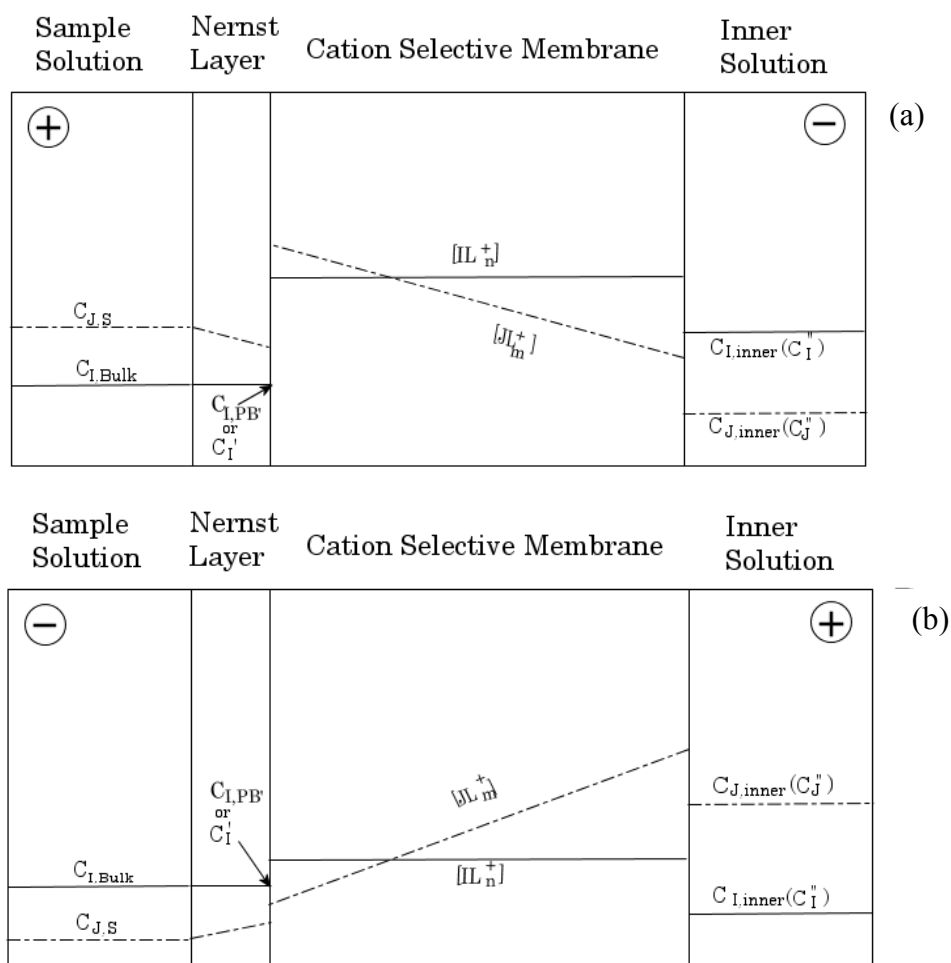
Figure 4.11: Schematic showing the concentration gradients present in a membrane exposed to a small negative (a) and positive (b) current. [237]

Unfortunately, in order to obtain minimal concentration gradients, the inner filling solution or applied galvanostatic current needs to be carefully chosen to match the sample. This can be difficult in practical situations where samples can vary significantly, making it almost impossible to predict appropriate concentrations and currents. Due to these complexities, controlling fluxes through ion-exchange is discussed further and the galvanostatic control has been avoided. More information into the control of ion fluxes through current polarization can be found in the literature [237-241].

If the level of exchange on the inner side of the membrane is below that of the optimal value, $([IL_n^{z_I}]'' > [IL_n^{z_I}]')$, then a concentration gradient can still exist (see

Figure 4.12 (a)), leading to primary ion leaching and higher limits of detection (Figure 4.12 (b)).
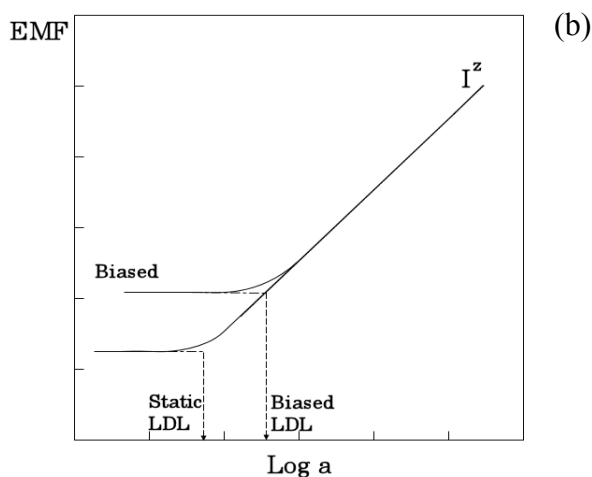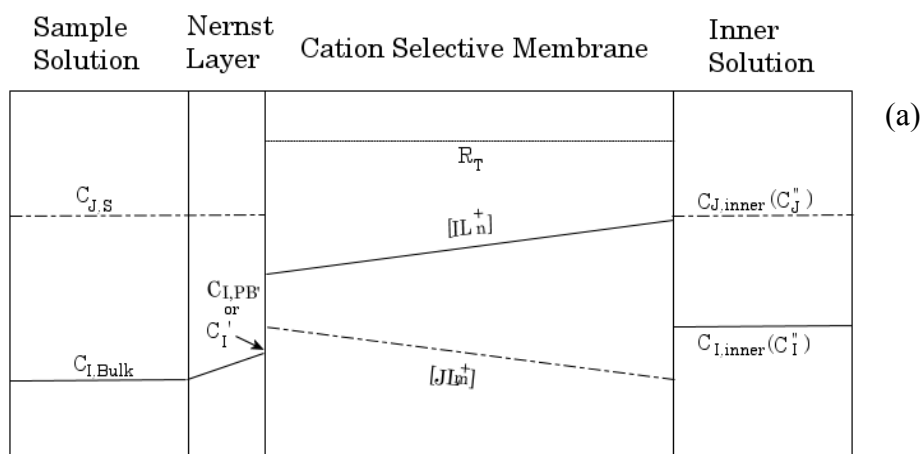
Figure 4.12: Schematic representation of concentration profiles showing a less than optimal partial extraction on the inner membrane side ($[IL_n^{z_I}]'' > [IL_n^{z_I}]'$) (a) leading to the biased detection limit in the response curve (b). [221]

On the other hand, if the level of partial exchange of the primary ion at the inner membrane side is higher than the optimal level ($[IL_n^{z_I}]'' < [IL_n^{z_I}]'$), then the reverse of Figure 4.12 is observed and an inward flux of primary ions occurs (Figure 4.13 (a)). This leads to a depletion of the primary ion at the sensed Nernst layer, compared to the bulk sample concentration. The depletion is observed as a lower than expected EMF at the relevant bulk concentration in the response curve (Figure 4.13 (b)). The depletion at the membrane/sample interface only becomes prevalent below a certain sample bulk concentration $c_{I,bulk}$. Above this level, the electrode behaves according to

the Nernst equation. The level of primary ion exchange at the membrane/filling solution interface dictates the magnitude of the super-Nernstian response.
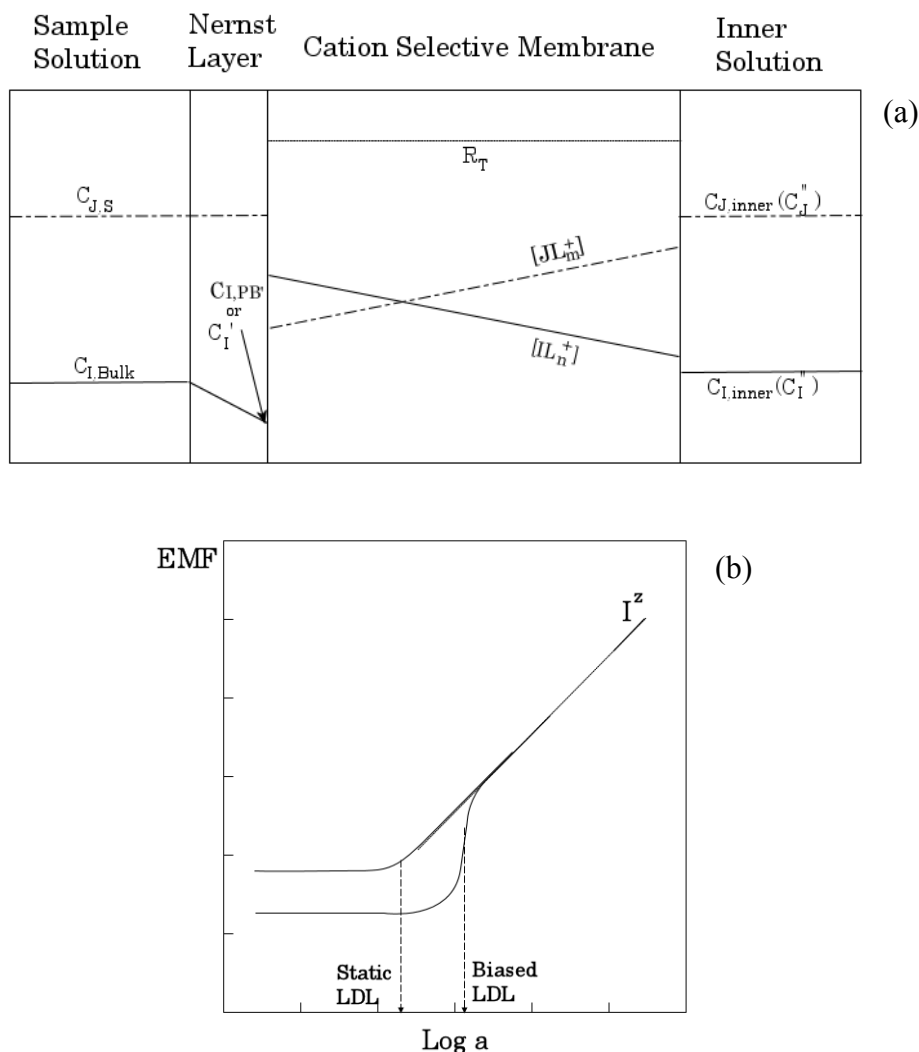
Figure 4.13: Schematic representation of concentration profiles showing a greater than optimal partial extraction on the inner membrane side ($[IL_n^{z_I}]'' < [IL_n^{z_I}]'$) (a) leading to the super-Nernstian step in the response curve (b). [221]

This is where the new function for determining the limit of detection, discussed in Section 4.1.2, becomes important. Under the IUPAC recommendations, the detection limits observed in electrodes experiencing super-Nernstian steps are exceptional. However, electrodes experiencing these steps are of limited practical use in low concentrations, as a result of the shifted potential away from the standard linear response. The new formalism discussed in reference [208] states that the limit of detection is where the measured potential of the bulk concentration deviates in either

direction by more than (RT/z_lF) ln 2 from the ideal Nernstian response. Electrodes showing a slight super-Nernstian response can be within these limits allowing for lower detection limits by many orders of magnitude. Even though super-Nerstian steps are of little practical use in routine calibrations and measurements, two beneficial uses have been found. One such application is the use of two super-Nernstian electrodes, each having a potential drop occurring at different concentrations, in determining ion concentrations with high sensitivity [242]. Electrodes that exhibit a super-Nernstian step can also be used in determining unbiased selectivity coefficients, as there is no release of primary ions into the sample to perturb the response [224].

The response function can be predicted for various levels of primary ion exchange based on selectivities, and inner filling solution concentrations. The useful measuring range determined from the linear region of the calibration graph, changes significantly from the optimal level of ion-exchange to the poorest experienced for both low and excessive levels of exchange at the inner membrane interface, as shown in Figure 4.14 [208, 243].
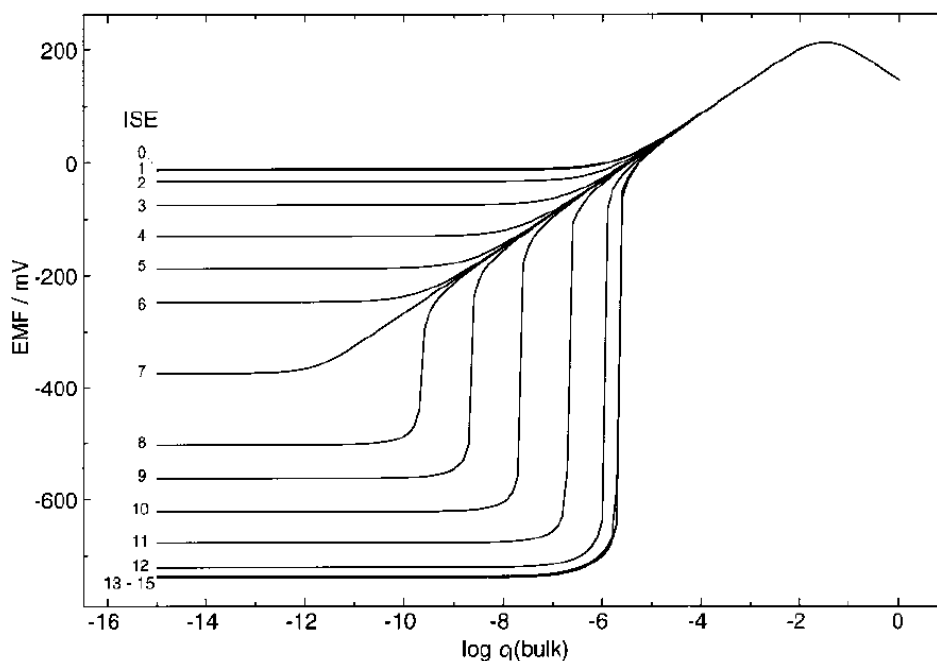
Figure 4.14: Calculated EMF response curves for a series of ISEs with each having different concentrations of primary ion in the inner filling solution. The curves are labelled with the negative logarithm of the primary ion concentration. Picture taken from [208].

If the primary ion complex in the membrane is strong (high stability constant) then the concentration of uncomplexed ionophore is constant. The ionophore is present in large excess compared to the ion-exchanger and a change in concentration of the complex is always proportional to a change in concentration of free primary ion within the membrane. The concentration of the complex in a membrane without interference from coextraction and a stoichiometry of 1:1 is equal to the ion-exchanger R$_T$, $[IL_n^{z_I^+}] = R_T/z_I$. The membrane potential can therefore be written as;

$$E_M = E_I^0 + \frac{RT}{z_I F} \ln \frac{R_T}{z_I} + \frac{RT}{z_I F} \ln \frac{c_I}{[IL_n^{z_I^+}]}$$

Equation 4.36

Combining Equation 4.36 with 4.18, the relationship between membrane selectivity and phase boundary concentrations can be made, via Equation 4.37.

$$\frac{c_{I,PB}}{[IL_n^{z_I}]''} = \frac{z_I}{R_T}\left[\frac{1}{2}\sum_{i(1)} K_{Ii(1)}^{pot\ 1/z_I} c_{i(1),S} + \sqrt{\left(\frac{1}{2}\sum_{i(1)} K_{Ii(1)}^{pot\ 1/z_I} c_{i(1),S}\right)^2 + \sum_{i(2)} K_{Ii(2)}^{pot\ 2/z_I} c_{i(2),S}}\right]^{z_I}$$

Equation 4.37

The concentration of primary ion complex $[IL_n^{z_I}]''$ on the inner side of the membrane can be calculated by using $c_{I,PB} = c_{I,Bulk}$. The concentration at the phase boundary ($c_{I,PB}$) is equal to the bulk primary ion concentration ($c_{I,Bulk}$), due to the high total primary ion concentration at the inner solution.

Equation 4.36 can also be applied to the sample membrane interface, and by combining it with Equation 4.32, the phase boundary concentration of the primary ion can be calculated as a function of q, (see Equation 4.38).

$$c_I = \frac{1}{2}\left(c_{I,bulk} - \sum K_{IJ}^{pot} c_J + [IL_n^{z_I^+}]'q - \frac{qR_T}{z_I} + \left(\left(c_{I,bulk} - \sum K_{IJ}^{pot} c_J + [IL_n^{z_I^+}]'q - \frac{qR_T}{z_I}\right)^2 + \left(4\sum K_{IJ}^{pot} c_J \left([IL_n^{z_I^+}]'q + c_{I,bulk}\right)\right)\right)^{1/2}\right)$$

Equation 4.38

The calculated phase boundary concentration ($c_{I,PB}$) can now be inserted into Equation 4.18 in the place of bulk primary ion concentration ($c_{I,Bulk}$), and used to predict the theoretical response function for a given ionic background concentration. Considering that the inner concentration of the complex is fixed $[IL_n^{z_I}]''$, the combined equations of 4.18 and 4.38 simplify to Equation 4.39.

$$E = E_I^0 + \frac{RT}{z_I F}\ln\left(\frac{1}{2}\left(c_{I,bulk} + \sum K_{IJ}^{pot}c_J\right) + \frac{1}{2}\left(\left(c_{I,bulk} - \sum K_{IJ}^{pot}c_J\right)^2 + 4\sum K_{IJ}^{pot}c_J\left(q\frac{R_T}{z_I} + c_{I,bulk}\right)\right)^{1/2}\right)$$

Equation 4.39

Since the bulk concentration at the detection limit is theoretically zero ($c_{I,Bulk} = 0$), Equation 4.39 can be simplified to:

$$E = E_I^0 + \frac{RT}{z_I F}\ln\left(\frac{1}{2}\sum K_{IJ}^{pot}c_J + \frac{1}{2}\left(\left(\sum K_{IJ}^{pot}c_J\right)^2 + \frac{qR_T}{z_I}4\sum K_{IJ}^{pot}c_J\right)^{1/2}\right) \quad \text{Equation 4.40}$$

The logarithmic detection limit can now be determined by the log term in Equation 4.40.

$$\log c_I(DL) = \log\left(\frac{1}{2}\sum K_{IJ}^{pot}c_J + \frac{1}{2}\left(\left(\sum K_{IJ}^{pot}c_J\right)^2 + \frac{qR_T}{z_I}4\sum K_{IJ}^{pot}c_J\right)^{1/2}\right) \text{Equation 4.41}$$

If ion fluxes in the system are not relevant ($4\frac{qR_T}{z_I} << K_{IJ}^{pot}$), then Equation 4.41 reduces to the static detection limit in Equation 4.19. If, however, the fluxes are significant ($4\frac{qR_T}{z_I} >> K_{IJ}^{pot}$), then Equation 4.41 simplifies to,

$$\log c_I(DL) = \frac{1}{2}\log\left(\frac{qR_T}{z_I}\sum K_{IJ}^{pot}c_J\right)$$

Equation 4.42

Alternatively Equation 4.43 can be used for other charge combinations [220].

$$\log c_I(DL) = \left(\frac{1}{2} + (z_J - z_I)\frac{1}{6}\right)\log\left(\left(\frac{qR_T}{z_I}\right)^{z_I/z_J} \sum K_{IJ}^{pot} c_J^{z_I/z_J}\right)$$

<div align="right">Equation 4.43</div>

Even though detection limits can be theoretically predicted from the above equations, experimental results are often inferior to these as a consequence of the assumptions made to keep the model simple. They do, however, provide an insight into the response mechanisms of membrane electrodes, which is beneficial to experimental design.

4.4.   Determination of the Response Towards Thallium(I)

4.4.1.   Calibration and Detection Limits

The analysis of heavy metals in the environment is extremely important due to their toxic nature and the potential for harm to both plants and animals. Thallium is often overlooked as a potential threat to human health due to its limited use in today's society. However, thallium still has the potential to cause adverse health effects especially in areas of zinc and lead smelting, coal burning, and may also feature in homicide cases. As thallium is odorless and tasteless it was successfully used as a poison, but has now been banned in many western countries. In spite of this, both intentional and unintentional poisonings still occur today and, since chronic thallium uptake mimics other diseases, it is often diagnosed too late [244]. An inexpensive and quick analysis of thallium in the clinical and environmental fields would be beneficial.

Calixarene (1)   R = *t*-butyl
Calixarene (2)   R = H

Calixarene (3)   R = *t*-butyl
Calixarene (4)   R = H
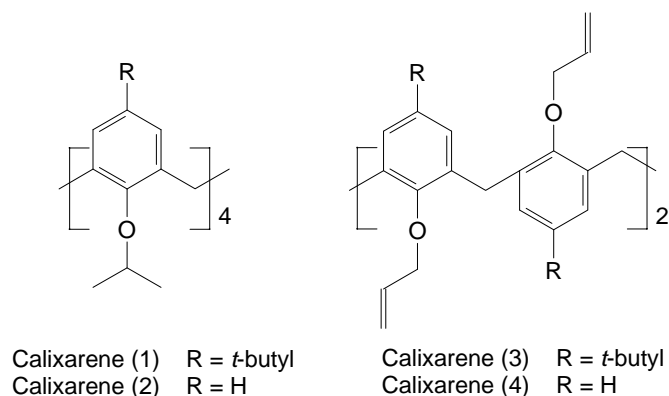
Figure 4.15. Structures of the calixarenes used in this chapter.

Of the five calixarenes synthesized for use as thallium ionophores, only three are of practical use in plasticized PVC membranes. Calixarene (2) crystallised in the membrane, rendering it useless as an ionophore. The ion-selective electrode membrane is essentially a supported liquid membrane in which the ionophore and anion-exchanger are able to freely move and form complexes with a target ion. Once the ligand is bound within a crystal lattice, it is prevented from complexing with ions. The response observed with this membrane would be the result of uncomplexed ions or from impurities dispersed within the polymer matrix. A Nernstian response may still be observed for a given ion, as long as the concentration of the ion within the membrane is kept constant. However, the selectivity of the membrane will follow the lipophilicity of the ions within the membrane (i.e., the Hoffmeister series) and will not be dictated by the formation of a complex between the ion and the calixarene. This would be impractical due to the membrane being relatively unselective.

As a consequence of the low solubility of the synthesized calixarene (2), only three out of a potential five thallium ionophores were tested. One of the criteria of a successful ionophore is that it requires significantly large or numerous lipophilic groups for it to remain in the membrane phase and not leach into the sample or form crystals within the membrane. This is the crucial difference between calixarenes (1) and (2), which have very similar structures but differ in the number of lipophilic groups attached to the main binding site. Calixarene (1) has four *tert*-butyl groups at the para position which make it more soluble in the plasticized PVC than the similar calixarene (2) without the *tert*-butyl groups. The solubility of calixarene (2) could be

improved possibly by attaching additional functional groups to areas which would not affect the binding of the compound. This could be achieved by attaching longer chains to the isopropyl group on the lower rim, or by groups other than *tert*-butyl on the upper rim, such as di-allyl or propyl, which are presumed not to interfere significantly with the complexing mechanism of the present calixarenes with thallium.

Solubility issues with the 1,3-alternate calixarene (3) were also observed, with crystals appearing in some of the membranes, but not others. The crystals were first observed in a membrane which used 2-fluoro-2′-nitrodiphenyl ether (FNDPE) as the plasticizer. FNDPE was initially used as a plasticizer so that a comparison could be made against similar calixarenes produced by Kimura et. al. [88]. Since selectivities can shift depending on the plasticizer used [47], it was decided to keep all variables constant if a comparison was to be made in a vast range of trials. However the FNDPE membrane that crystallised contained a relatively large concentration of calixarene, and this could be prevented by reducing the amount of ionophore. It was decided to change the plasticizer to one that is more commonly used e.g. Bis(2-ethylhexyl) sebacate (DOS) or 2-nitrophenyl octyl ether (o-NOPE), which would allow for a wider comparison with other ionophores. Even with the use of DOS and o-NOPE as plasticizers, crystals were still apparent on several occasions.

It does appear unusual that in the 1,3-alternate calixarenes (3) and (4), the solubility trend is the opposite of that observed in the cone conformer calixarenes (1) and (2). This could be due to many factors that are outside the scope of this thesis. However, it does seem unusual that the calixarene with the higher degree of lipophilic functionalities crystallizes more readily than the one with fewer groups. As a result of the limitied solubility of calixarene (3), only specific tests were carried out. The limited solubility of calixarenes (2) and (3) resulted in most of the tests being carried out on calixarenes (1) and (4).

The response curves of calixarenes (1), (3) and (4) incorporated into plasticized PVC membranes and assembled in the conventional setup (Figure 4.1) are presented in Figure 4.16.
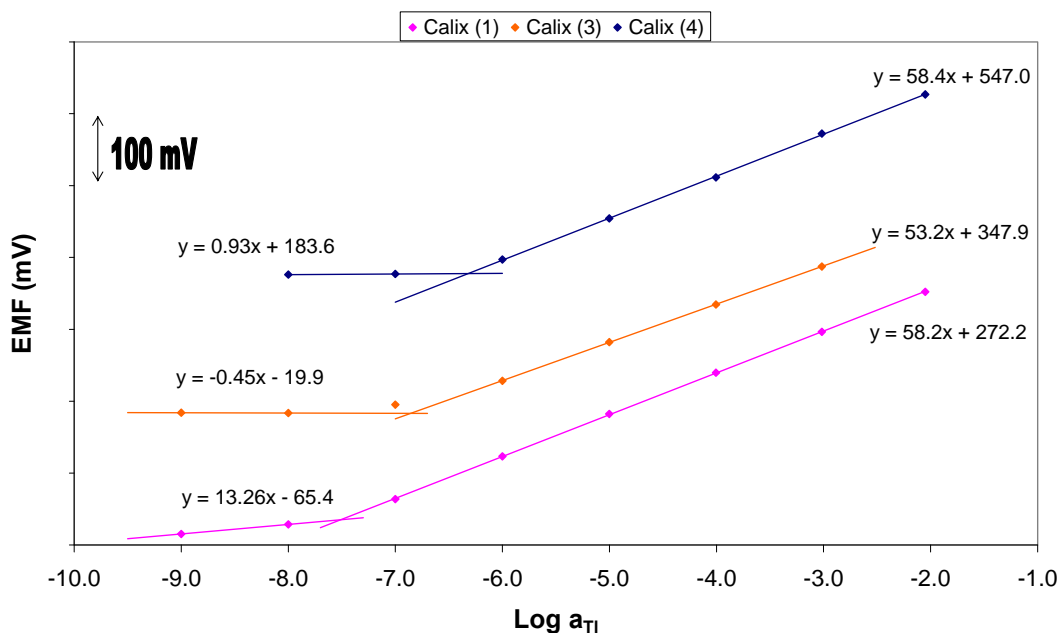
Figure 4.16: Calibration Curves of calixarenes (1), (3) and (4) with thallium(I) using the traditional ISE setup with a high concentration of thallium salt in the inner solution. The electrodes E^0 values have been offset for clarity.

The thallium(I) selective electrodes based on calixarenes (1), (3) and (4) show a Nernst response to changes in activity of Tl^+ over the concentration range of 1×10^{-1} to 4.7×10^{-7} M. The upper detection limit has not been displayed in Figure 4.16, as it often occurs between 10^{-2} and 10^{-1} M a consequence of co-extraction (Donnan failure), see Sections 4.1.2 and 4.2 of this Chapter. Most often, the upper limit of detection is of little concern in ISEs and analytical chemistry. It is only a concern in samples of high primary ion concentration and may be circumvented by sample dilution.

The response of around 59 mV decade^{-1} demonstrates that these membranes, incorporating the relevant calixarenes, behaves ideally according to the Nernst equation. The lower response of Calixarene (3) could be due to either the membrane loosing its permselectivity at high thallium(I) concentrations or the presence of impurities which elevate the potential at low thallium concentrations. Further tests would determine the exact cause of the lower response. To prove that the response is directly related to the complexation of thallium(I) with the calixarene, a membrane should be prepared from non-commercial polymers and plasticizer. The low level of

impurities found in commercial polymers and plasticizers can act as ion sites, thereby producing a Nernst response in membranes that do not contain any ionophore [28, 47]. By removing any chance of obtaining a Nernst response as a result of impurities, one would be able to determine if the response is a direct result of the ionophore (calixarene) complexation. Manufacturing of plasticizers and PVC is impractical, both from a cost and time perspective, and other tests can be used to determine if the ionophore is complexing with the primary ion. Testing the selectivity and complex formation constant of the ionophore can determine whether the response is due to the ionophore or impurities, and is discussed later in this Chapter. The lower limits of detection for thallium(I), determined using the intersections of the linear regions of the response curves and at the location along the response curve deviating by more than 17.8 mV in Figure 4.16, are displayed in Table 4.1.

Table 4.1: Response towards thallium(I) and lower detection limits of calixarenes (1), (3) and (4) with the traditional ISE setup.

	Slope mV decade^{-1}	LDL (IUPAC.)		LDL (new definition)	
		Log a_i	Concentration x 10^{-7} M	Log a_i	Concentration x 10^{-7} M
Calixarene 1	58.18	-7.52	0.31	~ -7.82	0.15
Calixarene 3	53.20	-6.85	1.41	~ -6.90	1.25
Calixarene 4	58.42	-6.32	4.76	~ -6.45	3.57

Table 4.1 shows the lower detection limits of the Tl^+ sensors calculated via two separate methods. IUPAC states that the LDL of ISEs occurs at the point of intersection of two linear regions of the calibration graph. The new definition states that the LDL occurs when the potential differs by more than (RT/z_IF) ln 2 from the upper linear region of the calibration graph and is required when a super-Nernst response is observed. The two definitions are almost equal for electrodes that behave ideally according to the Nernst equation. The LDL based on the new definition is only an estimate as it occurred between two points on the calibration graph.

The lower detection limits displayed in Table 4.1 are characteristic for ISEs with a conventional electrode design, incorporating an inner filling solution of a highly concentrated primary ion. The LDL is a result of primary ion leaching from the membrane into the sample solution, or more precisely the Nernst diffusion layer on

the sample side of the membrane, and therefore perturbing the sensor response [220, 223]. Since the electrode responds to changes in the activity at the membrane/solution phase boundary, even the release of a minute fraction of ions from the membrane is enough to alter the EMF in dilute solutions. The response at low primary ion concentrations is governed solely by primary ion-release, which is why a constant potential is achieved at these low activities. Even though ISE measurements are carried out under near zero-current conditions, ions from the highly concentrated inner filling solution can migrate outwards into the sample. Zero-current conditions are maintained by the simultaneous incorporation of an interfering ion from the sample into the membrane and subsequent flux in the opposite direction, (see Figure 4.9). The samples prepared for the calibration graphs in Figure 4.16 only contained the primary ion salt and therefore the interfering ion, which moves in the opposite direction to that of the primary ion, would have to be that of H^+ from water. The processes responsible for the LDLs displayed in Table 4.1, are co-extraction, ion-exchange and diffusion, which were discussed in Section 4.2 of this Chapter.

The lower detection limit of calixarene (4) may be slightly better than expressed here as a severe upward drift was observed in low thallium(I) concentrations as a consequence of the reference electrolyte leaching into the sample and being detected. The reference electrolyte was changed to lithium acetate for the remainder of the electrode tests in order to prevent further interferences. The change to lithium acetate as the reference electrolyte alleviated the upward drift caused at low analyte concentrations.

Until recently, the LDL displayed in Table 4.1 was thought to be an optimum level achievable with these devices, and often led to the limited use of ISEs in analytical chemistry. However, now that the processes responsible for these LDL are understood, techniques have been developed to counteract them and have allowed a reduction in LDLs for a range of analytes. The reduction in the detection limits are discussed later in this Chapter.

4.4.2. Response Times

All calibrations were conducted with solutions starting from the most concentrated to the least concentrated. The response time trace for one of the calixarenes is shown in Figure 4.17. The other two calixarenes show similar trends and are not displayed. The potential was said to be stable if it did not change by more than 1 mV over 60 seconds.
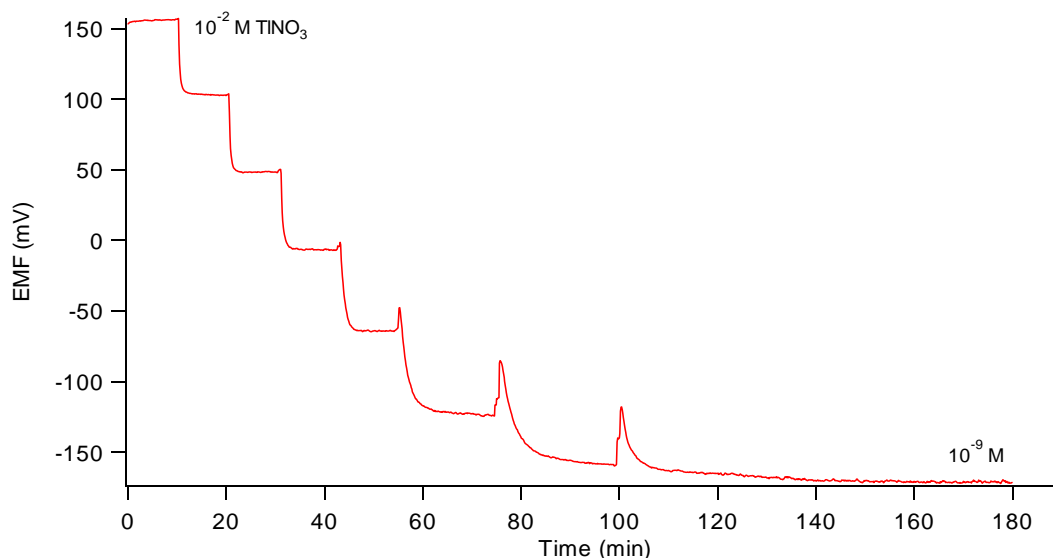
Figure 4.17: Response of a liquid contact electrode incorporating calixarene (1) as the ionophore in the membrane.

The time taken for the potential to stabilise in high concentrations was in the order of seconds, while at lower concentrations it took considerably longer. Short response times are desirable in applications where there is a high sample throughput. In the case of thallium detection, high sample throughputs are often not needed as poisonings and environmental spills are usually random and single events, and do not require the same analysis frequency as say potassium analyses in surgery. A relatively quick determination is still beneficial in analytical chemistry.

4.5. Determination of the Complex Formation Constants

The determination of the complex formation constant between an ionophore and an ion can be achieved through a variety of methods. Since binding constants can be

affected by the solvent, it was decided that the best method of assessing the ionophore/ion complex was in the membrane itself [245]. A method recently developed by Russian researchers and refined by the Bakker group, allows complex formation constants to be determined in a membrane medium [245]. The in-situ measurements are carried out with two membranes, one with and one without ionophore, pressed together. The results of several calixarene complex formation constants are displayed in Table 4.2. The experimental setup was validated with a sodium selective calixarene that has been tested previously with this method. A good correlation between the literature value (7.60 ± 0.08 [245]) and the experimental value (7.89 ± 0.1) shows that the experimental setup is satisfactory.

Table 4.2: Complex formation constants of calixarenes (1) and (4) with thallium and sodium, and a sodium selective calixarene with sodium. Values were determined via the sandwich membrane technique.

	Ionophore L_T (mmol kg^{-1})	Anionic sites R_T (mmol kg^{-1})	Membrane Potential ΔEMF (mV)	Formation Constant Log β_{ILn}
Calixarene (1) with Tl$^+$	12.36	5.93	251.3 ± 2	6.44 ± 0.04
Calixarene (4) with Tl$^+$ with Na$^+$	11.73 11.73	5.12 5.12	216.8 ± 3 3.97 ± 2	5.85 ± 0.05 2.24 ± 0.03
Na$^+$ Selective Calixarene	9.80	5.09	329.2 ± 6	7.89 ± 0.10

The potential difference is obtained by subtracting the potential of the membrane without ionophore from that of a two membrane system consisting of the membrane without ionophore pressed against one with ionophore. Both membranes are conditioned in solutions of the same concentration, and the potentials measured with identical concentrations as the conditioning solutions on either side of the membranes. Essentially, the objective of the two membrane system is to separate the phase boundary potentials, which result in a potential that is related to the activity ratio of the measuring ion on both parts of the membrane [245]. The large potential difference is expected if the free thallium concentration differs significantly between the two membranes, as a result of the binding characteristics of calixarenes (1) and (4), which are only present in one membrane [245]. The membrane species

eventually diffuse between both membranes, and the potential decreases back to that of the single membrane as a consequence of reaching equilibrium.

The calculations were conducted without considering ion-pairing, as it has been demonstrated that the response due to ion-pairing is minimal, since it is only the square-root of the ratio of the two ion-pair formation constants. The effect due to ion-pairing can be kept low by incorporating an inert lipophilic salt or using the largest of the anionic site additives, tetrakis-[3,5-bis(trifluoromethyl)phenyl]borate. The complex formation constants were calculated using Equation 4.44. The derivation of Equation 4.44 can be viewed in the literature [245].

$$Log\beta = \left(L_T - \frac{nR_T}{z_I} \right)^{-n} \exp\left(\frac{E_m z_I F}{RT} \right)$$

<div align="right">Equation 4.44</div>

The stoichiometry (n) of all the calixarenes is assumed to be 1, as has been confirmed for calixarene (4), using an NMR technique (see Section (3.6.2)), and the sodium calixarene from the literature are both 1. It is also reasonable to assume a 1:1 complex based on the calixarene's structure and the relevant binding sites.

The complex formation constants displayed in Table 4.2 demonstrate that the ligand is binding to the Tl^+ ion, and that the response is dictated by this complexation and not from membrane impurities. This demonstrates that the calibration graphs displayed in Figure 4.16 are directly related to the Tl^+/calixarene complex in the membrane and changes in the activity of the sample. The complex formation constant of calixarene (4) with Na^+ was also determined, so that an evaluation could be made of the strength of the thallium(I) binding, as opposed to a common interferent. The results show that this calixarene essentially forms no complex with sodium in the membrane. The potential increase of this calixarene in a sandwich membrane conditioned in NaCl is only 4 mV.

The complex formation constants observed by the current series of thallium binding calixarenes are somewhat lower than other calixarenes with various ions. Calixarenes such as 4-*tert*-butyl-calix[4]arene-tetrakis(N,N-dimethylthioacetamide), and tert-

butyl-calix[4]arene-tetraethyl ester show complex formation constants of 15.9 for Pb^{2+} and 7.9 for Na^+ respectively. The lower formation constants of the thallium calixarenes is a consequence of the weaker cation π-interactions, as opposed to the typically stronger coordination through sulfur, nitrogen and oxygen atoms [99]. Even though π-interactions towards soft metals are weaker, they are relatively selective, which is a vital requirement in ISEs. The stronger thallium binding of calixarene (1) (log β = 6.44) compared to that of (4) (log β = 5.85) is assumed to be a result of the two different structures. The binding sites of the calixarenes with thallium(I) were determined to be at the aromatic rings, in the hydrophobic cavity (see Section 3.6). Calixarene (1) is in the cone conformer, whereas calixarene (4) is in the 1,3-alternate conformation. The increased binding strength could be attributed to either the different conformations of the two compounds or the presence of the *tert*-butyl groups on the upper rim of calixarene (1).

4.6. Determination of the Ionophore Selectivity

A vital characteristic of an ISE is its selectivity towards the primary ion over interfering ions. The selectivity determines whether the sensor can be used in practical samples that may contain a vast range of cations, anions and organic ligands. Table 4.3 shows the selectivity coefficients, log $K_{I,J}^{pot}$, of calixarenes (1), (3) and (4) incorporated into PVC/DOS membranes. Included in Table 4.3 are the selectivity coefficients against thallium(I) of a membrane without ionophore.

The selectivity coefficients were determined via the separate solution method (SSM) where the membrane had not contacted the primary ion prior to the measurements. The membranes were conditioned in solutions containing only an interfering ion and the electrode's inner filling solution also contained an interfering ion. By not allowing the membrane to come into contact with the primary ion prior to the measurements, a more accurate determination of true selectivities of an ionophore can be made as a result of minimal ions being released into the sample. Initially, membranes were conditioned with the primary ion, which resulted in the release of these ions from the membrane into the sample and consequently perturbing the

response of highly discriminated ions. Since the membrane requires the incorporation of ions to establish a phase boundary potential, an interfering ion is chosen which will lead to minimal ion fluxes. The selectivity determinations are then carried out from the most discriminated ion to the primary ion. For the selectivity coefficients to be valid, a Nernstian response is a prerequisite for each ion. The response curves of all interfering ions tested for each of the membranes are displayed in Figure 4.18 to Figure 4.21.

Table 4.3: Potentiometric selectivity coefficients, log $K_{I,J}^{pot}$, obtained with DOS/PVC membranes, incorporating the ion exchanger NaTFPB and ionophores (1), (3) and (4).

Ion	NaTFPB	Calixarene (1)	Calixarene (3)	Calixarene (4)
Ag^+	-0.54	-1.26	-0.89	-1.16
$N(Et)_4^+$				-1.25
Cs^+	0.02	-3.03	-2.75	-2.17
NH_4^+	-0.47	-3.57	-3.20	-2.71
K^+	-0.17	-3.33	-3.13	-2.77
H^+	-0.61	-3.70	-3.62	-3.66
Na^+	-0.77	-3.64	-3.55	-3.74
Li^+	-1.07	-4.43	-3.93	-3.97
Pb^{2+}	-1.67	-4.84	-4.32	-4.52
Al^{3+}	-2.56	-5.84	-5.64	-5.62
Cd^{2+}	-3.14	-6.19	-5.83	-5.57
Cu^{2+}	-2.75	-5.89	-5.51	-5.81
Ba^{2+}	-3.01	-6.03	-5.90	-5.84
Ca^{2+}	-3.28	-5.93	-6.08	-6.01
Zn^{2+}	-3.40	-6.14	-6.16	-6.12

All mean selectivity determinations were carried out with a minimum of three electrodes, between the concentrations of 10^{-2} to 10^{-4} M, standard deviations: 0.01-0.5.

The response curves show that Nernstian behaviour is observed for all ions in the observed concentration ranges and the selectivity coefficients are not affected by biases [224]. This behaviour can only be observed for highly discriminated ions if the membrane has not previously been in contact with preferred ions. If the

membrane had come into contact with a preferred ion, then biases would have resulted in highly discriminated ions as a result of ion release into the sample. This was also observed when the reference electrode contained a bridge electrolyte of NH_4NO_3 resulting in significant electrode drift. The reference electrolyte had to be changed to a weak interfering ion, e.g. $LiCH_3COO$. Responses that deviated away from the ideal Nernstian values are a consequence of H^+ interferences with the calibrations. This was often observed for highly discriminated ions.

The trends observed in Figure 4.18 for a membrane in the absence of ionophore followed the Hofmeister series which is based on the lipophilicity of the ions in the membrane [25]. The PVC/DOS membranes which do not include any ionophore, still managed to produce a cationic Nernstian response as a consequence of ionic impurities, which act as ion sites [28, 47]. Thallium easily enters the lipophilic membrane, as it is one of the highest cations in the Hofmeister series and Figure 4.18. It is surrounded by cesium and potassium which have similar chemical properties [58].
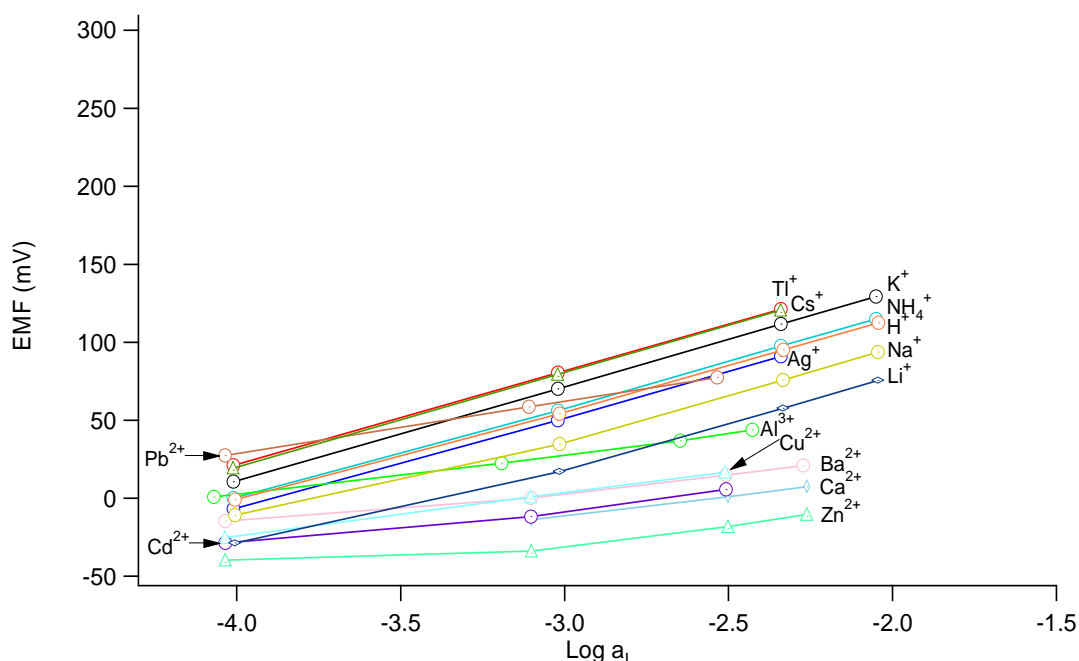
Figure 4.18: Selectivity response of the ISE membrane based on PVC/DOS incorporating NaTFPB but no ionophore.

When the calixarenes are incorporated into the membrane, the selectivity series order only changes slightly, however it differs in magnitude. For all ionophores, an increase in EMF is observed for the cations thallium and silver. An increase in EMF is also present with calixarene (4) for cations such as cesium, potassium and ammonium. The remainder of the cations follow the ion lipophilicity, which could be attributed to the membrane impurities dictating the EMF response and not that of the ionophore. Since the thallium complexes are not very strong due to the moderate binding capabilities of π-interactions, a large difference for the primary ion, is not observed between the potential of the membrane with and without ionophore [246]. This lack in potential change could explain the higher than expected selectivity of highly discriminated ions, for example, a potential is observed for sodium which has a complex formation constant of almost 0 determined through the sandwich membrane technique. If a membrane contained the ionophore and no impurity sites then a Nernstian response would not be observed for this membrane when exposed to changes in Na^+ activity. The actual selectivity of highly discriminated ions such as Ca^{2+}, Zn^{2+}, Al^{3+}, and Cd^{2+}, may be better by many orders of magnitude if the impurity sites could be removed, or the membrane lipophilicity altered. Ionophores which have greater potential differences between the primary and interfering ions can show selectivities log $K_{I,J}^{pot}$ down to -9/-10 .
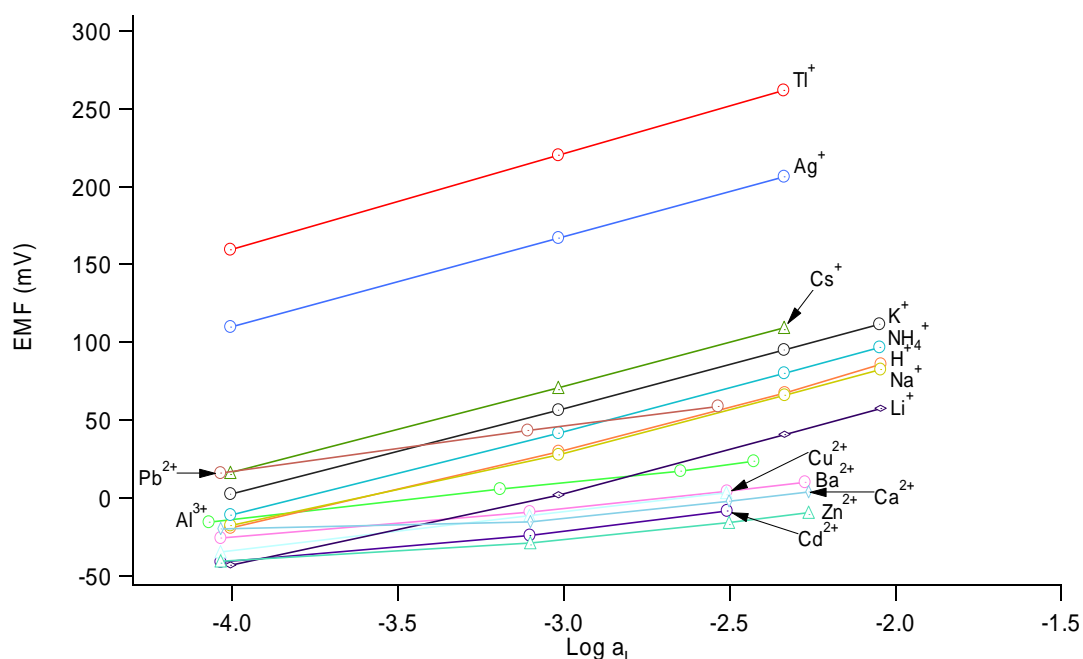
Figure 4.19: Selectivity response of the ISE membrane based on PVC/DOS incorporating NaTFPB and calixarene (1)

Silver is a common interferent with all of the above calixarene ionophores, as it also exhibits π-bonding through the aromatic cavity. The selectivity is better for thallium, as the ionic radius for silver is smaller (115 pm as opposed to 150 pm) and therefore the distance between the aromatic rings and the silver ion is greater, leading to a weaker interaction [193]. The slightly higher thallium selectivity of calixarene (1) over silver may be the result of the presence of an additional two aromatic units at the binding site. For the desired applications of environmental monitoring, silver is not such a significant interferent, with mean soil concentrations of <0.01 to 5 ppm with an average of 0.1 ppm and average water concentrations of 0.2 ppb (fresh water), and 0.25 ppb (salt water) [247].
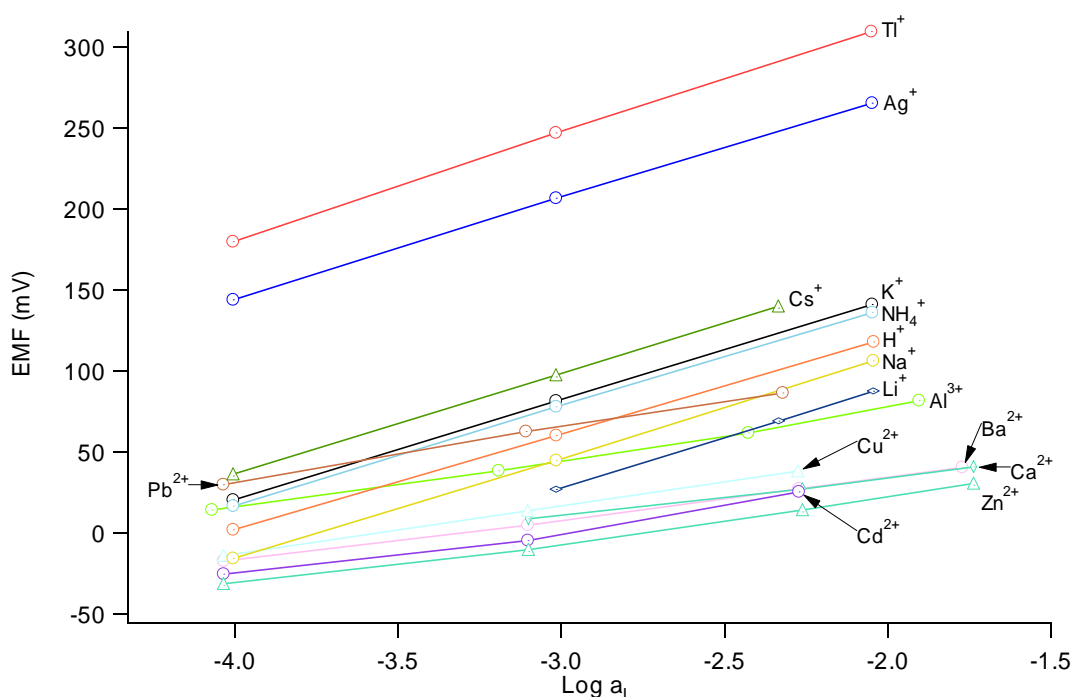
Figure 4.20: Selectivity response of the ISE membrane based on PVC/DOS incorporating NaTFPB and calixarene (3)

Calixarene (4) experiences a reduced selectivity for K^+, Cs^+ and NH_4^+, compared to the other ionophores. This trend has also been observed in solvent extraction data where the 1,3-alternate calixarene extracted potassium picrate into an organic solvent [156]. The increased binding of these ions may be a consequence of the inverted aromatic rings, which brings oxygen atoms into close proximity of the binding site. The same trend is lacking in the other 1,3-alternate calixarene (3), which could be a consequence of the bulky *tert*-butyl groups hindering the binding site.
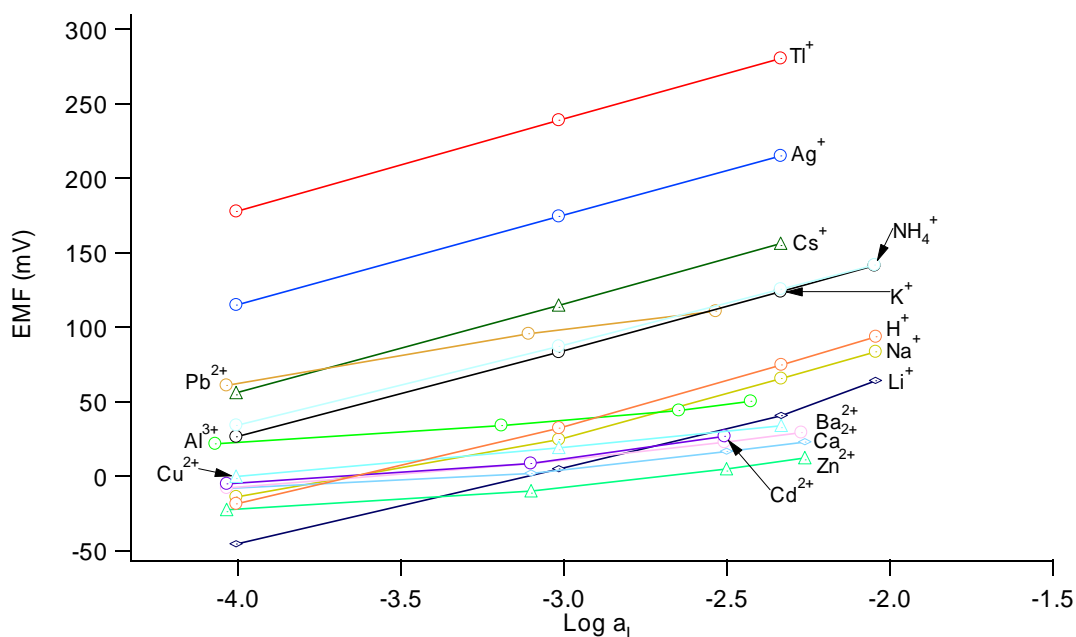
Figure 4.21: Selectivity response of the ISE membrane based on PVC/DOS incorporating NaTFPB and calixarene (4)

The three synthesized calixarenes exhibit alkali selectivities that are comparable to or far better than other compounds trialed in the literature [76, 77, 80, 82, 83, 87, 92, 94-96, 248]. The alkaline earth and transition metal selectivities presented above are also far superior to values presented in the literature. The enhanced selectivity could be due to two reasons; a) the lack of significant binding groups in the above calixarenes, which excludes a vast range of ions that could complex, or b) the new method of determining selectivity coefficients, which removes biases from the leaching of the primary ion into the sample.

The compounds tested as thallium(I) ionophores in the literature consisted of sulfur containing macrocycles, crown ethers, a complex indeno pyran compound and thallium(I) salts of O,O'-didecyl dithiophosphate or hetropoly acids to name a few, which contain a vast range of significant binding sites, not only for thallium, but also for other metals.

However, it was found that the selectivity of alkali metals for the above series of calixarenes was inferior to similar calixarenes reported in the literature [88, 91, 99,

246]. The selectivity coefficients for most of the similar derivatives were conducted in membranes which used FNDPE as the plasticizer. To allow for a greater comparison between other ionophores, it was decided to change the plasticizer to DOS, as it is a more common and well known plasticizer.

An attempt to improve the thallium(I) selectivity by increasing the cavity size was reported by Katsu, T. et. al. [91], and an improvement for thallium over silver was observed. However, the lower rim substituents consisted of esters, which are known to be hard-donor sites and consequently suffered from alkali and alkaline earth metal interferences. An attempt was made to produce a similar sized calixarene where iso-propyl groups were attached to the lower rim instead of the ester groups. The desired compound was synthesized but unfortunately calixarene (5) did not make it to the ISE testing stages as time constraints prevented this. Apart from the slightly diminished alkali selectivity of the above ionophores over similar derivatives, they did show an improved selectivity for the alkaline earth and transition metals. The discrimination over the alkali metals is good, but enhanced selectivity is desirable, if they are to be used in clinical analyses where these ions are in high concentrations.

4.7. Lowering the Detection Limit of Polymeric ISEs Incorporating Calixarenes for Thallium(I) Analysis.

In addition to ionophore selectivity, the lower detection limit of polymeric ISEs is another very important factor in the applicability of these sensors. Traditionally, ISEs exhibit detection limits in the micromolar range and were thought to be of limited practical use, especially in the monitoring of trace levels in environmental and clinical samples [201, 224]. It was initially thought that the solvent polymeric membrane had no influence on the sample composition, and that the phase boundary at the membrane and solution resembled that of the bulk sample, even though it had been known for decades to differ in solid-state and liquid membranes [243, 249]. Over the last decade, however, the response of polymeric membranes and the mechanism behind the response has been better understood.

It is now well documented that the response of traditional ISEs at low analyte concentrations is affected by ion-fluxes within the membrane. These ion-fluxes not only affect the selectivities, but also perturb the sensor's lower detection limit. In the presence of these ion fluxes, the primary ion concentration in the Nernst diffusion layer deviates from that of the bulk, which is displayed as a higher or lower than expected phase boundary potential depending on the direction of the ion flux [237]. Ion fluxes in the direction of the sample cause an increase in the concentration of primary ions in the phase boundary layer of the sample and a concomitant sub-Nernstian response, whilst an inward flux results in the depletion of the primary ion in this region and an apparent super-Nernstian response. Primary ion release into the sample, as a consequence of co-extraction, ion-exchange and diffusion (see section 4.2), results in higher than expected detection limits and selectivities. Since membranes contain about 10 mM of analyte ions, it only takes a minute fraction of these ions to be released into the phase boundary to affect the response. A series of methods have been established to reduce these detrimental ion-fluxes, which has led to a reduction in the detection limits of a variety of ionophores.

The changes in experimental setup has led to a reduction in detection limits of a series of cations including Ca^{2+} [224], Ag^+ [220], Cd^{2+} [212], Pb^{2+} [250], K^+ [219], Cu^{2+} [251] and NH_4^+ [219]. In an attempt to reduce the detection limit of the current series of thallium(I) selective calixarene ionophores, several of these methods have been attempted. Once the ion fluxes are controlled, the lower detection limit is determined by the ion-exchange selectivity of the membrane. The detection limits of thallium(I) ISEs in the literature, which use the traditional electrode setup, all lie in the micromolar range [76, 83, 88, 91, 92, 95, 98].

The urine thallium concentration, determined by ICP-MS, of two poisoned victims five days after a poisoning event were 7.1×10^{-5} M and 5.6×10^{-5} M, which is bordering on the limit of detection of traditional ISEs, and is also significantly higher than the background levels of thallium in urine of 0 to 5×10^{-8} M [72]. The same victims' blood levels were determined to be 1×10^{-5} M and 4.7×10^{-6} M respectively, also bordering on the detection limits. Upon treatment, the victims thallium concentrations in both urine and blood decreased significantly, 455 ng/g down to 4.7 ng/g in blood over a period of two months [72].

The monitoring of thallium in environmental samples would be inherently more difficult than in poisoning victims due to the ultra low concentrations. Thallium levels in streams near Zn-Pb metal smelting plants have been reported at concentrations between 16 nM and 0.8 nM, which is very much beyond the above series of thallium ISEs [56]. If environmental and clinical measurements are to be carried out using ISEs then the current limit of detection has to be significantly lowered to nano-molar levels or less. In the following sections, attempts have been made to reduce the detection limit of the thallium(I) ISE by addressing the concentration gradients and ion fluxes through techniques previously tested with other cations.

4.7.1.   Reducing the Lower Detection Limit with the use of an EDTA Buffered Inner Filling Solution.

Ion fluxes are a result of concentration gradients in the membrane, which are established when ion concentrations on either side of the membrane differ significantly. The release of primary ions into the Nernst diffusion layer (stagnant layer) is a consequence of co-extraction, ion-exchange and diffusion, and occurs in electrodes where the inner filling solution consists of a high concentration of primary ion. The detection limits expressed in Table 4.1 are directly influenced by these ion fluxes, and show values that would be unacceptable for determinations of thallium in environmental or clinical samples.

One of the first methods used in reducing concentration polarization and ion fluxes was to incorporate EDTA in the inner filling solution, which acts as an ion buffer. The EDTA binds with the thallium reducing its activity in the inner solution, and subsequently reduces the ion fluxes from the membrane into the Nernst layer, whilst maintaining a relatively concentrated solution with an interfering ion [224]. The EDTA also helps to maintain a constant and low concentration of free thallium in the inner solution which is required for a stable inner phase boundary potential. EDTA is used as the buffering agent as it has one of the highest stability constants with thallium (Log K = 6.41), for the majority of the common organic ligands [62, 252].

There are two other similar compounds, PDTA and CDTA which have slightly better stability constants with thallium, 7.02 and 6.70 respectively, but are excessively expensive, and therefore it was decided to use the more readily available EDTA as the ion buffering agent [62, 252]. The calibration graph for two ISEs containing an inner filling solution consisting of approximately 5×10^{-2} M Na_2EDTA, 10^{-4} M $TlNO_3$ at pH ~9.0 and based on membranes incorporating calixarenes (1) (3) and (4) are displayed in Figure 4.22. Exact compositions of the membranes and relevant inner filling solutions can be viewed in the experimental part of this Chapter.
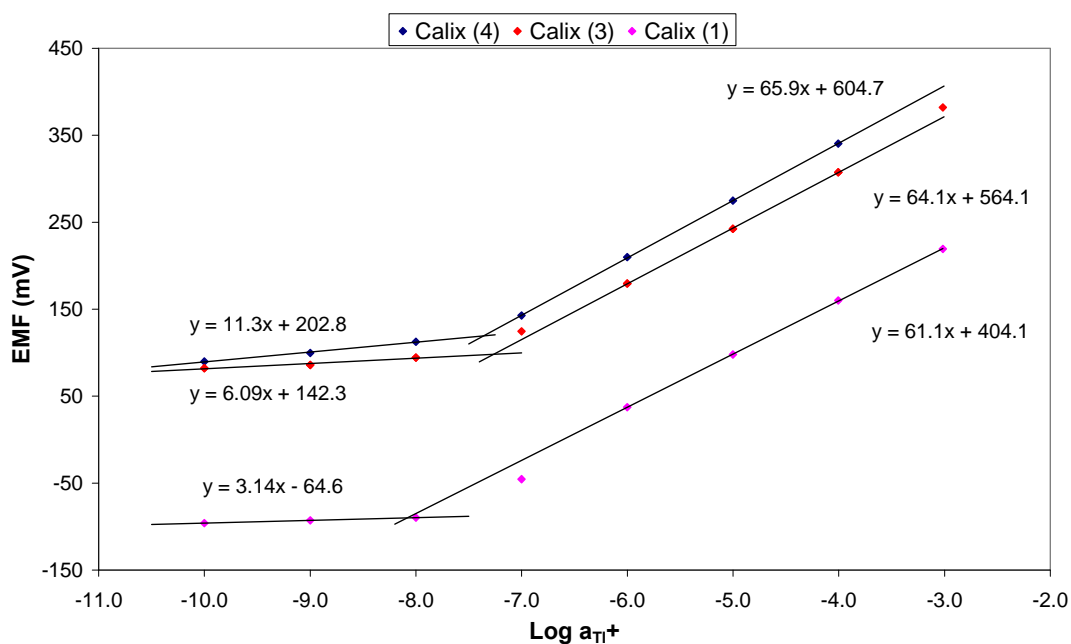
Figure 4.22: Calibration graph of membranes containing calixarenes (1), (3) and (4) with an EDTA buffered inner filling solution.

The experimental and calculated limits of detection of the various calixarenes are displayed in Table 4.4.

Table 4.4: Limits of detection of three calixarenes with an EDTA buffered inner filling solution and calculated limits based on selectivity data and membrane composition.

Calixarene	Experimental and Calculated Limits of Detection (nM)			
	Experimental		Calculated	
	IUPAC.	New Def.	Static	Dynamic
Calixarene (1)	8.32	~151	0.20	24.3
Calixarene (3)	54.4	~55.5	0.24	26.7
Calixarene (4)	43.9	~30.8	0.22	36.4

The limits of detection for the current series of calixarene ISEs have been reduced through the use of a buffered inner filling solution. The lower limits have been reached by controlling ion fluxes within the membrane, which prevents the release of primary ions into the sensed Nernst diffusion layer. The fluxes have been reduced by lowering the free thallium(I) concentration in the inner filling solution to values of 18.6, 16.2 and 19.5 nM for calixarenes (1), (3) and (4) respectively. As a consequence of the weak binding strength of EDTA with thallium(I) the inner solution concentration could not be lowered further, which would help to reduce detection limits to lower levels. The free metal concentrations of the inner filling solutions of electrodes published in the literature are considerably lower with values often around 10^{-11} M [212]. The free metal concentrations of metals other than thallium are able to be at lower levels as a result of the better binding of the cations with EDTA.

The detection limits of all calixarenes have been reduced by about an order of magnitude through the use of an inner ion-buffering system. The membranes of calixarene (3) and (4) were conditioned in 10^{-4} M $TlNO_3$ which could be responsible for the higher values compared to calixarene (1), which was conditioned in 10^{-7} M $TlNO_3$. The higher concentration of the conditioning solution may lead to the co-extraction of $TlNO_3$ into the membrane, which is then released at low sample concentrations.

Calixarenes (3) and (4) show little difference between the detection limits obtained through the IUPAC method and that of the new definition. The large discrepancy between the two detection limits of calixarene (1) is a result of the small super-Nernstian step occurring around a thallium concentration of 10^{-7} M. The super-Nernstian step occurs when the primary ion is depleted at the phase boundary, as a consequence of extensive ion-exchange into the membrane and ion-fluxes in the direction of the inner filling solution. Below the apparent super-Nernstian step, the potential is no longer determined by $a_{Tl,Bulk}$, but by the ion-exchange of Tl^+ into the membrane and Na^+ into the sample solution.

The response of calixarene (1) could be corrected by optimising the concentrations of the inner filling solution, resulting in a reduced inward flux of primary ions at low sample concentrations. The inner solution would only have to be changed slightly as the super-Nernstian step was only a fraction over the maximum deviation allowed under the new definition (17.8 mV). The goal of this work was to apply the various techniques to reduce the detection limits and full optimization should be carried out in future work. The response of calixarene (4) showed no super-Nernstian step as a consequence of the conditioning solution, which released ions into the sample at low concentrations and counteracted a possible super-Nernst step. A schematic representation of the concentration gradients occurring when a buffered inner filling solution is applied are shown in Figure 4.12 and Figure 4.13.

Based on the static method for determining the lower detection limits, Equation 4.19, the optimum lower limits in a sample with no background electrolyte are 0.20, 0.24 and 0.22 nM for calixarene (1), (3) and (4), respectively. The values used in calculating this lower limit of detection are based on the assumption that Tl^+ and H^+ are the only cations present in the solution, and that the pH of thallium(I) nitrate solutions is about 6. The detection limits predicted by the static method are often unrealistic, as ion fluxes play a significant role in the EMF response at low concentrations.

The dynamic model is a more accurate estimation of the true detection limit because it takes into account ion fluxes in addition to selectivities. Using Equation 4.42, the lower detection limits from the dynamic model were calculated. The calculated

values are displayed in Table 4.4 and show the expected detection limits when ion fluxes are taken into account. The q value in Equation 4.42 was estimated with the known diffusion coefficient of thallium(I) in water of $D_{aq} = 2.0 \times 10^{-5}$ cm^{2}s^{-1} [253], and that of the ionophore complex in the membrane to be $D_{org} = 10^{-8}$ cm^{2}s^{-1} [222], with equal diffusion layer thicknesses in the aqueous and membrane phases $\delta_{aq} = \delta_{org}$, and was determined to be q = 0.0005. The calculated limits of detection for the dynamic model closely resemble those obtained from the experimental calibration graphs, which demonstrates that the lower detection limit of this series of ionophores has been reached when the sample only consists of the primary ion and water. This is due to the poor selectivity of H^+ over Tl^+, which starts to interfere at low thallium(I) concentrations.

The detection limits of calixarenes (3) and (4) are still not seen as being optimized based on the limits calculated by the dynamic model. In an attempt to reduce the limit further for calixarene (4), the inner filling solution was slightly changed to reduce the activity of thallium. The result of increasing the pH of the inner filling solution is displayed in Figure 4.23. As a consequence of the limited solubility of calixarene (3) and therefore not knowing the true concentration of the calixarene in the membrane, it was decided not to pursue this ionophore further.

The detection limit of the ISE when the pH in the inner filling solution is elevated was 40 nM, based on the IUPAC method and 231 nM according to the new definition. The new inner filling solution resulted in a super-Nerstian step, suggesting that the optimal inner filling solution was achieved in the first calibration (Figure 4.22) and that the new filling solution caused a flux of primary ions in the direction of the inner side of the membrane and a depletion of Tl^+ ions in the sample at micro-molar concentrations. The concentration of free thallium(I) in the inner filling solution with the reduced acidity was 10.4 nM, which is lower than that of 19.5 nM displayed in Figure 4.22.
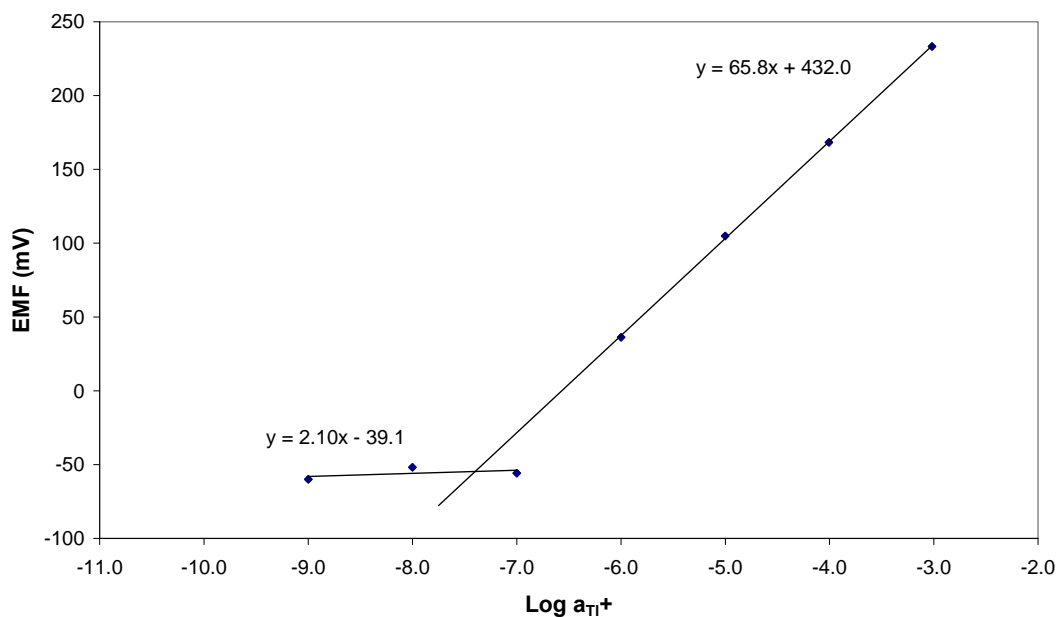
Figure 4.23: Calibration graph of a membrane incorporating calixarene (4) with an EDTA buffered inner filling solution at a higher pH than the one used in Figure 4.22.

The new setup was unsuccessful in lowering the detection limit to that predicted by the dynamic model, and an alternative method was required. It was decided that the conditioning solution was having an influence on the lower detection limit of membranes incorporating calixarene (4). The inner filling solution was changed back to the optimized concentrations displayed above (see Figure 4.22), and the membrane was conditioned in 10^{-7} M TlNO$_3$. The results displayed in Figure 4.24 demonstrate that the conditioning solution is a very important factor if low detection limits are required. Detection limits of 11.5 nM (IUPAC.) and 162 nM (new definition) were obtained with the new experimental method. The detection limit looks to have been reduced from the original EDTA calibration graph (Figure 4.22) according to the IUPAC. definition, but the change in conditioning solution has resulted in a slight super-Nernstian step, which is large enough to exceed the new definitions limits of 17.8 mV, therefore increasing the lower limit. The inner filling solution needs to be optimized once again based on the new conditioning solution to reduce the super-Nernst step to below that of 17.8 mV. The optimal lower detection limit based on the dynamic model of calixarene (4) does look to be achievable if the appropriate conditions are employed. The inner filling solution requires the optimum concentrations of thallium nitrate and EDTA at the appropriate pH for the ion-fluxes

to be minimal. With further testing of different concentrations in the inner solutions, the correct thallium buffer level would be established and the detection limit for calixarene (4) should be achieved to levels similar to that of calixarene (1).
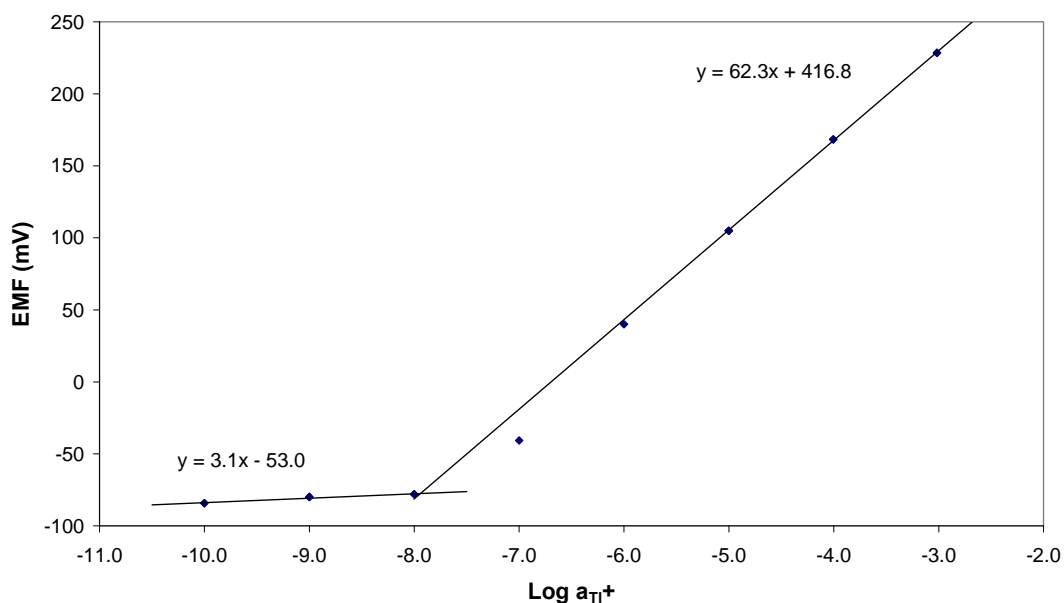
Figure 4.24: Calibration Graph of a membrane incorporating calixarene (4) with an EDTA buffered inner filling solution. Electrodes were conditioned in 10^{-7} M thallium(I) nitrate.

4.7.1.1. Lowering the Detection Limit by Reducing the Influence of H^+ Ions.

To try and improve the detection limit further, attempts were carried out to lower the concentration of H^+ in the sample solution, therefore reducing its influence in low analyte concentrations. Since the selectivity of K^+ and Na^+ closely resembled that of H^+, the hydroxides of these ions could not be used as they would also interfere at low thallium concentrations. It was decided that the hydroxide of lithium would be used as its selectivity is slightly lower than potassium and sodium. The calibration graph for an electrode which contained calixarene(1) as the ionophore and LiOH as the background electrolyte is displayed in Figure 4.25.
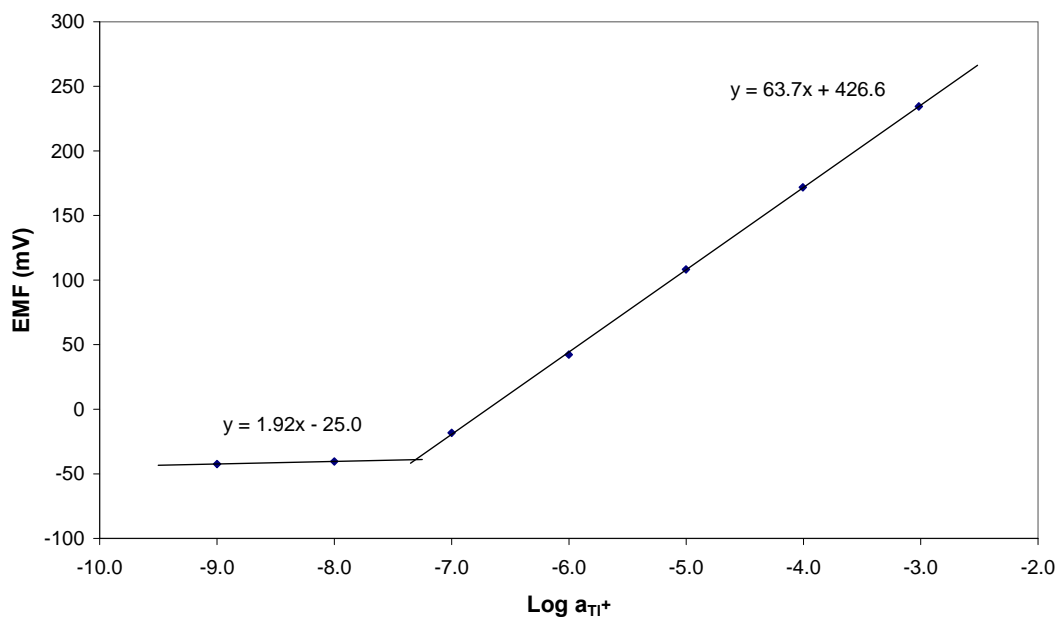
Figure 4.25: Calibration graph of a membrane incorporating calixarene (1), in thallium solutions which contained a constant LiOH background concentration.

When the H^+ concentration is reduced to 0.16 µM with the use of lithium hydroxide, the detection limit does not improve as one would hope. The experimental detection limit in a background of 10^{-4} M LiOH is 49.1 nM, which is an increase on the value determined by the IUPAC definition but an improvement based on the new definition. A dynamic detection limit of 1.37 µM is calculated from Equation 4.42 when both H^+ and Li^+ ions are in solution, which is actually larger than the obtained experimental result. Due to the selectivities of the synthesized calixarenes, an alternative to reducing the pH of the various solutions is desired.

An alternative to using a metal hydroxide as the pH adjuster, is tris(hydroxymethyl)amino methane (TRIS). Prior to adding TRIS to the thallium(I) calibration solutions, its selectivity was tested. Selectivity values $K_{Tl,Tris}^{pot}$ were determined to be -7.2 and -6.88 for calixarenes (1) and (4) respectively. However, these values are only estimates, as sub-Nernstian slopes were recorded for the TRIS calibration, which only consisted of two points/concentrations as there was no change in potential between the concentrations of 10^{-4} and 10^{-3} M. The two higher concentrations also suffered from upward drift, which could be the result of the reference electrolyte ion (Li) interfering in the reading. Similar drifts were observed

in early work when the reference electrolyte consisted of NH_4NO_3, which interfered with highly selective ions. As a result of this, the selectivity can only be an estimate, but based on the trends, it does look to be significantly low enough to be added to calibration solutions to reduce the H^+ concentration. The calibration graphs of calixarenes (1) and (4) incorporating a standard concentration of 10^{-4} M TRIS in the thallium(I) standards is presented in Figure 4.26.

The addition of TRIS to the thallium standards increased the pH to around 8.0. According to the dynamic detection limit model, this should have decreased the best achievable lower limit of calixarenes (1) and (4) to 4.96 and 6.23 nM respectively, based on the pH and the estimated selectivities of TRIS. Unfortunately the experimental detection limits were measured to be 38.9 and 35.5 nM for calixarenes (1) and (4) respectively, and this is considerably higher than the optimal levels predicted by the calculations. To ensure that the optimal detection limits have been reached, both the membrane and electrode parameters require further optimization.
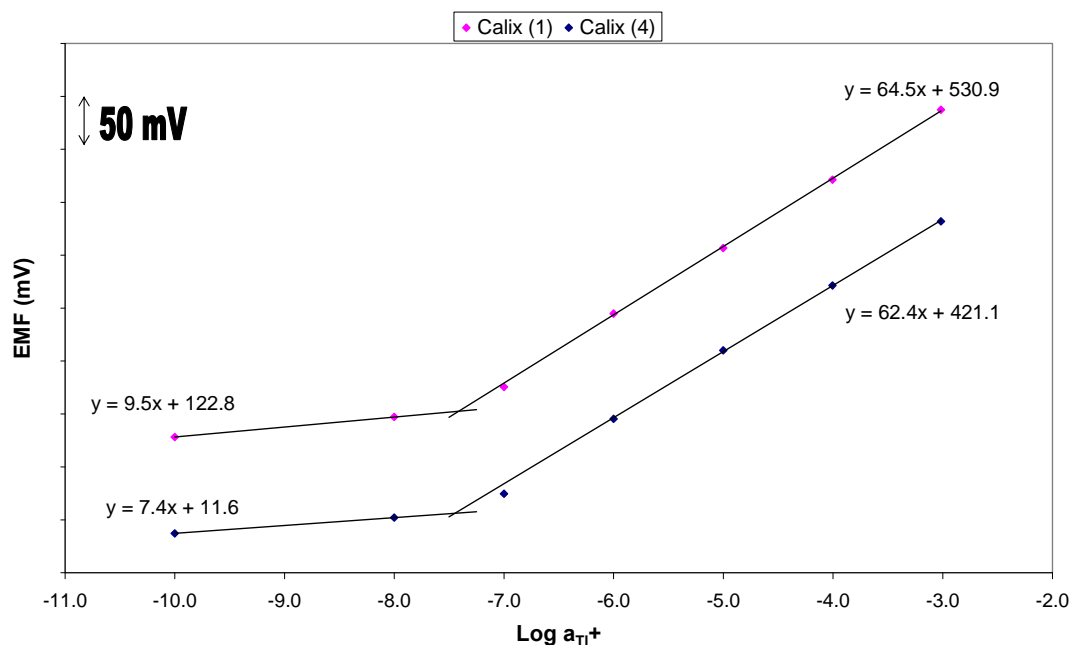
Figure 4.26: Calibration graphs of calixarenes (1) and (4) incorporating an EDTA buffered inner filling solution and thallium(I) nitrate standard solutions with a constant concentration of TRIS. E^0 values differ as the data was separated for clarity.

It was decided to try to further increase the pH of the sample solutions to determine its effect on the electrode's lower detection limit. The pH was increased to around 9 for the various concentrations of thallium(I) nitrate by having a constant background concentration of 10^{-2} M TRIS. The increased pH had little effect on the detection limit with it increasing slightly from the values obtained from Figure 4.26. This suggests that the interference from H^+ is not the determining factor regarding the lower limit of detection with the thallium ISEs. Notwithstanding, the increased TRIS concentration may be counteracting the reduced H^+ interference, thereby hindering the effects of lowering the H^+ concentration.

The lower detection limit of the current series of thallium selective ionophores may have been reached as the values increased when the pH was altered, suggesting that the original EDTA buffered inner filling solutions with no background electrolyte in the sample was the optimum setup.

The lower detection limit may not be reduced further with this series of thallium selective ionophores, even through optimisation of the EDTA inner filling solution, as the optimum values obtained in Chapter 5 with a solid-contact ISE were similar to those obtained with the EDTA inner filling solution (see Chapter 5, Section 5.7.1). Idealistically, SC-ISEs should have little or no ion fluxes from the inner side of the membrane, as there ought to be no inner filling solution where ions can congregate at high concentrations, thereby leading to a non-biased lower detection limit. This outcome suggests that there are other factors dictating the lower detection limit of this series of thallium(I) selective calixarenes. One of the unusual features of calixarenes is that they can incorporate neutral organic molecules, the lower detection limit may be influenced by uncontrollable interferences occurring in the membrane with these ionophores (see Chapter 3, Section 3.5.1 and 3.5.2).

4.7.2. Lowering the Detection Limit Through the Incorporation of an Exchangeable Interfering Ion on the Inner Membrane Side.

One of the disadvantages of using EDTA as an inner filling solution is the deterioration in performance over time, as a consequence of the partitioning of the EDTA-complex into the organic membrane phase [212, 220]. To alleviate the problems of inner solutions which contain complexing agents, alternate methods have been proposed. One such method is to incorporate an exchangeable ion in place of EDTA at the inner side of the membrane. The added ion exchanges with a proportion of the primary ions at the inner side of the membrane therefore reducing its concentration within the membrane and suppressing the outward flux of ions at low sample concentrations.

The exchanging ion was chosen to be the tetraethyl ammonium ion, which has a selectivity coefficient of $K^{pot}_{Tl^+, Et_4N^+}$ = -1.25 for calixarene (4). The percentage of exchange can be calculated using Equation 4.45.

$$\frac{a_I}{a_I + \Sigma K^{pot}_{I,J} a_J} = \frac{[IL^{z_I}_n]}{[I]}$$

Equation 4.45

where $[I]$ is equal to the concentration of the anion exchanger R_t, and $[IL^{z_I}_n]$ is the concentration of primary ion complex in the membrane. The calibration graphs with a PVC/DOS membrane incorporating calixarene (4) as the ionophore and different exchange rates of Et_4N^+ are displayed in Figure 4.27.
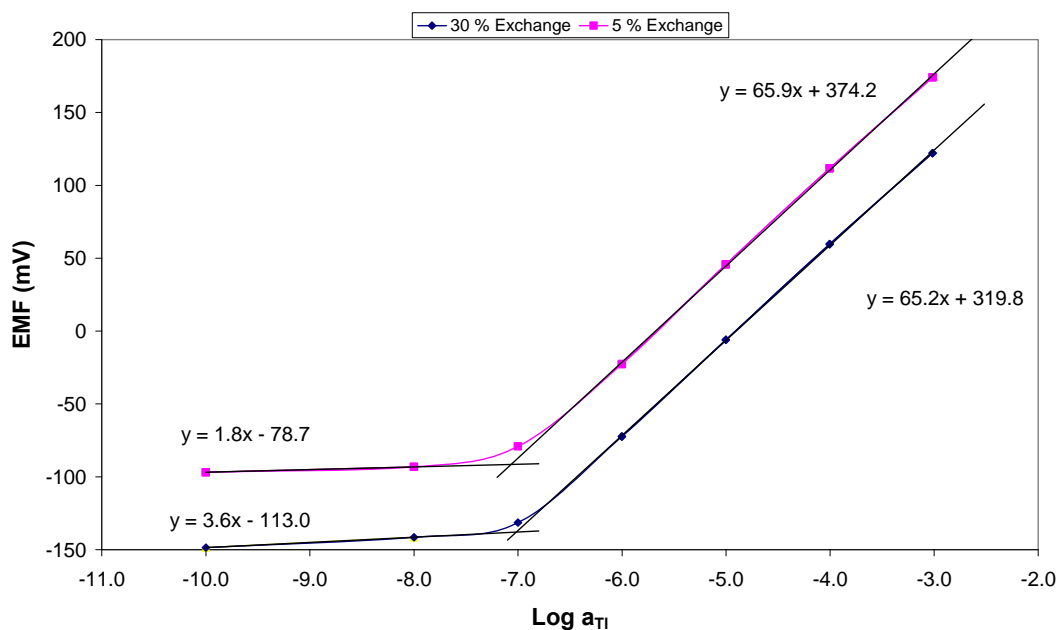
Figure 4.27: Calibration graphs of PVC/DOS membranes with different concentrations of Et_4NNO_3 in the inner solution, to maintain a level of exchange between the primary ion Tl^+ and interfering ion Et_4N^+ of 30 % and 5 % respectively.

The detection limits with different inner solutions of Tl^+ and $Et4N^+$, were determined to be 9.77 x 10^{-8} M and 8.61 x 10^{-8} M for 30 % and 5 % exchange respectively. The detection limit has been reduced from the value obtained with the traditional setup, but is inferior to that obtained with EDTA as the inner solution.

The detection limits obtained using the exchangeable ions on the inner side of the membrane are higher than the ones predicted by the dynamic model calculation (see Table 4.4), which suggests that co-extraction is still a factor at the inner membrane side producing an outward flux of primary ions. The flux of primary ions is not as prevalent as in the traditional setup due to some of the ionic sites being consumed by the exchanged ion Et_4N^+. A higher level of exchange should be tested to ensure that the optimal value has been achieved, and is to be carried out in future work.

4.8.   Experimental

4.8.1.   Reagents

Poly(vinyl chloride) (PVC), bis(2-ethylhexyl) sebacate (DOS), 2-nitrophenyl octyl ether (o-NOPE), 2-fluoro-2'-nitrodiphenyl ether (FNDPE), sodium tetrakis-[3,5-bis(trifluoromethyl)phenyl]borate (NaTFPB), potassium tetrakis(p-chlorophenyl) borate (KTpClPB), were obtained from Fluka. Tetrahydrofuran (THF) anhydrous, inhibitor free, 99.9 % purity was obtained from Sigma-Aldrich. Silver nitrate, copper nitrate, potassium nitrate, lead nitrate, calcium nitrate, Na-EDTA and tris(hydroxymethyl)amino methane were obtained from Univar as AR grade. Cesium nitrate, ammonium nitrate and lithium nitrate were obtained from Merck as AR grade. Barium nitrate was obtained from Sigma-Aldrich as AR grade. Zinc nitrate and aluminium nitrate was obtained from BDH Chemicals as AR grade. Cadmium nitrate was obtained from Fluka as purum p.a. grade. Sodium chloride was obtained from Chem supply as AR grade. Lithium acetate was obtained from Aldrich with 99.99 % purity. Thallium nitrate was obtained from Aldrich with 99.9 % purity. Aqueous solutions were prepared with Milli-Q water (PURELAB). All ionophores were prepared in our laboratory as described in Section 2.7.3.

4.8.2.   ISE Membranes

Membranes approximately 300 μm in thicknesses were prepared by pouring 580 mg of membrane components dissolved in THF into a glass ring of 45 mm internal diameter fixed on a glass Petri dish, and allowing the solvent to evaporate. Exact membrane compositions are displayed in Table 4.5 below.

Table 4.5: Compositions of the various membranes used throughout the chapter.

Membranes	PVC	Plasticiser	Ion-exchanger		Ionophore	
	(mg)	(mg)	(mg)	mmol/kg	(mg)	mmol/kg
Figure 4.16						
Calixarene (1)	192.8	380.2 *	3.06	5.93	5.88	12.36
Calixarene (3)	180.8	402.6 *	3.06	5.84	5.04	10.53
Calixarene (4)	191.4	478.5 +	3.83	6.07	38.28	91.95
Table 4.2						
Calixarene (1)	192.8	380.2 *	3.06	5.93	5.88	12.36
No Ionophore	190.0	381.4 *	2.60	5.11	0	0
Calixarene (4)	190.1	380.6 *	2.62	5.12	3.96	11.73
No Ionophore	191.6	380.0 *	2.59	5.09	0	0
Na Calixarene	189.7	381.3 *	2.66	5.18	5.57	9.68
No Ionophore	190.1	381.3 *	2.58	5.07	0	0
Table 4.3						
No Ionophore	190.0	381.41 *	2.60	5.11	0	0
Calixarene (1)	192.8	380.2 *	3.06	5.93	5.88	12.36
Calixarene (3) #1	129.9	260.7 *	2.12	6.01	5.03	15.63
#2	180.3	402.6 *	3.06	5.84	5.04	10.53
Calixarene (4) #1	130.3	265.5 *	2.25	6.32	3.94	16.76
#2	194.3	380.6 *	2.61	5.05	5.08	14.91
Figure 4.22						
Calixarene (1)	192.8	380.2 *	3.06	5.93	5.88	12.36
Calixarene (3)	191.4	481.3 ~	3.76	5.93	38.4	66.42
Calixarene (4)	251.3	526.0 ~	5.00 †	12.09	50.9	104.5
Figure 4.23 & Figure 4.24						
Calixarene (4)	194.3	380.6 *	2.61	5.05	5.08	14.91
Figure 4.25						
Calixarene (1)	192.8	380.2 *	3.06	5.93	5.88	12.36
Figure 4.26						
Calixarene (1)	192.8	380.2 *	3.06	5.93	5.88	12.36
Calixarene (4)	194.3	380.6 *	2.61	5.05	5.08	14.91
Figure 4.27						
Calixarene (4)	90.39	182.8 *	1.46	5.94	2.50	15.42

* denotes DOS as a plasticizer whilst + o-NOPE and ~ FNDPE. † denotes the use of KTpClPB. Two different membranes were used in the determination of selectivity coefficients (Table 4.3) for calixarenes (3) and (4). Both #1 membranes above were prepared in glass rings of 33 mm internal diameter instead of the usual 45 mm.

4.8.3. EMF Measurements

Potential measurements were conducted on either an ACM Potential-20 instrument (Cumbria, UK) or a Lawson Lab Inc. EMF-16 electrode monitor (Malvern, PA 19355, USA), in magnetically stirred solutions, except for the sandwich membrane

trials where no stirring was utilized. All measurements were corrected for liquid junction potentials according to the Henderson equation and activities were calculated using the Debye-Huckel approximation. The reference electrode was a Orion Thermo double junction Ag/AgCl model 90-02, with 3 M KCl inner electrolyte and a 1 M LiCH$_3$COO bridge electrolyte, except in calixarene (4) initial calibration run (Figure 4.16) where 1 M NH$_4$NO$_3$ was used. All potential readings were carried at standard temperature and pressures. All pH measurements were carried out with an Orion pH meter model 290A.

4.8.4. Preparation of Calibration and Detection Limit Electrodes

The electrodes for determining the calibration graphs and detection limits in Section 4.4 were prepared via the following means; disks of approximately 4 mm diameter were punched from the above membranes and attached to PVC tubing 3 mm i.d., by means of a THF/PVC slurry. The electrodes were assembled with an Ag/AgCl inner reference electrode in a 10^{-2} M NaCl electrolyte connected to a membrane electrolyte of 10^{-3} M TlNO$_3$, through a diaphragm. The membranes were conditioned in 10^{-3} M TlNO$_3$ for at least 16 hours. Calibration runs were conducted with thallium(I) nitrate solutions, with no background electrolyte, between the concentrations range 10^{-2}-10^{-9} M, starting with the most concentrated solution. Between each concentration, the electrodes were thoroughly rinsed with Milli-Q water. The results consisted of mean values of a minimum of three electrodes.

4.8.5. Preparation of Low Detection Limit Electrodes

Electrodes were prepared similar to the above method with the relevant membranes, but consisted of different inner filling solutions. The inner filling solutions for the relevant electrodes are summarised in Table 4.6 and Table 4.7. Inner filling solutions were separated from the electrolyte of the internal reference electrode (10^{-2} M NaCl) by means of a diaphragm. Membranes were conditioned in 10^{-4} M TlNO$_3$ unless stated, when they were conditioned in 10^{-7} M TlNO$_3$. Calibrations were conducted

with $TlNO_3$ solutions, between the concentrations of 10^{-3}-10^{-10} M, starting with the most concentrated solution. Solutions contained no background electrolyte except for the calibrations displayed in Figure 4.25 and Figure 4.26, which contained a background electrolyte of 10^{-4} M LiOH and 10^{-4} M tris(hydroxymethyl)amino methane respectively. The high pH in the inner side of the membrane was achieved through the addition of NaOH to the thallium/EDTA solution.

Table 4.6: Compositions of the various EDTA inner filling solutions used throughout this chapter.

Membrane	Tl^+ Concentration	Na_2EDTA Concentration	pH	Log Tl Activity
Figure 4.22				
Calixarene (1)	10^{-4} M	0.05 M	9.03	-7.86
Calixarene (3)			9.12	-7.93
Calixarene (4)			9.00	-7.84
Figure 4.23				
Calixarene (4)	10^{-4} M	0.05 M	9.46	-8.12
Figure 4.24				
Calixarene (4)	10^{-4} M	0.05 M	9.03	-7.86
Figure 4.25				
Calixarene (1)	10^{-4} M	0.05 M	9.03	-7.86
Figure 4.26				
Calixarene (1)	10^{-4} M	0.05 M	9.03	-7.86
Calixarene (4)				

Thallium activities in the EDTA buffered inner filling solutions were calculated through the computer software Visual MINTEQ version 2.40b, which is based on the original program MINTEQA2 version 4.0 designed by CEAM, EDP in the USA.

Table 4.7: Compositions of the two Et_4N^+ inner filling solutions used in Section 4.7.2 of this Chapter.

Membrane	Tl^+ Concentration	Et_4NNO_3 Concentration	% Exchange
Figure 4.26	10^{-4} M	0.053 mM	5
	10^{-4} M	0.43 mM	30

4.8.6.   Preparation of Electrodes Used in the Sandwich Membrane Tests

Disks of approximately 6 mm diameter were cut from the membranes prepared above with a cork borer and conditioned overnight in their respective chloride based solutions. Thallium(I) chloride (0.01 M) was used with membranes incorporating calixarenes (1) and (4) and no ionophore, while sodium chloride (0.01 M) was employed for membranes incorporating calixarene (4), the sodium selective calixarene (*tert*-butylcalix[4]arene tetraethyl ester), along with no ionophore. Measurements were initially conducted on a membrane which contained no ionophore using a Philips electrode IS-561, which contained an inner solution equivalent in concentration to that of the conditioning and sample solutions. Measurements were conducted against an Orion Ag/AgCl double junction reference electrode with a bridge electrolyte of 1 M $LiCH_3COO$, in unstirred solutions. The membrane containing no ionophore was quickly dried with tissue paper before being pressed together with a membrane that contained the desired ionophore. The sandwich membrane was promptly placed back in the Philips electrode body where the potential was measured for the same solution as the single membrane. Stabilization occurred within about one minute of pressing the two membranes together. Prior to measurements, the Philips electrode was checked for air bubbles. Potential differences were determined by subtracting the potential of the membrane which contained no ionophore from that of the sandwich membrane potential. Standard deviations were determined with sample populations of n = 4 for calixarene (1), n = 18 for calixarene (4) with Tl, n = 4 for calixarene (4) with sodium and n = 19 for the sodium selective calixarene.

4.8.7.   Preparation of the Electrodes Used in the Selectivity Determinations

Electrodes were prepared with the same fashion as those used in the calibrations, using the membrane compositions displayed in Table 4.5. The membranes of all electrodes were conditioned in 10^{-2} M NaCl overnight and contained an identical

inner filling solution. Calibrations of the interfering ions were conducted with nitrate solutions, except for sodium and cesium, where chloride was the counter ion, using a measuring sequence of the most discriminatory ion first to the least with thallium being the last. Calibrations graphs were recorded in solutions of increasing ionic strength between the concentrations of 10^{-4} to 10^{-2} M. Electrodes were thoroughly washed with Milli-Q water after each element run.

5. Solid Contact Ion-Selective Electrodes

5.1. Introduction

Solid contact ion selective electrodes have been reported in the literature for many years [254-256]. The primary objective of solid contact ISEs was to eliminate the need for an internal filling solution on the inner side of the polymer membrane. The focus of this design was to enhance miniaturization and microfabrication with low cost, robustness and mechanical flexibility [257]. In eliminating the aqueous inner solution the electrodes could be mounted horizontally, vertically or inverted, which would be beneficial in the clinical, medical and process fields [257, 258].

The initial design was to directly cast the membrane cocktail onto solid supports, which consisted of wires or flat coupons of platinum, silver, gold or graphite [254-256]. The coated wire (CW) electrodes were prepared by dipping the wire in a solution containing the appropriate membrane ingredients several times to form a small bead at the wire tip [259]. The other forms of solid contact (SC) electrodes were prepared by drop casting a known volume of membrane solution onto a flat conducting substrate then allowing the solvent to evaporate (see Figure 5.1). While these electrodes were robust and simple to prepare, they suffered from long-term potential instability, low reproducibility and only moderate limits of detection [260].
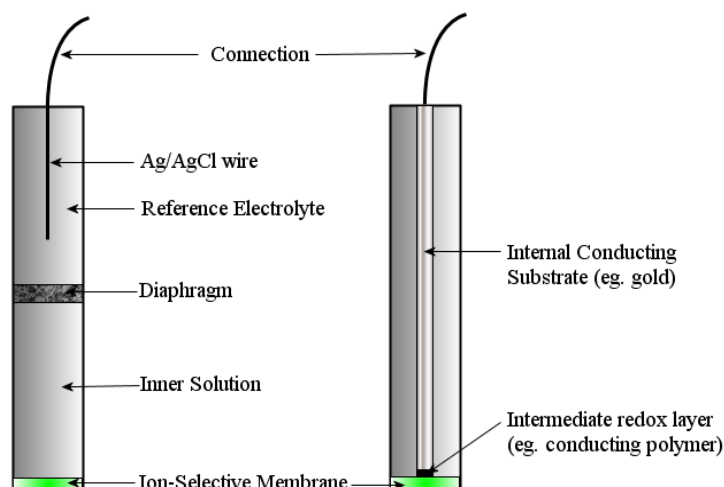
Figure 5.1: Solid Contact (SC-ISE) electrode compared against a standard inner-liquid ion-selective electrode (IL-ISE).

5.2. Response Mechanism of Solid Contact Electrodes

In a conventional ISE design, the inner side of the membrane consists of an Ag/AgCl/chloride solution reference system (Equation 5.1).

$$AgCl_{(s)} + e^- \rightleftharpoons Ag_{(s)} + Cl^-$$

Equation 5.1

This construction leads to a well-defined EMF potential with long-term stability [261]. In solid contact electrodes, the internal Ag/AgCl reference system is removed (see Figure 5.1). The removal of the well defined reversible thermodynamic system resulted in electrodes with poor stability and were only useful for specific applications, such as chromatographic detectors [255, 262, 263]. The poor stability was associated with a blocked interface between the solid substrate and the polymer membrane. This is a consequence of a conflict between the ionic conductivity of the membrane and the electronic conductivity of the substrate, which results in a high charge transfer resistance between the two.

In the initial years of SC-ISE research, there was no well-defined redox couple at the substrate/membrane interface resulting in an insufficient ion-to-electron transfer and undesirable potential drifts. Many authors in the literature have suggested the formation of an oxygen half-cell at the ion conducting interface, since the membrane is permeable to both oxygen and water [255, 261, 264]. Impurities introduced from the membrane ingredients or the substrate that have redox active capabilities may also contribute to the process between the two phases. The response mechanism of SC-ISEs both without (A) and with (B) redox-active components is illustrated in Figure 5.2.

Since the electrode is permeable to water, it can diffuse through the membrane and establish a layer or pockets between the membrane and solid substrate. This second internal aqueous layer introduces a new phase boundary, which often results in potential drifts due to the movement of ions. The problems associated with the water layer are discussed in more detail in Section 5.5. In order to obtain a stable reproducible SC-ISE it has been suggested that the solid substrate must contain a

well defined redox couple to facilitate the transfer from ionic to electronic charge, in addition to being highly lipophlic to prevent the formation of a water layer.
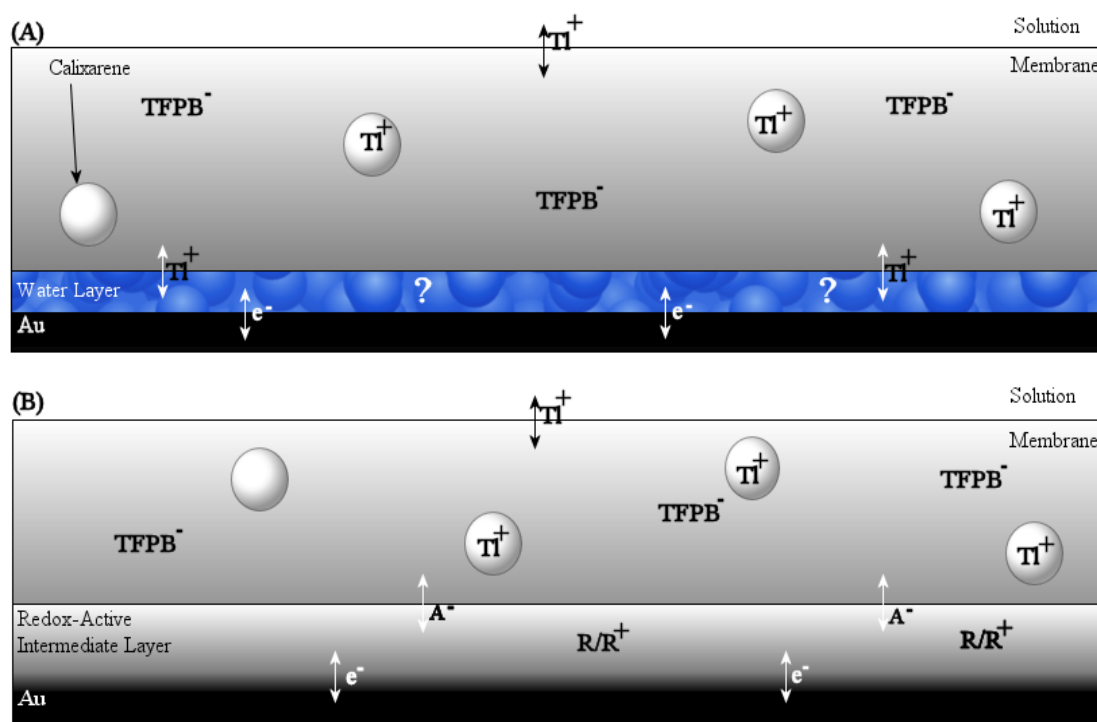
Figure 5.2: Response Mechanism of SCISEs: (A) A SCISEs without a controlled redox process and (B) a SC with a redox-active compound on the solid electronic substrate.

One technique studied so far to alleviate the problems associated with SC-ISEs, whilst still maintaining the superior response characteristics and stability of LC-ISEs, was the use of hydrogel as an intermediate layer between the membrane and solid substrate [260, 265, 266]. In this system, a thin layer of hydrogel consisting of poly(2-hydroxyethyl methacrylate) loaded with the primary ion as a chloride salt, was drop cast over the conductive substrate [260]. This system alleviated some of the problems of a blocked interface, but still was restricted from true minaturaisation due to the semi-aqueous system. Gyurcsányi and co-workers have conducted a side-by-side comparison of hydrogel and conducting polymer based inner contacts and concluded that the latter was superior to the hydrogel inner contacts in several of the tests [260]. Given these factors, it was decided that SC-ISE based on conducting polymers should be pursued.

A significant proportion of research has been dedicated to the formation of a well-defined redox half-cell between the membrane (ionic conductivity) and the solid substrate (electronic conductivity). The utilisation of redox active self-assembled monolayers (SAMs), conducting polymers, lipophilic silver-ligand complexes, an epoxy layer loaded with metal and carbon substrate electrodes have all been studied, and in some cases have overcome the stability problems observed with the blocked interface [257, 260, 267, 268]. The work conducted in this research focuses on the use of conducting polymers e.g. polypyrrole and poly(3-octylthiophene) and a water insoluble redox active organic salt (lanthanum 2,6-dichlorophenolindophenol (La-DCPI)) to act as the ion-to-electron transducer, between membrane and solid substrate.

5.3. Conducting Polymers

Conducting polymers (CPs) are potentially electrically active due to their highly conjugated backbone. The overlapping p_z orbitals, as a result of the alternating single (σ) and double (π) bonds, allow for transition of electrons and subsequently current flow when either there is an excess or deficiency of π-electrons along the chain. This provides these organic compounds with their unique electrical and optical properties. Examples of several conducting polymers are illustrated in Figure 5.3.

Initially these polymers are insulators or semi-conductors due to the localisation of the π-electrons along the carbon backbone. It was first discovered in 1968 that the conductivity of polyacetylene could be varied over a range of 10^{-9} to 10^{-2} S cm^{-1} by exposure to Lewis acids and bases [269]. It was not until 1976 that scientists discovered that partial oxidation of polyacetylene by electron attracting species, e.g. I_2, led to a dramatic increase in electrical conductivity [269, 270]. This discovery resulted in the scientists receiving a Nobel Prize in Chemistry in 2000 and changed the way people viewed polymers. De-localisation of the π-electrons along the polymer backbone can be achieved through either partial oxidation (p-doping) or reduction (n-doping).

A)

B)

C)

D)

E)
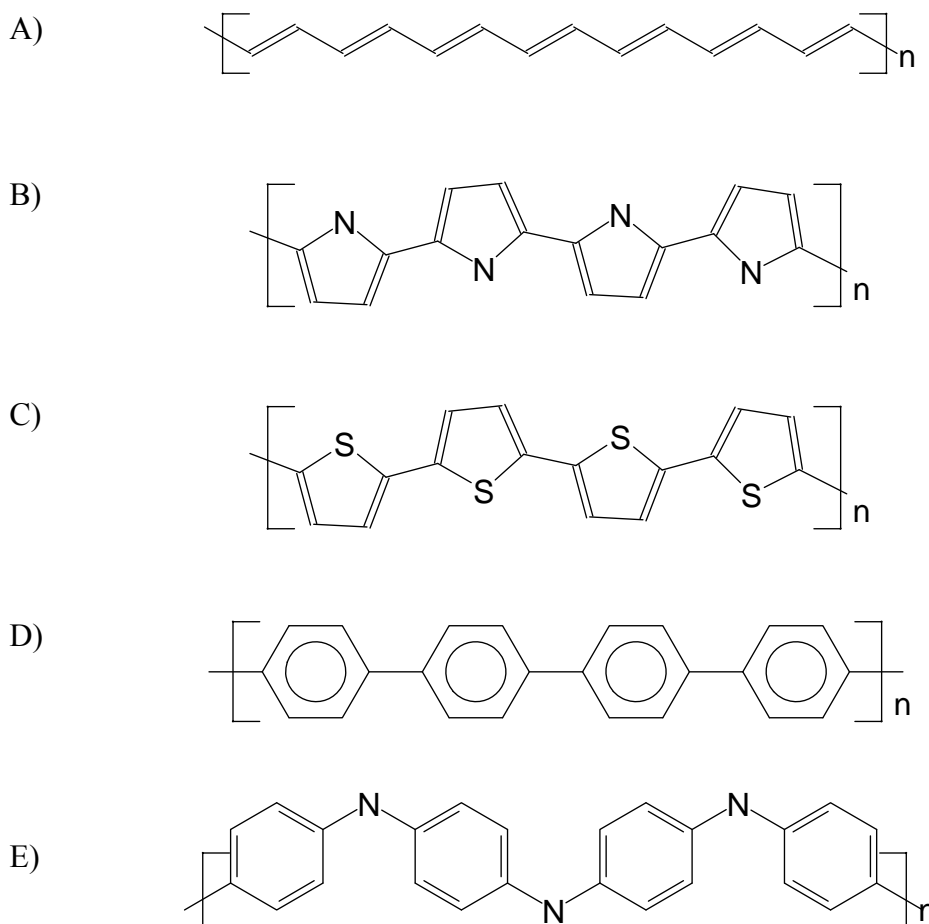
Figure 5.3: Structures of some common conducting polymers. A) Polyacetylene, B) Polypyrrole, C) Polythiophene, D) Poly(p-phenylene), E) Polyaniline

5.3.1. Doping of Conjugated Polymers

The term doping originates from the physics field of inorganic semiconductors and is utilised in conducting polymers, as it changes the oxidation state without manipulating the structure. In CPs, the term doping describes the oxidation or reduction of the molecule's conjugated backbone. Oxidation or reduction leads to the carbon chain becoming positive, or negative respectively. Doping can be accomplished via several methods, chemical, electrochemical, ion implantation and photochemical [271, 272]. In each case, the polymer doping is always accompanied by a counter ion to maintain electroneutrality. The counterion (dopant) incorporated into the polymer can significantly change its chemical properties and must therefore

be carefully chosen based on the desired task. The doping level is a measure of the oxidation/reduction of the polymer and is calculated from the proportion of dopant ions per monomer unit, e.g. a doping level of 0.20 (or 20 %) indicates that there is one dopant ion per five monomer units.

Chemical doping is carried out on the polymer by either an electron acceptor, through oxidation (oxidant, A) or an electron donor, through reduction (reductor, B), following reactions 5.2 and 5.3:

$$p\text{-doping} \qquad (P)_n + A \rightarrow (P)_n^+ A^- \qquad \qquad \text{Equation 5.2}$$

$$n\text{-doping} \qquad (P)_n + B \rightarrow (P)_n^- B^+ \qquad \qquad \text{Equation 5.3}$$
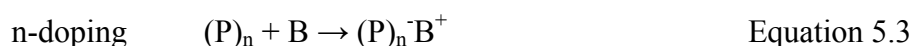
where A^- and B^+ are the dopants. Chemical oxidation/reduction can occur via exposure of the polymer to I_2 or AsF_5 vapours, $FeCl_3$, $Fe(NO_3)_3$, $CuCl_2$ or sodium naphthalide to name a few [269, 271]. The doping level is dictated by the vapour pressure of the dopant or its concentration, the doping time, the temperature of the reaction and the polymer type [271].

In electrochemical doping, the monomer/polymer is exposed to an applied potential, leading to the oxidized or reduced forms, which is shown in Equations 5.4 and 5.5.

$$p\text{-doping} \qquad P + C^- \rightarrow 1/n \, (P)_n^+ C^- + e^- \qquad \qquad \text{Equation 5.4}$$

$$n\text{-doping} \qquad P + D^+ + e^- \rightarrow 1/n \, (P)_n^- D^+ \qquad \qquad \text{Equation 5.5}$$
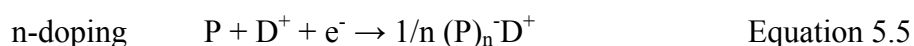
Both C^- and D^+ are the relevant counterions that are incorporated into the polymer upon its oxidation/reduction to maintain electroneutrality. The electrochemical oxidation of pyrrole will be discussed further in Section 5.3.2.

Electrochemical doping is preferred to chemical doping as it allows for better control of the doping level. Any doping level can be achieved by the application of a constant potential over a length of time, and the level at which the polymer is doped is directly related to the voltage at electrochemical equilibrium, as determined by a reduction in current to zero [270]. The conductivity of the polymer can be

significantly increased from 10^{-10}-10^{-5} S cm^{-1} (non-doped) to ~1-10^{4} S cm^{-1} (fully doped) [272, 273]. As a result of the advantages of electrochemical doping over chemical doping, it was decided to only pursue the former in the current research.

5.3.2. Polypyrrole and Poly(3-octylthiophene) as Ion-to-Electron Transducers.

Poylpyrrole

Polypyrrole is a well-known conducting polymer and has been routinely used for many years due to its high conductivity, remarkable stability, simple preparation and well know properties [274, 275]. Polypyrrole was the first conducting polymer incorporated in ISEs [276]. Dong et al. tested the response of an anion-doped polypyrrole film on glassy carbon for chloride ions [276]. The reaction equation and associated mechanism for the electrochemical conversion of pyrrole to polypyrrole are shown in Figure 5.4 and Figure 5.5 respectively.
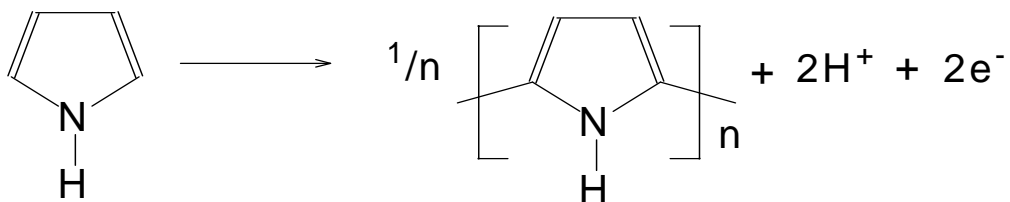
Figure 5.4: Equation for the electropolymerisation of polypyrrole
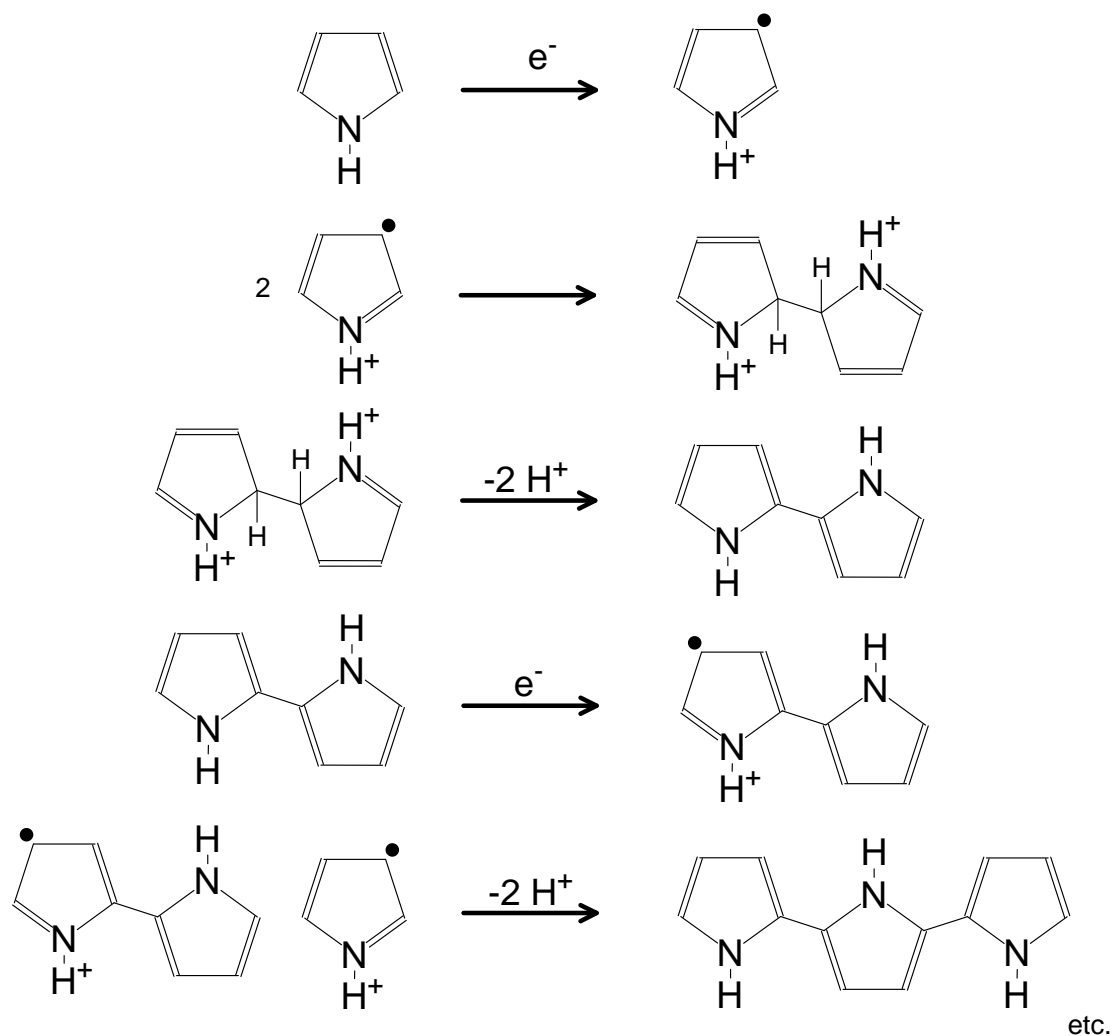
Figure 5.5: Mechanism for the electrochemical deposition of pyrrole to polypyrrole.

The first step involves the oxidation of the pyrrole to its radical cation. The second step of the synthesis is a free radical-radical coupling mechanism. In the first and second stages, the chosen solvent, counterion and possibly even the monomer compensate for the natural repulsion of the pyrrole radicals [277]. The production of the dihydrodimer dication in the second step is followed by the loss of two protons and rearomaritisation to produce the dimer [269]. The oxidation of the dimer occurs more readily promoting further coupling. This process continues until the maximum solubility of the oligomer in the electrolyte is reached, after which it precipitates on the electrode surface [269]. A counter ion is eventually incorporated into the polymer, when the charge on the growing chain is significant enough to support it [277]. The polymerisation proceeds with an electrochemical stoichiometry of 2.2-2.3 Farady mol^{-1}. Of the 2.2-2.3, 0.2 is reserved for the reversible oxidation of the

polymer (doping), with the majority of the charge being used for the oxidation of the monomer/dimer etc. [269].

In order for the polymerisation to proceed as intended, certain conditions in the electrochemistry, electrode material, solvent, counterion and monomer must be met [269, 277]. The applied potential must be above a certain level, otherwise the rate of polymerization will prevent the precipitation of the polymer. The monomer must also be in a relatively high concentration in order to avoid competitive reactions of the free radicals [269]. At high anodic potentials or low monomer concentrations the polymer can undergo degradation instead of deposition. In most instances, the solvent must not contain oxygen or be highly nucleophilic, as these can react with the intermediate radicals. In addition, it needs to have a high enough dielectric constant to ensure sufficient conductivity. The electrical conductivity of the solvent is increased with the addition of a soluble salt, which is eventually incorporated into the deposited polymer. In the case of polypyrrole, water is used as the solvent as pyrrole is soluble in this media. The deposition of the insoluble polymer on the electrode may be discouraged if the surface is extremely polar at the used potential [269, 277].

In the case of polypyrrole, the choice of counterion that is incorporated between the polymer planes can greatly affect the conductivity/potentiometric response of the polymer [277]. In addition to the type of counterion, its concentration in the polymer also has an effect on the conductivity. The conductivity is related to the nucleophilicity of the incorporated counterion, with a decrease in conductivity as the electron affinity of the counterion increases [277]. The addition of extra functional groups on the pyrrole chain also lowers the conductivity of the polymer due to steric effects. These substituents can also have an effect on electropolymerisation by affecting the conjugation and subsequently its oxidising capabilities.

Polypyrrole can also act as the ion sensing membrane if appropriate techniques are employed. In the oxidised state, the polymer layer can exhibit an ion conductivity and slight permselectivity towards anions, whereas in the reduced state, the polymer is more permselective towards cations [273, 277-279]. The cation selectivity is achieved by incorporating large bulky anions in the polymer, so when the polymer is undergoing reduction, the anion is prevented from leaving the polymer and, as a

result, a cation is incorporated into the polymer to maintain electroneutrality [277, 280]. Such bulky anions include dodecyl sulfate, poly(4styrenosulfanate) ions, naphthalenosulfonate, polyvinyl sulfonate or hexacyanoferrate [277, 279]. When a small mobile anion is incorporated in the doping process (Cl^-, NO_3^-), the anion is able to freely exchange with the electrolyte. However, the selectivity of polypyrrole is trivial compared to other sensors, but can be greatly increased by incorporating complexing ligands or ionophores into the conducting polymer membrane [273, 280-282]. The cationic, anionic and redox responses of polypyrrole are shown in Figure 5.6.
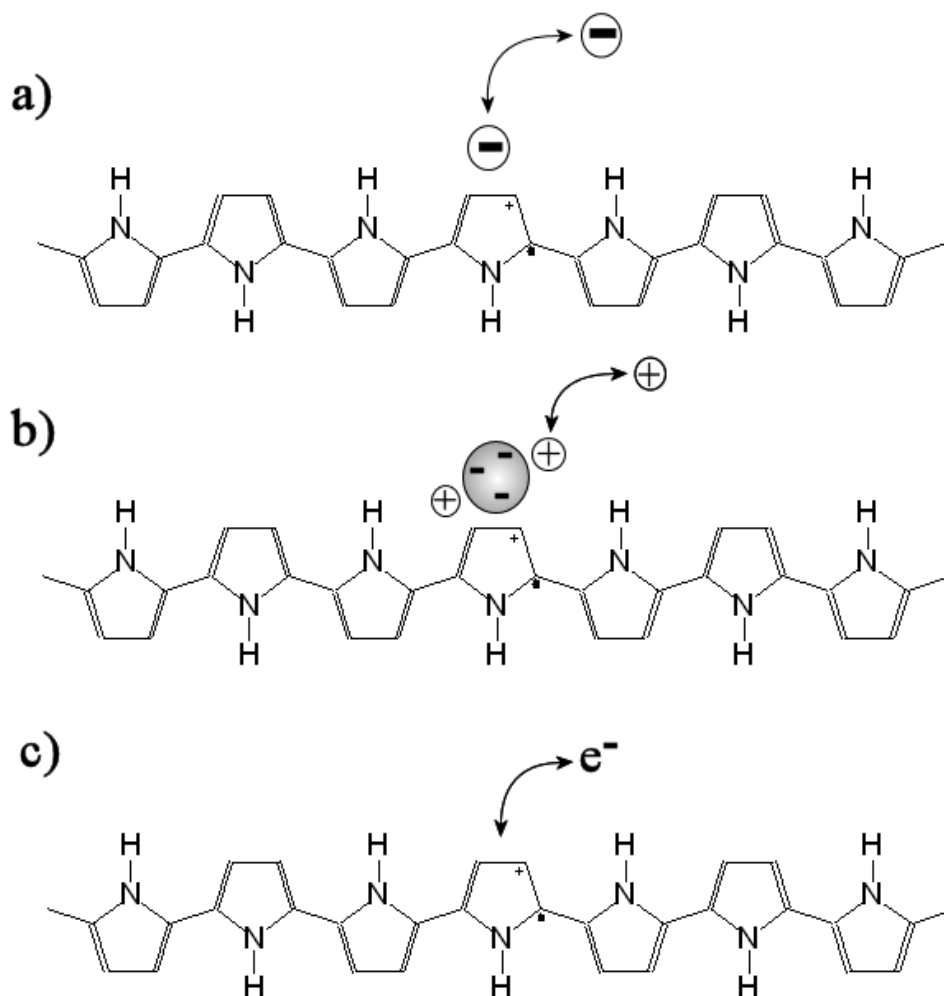
Figure 5.6: Response mechanisms of polypyrrole films a) anionic b) cationic c) redox [273].

In addition to the cationic and anionic responses, polypyrrole also exhibits redox sensitivity (see Figure 5.6 c). The response can be either metallic or non-metallic in nature, based on the electron transfer, and can be utilized for measurements of the

monomer and other neutral species such as oxygen and ammonia, in addition to redox potentiometric measurements [273, 283-288]. Many of the conducting polymers also exhibit pH sensitivity. With a significant range of functions that could contribute to the overall response, the practical application of conducting polymers as sensing materials is difficult. Attempts to overcome these flaws has led to the incorporation of ion recognition sites (see Figure 5.7).
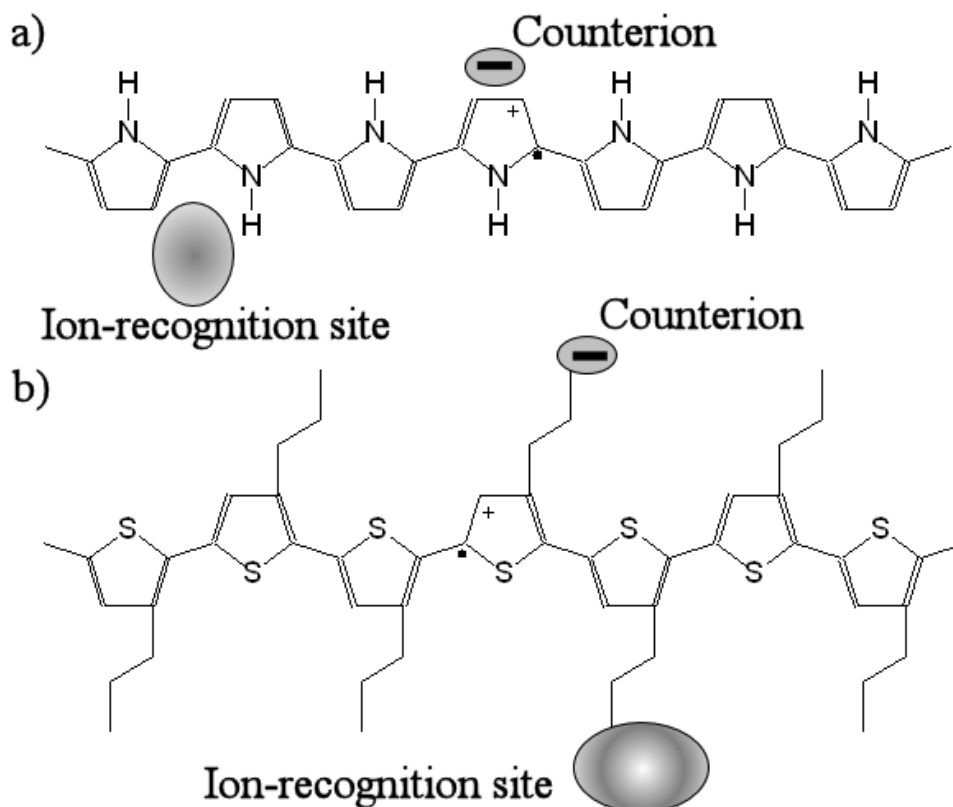
Figure 5.7: Incorporated electrically neutral ion-recognition sites a) physically trapped in polypyrrole b) covalently bonded in polythiophene. [273]

An alternative to using the conducting polymer directly as the ion sensing material is to coat the polymer with a classical ionophore-based ion-selective polymeric membrane. This renders the selectivity of the sensor entirely dependent upon the ionophore supporting membrane, while the underlying conducting polymer acts solely as an ion-to-electron transducer. Solid contact electrodes incorporating this experimental design were chosen to test the current series of thallium selective ionophores due to the combined advantages of the selectivity of ionophore based

polymeric membranes and the ion-to-electron transduction advantages of the conducting polymers.

The incorporation of ion-recognition sites into the conducting polymer is still of significant interest as it has the potential to develop durable micro and nanosized ion sensors [289]

Poly(3-octylthiophene)

The electrochemical synthesis of polythiophenes was first reported in 1982 by Tourillion, G. and Garnier, F., and these polymers displayed conductivities up to 10-10^2 S cm^{-1} [290]. The electropolymerisation of polythiophene is carried out at elevated potentials, which results in overoxidising the polymer according to Figure 5.8, and poor quality films. Incorporation of a linear hydrocarbon chain at the third carbon in the thio ring increases the oxidizing potential resulting in better quality polymer films. The degree of polymerization for alkylthiophenes is in the order of a few hundred, compared to 10-35 for polythiophene and can reach conductivities of up to 100 S cm^{-1} [269, 291]. However, the presence of branched hydrocarbon chains can diminish the conductivity of the polymer as a consequence of the reduced conjugation of the polymer backbone [269].
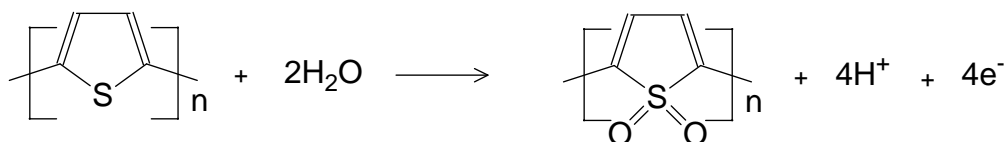
Figure 5.8: Over oxidation of Polythiophene resulting in a deterioration in the chemical and physical properties [277].

The mechanism for electropolymerisation of polythiophenes is essentially the same as polypyrrole (Figure 5.5), with the formation of radical cations that react with one another and other monomer units to form the polymer [277]. Counter ions are also incorporated into the polymer backbone upon polymerisation. As in polypyrroles, polythiophenes also exhibit ion exchange characteristics. However, the incorporation of appropriate counterions is often difficult as the electropolymerisation is solely carried out in nonaqueous solvents such as acetonitrile or propylene carbonate, in

addition to the higher anodic potentials required [277]. The presence of water in the polymerization of thiophene also resulted in a degradation of the conjugation length, conductivity and polymer film quality.

One advantage of polythiophenes over polypyrroles is the ease of incorporating additional functional groups to the polymer backbone, which can act as ion recognition sites as well as changing hydrophilicity [277]. Another potential advantage of polythiophenes in solid contact ISEs over polypyrole is their increased hydrophobic nature, which could be beneficial in the prevention of a water layer between the membrane and the solid conducting substrate, as discussed in Section 5.5. Polyalkylthiophenes also have the advantage of being soluble in organic solvents, which allow them to be dissolved and drop cast instead of direct electropolymerisation onto the electrode surface. In this Chapter, poly(3-octylthiophene) was chosen as an ion-to-electron transducer between a gold substrate and a thallium(I) selective methylmethacrylate/decylmethacrylate copolymer membrane.

5.3.3.   Spontaneous Charging/Discharging of Conducting Polymers.

A characteristic of conducting polymers that influences the potentiometric response of SC-ISEs is that of spontaneous charging/discharging. The spontaneous charging/discharging leads to ion fluxes similar to those observed in LC-ISEs, which results in biases in the detection limits and selectivities. The phenomenon results in an alteration of the ion concentration of the conducting polymer, especially over an extended period of time depending on the applied solutions. The perturbation in response is not only a result of the charging/discharging occurring simultaneously with the measurements, but also the same phenomenon that leads to the accumulation or release of ions in the conducting polymer phase over the sensor's lifetime [292, 293]. In high concentration conditioning solutions, discharging of the polymer will predominate over charging as the inward flux of primary ions influences the polymer interface. In the case of polypyrrole, deprotonation occurs to compensate for the high level of immobilized anion accumulated during doping, as the exchange of cations

from the ion-selective membrane occurs. In other polymers, discharging may occur through the loss of previously accumulated cations. Dissolved oxygen permeating through the membrane can also influence charging. The term discharging actually describes the process occurring at an uncovered polymer or a system covered with an anion-sensitive membrane, which results in a loss of charge. It should be noted that in a system with a cation selective membrane covering a conducting polymer, the process is actually ion-exchange [293]. Michalska and co-workers estimated that the concentration of cations incorporated into the polypyrrole with chloride as the doping anion, could be as high as 0.15 M or 0.16 mol kg^{-1} [293]. This has serious implications for detection limits, as it is similar to the concentrations of primary ions in the inner compartment of LC-ISEs, which fall victim to high outward fluxes and ion leaching. The pH of the conditioning solution also had a dramatic influence on the response of the electrodes due to the deprotonation of the polypyrrole. To reduce the effect of spontaneous charging/discharging, it was recommended to condition the electrode in such a way that the concentration of interfering ion would be predominantly higher than that of the primary ion [293].

5.4. Other Redox-Active Systems used in Solid-Contact Ion-Selective Electrodes

An alternative to conducting polymers acting as ion-to-electron transducers is the use of redox active components which have both ionic and electronic capabilities. Such components tested to date include lipophilic silver complexes and redox active self assembled monolayers (SAM) of large organic molecules [263, 267, 294]. These types of systems showed improved potential stability compared to a SC-ISE without an intermediate layer. The large organic molecules were also thought to prevent the formation of a water layer between the membrane and the substrate due to their lipophilicity. However, a water layer test still showed the presence of water, but was overcome by the incorporation of n-octanethiol into the SAMs. The lower detection limits of these electrodes were still in the micromolar range, which suggests that ions were still leaching from the membrane. Recently, a new redox active organic complex (lanthanum 2,6-dichlorophenolindophenol (La-DCPI)), was incorporated into a screen printed SC electrode system for the determination of ascorbic acid [295,

296]. The La-DCPI complex, structure shown in Appendix VI, enhanced the potentiometric performance of the screen printed solid contact electrode. The DCPI exhibits a totally reversible behaviour and the lanthanum salt is sparingly soluble in aqueous media, which will prevent leaching [296]. In the present research, we intend to utilise the excellent redox characteristics of the La-DCPI complex to improve the stability and sensitivity of a SC-ISE incorporating one of the current series of thallium(I) selective calixarenes.

5.5.   Detection Limits of Solid Contact Electrodes

A significant problem with the experimental setup of the conventional inner filling solution method is the presence of zero-current ion fluxes in the membrane. Unless addressed, these fluxes, which are in the order of less than 1 pmol $cm^{-2}s^{-1}$, influence the unstirred Nernst diffusion layer and result in detection limits of $\sim 10^{-6}$ M [261]. This outward flux is observed even if the sample solution does not contain any analyte at all, producing a biased limit of detection. The fluxes originate from the high concentration of primary ions in the inner filling solution migrating outward into the less concentrated sample solution, and inadvertently render the sensor useless to low analyte concentrations or highly discriminated interfering ions. Ways to reduce the detection limit of the inner filling solution method were discussed earlier in Chapter 4.

With the removal of the inner solution in solid contact electrodes, this problem should have been eliminated. However, since the membrane is permeable to water, it has been shown that a small water layer or droplets could be established between the membrane and the solid substrate and congregate ions at relatively high concentrations [261]. The EMF instabilities observed are a direct result of the aqueous layer changing in composition as carbon dioxide/oxygen and ions permeate through the membrane [260, 261, 297]. The EMF in solid contact electrodes with an internal water layer is primarily made up of three phase boundary potentials; The sample/membrane, the membrane/inner aqueous layer and the inner-aqueous layer/solid conductive substrate, all contribute to the overall potential of the sensor .[261]. The very small volume established between the membrane and the inner

contact is very sensitive to changes in ion concentration, which is completely determined by the membrane [261]. A minor change in ion concentration in such a small volume would lead to a significant result on the phase boundary potential on the inner side of the membrane and therefore a significantly visible potential change [297].

Spontaneous charging/discharging of the conducting polymer also influences the detection limit of SC-ISEs. As discussed is Section 5.3.3, the conditioning of the SC-ISE in relatively high concentrations of primary ion can increase the limit of detection significantly.

Several electrochemical methods can be used to evaluate the presence of a water layer in solid contact systems and are discussed in Sections 5.5.1 to 5.5.3.

5.5.1.   Potentiometric Water Layer Test

This type of test was first utilised by Fibbioli, M., et al. [261] to prove the presence of a water layer between the PVC membrane and the solid conducting substrate. In this test, the sensor is first conditioned in a moderate concentration of primary ion. Once a stable potential is observed for the primary ion, the solution is changed to an interfering ion of high concentration. If an aqueous layer is present between the membrane and the solid substrate, an upward potential drift after the initial negative drop is observed for the interfering ion (see Figure 5.9). The instantaneous negative drop in EMF, when the solution is changed from the primary ion to the interfering ion, is a direct result of the membranes selectivity behavior on the outer phase boundary [263]. The subsequent upward positive drift after the initial negative drop is a direct consequence of interfering ions reaching the inner aqueous layer where they are preferentially exchanged with the primary ions as a result of the membrane's selectivity. The exchange of ions on the inner membrane side leads to a rapid change in composition in the very small volume in the inner layer, and as a direct consequence, a highly visible drift of the inner phase boundary potential is observed [261, 297]. When the sensor is again exposed to the initial concentration of primary ion the reverse effect occurs. The initial positive jump is followed by a slow potential

decrease which is attributed to the primary ions being exchanged with the interfering ions in the internal water layer. The second drift is slower due to the preference of the membrane towards the primary ion over the interferent. A theoretical model based on an ISE with a very thin inner solution has been developed to describe the response observed [261]. Utilising conducting polymers and redox-active self assembled monolayers, the water layer could be removed with stable potentials resulting (see Figure 5.9 (b)).
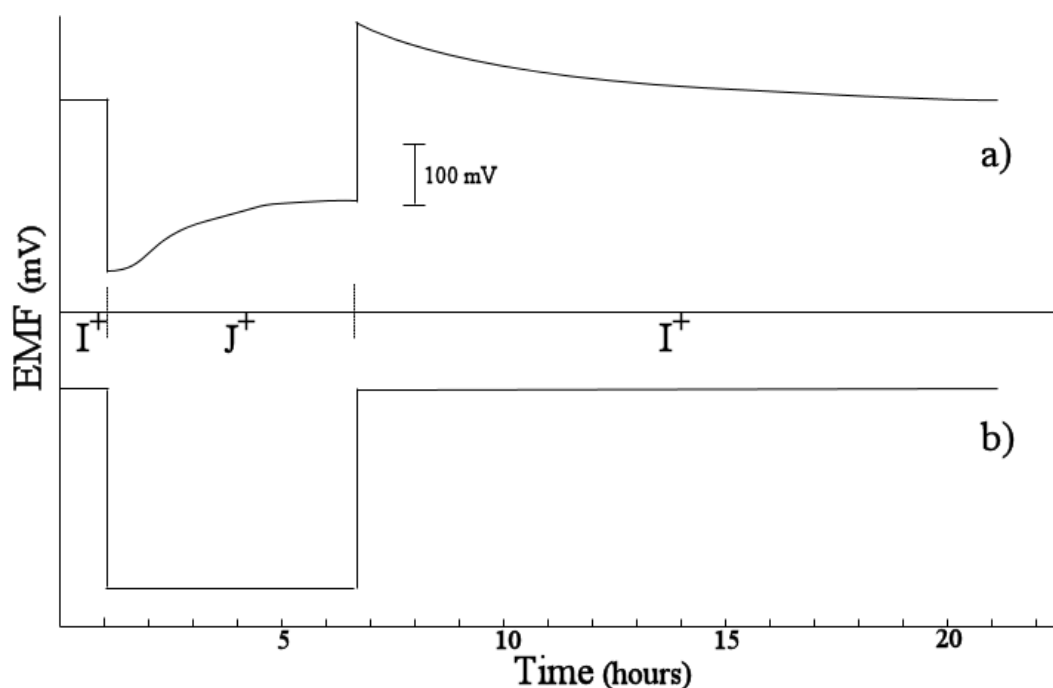
Figure 5.9: Schematic representations of response curves for solid contact electrodes with (a) and without (b) the presence of a water layer between the ion-selective membrane and the electronic conducting substrate. I^+ and J^+ represent the primary and interfering ions respectively [261].

5.5.2.   Oxygen-Redox Buffering Test for the Solid Contact

This test is designed to monitor the influence of bubbling argon (or nitrogen) and oxygen through the sample solution. By alternating the different gases, conclusions can be proposed to the handling capabilities of the electrode towards redox-active species in solution that can diffuse through the membrane. An example of an oxygen-redox test on three different SCISEs can be viewed in Figure 5.10. Figure

5.10 shows the influence of poly(3-octylthiophene) (POT) on the electrodes response to changes in oxygen concentration in the sample solution. The electrode without the POT showed potential drifts when the gas was changed from argon to oxygen then back to argon. When a conducting polymer was introduced between the membrane and the solid gold substrate the sensitivity towards oxygen was prevented and a constant potential was obtained.

The removal of the miniscule water-layer, or the introduction of an appropriate ion-to-electron transducer between the membrane and solid substrate reduces the possibility of an oxygen half-cell forming, which would be perturbed by differences in oxygen concentrations in sample solutions. It is also possible that a water layer may form, but the solid contact is able to buffer against the oxygen redox process and therefore eliminate a significant potential drift.
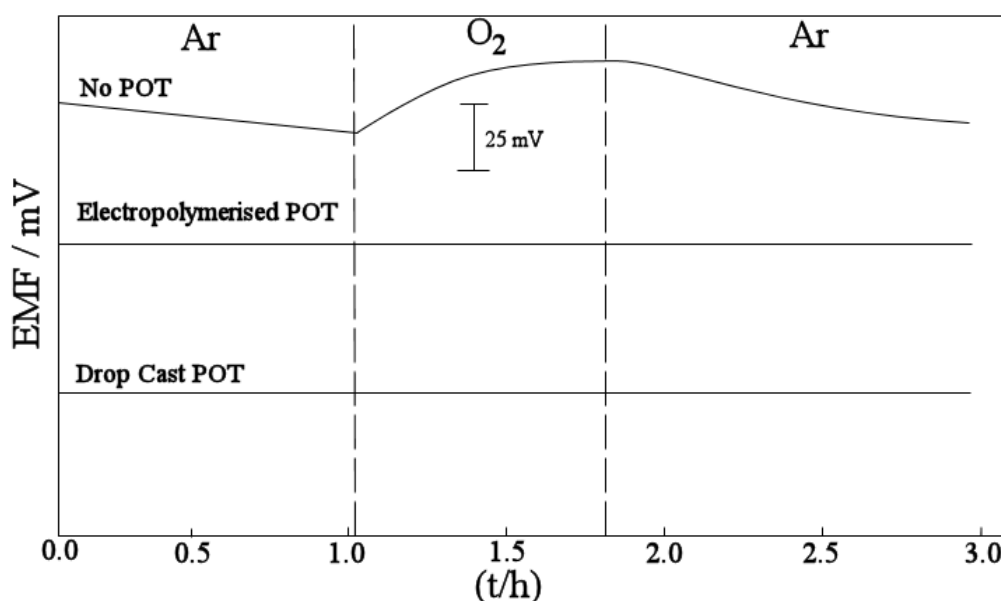
Figure 5.10: Example of an oxygen-redox test on SC-ISEs with and without a conducting polymer as an ion-to-electron transducer [297].

5.5.3. Electrochemical Impedence Spectroscopy

Electrochemical impedence spectroscopy (EIS) is a useful and powerful tool for understanding electrochemical systems for a variety of applications. EIS allows for

the separation and characterization of various individual kinetic processes through a non-destructive steady-state technique by probing the relaxation phenomena over a variety of frequencies [298-300]. Initially, EIS found widespread use in the corrosion area and has provided a plethora of information on the mechanistics of electrochemical systems. Processes such as electrochemical reaction rates, corrosion behaviour, diffusion, passivation, adsorption and film thickness can be determined from the resistance and capacitance displayed in the EIS spectra [299]. Over recent decades EIS has also provided information on various adsorption and charge transfer processes of sensors [257, 282, 300-305].

EIS works by applying an AC potential (usually sinusoidal) of a small amplitude to an electrochemical system, then measuring the AC current signal containing its excitation frequency and its harmonics [306]. The excitation signal can be expressed as;

$$E_t = E_0 \sin(wt)$$

Equation 5.6

and the measured current signal as;

$$I_t = I_0 \sin(wt + \phi)$$

Equation 5.7

where E_t and I_t are the potential and current response at time t (sec), E_0 and I_0 are the amplitude of the applied signal and maximum amplitude of the measured current respectively, $w = 2\pi f$ (f = frequency in Hertz (Hz)), ϕ is the phase angle between the perturbation and the response signals and I is the amplitude of the measured signal [299, 306, 307]. The impedance of a system can now be calculated according to Equation 5.8, which is an analogue of Ohms law [299, 306].

$$Z = \frac{E_t}{I_t} = \frac{E_0 \sin(wt)}{I_0 \sin(wt + \phi)} = Z_0 \frac{\sin(wt)}{\sin(wt + \phi)}$$

Equation 5.8

The impedance is expressed as a function of magnitude (Z_0) and phase shift (f) and is therefore a vector quantity that has a real component (Z') and an imaginary component ($-Z''$). A plot of $-Z''$ vs Z' (Nyquist or complex plane plot) displays the impedance obtained at different frequencies at a given potential, as shown in Figure 5.11.
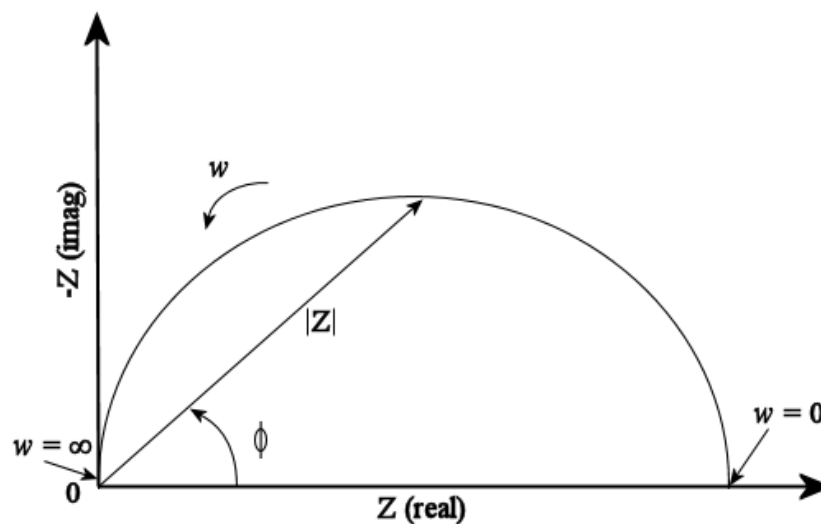
Figure 5.11: A schematic representation of a complex plane plot (Nyquist plot) of a simple single time constant.

The simple semicircle displayed in Figure 5.11 is a result of a single time constant which can be represented by the circuit diagram below.
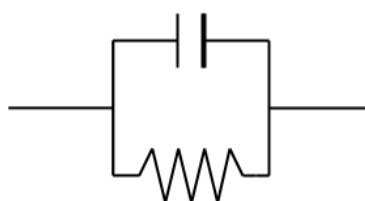
Figure 5.12: A simple equivalent circuit with one time constant displayed as a resistor and capacitor in parallel.

Often, electrochemical systems are more complicated with several time constants being present, which may manifest themselves as partial semicircles on the Nyquist plot. Various equivalent circuits made from resistors, capacitors and inductors can be constructed in various arrangements to model the data and help extract the

mechanistics of the system. The typical Randles circuit can be used to model a range of electrochemical systems (see Figure 5.13) [307].
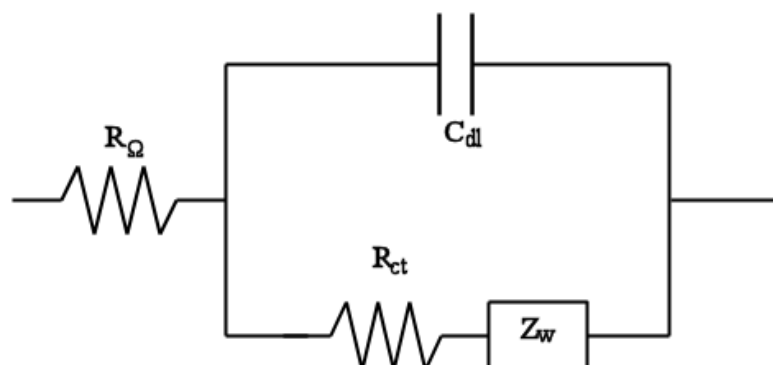
Figure 5.13: Randles circuit. C_{dl} = double-layer capacitance, R_{ct} = charge transfer resistance, R_{Ω} = uncompensated resistance (solution resistance), Z_w = Warburg impedance (diffusion).

The uncompensated resistance (R_{Ω}) is a result of the solution resistance between the working and reference electrodes, whilst that of the Warburg impedance is a result of the semi-infinite linear diffusion process in the system. A more detailed description of how EIS works and the various circuit models can be found in the literature [306, 308-311].

EIS has been used to understand processes associated with ISEs for many years, especially in relation to interfacial properties of PVC based membranes electrodes [300, 312]. The technique has been used to probe the effect of plasticizer content, membrane thickness, ionophore/anion exchanger ratio, ionic site concentration, pH, and type of plasticizer on the impedance of the ion-sensing membrane [312-314]. In addition to liquid contact ISEs, EIS has been intensively use with SC-ISEs, particularly for those that use conducting polymers as an intermediate layer between the membrane and the solid substrate [257, 281, 282, 294, 305, 315-319].

In this thesis, EIS is used to gain information on the interface between the ion conducting membrane and the electron conducting substrate in SC-ISEs. We will use the technique to determine if water layers or water droplets formed between the ionic conducting membrane and the electronic conducting substrate by probing the

response of the electrode over time from the initial point of contact with the measuring solution.

5.6.   Polymer Matrices of Solid Contact ISEs

Although PVC has been the most widely used polymer matrix, it still has disadvantages. One of the most important disadvantages is the leaching of plasticiser from the membrane into the sample. The leaching of plasticiser into the sample causes the sensor's potential to drift especially over long periods, and also contaminates the sample solution [28]. With true miniaturisation and the reduction in sample volumes, minute amounts of plasticiser leaching could be critical, especially in in-situ biological applications where the leaching plasticiser could result in irritation or other toxic effects. However, a reduction in the level of plasticiser decreases the diffusion co-efficient in PVC membranes, which can lead to ionophore inactivity and a slowing of membrane response [320]. Decreasing the plasticiser (or membrane solvent) can also lead to a reduction in the solubility of an ionophore or ion-exchange within the membrane and subsequently affect the sensors selectivity and sensitivity. However, PVC with lower levels of plasticiser exhibit better adhesion properties in SC-ISEs [263]. Better adhesion between the membrane and solid conducting substrate discourages the formation of a water layer.

To overcome the problems associated with PVC based membranes, other polymers such as polyurethane, polyacrylates and methacrylates and ones based on silicon rubber have been tested, but with moderate success.

Polyurethane (Tecoflex®) has been tested in membranes with minimal or no plasticiser, without loss of the sensor response characteristics [321, 322]. The use of this polymer in membrane cocktails has been shown to increase biocompatibility by limiting the plasticiser content of the membrane [321]. The first polymethacrylates tested suffered from incompatibilities with the various plasticisers used, as well as the excessive volumes required compared to PVC membranes [320]. High levels of plasticiser are undesirable for a number of reasons: 1) high levels promote the leaching of membrane components, which reduce the sensors lifetime and perturbs

the electrode response, as discussed above; 2) The toxicity of excluded plasticiser in biological applications; 3) The relative expense compared to the amount used in PVC membranes, which would be significant enough in large-scale applications; 4) High levels required for optimal response can reduce mechanical strength and therefore limit the available applications of the sensor; 5) Difficulties in sensor minaturisation and true "reagentless" solid-state electrodes, which can lead to fabrication through photolithography/photocuring [28, 323].

Recently, a series of plasticiser free polyacrylate and poly(n-alkyl)acrylate co-polymers have been tested in both conventional and solid contact ISEs with excellent results [28, 278, 297, 320, 323-325]. The plasticiser free nature of this new series of ISE polymers promotes the minaturisation of these sensors and increases the breadth of possible analytical tests as a result of greater biocompatibility. The diffusion coefficient of these membranes is in the order of a thousand times lower than in plasticised PVC membranes; however, they still produce steady and quick response ISEs [230].

PVC based membranes require plasticisers to reduce the glass transition temperature (T_g) below that of room temperature. The co-polymers of the methacrylates with the correct proportions of each of the monomer units have a sufficiently low T_g to be utilised without the incorporation of plasticisers. The T_g in methacrylate co-polymers is partially the result of the quantities of monomers used in its preparation. Other factors such as method of measurement, aging of the polymer and the polymer molecular weight also play an important role [320]. As a consequence of the many factors that make up the polymer's T_g, only an estimate can be made prior to its preparation. A T_g range can be determined using the Fox equation (Equation 5.9) [28, 320]

$$\frac{1}{T_g(co)} = \frac{F_a}{T_g(a)} + \frac{F_b}{T_g(b)}$$
<div align="right">Equation 5.9</div>

where $T_g(a)$ and $T_g(b)$ are the glass transition temperatures of the homopolymers of the respective monomers in Kelvin. F_a and F_b are the weight fractions of the

monomers and $T_g(co)$ is the calculated glass transition temperature of the co-polymer also in Kelvin.

The glass transition temperatures of the homopolymers of the two monomers are 105 ˚C for MMA and −30 ˚C for DMA. The presence of the MMA improves the film forming properties of the membrane whilst the DMA acts as the plasticiser in membranes by reducing the glass transition temperature [28]. The co-polymer is produced via free radical initiation in a homogeneous solution. This method is chosen as it introduces very few impurities into the final membrane. Impurities remaining from the manufacture of PVC and the various plasticisers act as anionic sites in the membrane. These impurities are the reason PVC membranes with no additional ionic sites can produce a cationic Nernstian response. Bakker and co-workers demonstrated that the MMA-DMA co-polymer produced no response to sample ions as a result of the lack of binding sites [28].

As a result of the good properties and excellent electrode behaviour shown recently for the co-polymer of methyl methacrylate (MMA) and decyl methacrylate (DMA), it was desirable to test this membrane support with one of the previous series of thallium sensing calixarenes.

5.7. Response of Solid Contact ISEs Incorporating a Calixarene as an Ionophore for Thallium(I) Detection

The calixarenes that were presented in Chapter 4 using a conventional liquid contact configuration showed excellent response to changes in thallium activity and good selectivity over a range of interfering ions. It was also demonstrated that the lower detection limit could be reduced by controlling ion fluxes within the membrane through the application of a controlled inner filling solution. One of the benefits of SC-ISEs is that the inner solution is absent, which ideally would result in zero ion fluxes from the inner side of the membrane to the outer and no analyte release into the sample. However, the process of SC-ISEs is not as simple as it initially appears and other problems occur in many parts of their design. Despite this, SC-ISEs have many potential advantages over their conventional liquid contact counterparts.

The following section will present work on the incorporation of calixarene (4) into a SC-ISE, to be used for thallium(I) detection and aiming to overcome the problems of its liquid contact counterpart as described in Chapter 4. Various tests will be carried out to ensure that the SCs are working adequately and do not suffer from known problems. Several types of SC-ISEs will be tested to predict the best electrode for future development.

5.7.1. Calibration and Detection Limits of the Solid Contact Ion-Selective Electrodes

Many different types of SC-ISEs have been tested throughout the literature with varying results [254-260, 267, 268, 280, 282, 295, 323]. It was decided to test the calixarene (4) ionophore in four types of SC-ISEs, consisting of: a) a graphite conducting substrate covered with a redox-active insoluble salt with a plasticized PVC membrane as the sensing material, (Graphite Contact); b) a gold conducting substrate covered with a plasticized PVC membrane, (Plain-Au-SC); c) a gold conducting substrate covered with polypyrrole then a plasticized PVC membrane (PPy-SC); and d) a gold conducting substrate covered with poly(3-octylthiophene) then a plasticizer free MMA-DMA membrane as the sensing substrate (POT-SC). Graphical representations of the SC-ISE designs are displayed in Figure 5.14.
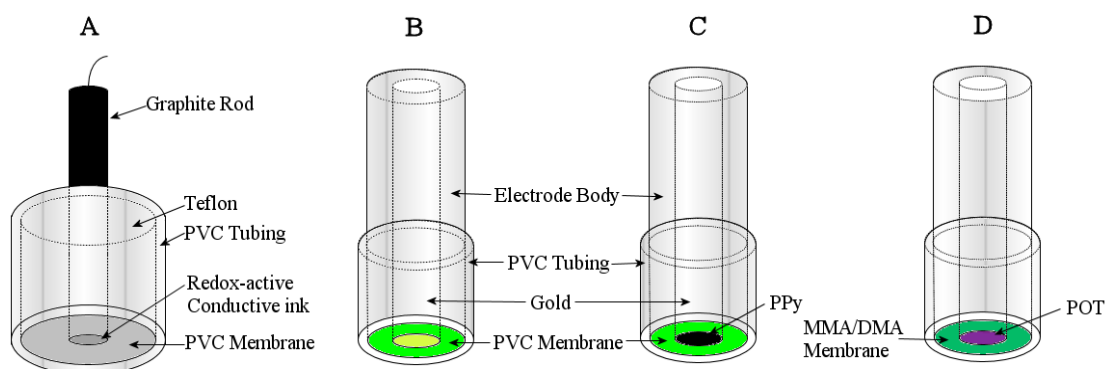
Figure 5.14: Graphical representations of the various solid contact ion-selective electrodes tested in this chapter. A) Graphite Contact, B) Plain-Au-SC, C) PPy-SC, D) POT-SC.

The gold disc electrodes used in the study were obtained as standard solid state electrodes available from a commercial source, whereas the graphite ISEs were constructed from spectroscopic grade graphite that was cleaned prior to use, then encased in Teflon.

The ideal advantage of SC-ISEs over the conventional inner solution counterparts is that they contain no inner solution which eliminates ion gradients in the membrane and provides an unbiased lower detection limit. Unfortunately, it has been found by different research groups that a water film or droplets develop between the membrane and the conducting substrate where ions can congregate at relatively high concentrations and lead to the same biased results as in inner liquid contact ISEs [259-261, 263, 267, 326, 327]. Apart from the bias in lower detection limits and selectivities, the inner water layer resulted in potential fluctuations as a result of an ill defined redox half-cell [255, 261, 264]. The established redox couple in the water layer was that of an oxygen half-cell which reacted to changes in temperature and more importantly partial pressures of oxygen in the sample. It is apparent that one of the major problems facing SC-ISEs stem from the inner water layer between the membrane and solid conducting substrate.

Over the past few years measures have been employed to remove the water layer and also establish a well defined ion-to-electron transducer system. The calibration graphs of the four electrodes obtained by changing the Tl^+ activity are displayed in Figure 5.15.
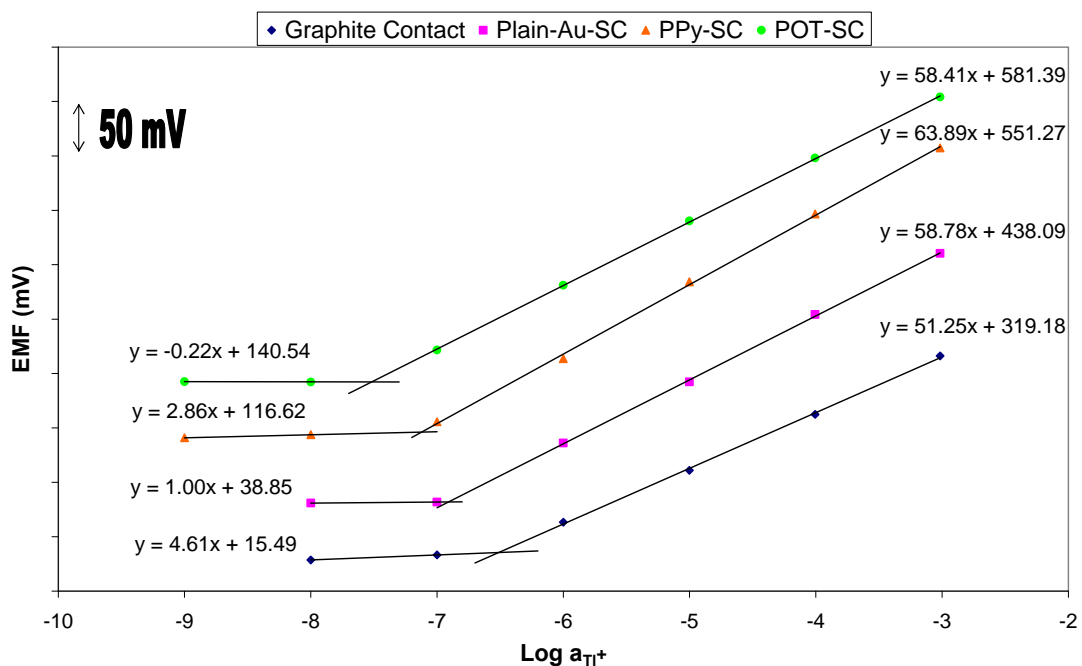
Figure 5.15: Calibration graphs of solid contact ISEs using calixarene (4) as the ionophore. E^0 values of the calibrations are different as they have been separated by uniform addition to the obtained values. Electrodes consist of one graphite based substrate and three gold based substrates.

All electrodes show good Nernstian responses over a wide concentration range, with electrodes, "Plain-Au-SC" and "POT-SC" producing the best response. The graphite electrode showed a slightly sub-Nernst response of 51.3 mV/decade, which could be due to the conductive ink and redox-salt leaching into the membrane. When the membrane cocktail was drop cast over the redox-active ink, it appeared to have dissolved in the PVC membrane solvent and had become incorporated into the membrane cocktail. The graphite electrode consisted of a graphite rod coated with a conductive ink which contained 5% w/w La-DCPI that was surrounded in a Teflon body, the coated graphite rod and the Teflon body was then coated with the plasticized PVC membrane incorporating calixarene (4) and NaTFPB. The electrode "PPy-SC" produced a slightly super-Nernst response, which might be due to the conducting-polymer polypyrrole being used as the ion-to-electron transducer. The "PPy-SC" electrode consisted of a gold substrate covered with polypyrrole, that was electropolymerised on the gold surface in the presence of potsssium hexacyanoferrate(II)/(III), which was then covered with a plasticized PVC membrane incorporating calixarene (4) and NaTFPB.

The detection limits of the four different types of SCISEs are displayed in Table 5.1.

Table 5.1. Lower detection limits with thallium(I) of four types of solid contact ion-selective electrodes using calixarene (4) as the ionophore

Electrode	Support	Membrane Matrix	Log a_{Tl^+}	Lower Detection Limit
Graphite Contact	Graphite	Plasticised PVC	-6.51	0.31 μM
Plain-Au-SC	Gold	Plasticised PVC	-6.91	0.12 μM
PPy-SC	Gold	Plasticised PVC	-7.12	75.8 nM
POT-SC	Gold	MMA/DMA Co-Polymer	-7.52	30.2 nM

The graphite electrode produced a detection limit similar to that obtained in Chapter 4 which consisted of an inner filling solution of a highly concentrated salt of the primary ion. The detection limit in cases of highly concentrated inner solutions is influenced by ion fluxes of primary ions in the membrane, which leads to ions being released in the sensed Nernst diffusion layer and biasing the lower detection limit. The graphite electrode should ideally be void of an inner aqueous solution and provide improved detection limits. However, the detection limit obtained with the graphite electrode indicates that an inner aqueous layer may exist, where ions can congregate at relatively high concentrations and perturb the response at low sample activities as a consequence of ion fluxes. The conductive graphite based ink was designed to expel water from the inner contact through a highly hydrophobic medium between the membrane and the conducting substrate. Further tests to determine the presence of a water layer or water pockets between the membrane and the graphite rod are presented in the following Sections.

The electrode "Plain-Au-SC", consists of a gold substrate covered solely by a plasticized PVC membrane containing the ionophore (calixarene (4)) and NaTFPB. Similar to the graphite electrode a detection limit in the micromolar region is indicative of a water layer between the membrane and gold surface. This is not surprising since many groups have reported problems associated with SC consisting of just a substrate coated with the ion-sensing membrane [256, 260, 261, 305, 327, 328]. The solid contacts of this design are subjected to the same ion fluxes that occur

in their liquid contact counterparts, and are therefore limited to the same detection limits [305, 327].

The detection limit was improved slightly through the incorporation of a conductive polymer between the ionic conducting membrane and the electronic conducting substrate, "PPy-SC" in Figure 5.15. The purpose of the conducting polymer is to act as an ion-to-electron transducer whilst preventing the formation of a water layer through a highly hydrophobic polymer. The electrode with the intermediate layer of polypyrrole shows a detection limit that is inferior to that obtained with the liquid inner contact and an EDTA buffer, see Section 4.7.1. This could be due to the process of spontaneous charging/discharging that can occur in conducting polymers under operating conditions, and has shown to affect both detection limits and selectivities [292, 293, 329]. It has also been demonstrated by Sutter, J. et. al. that the preparation of the conducting polymer layer is crucial to the absence of a water layer and enhanced electrode response [326]. Soaking the conducting polymer after electropolymerisation in water for several hours aided in the prevention of a water layer and detection limits down to nanomolar levels [326]. Even though the experimental procedure from the literature was followed, slight personal variations may lead to imperfections and as a consequence a higher than expected detection limit. A better understanding of the electrode preparation and its ramifications for the sensor response is required if the detection limit of the thallium SC-ISE using polypyrrole as the intermediate layer is to be reduced further.

The selectivity of calixarene (4) with respect to the H^+ ion may also contribute to the inferior detection limit as polypyrrole can be affected by pH. The choice of the doping anion also affects the sensor's response, with some having little prevention of water layer formation. Based on the literature it was decided to polymerise the pyrrole in the presence of potassium hexacyanoferrate(II)/(III) to achieve the best results.

The best detection limit of the tested SC-ISEs occurred with the use of a gold substrate coated with POT and then a layer of MMA-DMA copolymer, which included calixarene (4) as the ionophore and NaTFPB as the ion-exchanger, (POT-SC). The lower detection limit of 30.2 nM is in agreement with the value obtained

from the liquid contact which contained an EDTA buffered inner filling solution. This suggested that the inner water layer between the membrane and the gold substrate has been removed as there is no sign of ion fluxes in the membrane leading to the leaching of the primary ion into the sample. According to the calculation for the lowest possible detection limit based on the dynamic model, the optimal detection limit has been reached for this ionophore in a sample of only thallium(I) nitrate. The absence of the water layer could be a result of the highly lipophilic polymer POT used as an ion-to-electron transducer, therefore repelling water away from this region [289]. POT has the highest lipophilicity of all of the conducting polymers used in ISEs and lacks basic functionalities preventing spontaneous discharge [297]. The prevention of the water layer could also be a result of the good adhesive properties and water excluding properties of the MMA-DMA copolymer [297].

Based on the calibration graphs, the most promising electrode looks to be that of the POT/MMA-DMA system. As was the case in the liquid contact ISEs the lower detection limit may be dictated by the H^+ ion in the solution. An attempt was made to reduce the pH of the solution with LiOH, but it was found that to reduce the H^+ concentration significantly, a moderate proportion of lithium had to be added, which also interfered with the ISE's response. Attempts to lower the detection limit further by increasing the sample pH were unsuccessful, suggesting that alternate reasons are responsible for the lower detection limit in the current series of thallium ISEs. This is further supported by the lower detection limit of the "POT-SC" electrode, which should be devoid of an inner solution resulting in no ion fluxes towards the sample and a lower detection limit than the EDTA inner filling solution electrodes. If no water layer is present in the "POT-SC" electrode then the lowest possible detection limit may have been reached for this series of thallium ionophores. The reason for the slightly higher than expected detection limit for the synthesised series of thallium selective ionophores is unknown and may be the result of factors that are out of our control. One of the factors influencing the response could be unusual calixarene interactions occurring with other organic molecules in the membrane which is a consequence of the unique properties of these calixarenes.

However, to confirm the presence or absence of water layers based on the calibration results further tests were performed.

5.7.2. Time Responses of the Four Solid-Contact Thallium(I) Ion-Selective Electrodes.

The time responses of the calibration graphs conducted on the four SC-ISEs are displayed in Figure 5.16. The solid contact electrodes showed similar trends to that of the inner liquid contact counterparts. A steady response was achieved in a matter of seconds for concentrated samples whilst it took considerably longer periods for dilute samples. The four SC-ISEs show good response rates to changes in thallium(I) concentration in the sample. The slight positive drift in samples of low thallium(I) concentration could be due to thallium(I) ions leaching into the sample as a consequence of the high concentration of the conditioning solution used. The electrodes were conditioned in 10^{-4} M TlNO$_3$, which may have lead to some co-extraction in the membrane and subsequent release in dilute samples. Conditioning the membrane in 10^{-7} M TlNO$_3$ after the 10^{-4} M solution may have prevented this and lowered the detection limit slightly.
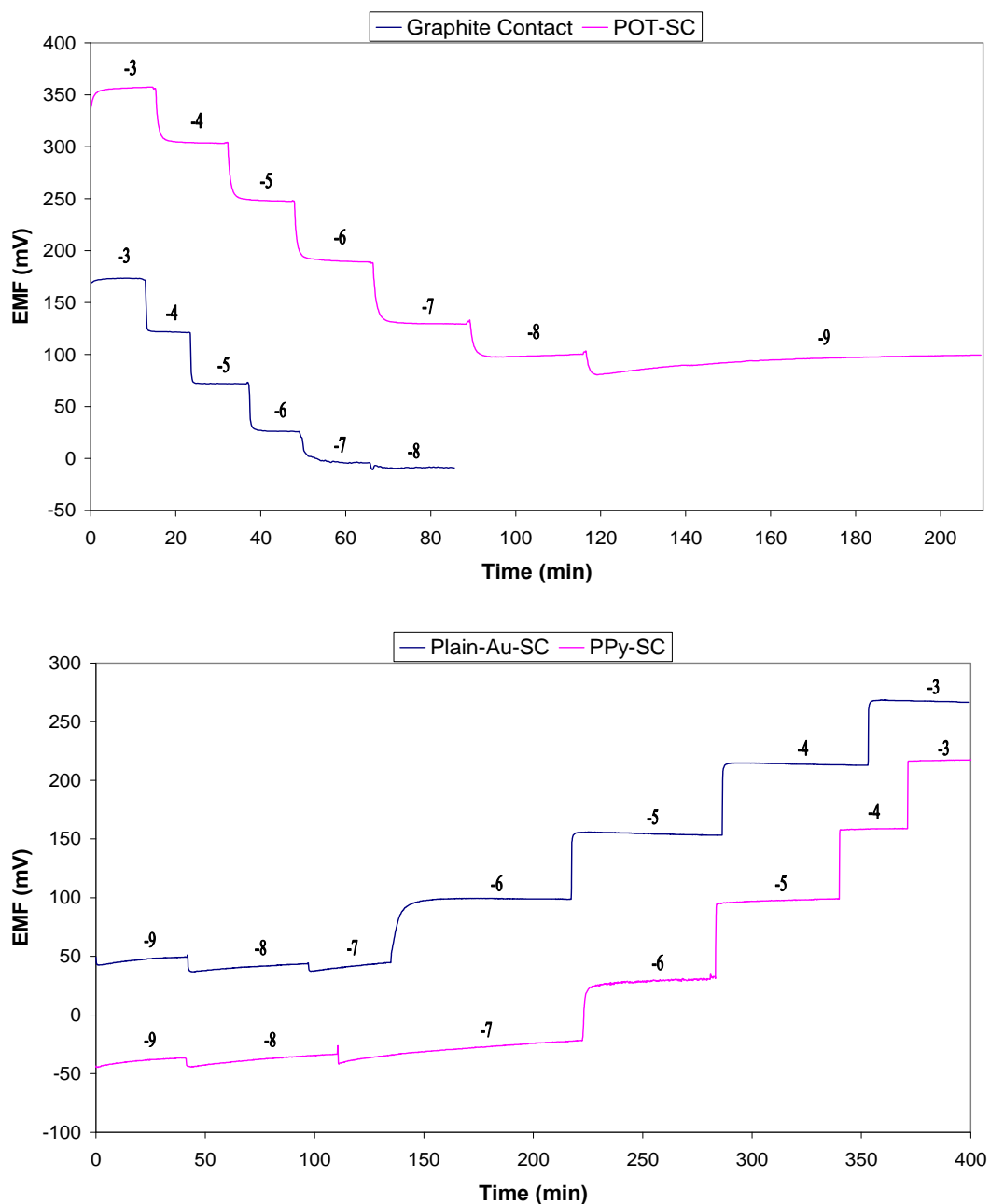
Figure 5.16: Time responses of the four solid-contact ion-selective electrodes incorporating Calixarene (4) as the ionophore in the membrane.

5.7.3. Determination of the Presence of a Water Layer in the Four Solid-Contact Thallium Ion-Selective Electrodes.

5.7.3.1. Potentiometric Water Layer Test

The potentiometric water layer test has been used for several years to evaluate a SC sensor's ability to exclude water from the contact between the conducting substrate and the ion-sensing membrane [261, 263, 297, 326, 328]. Since the removal of the water layer is crucial in producing SC-ISEs with low detection limits, it is vital that the water layer is removed in thallium(I) based sensing electrodes as sample concentrations would primarily fall within the nanomolar region. The water layer tests obtained by changing the sample solution from a low concentration of Tl^+ to a high concentration of interferent then back to the initial Tl^+ is displayed in Figure 5.17.

In the following test, a water layer is indicated if the potential rises after the initial drop in the first sample change, then a decrease after a potential rise in the second sample change back to the initial solution. The potential rise after the initial drop is a consequence of ions exchanging on the inner side of the membrane, which changes the composition of the inner solution rapidly. The potential drop after the second sample change is the reverse effect with interfering ions being exchanged back into the membrane phase [261].
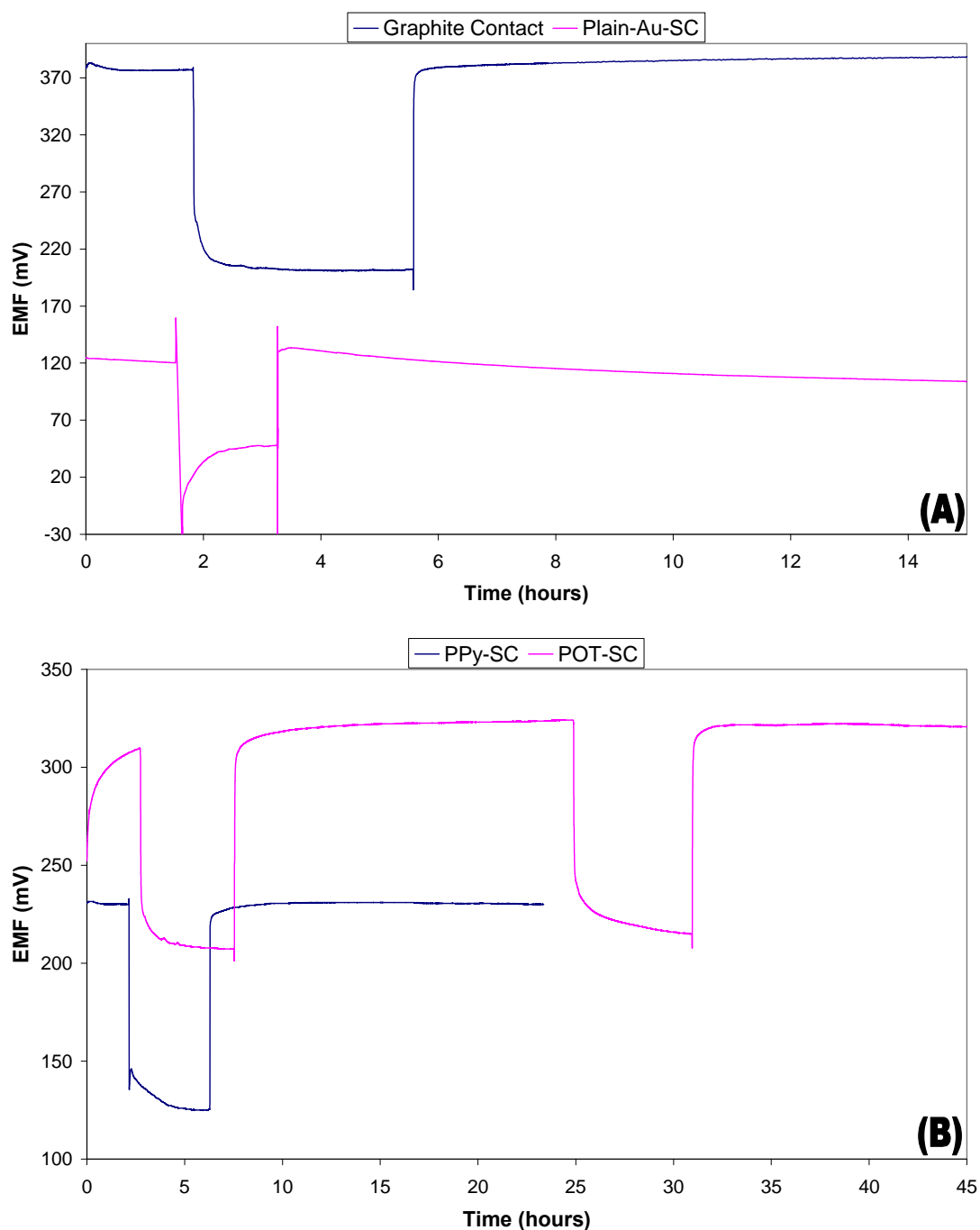
Figure 5.17: Results of the water layer tests for the four Tl^+ selective SCISEs. Graphite contact and Plain-Au-SC (A) and PPy-SC and POT-SC (B). Initially EMFs of the four electrodes were recorded in the primary ion (Tl^+), then changed to an interfering ion (Na^+) for several hours, then changed back to the primary ion once more.

All four electrodes show a potential drop of around 100 mV by changing the sample solution from a primary ion to an interfering ion. The only electrode that showed the presence of a water layer by the increase in potential after the initial decrease was that of the "Plain-Au-SC". This was to be expected as it is now well known that water penetrates the plasticised membrane and lodges between the gold substrate and the membrane [263, 330]. The "Plain-Au-SC" electrode data shows the fast exchange for the thallium entering the membrane from the inner side and fluxing outwards to the sample and then the slow exchange of thallium back into the water layer on the inner side of the membrane when the solution is changed back to the primary ion. This test confirms that the detection limit shown in Figure 5.15, for the "Plain-Au-SC" is a result of fluxes in the membrane leading to biases in the electrodes response. At the start of each trial with the "Plain-Au-SC" electrode, the response slowly drifted, which could be a consequence of the ill defined redox process occurring in the between the membrane and the gold substrate. The ion-to-electron conversion at the electrode interface is hypothesised to be that of an oxygen half cell, which is sensitive to minor changes in the sample and may be further evidence of water at the gold surface.

It is surprising that the "Graphite Contact" did not show the presence of a water layer, as the detection limit in Figure 5.15 for this electrode occurs in the micro molar region, which suggests ion fluxes are present perturbing the electrodes response at low analyte concentrations. The electrode's response in the calibration may be due to other factors such as leaching of the conductive ink into the polymer, leading to an increase in the lower detection limit. More work is required on this electrode to determine the cause of the high detection limit.

The "PPy-SC" and the "POT-SC" did not show the presence of water layers which is to be expected based on the lower detection limits presented in Figure 5.15. The "POT-SC" electrode did not stabilise quickly which is a consequence of the lower diffusion coefficient compared to plasticised PVC membranes. To counteract this, thinner membranes are used to show the ion-exchange occurring within an acceptable time frame. Even though the membrane thickness had been reduced from that of their inner liquid counterparts, it might not be sufficiently thin to allow an ion-exchange at the inner side of the membrane in the allowed time frame. To rule

out possible errors due to membrane thickness, membranes thinner than 100 μm should have been used, or even longer analysis times. Even so, the potentials were decreasing slowly for more than five hours without showing the slightest increase as a result of ion exchange on the inner side of the membrane.

The water layer test was conducted twice for the electrode "POT-SC" on the same run as the potential was not stable after only one night of conditioning. After a second night in 10^{-4} M TlNO$_3$ the electrodes response was stable. The long conditioning time is a result of the diffusion coefficient of the MMA-DMA copolymer which can be up to three orders of magnitude lower compared to plasticised PVC [230, 297].

Apart from the "Graphite Contact" the potential water layer test is consistent with the findings from the calibration graphs and the lower detection limits. This demonstrates that the best responses are achieved with solid contacts that have intermediate systems between the electric conducting substrate and the ion conducting membrane.

5.7.3.2. Electrochemical Impedance Spectroscopy Water Layer Test

EIS is a powerful tool for the characterisation of electrochemical systems which are influenced by a variety of factors e.g. surface adsorption of molecules, or the impact of water in the matrix. Solid contact polymeric ISEs have previously been characterised by EIS, but were often only conducted at one particular point in time [257, 281, 282, 294, 305, 313, 315, 316]. The singular spectra obtained from these experiments provided valuable results, however, fluctuations over time due to changes in the electrochemical system are missed. Experiments that were conducted over a period of time only analysed the long-term stability of the electrodes and their respective membranes [317, 318]. Since EIS can be conducted in-situ we propose here to characterise the sensor from first contact with the solution until at least forty-eight hours after this initial contact. Impedance scans were conducted every hour from the initial point of solution contact. The complex-plane plots (or Nyquist plots)

of chosen hours for the four SC-ISEs are displayed in Figure 5.18 to 5.22. All four plots show large high-frequency semicircles which are indicative of the ISE membrane bulk resistance in parallel with its geometric capacitance [282, 302, 318]. The semi-circles at low-frequencies are assigned to the interfacial impedance of the charge transfer resistance and double-layer capacitance at either the membrane/substrate or membrane/solution interfaces [282, 304, 305, 316, 318]. The solution resistance is masked by the large resistance of the membrane and is therefore not seen on the raw or unexpanded plots.
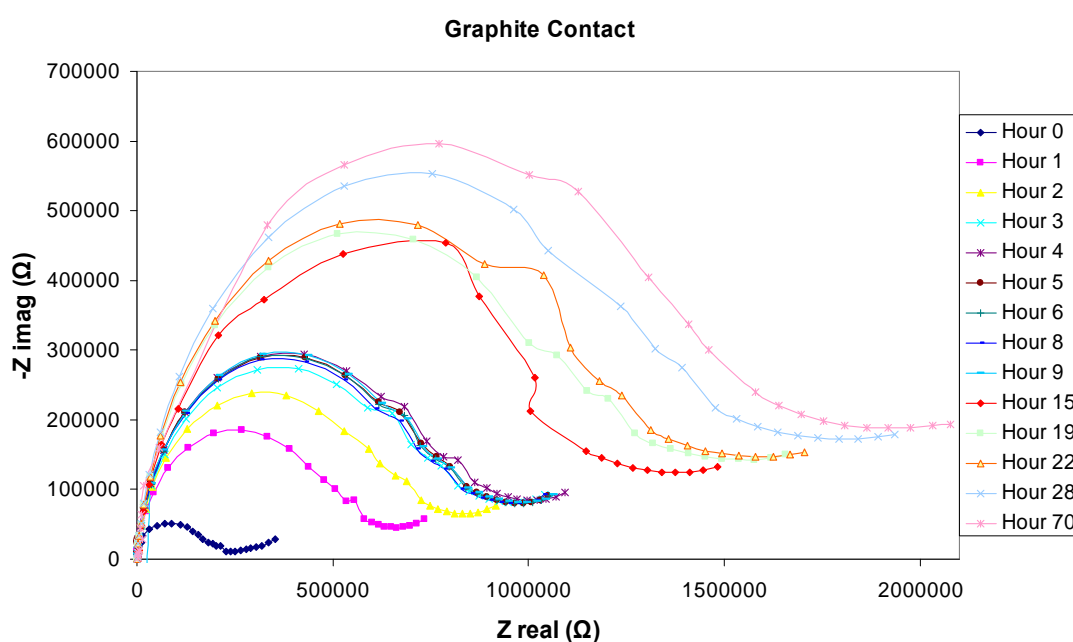
Figure 5.18: Complex plane plots of the Graphite Contact electrode in a solution of 10^{-2} M TlNO$_3$ over a period of 70 hours after initial contact with the conditioning solution

The bulk membrane impedance of the graphite electrode increases over the period of three hours from when it is initially placed in the solution from approximately 170 kΩ to 725 kΩ. This increase is attributed to the intake of water, drawing ions or charged molecules out of the continuous membrane into pockets of isolated water, as explained by Buck and co-workers [302]. The impedance stabilizes over the next few hours (3-9) once the membrane has incorporated the maximum loading of water.

The high-frequency semicircle in the scans tails off at midrange frequencies which could be due to another small time-constant overlapping with the membrane impedance. The additional time constant is more than likely due to the La-DCPI redox mediator between the membrane and the graphite rod. The second semicircle is more prominent after initial contact (Hour 0), as ions haven't yet reached the inner side of the membrane to change the nature of the redox compound and influence its charge transfer.

After ten hours of conditioning the electrodes behaviour is unusual, as the membrane bulk impedance rises yet again. Additionally data points around the second semicircle become increasingly scattered. A significant number of spectra were rejected due to poor statistics around this region. The reason behind the increase in membrane impedance and the scattering of the second semicircle is unclear; however it is postulated to be a result of the redox mediator (La-DCPI) in the conductive graphite based ink and the plasticized PVC membrane changing its electrochemical properties. A possible explanation could be that the conductive ink with the redox mediator could be leaking into the membrane and therefore preventing a uniform charge transfer from the membrane to the graphite rod. More tests are required to pin point the reason behind the sudden change in electrode characteristics. The presence of a water layer could not be detected; this would have been indicated by a sudden decrease in membrane response after ten hours due to water and ions lowering the contact resistance between the membrane and electrode. The change in the electrochemical properties of the redox mediator and membrane system may be the cause behind the low detection limit and the lack of potential drifts in the potential water layer test in Section 5.7.3.1.

At the point of immersion in the solution the "Plain-Au-SC" electrode has a bulk resistance of around 223 kΩ. Within the first hour, this has increased slightly to 237 kΩ, which is likely to again be a result of water entering the membrane as pockets and drawing ions out of the continuous matrix into them or alternatively areas of hydrophobic impurities, which have formed throughout [302]. The impedance of the high-frequency semicircle then decreases slowly over several hours back to the original value.

Figure 5.19: Complex plane plots of Plain-Au-SC in a solution of 10^{-2} M TlNO$_3$ over a period of 48 hours after initial contact with the conditioning solution.
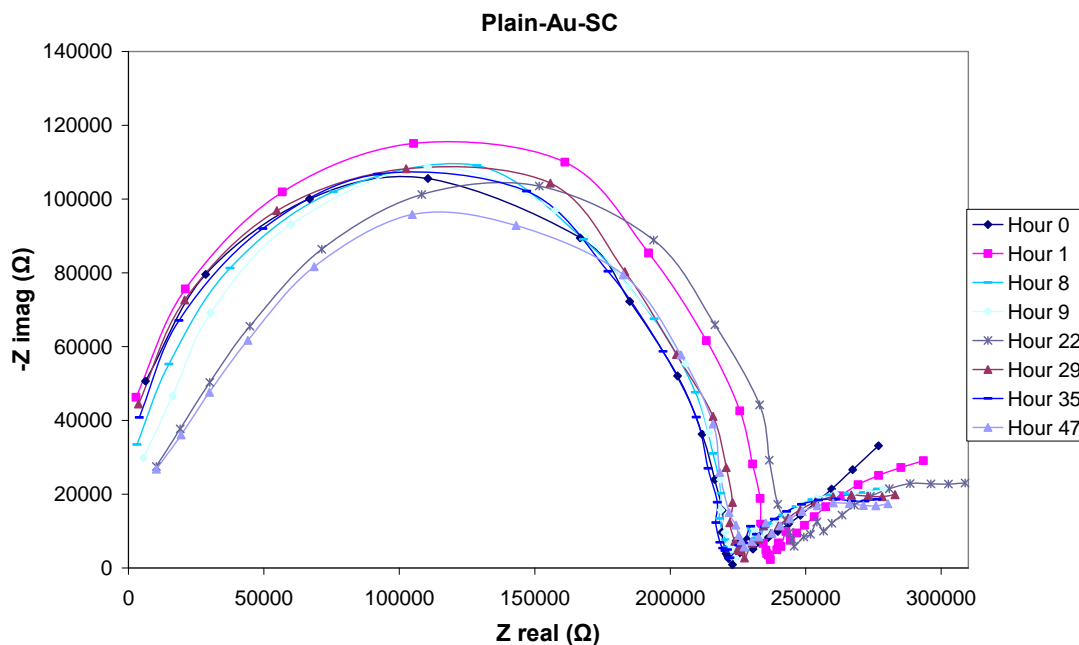
It was initially thought that the impedance drop was due to water reaching the interface between the membrane and the substrate, therefore lowering the contact resistance experienced at this boundary. Other tests recently conducted in the Group have shown that the impedance increases over time, stabilizes slightly, and then decreases as water infiltrates the membrane/substrate interface. Once the maximum amount of water has entered the space between the membrane and the substrate the impedance stabilizes once again. Complex-plane plots of a tested Ca^{2+}-selective SC-ISE consisting of a PVC/DOS membrane over plain gold showing a water layer is displayed in Appendix VII. However the bulk membrane impedance of "Plain-Au-SC" again slowly increases to 245 kΩ at 22 hours where it then returns back to the original value. This second rise and fall in impedance could not be the result of a water layer and therefore has to be from another factor controlling the system. The fluctuations could possibly be due to other electrical interferences based on the day/night cycle affecting the electrodes response as a result of increased electrical activity during the day. All EIS tests were conducted in a dark cell which eliminates any photochemical effects but does not prevent stray electrical effects.

One characteristic that is missing from the above complex plane impedance plots that is seen in other plots is the large increase in impedance when the electrode is initially placed in the solution. An example of the large increase in impedance at the start of conditioning is shown for the "Graphite Contact" electrode in Figure 5.18 and also in Figure 5.20, which was conducted on a calcium selective PVC/DOS solid contact electrode. The significant increase in impedance is from the immobilization of ionic species in aqueous regions in the membrane which are formed from water entering the membrane and congregating in hydrophilic impurities [302].

The initial increase in impedance may be a result of the larger AC amplitude used on the gold electrodes. An AC amplitude of 50 mV was used to diminish the effects of noise and this may accelerate the process of water intake and therefore not be seen on the initial complex plan plots. The graphite electrode in Figure 5.18 used FNDPE as the plasticizer whereas the "Plain-Au-SC" used DOS, which also may have affected the intake of water.

Figure 5.20: Complex plane plots of a Ca^{2+}-selective SC-ISE in 10^{-3} M $CaCl_2$ over a period of 6 hours after initial contact with the conditioning solution. The spectra shows the increase in impedance from the initial point of contact, which is said to be due to water infiltrating the membrane and drawing ions out of the continuous membrane into localized pockets.

It is also interesting to note the changes in the low-frequency semi-circle at the start of the test in Figure 5.19. Initially, the second time constant looks to be due to Warburg diffusion, but quickly changes to a second semi-circle after only a couple of hours conditioning, after which it remains constant. The second semicircle is known to occur from charge transfer and double layer capacitance at the electrochemical interface. There is a definite change occurring at the membrane/substrate interface over the first few hours. Since water and oxygen are able to travel through the membrane, an oxygen half-cell establishes itself at the gold surface therefore increasing the low-frequency capacitance and decreasing the charge-transfer resistance, which is characteristic for unblocked interfaces [305]. Initially there is a blocked interface and no second time constant as a result of water not reaching the interface yet. After only a few hours, a water layer has established and with it an oxygen redox half cell lowering the charge transfer resistance at the membrane/substrate interface.

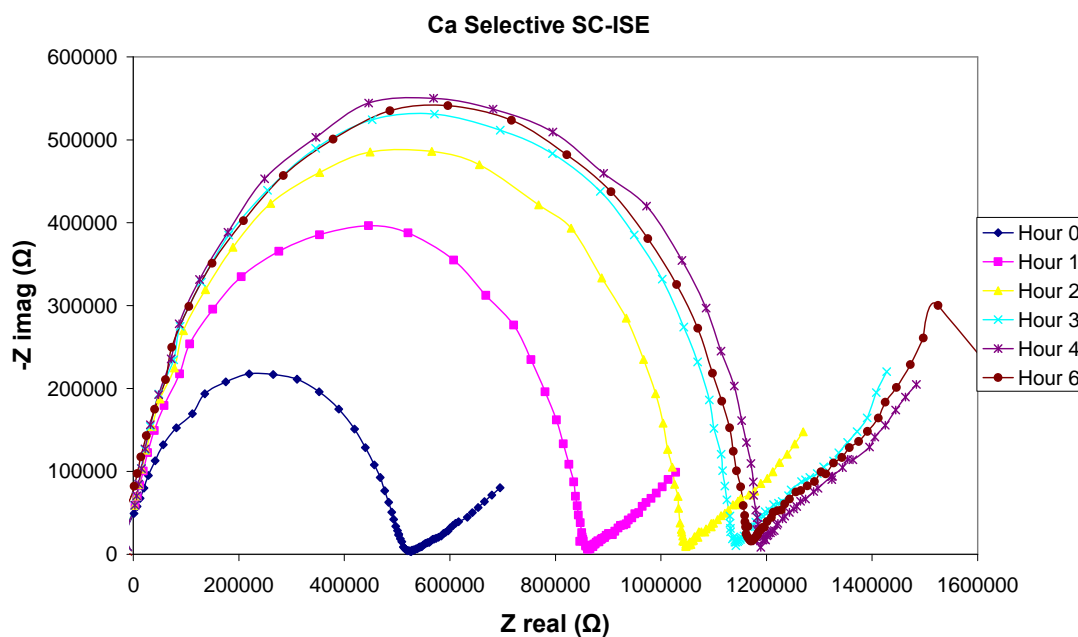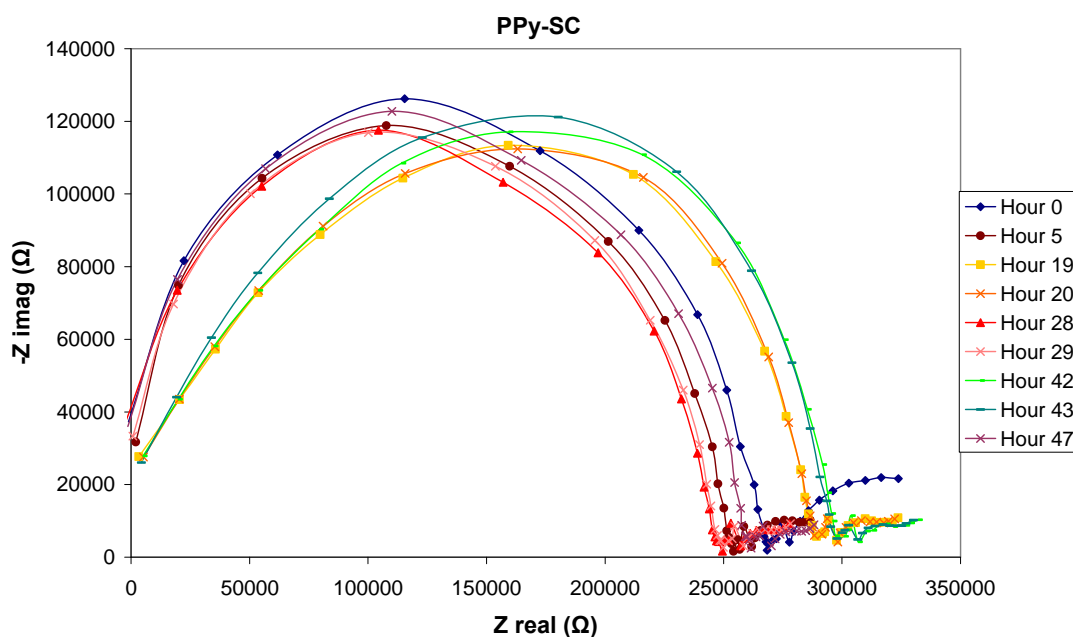

Figure 5.21: Complex plane plots of PPy-SC in a solution of 10^{-2} M TlNO$_3$ over a period of 48 hours after initial contact with the conditioning solution.

The low-frequency semicircle for the electrode containing polypyrrole as the intermediate layer between the membrane and the substrate is prominent from the initial scan (Figure 5.21) unlike the first run in Figure 5.19. The low-frequency

semicircle is due to the capacitance and charge transferring capabilities of the polypyrrole. Since polypyrrole is able to act as an ion-to-electron transducer from time zero, no system between the ionic conducting membrane and the electronic conducting substrate needs to be established. The decrease after the first hour could be due to ions reaching the polypyrrole therefore changing the charge-transfer characteristics. This demonstrates the importance of the intermediate conducting polymer layer in SC-ISEs.

According to other authors, the impedance of the high-frequency semicircle for electrodes containing the polypyrrole should be less than that of membranes on plain gold [257, 305]. This is a result of allowing well defined charge transfer across the membrane/substrate interface in place of the blocked system, as is the case in the plain gold. However, the bulk membrane impedance for both the plain gold electrode and the polypyrrole intermediate electrode are similar. The reason for the similar impedances is not yet understood.

As was the case in the plain gold electrode (Plain-Au-SC), the bulk membrane impedance fluctuates by about 18 % over time (commensurate with the EIS experimental error of about 10 %). The up and down fluctuations over time suggest that a water layer is not present, which is to be expected with the polypyrrole intermediate layer. The preparation of the solid contact is crucial to the electrodes response characteristics. Slight imperfections between the gold and the membrane may allow water to congregate in pockets and cause drifts later in low analyte concentrations. As the impedance plots for the "Plain-Au-SC" and the "PPy-SC" are similar, it suggests that the "Plain-Au-SC" may have been prepared slightly differently to the one used in Figure 5.17, which shows a water layer when changing from the primary ion to an interfering ion.
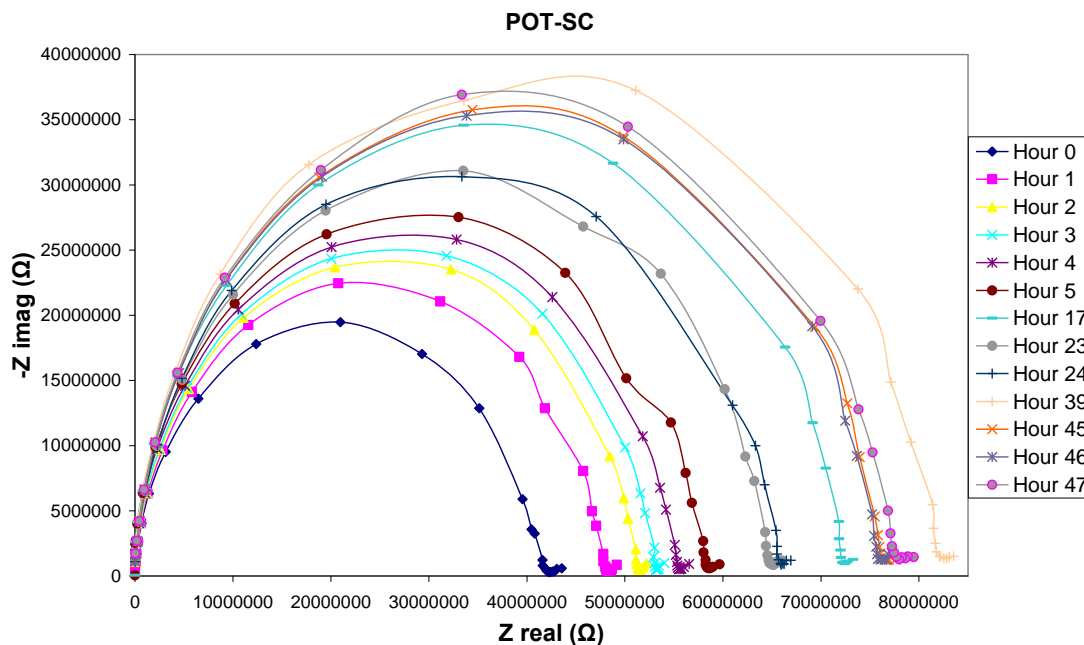
Figure 5.22: Complex plane plots of POT-SC in a solution of 10^{-2} M TlNO$_3$ over a period of 48 hours after initial contact with the conditioning solution.

The bulk membrane impedance in the case of the co-polymer electrode (POT-SC) is significantly higher than the PVC/DOS membranes. The high impedance is a direct result of the in-house prepared membrane matrix, as opposed to the commercially bought matrix of PVC and plasticisers. The bought supports contain impurities, which increase the conductivity of the membranes and therefore lowers impedance [28, 47, 302, 331]. Since the MMA-DMA co-polymer is manufactured in house and requires no additional plasticisers hence impurity levels are low. Since the diffusion coefficient of the co-polymer membrane is lower than that of the plasticised PVC, the incorporation of water into the membrane takes significantly longer, which shows as the characteristic impedance increase in Figure 5.22 when conditioning the membranes.

The low-frequency semicircle responsible for the capacitance and charge-transfer at the gold interface is hard to determine as a result of the large bulk membrane impedance. By amplifying the region of the low-frequency semicircle, a slight resemblance of a time constant due to the POT is present. If an observation is to be made on the low-frequency semicircle, the bulk membrane resistance needs to be

reduced, which can be achieved by the addition of a lipophilic salt such as ETH-500 or by reducing the thickness of the membrane.

The determination of a water layer is again inconclusive, as the impedance rises then falls twice over the 48 hours. Similar to the other electrodes, the co-polymer membrane with POT looked to be influenced by a cyclic effect. Despite the fact all measurements were conducted in the dark, stray electrical and/or temperature effects maybe the cause of the fluctuations in these types of tests. Future tests should be conducted inside a Faraday cage in a uniform temperature laboratory to rule out any unforseen errors.

The use of EIS to determine water layers needs to be examined further, so that a defined set of parameters is established. The lack of a positive water layer for the "Plain-Au-SC" electrode in the EIS spectra suggests that the contact may have been prepared in such a way as to prevent a water layer from forming. This demonstrates that SC-ISEs still require more research and that further tests through the use of EIS are needed. The data based on the thallium ionophores are not conclusive enough to suggest water layers or pockets; however, other ionophores and membranes have been tested with this technique and have demonstrated the presence of a water film.

5.7.3.3.   Sensitivity to Oxygen of the Four Solid-Contact Ion-Selective Electrodes

One of the critical factors in developing high-quality working SC-ISEs is a stable transfer from the ionic conducting membrane to the electron conducting substrate [289]. Potential instabilities of initial SC-ISEs due to the blocked interface between the membrane and the substrate rendered them of little practicality. The potential drifts were said to be due to an oxygen half-cell between the membrane and the substrate, which was easily affected by changes in the sample, as the membrane is permeable to both water and oxygen [261, 264]. The conducting polymer used in SC-ISEs has two functions, one of which is to supply a stable and well defined transfer from the ionic to electric form. Another method used to act as an ion-to-electron transducer is redox-active self assembled monolayers [261, 263, 267].

Of the four SC-ISEs, two contained conducting polymers (Polypyrrole and Poly(3-octylthiophene)), one a redox-active organic salt in a conductive ink, and the last no intermediate layer between the membrane and the substrate. The four electrodes' ion-to-electron transduction and potential stability were tested by changing the oxygen concentration in the sample by purging with different gasses. The results of the four electrodes can be viewed in Figure 5.23.
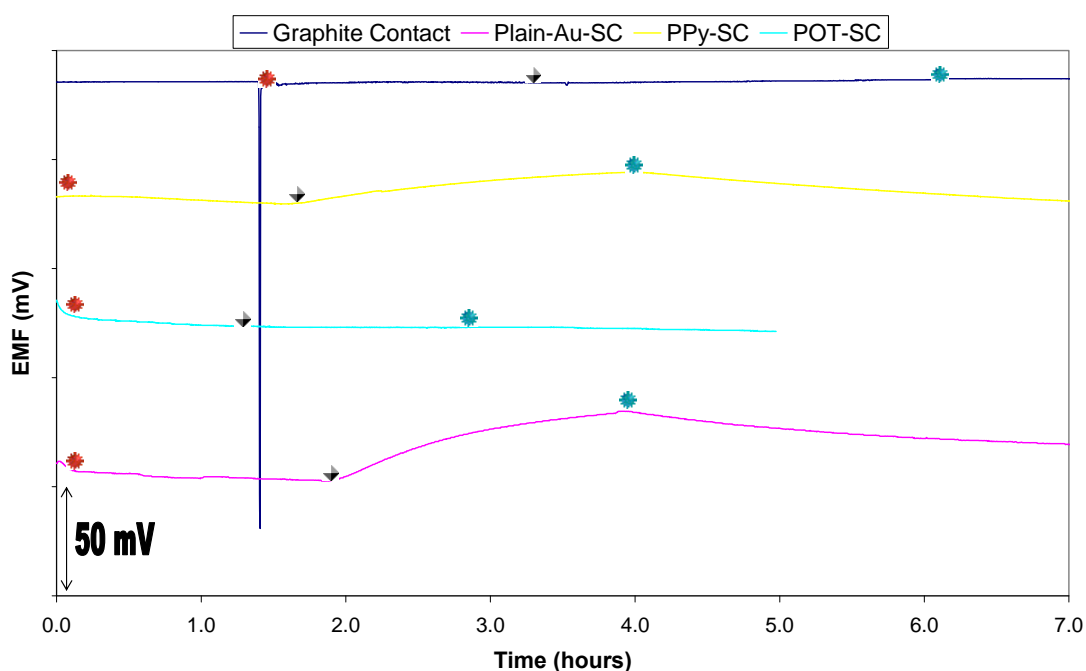
Figure 5.23: The influence of oxygen on the four thallium(I) SCISEs, with Graphite Contact, Plain-Au-SC, PPy-SC and POT-SC. ✸ The point where argon was first bubbled through the solution. ➥ The point where the gas bubbling through the solution was changed from argon to oxygen. ✸ The point where the gas was changed back to argon.

Understandably, the biggest potential drifts of the four SC-ISEs were observed for the electrode that had no intermediate redox system between the ion-sensing membrane and the electron conducting substrate. The "Plain-Au-SC" electrode which consisted of a plasticised PVC membrane over a gold substrate, drifted in the order of 15 mV per hour, when the gas was changed from argon to oxygen. The polypyrrole solid contact (PPy-SC) with a potential drift around 7 mV hour^{-1}, was

not able to fully prevent the influence oxygen has on the system. This is in agreement with other results of polypyrrole on gold in the literature [326, 330].

The best results with respect to the sensors' redox capacity were electrodes which had little sensitivity to oxygen changes, and were experienced with the "Graphite Contact" and "POT-SC". The "Graphite Contact" showed the most stable response with a potential drift of <0.4 mV per hour. The incorporation of the La-DCPI water insoluble organic salt has either formed a well defined system at the membrane substrate interface, or the redox capacity of the La-DCPI is significantly larger than that of the oxygen half-cell, therefore masking its effect. The electrode incorporating the MMA-DMA co-polymer had a potential drift of ~-1 mV per hour, but was not influenced by the changes in oxygen levels in the sample. The stable response could be due to the stable redox couple of the POT (POT-POT^{+n}), which also prevents the formation of a water layer, but it could also be enhanced by the water repelling properties of the co-polymer. These results again demonstrate that the best response is observed for the "POT-SC", suggesting a quality SC electrode system.

5.7.4. Characterisation of membrane matrices by Small Angle Neutron Scattering

Small Angle Neutron Scattering (SANS) is a technique that is used to characterise the microstructure of a vast array of materials. SANS has been used to characterise a wide variety of systems, e.g. colloids/emulsions, nanomagnetic materials, polymer blend structure and compatibility, crystallisation kinetics, hydrogen storage, wine science and natural fibres [332]. One of the vital components of ISEs is the polymer, which supports the ionophore, anion exchanger and plasticiser when needed. The polymer should ideally be inert and not perturb the electrode's response in any way. This may not always be the case with Ye, Q. et al. demonstrating that the plasticised PVC membrane contained ~6 nm inhomogeneities throughout, which were assigned to crystalline PVC in the unplasticised state [333]. The spherical inhomogeneities were described by a polydisperse hard-sphere model, and can be seen as peaks in the SANS curves, see Figure 5.24.
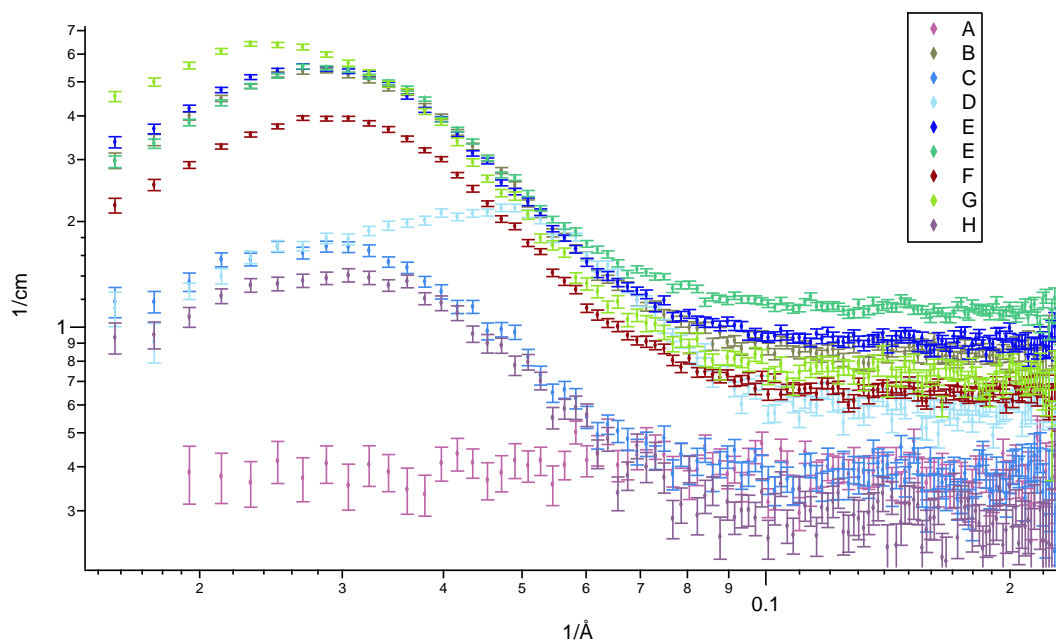
Figure 5.24: SANS curves of various membranes. Membranes: A, plain solvent cast PVC; B, PVC/DOS 1:2 ratio; C, PVC/FNDPE 1:2 ratio; D, PVC/DOS 2:1 ratio; E, Same as Membrane B only thicker; F, PVC/DOS/Ionophore; G, Membrane #4B of composition PVC/DOS/Ionophore/anion exchanger; H, Membrane #4C of composition PVC/FNDPE/Ionophore/anion exchanger.

Figure 5.24 shows the SANS curves of various membranes with different compositions. To gain a reference point for the instrument so that a comparison can be made to the Ye, Q. et al's paper, similar PVC/DOS membranes were run. The results shown in Figure 5.24 for the PVC/DOS membrane correlate well with the literature. Similar results were observed for the membrane containing lower plasticiser content, as there was a reduction in the average distance between the inhomogeneities.

Since FNDPE was used initially as the plasticiser, it was decided to test the membrane's microstructure compared to that of DOS. The size of the inhomogeneities is the same for FNDPE membrane as the DOS membrane with the peaks occurring in the same q-range. The lower intensity of the peak in the FNDPE membrane is due to a lower contrast between the inhomogeneities and the surrounding matrix [333]. Ye, O. concluded that the incorporation of a lipophilic salt had no effect on the microstructure of the membrane. However, our results

demonstrate that when the ionophore is incorporated into the membrane, (Membrane13), the SANS peak shifts to a slightly lower q value. This suggests the ionophore could be influencing the microstructure by increasing the average distance between the inhomogeneities.

The impact that heavy water has on the membrane microstructure was also tested with similar results to that of Ye, Q. et al. [333]. Ye, Q. et al. concluded that heavy water does not affect the crystalline PVC inhomogeneities and their separation, but does affect the membrane in another way, which can be seen in Figure 5.25, by the increase in intensity to the left of the main peak.
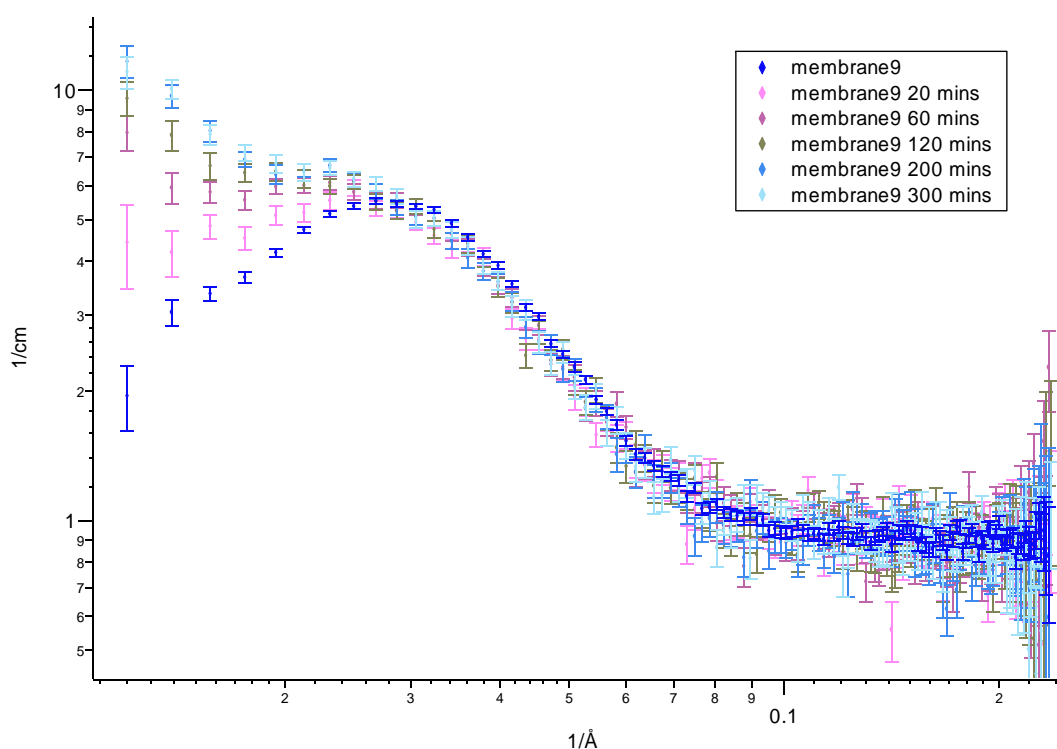
Figure 5.25: SANS curves of Membrane9 at different times of soaking in heavy water. Membrane9 consisted of DOS and PVC at a ratio of 2:1, with a thickness of 0.87 mm.

This rapid rise was assigned to a new water phase being created in the membrane and that only the asymptotically decaying part of the scattering pattern is visible due to the sensitivity of the instrument [333]. A mixed solution of HNO_3 and D_2O was also tested on a membrane containing PVC/DOS/ionophore/anion exchanger to determine if there was any effect that ions have on the water uptake. The results were identical

to that of Figure 5.25, suggesting that ions do not play any role in the water uptake and do not change the nature of the polymers inhomogeneities.

It is not known if the inhomogenities in the plasticised PVC membranes affect the potentiometric response; however, the water uptake can have a dramatic effect on the detection limit if ions are co-extracted, and the formation of a water layer between the solid substrate and the membrane in the case of SC-ISEs. It was therefore decided to test the new MMA/DMA copolymer by SANS to determine if any inhomogeneities exist. The scattering patterns for the dry membrane and after soaking in heavy water are displayed in Figure 5.26.
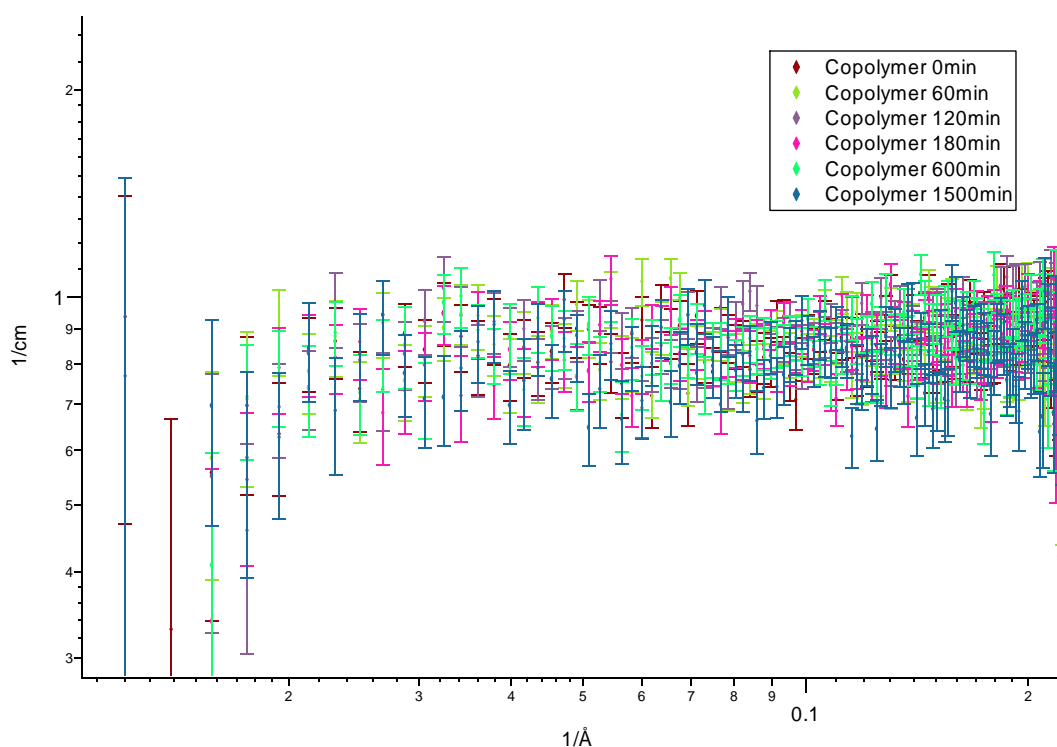
Figure 5.26: SANS curves of the MMA/DMA copolymer at different times of soaking in heavy water.

The scattering pattern for the dry membrane shows no signs of inhomogeneities in the polymer. This is not to say there are no inhomogeneities occuring, they maybe outside the sensitivity of this instrument or have too small a contrast. However, it is unlikely that the co-polymer contains inhomogeneities, as the matrix is made up of only one component and does not need additional plasticiser. The lack of inhomogeneities in the membrane could be another advantage of the self-plasticising

MMA-DMA copolymer over the more popular plasticised PVC system. The copolymer was also subjected to soaking in heavy water over a period of 25 hours to determine the effect water has on the matrix. Over the 25 hours in D_2O, there were no visible signs of water affecting the membrane as the SANS data did not show any change in the scattering intensities.

Despite MMA-DMA having a dramatically lower diffusion coefficient than the plasticised PVC membrane, the presence of a water phase should still have been seen after 25 hours, since it became apparent after only 20 minutes in Figure 5.25. Water does enter the MMA-DMA membranes because the EIS complex plan plots increased with time, which is attributed to water immobilising the ionic parts within the membrane.

The effect water has on the membrane cannot be determined with the current SANS instrument which has a q range of 0.01 to 0.12 Å^{-1}. Further tests need to be conducted as to the influence water has on the MMA-DMA copolymer membrane. The water excluding properties of the MMA-DMA are advantages for SC-ISEs as the adhesion on the electrodes surface may be a crucial factor in preventing water layers from forming. A polymer's water preventing qualities may help to exclude water from either the membrane itself, or the interface between the membrane and the solid substrate, which would lead to the optimum detection limit of the ionophore. The lack of microspheres in the polymer may also be beneficial towards the electrodes response by only having one continuous phase where the electrodes components are homogeneously distributed.

5.8.   Experimental

5.8.1.   Reagents

Pyrrole was obtained from Fluka and kept under an atmosphere of argon at reduced temperatures in the dark. Prior to use, the pyrrole was freshly distilled under reduced pressure and nitrogen. Poly(3-octylthiophene) (POT) was obtained from Sigma-Aldrich. Dry ethyl acetate was prepared by firstly washing with 5% sodium carbonate, then with saturated sodium chloride and dried over anhydrous magnesium sulphate prior to distillation. 2,2'Azobis(isobutyronitrile) (AIBN) was purified by recrystilisation from methanol. High molecular weight polyvinyl chloride was obtained from Fluka. 2-fluoro-2'-nitrodiphenyl ether (FNDPE), bis(2-ethylhexyl) sebacate (DOS), and sodium tetrakis-[3,5-bis(trifluoromethyl)phenyl]borate (NaTFPB) were obtained from Fluka. Tetrahydrofuran (THF) anhydrous, inhibitor free, 99.9% purity was obtained from Sigma-Aldrich. Diethylene glycole monoethyl ether was obtained from Sigma-Aldrich. Potassium hexacyanoferrate(III) was obtained from Chem Supply as LR grade. Chloroform was obtained from Selby Biolab as AR grade. Electrodag 423SS was obtained from Acheson Colloids Company which is made up of: graphite, ethylene glycol monobutyl ether acetate, carbon black, crystalline silica and vinyl resin. Carbon rods of 6.2 mm diameter were obtained from Proscitech. Methyl methacrylate was obtained from BDH Chemicals as AR grade and decyl methacrylate was obtained from Polysciences Inc. The MMA-DMA copolymer was synthesised as described previously . The first preparation contained methyl methacrylate (1.55 g, 15.5 mmol), decyl methacrylate (4.38 g, 19.4 mmol) and AIBN (3.4 mg) in dried ethyl acetate (5 mL) at 95°C. The second preparation contained methyl methacrylate (1.023 g, 10.2 mmol), decyl methacrylate (4.086 g, 18.1 mmol) and AIBN (3.4 mg) in dried ethyl acetate (5 mL) at 90°C. The glass transition temperature of preparation 1 was 7.9 °C and preparation 2 was -3.0 °C. The glass transition temperature was measured on a TA Instrument, DSC 2910 Differential scanning calorimeter with a cold stage attachment.

5.8.2.   Preparation of Solid Contacts

Spectroscopic grade graphite rods (7.0 mm diameter) were obtained from Proscitech and washed in acetone for two hours then with THF for 48 hours. The rods were then inserted into a Teflon body (see Figure 5.14) ready for the conductive ink coatings. The gold electrodes were rotating disc electrodes (Au of 3 mm diameter, tip diameter 10 mm, type 6.1204.320) obtained from Metrohm AG Switzerland and were polished with 0.3 μm alumina (Metrohm), then rinsed with Milli-Q water, acetone, 10^{-2} M HNO_3 and finally dichloromethane.

The conductive graphite based ink with La-DCPI was prepared by diluting the Electrodag with equal parts diethylene glycol monoethyl ether acetate then adding the saturated La-DCPI in acetone to make 5% w/w. The prepared ink was mixed thoroughly prior to deposition on the electrode tip. The conductive ink (20 μm) with La-DCPI was drop cast on the electrode surface and allowed to evaporate overnight. The plasticized membrane was then drop cast over the dry conductive ink with La-DCPI and left to dry overnight.

Polypyrrole (PPy) films on the gold electrode surfaces were achieved through potentiostatic electropolymerization. Electropolymerised PPy films were doped with potassium hexacyanoferrate(II)/(III) by applying a potential of 1 V for 40 seconds to the electrode submersed in an aqueous solution containing 0.5 M pyrrole and 0.5 M $K_4Fe(CN)_6$ that had been purged with argon. After electropolymerisation the electrodes were rinsed with water then left soaking in Mill-Q water for 4 hours and rinsed finally with fresh Milli-Q water, to remove any remaining doping electrolyte. Finally, the electrodes were dried at room temperature and rinsed with small portions of dried-THF prior to the membrane being drop cast. The potentiostat used for the electropolymerisation of the PPy was a Princeton Applied Research PARSTAT model 2263.

Poly(3-octylthiophene) (POT) films were prepared by drop casting 70 μL in 10 μL aliquots of a 0.25 mM POT in chloroform (calculated relative to the monomer). The

POT layer was allowed to dry over a few minutes prior to the drop casting of the membrane.

5.8.3. Preparation of Membranes

The compositions of the membranes used for the various SC-ISEs are displayed in Table 5.2

Table 5.2: Membrane compositions of the four SC-ISEs

Electrode	Polymer (%)	Plasticiser (%)	Ionophore (%)	Ion-Exchanger (%)	Thickness
Graphite Contact	PVC 65.5 mg (32.4)	FNDPE 133.6 mg (66.1)	Calixarene (4) 2.02 mg (1.0)	Na-TFPB 1.06 mg (0.5)	297 μm
Plain-Au-Contact	PVC 65.9 mg (31.8)	DOS 138.4 mg (66.7)	Calixarene (4) 1.98 mg (0.95)	Na-TFPB 1.12 mg (0.54)	110 μm
PPy-SC	PVC 65.9 mg (31.8)	DOS 138.4 mg (66.7)	Calixarene (4) 1.98 mg (0.95)	Na-TFPB 1.12 mg (0.54)	110 μm
POT-SC	MMA-DMA 196.2 mg (97.9)	-	Calixarene (4) 3.23 mg (1.6)	Na-TFPB 1.01 mg (0.5)	106 μm

For the "Graphite Contact", the membrane components were dissolved in dried-THF (2 mL). The membrane cocktail (400 μL) was drop cast over the electrode surface, then the THF was allowed to evaporate overnight. For the "Plain-Au-Contact" and the "PPy-SC electrodes", the membrane components were dissolved in dried-THF (2 mL). The membrane cocktail (100 μL) was then drop cast over the electrode surface in 2 x 50 μL increments. The THF was then allowed to evaporate overnight. For the "POT-SC" the membrane components were dissolved in dried dichloromethane. The membrane cocktail was then degassed for ten minutes by sonication before being drop cast onto the electrode surface. The membrane cocktail (100 μL) was drop cast onto the electrode surface in 2 x 50 μL increments. The membrane solvent (dichloromethane) was then allowed to evaporate overnight.

5.8.4.   EMF Measurements

EMF measurements were conducted on an ACM potential-20 potentiostat for the "Graphite Contact", "Plain-Au-SC" and "PPY-SC", and on a Lawson Lab potentiostat for the "POT-SC". The electrodes were maintained and run in the dark and beakers were pre-treated with 10^{-4} M nitric acid made up with purified nitric acid and Milli-Q water. All measurements were conducted with an Orion Thermo double-junction Ag/AgCl/3 M KCl reference electrode (type 90-02) containing a 1 M LiCH$_3$COO bridge electrolyte.

All EMF values were corrected for liquid-junctions potentials according to the Henderson equation and activity coefficients were calculated with the Debye-Huckel approximation. All electrodes were conditioned in 10^{-4} M TlNO$_3$ overnight except the "POT-SC", which was conditioned for 48 hours as a result of the slower diffusion coefficient of the MMA-DMA co-polymer. After conditioning and running in each of the calibration standards, the electrodes were washed excessively with Milli-Q water. Calibrations were conducted with 10^{-3}-10^{-9} M TlNO$_3$ solutions with no background electrolyte. All solutions for the calibrations were stirred at 250 rpm.

Water layer tests were conducted by initially measuring the potential of the electrodes in 10^{-4} M TlNO$_3$ solutions, then changing to 10^{-4}, 10^{-1}, and 10^{-2} M NaCl for the "Plain-Au-SC", "PPy-SC" and "POT-SC" electrodes respectively. After five hours in the NaCl solutions, all electrodes were changed back to their original 10^{-4} M TlNO$_3$ solution. All solutions for the water layer tests were unstirred and conducted at room temperature.

Oxygen-redox tests were conducted by allowing the potential to stabilise then bubbling argon through the solution over several hours. The gas was then changed to oxygen for several hours and then back again to argon. Care had to be taken to ensure bubbles were not trapped under the electrode on the surface of the membrane.

5.8.5.　　　EIS Measurements

EIS measurements were conducted on an EG&G Princeton Applied Research Potentiostat/Galvanostat Model 273A. The instrument was driven by Electrochemistry PowerSuite software version 2.52.0. No electrodes were conditioned in any solutions prior to their tests. All EIS spectra were collected at open circuit potential using an A.C. amplitude of $\pm$ 10 mV rms for the "Graphite Contact" and $\pm$ 50 mV rms for the "Au Contacts", in the frequency range from 100 kHz to 100 mHz. A conventional three elelctrode cell consisting of a platinum counter, double junction reference and the working electrodes were maintained in the dark during the tests. The electrolyte consisted of a 10^{-2} M $TlNO_3$ solution.

5.8.6.　　　Small Angle Neutron Scattering

All membranes, except the co-polymer membranes, were prepared by dissolving the components in dried THF, and then poured into glass rings of 23 mm internal diameter. The THF was then allowed to evaporate prior to putting the membranes into the SANS cuvettes. The co-polymer membrane that had previously been synthesised was placed into the SANS sample holders without further treatment. The compositions of the tested membranes are summarised in Table 5.3.

Membranes A to H were placed into dry cell cuvettes ready for analysis. A minimum of six measurements were conducted, with each measurement lasting 20 minutes. "Membrane9" was placed in a wet-cell cuvette and a measurement was carried out on the dry membrane for 10 minutes. Heavy water or D_2O was then added to the cuvette and measurements were carried out at 20, 60, 120, 200 and 300 minutes after the addition of heavy water, with each measurement lasting for 10 minutes. For the acid solution test, the membrane (membrane 10) was placed in a wet-cell cuvette and surrounded with 10^{-2} M HNO_3 in D_2O. Measurements were then carried out periodically over 24 hours. The MMA-DMA co-polymer was placed in a wet-cell cuvette and measured dry 17 times with each measurement lasting for 10 minutes.

D_2O was then placed in the cell to surround the co-polymer. Measurements were then taken at 60, 120, 180, 600 and 1500 minutes after the heavy water addition. All sample holders are quartz with 2 mm optical path length.

The small-angle neutron scattering measurements were performed on the AUSANS-spectrometer installed at the HIFAR research reactor located at Lucas Heights, Sydney, Australia. The spectrometer is equipped with a 64 cm x 64 cm detector with a 5 m sample-to-detector distance. The analysed q range is between 0.01 and 0.12 Å^{-1} at a wavelength of 5 Å. The scattering patterns were corrected for transmission, spectrometer background and cuvette scattering, in addition, were converted to absolute scattering cross section units using an A3 silica standard of known incoherent scattering.

Table 5.3. Composition of the various membranes used for the small angle neutron scattering

Membrane	Polymer (%)	Plasticiser (%)	Ionophore (%)	Ion-Exchanger (%)	Thickness
A	PVC (100)	-	-	-	0.53 mm
B	PVC (33.3)	DOS (66.6)	-	-	0.69 mm
C	PVC (33.3)	FNDPE (66.6)	-	-	0.55 mm
D	PVC (66.6)	DOS (33.3)	-	-	0.58 mm
E	PVC (33.3)	DOS (66.6)	-	-	0.87 mm
F	PVC (32.9)	DOS (65.8)	Calixarene (3) (1.3)	-	1.08 mm
G	PVC (33.7)	DOS (65.0)	Calixarene (4) (0.84)	Na-TFPB (0.49)	0.59 mm
H	PVC (33.8)	FNDPE (64.8)	Calixarene (4) (0.85)	Na-TFPB (0.58)	0.59 mm
Membrane9	PVC (33.3)	DOS (66.6)	-	-	0.87 mm
Membrane10	PVC (32.5)	DOS (65.9)	Calixarene (4) (1.04)	Na-TFPB (0.61)	1.4 mm
Co-Polymer	MMA-DMA (100)	-	-	-	-

6. Summary and Conclusion

Thallium is one of the most toxic naturally occurring elements known to mankind and has led to many deaths since its discovery in 1861 [58-60]. Even though thallium has limited uses as a result of its toxicity, deaths still occur today as a consequence of environmental spills, homicide and accidental intake. Often, thallium poisoning is not diagnosed in the early stages as the symptoms mimic those of other illnesses. An analytical tool capable of determining thallium in a vast range of samples at minimal cost would be beneficial, especially in poisoning cases where early treatment can result in a moderate recovery with some side effects [72].

The research goal of the work carried out in this thesis, was to develop a thallium(I) ion-selective electrode with good selectivity and low limits of detection. Currently, the present series of thallium(I) ISEs have moderate selectivities and poor limits of detection. Since thallium has chemical characteristics of both the heavy metals and alkali metals, it is often difficult to gain good selectivity against both [94, 95, 124, 190]. If the ionophore is designed with heavy metal binding sites such as sulfur, the electrode would tend to exhibit interferences from ions like silver and lead. If, on the other hand, the ionophore was designed with hard metal binding sites such as oxygen, the electrode would exhibit interferences from ions like potassium and sodium. The limits of detection in the various published literature fall within the micro-molar range, which are insufficient for practical samples where the expected concentrations of thallium would be below this level.

This thesis attempts to overcome these problems through the design of new ionophores which are tailored for selective complexation of thallium(I), then incorporate them into polymeric ISEs which have been designed to counteract the outward flux of ions that perturb the electrodes' response and lower the limits of detection. Calixarenes were chosen as the building blocks for the series of synthesized ionophores, as they possess many of the characteristics required for successful ionophores.

To overcome the varied binding nature of thallium, it was decided to pursue the complexing ability of π-electron systems. Even though π-electrons are known not to be strong binding sites, they are very selective and the electron rich cavity in the calixarene should provide an ideal coordinating location for the thallium ion [99]. The selectivity of the proposed compounds was to be further improved by manipulating the cavity so that only ions of a particular size or smaller would be permitted to enter allowing thallium to bind with the greatest strength relative to other smaller ions.

Based on these assumptions, five calixarene derivatives were chosen and successfully synthesized. Four calix[4]arene derivatives were synthesized with two in the cone conformation with attached isopropyl groups on the lower rim (calixarenes (1) and (2)) and two in the 1,3-alternate conformation with substituted allyl groups (calixarenes (3) and (4)). One calix[6]arene derivative was synthesized; however, substitution on the lower rim was only partially achieved with isopropyl groups. The synthesis of calixarenes (1) and (2) was initially difficult and required substantial amounts of alkylating agent (isopropylbromide) and base to promote the reaction and gained moderate yields of 34 % and 30 % respectively. The synthesis of the two 1,3-alternate derivatives, calixarenes (3) and (4), were significantly easier than calixarenes (1) and (2) and required substantially less time for their completion. Calixarene (3) was challenging as the *tert*-butyl groups or the low solubility in the solvent, prevented the direct full alkylation in the 1,3-alternate conformation. Even though the 1,3-alternate derivatives did require less time as a result of being able to heat the reaction, if the reaction was not vigorously refluxed then the desired product was not produced. Full substitution was achieved for calixarenes 1 to 4 with the desired products being synthesized with high purity.

During the characterization of the synthesized calixarenes, a very interesting property was discovered for calixarene (2), which encapsulates chloroform in the crystal structure and retains it at elevated temperatures. The chloroform was eventually released from the crystal structure at 125 °C, 64 °C above chloroform's boiling point. This may be beneficial in future applications, such as volatile solvent/gas storage or in catalytic applications, and should be pursued further to discover the full potential of this molecule. The other cone conformation calixarene (calixarene (1)) did

crystallize with chloroform between the calixarene molecules, but this was easily released as soon as the crystal had been exposed to the ambient atmosphere. The crystal structure of the 1,3-alternate calixarenes showed no sign of solvent incorporation.

Since the desired compounds had been successfully synthesized, the next objective was to determine their thallium binding characteristics. ^{1}H-NMR spectroscopy provided a simple and efficient means of determining a range of complexation properties of the four calixarenes. It was shown that the binding site of the calixarenes with thallium(I) is likely to be in the π-electron rich cavity. It was also discovered that the *tert*-butyl groups influenced the exchange kinetics between the complexed and uncomplexed states, with the observation of a faster exchange rate for the debutylated derivative.

Another interesting discovery was the observed "pinching" effect of calixarene (1) when thallium is bound within the aromatic cavity. The "breathing" motion of the calixarene molecule seems to be slowed down as a result of the ion binding to the π-electrons, which can be viewed in the NMR spectra as peak splitting for what were originally equivalent peaks for the uncomplexed molecule. Interestingly, silver does not exhibit this effect on the NMR spectrum for the complexed molecule indicating that the "breathing" motion of the molecule has not slowed significantly enough to be seen on the NMR time scale. This suggests that thallium is a better fit, to the cavity of the calixarene molecule than silver, as the calixarene still appears to possess symmetry in the silver complex as a result of the faster interconversion between the two pinched states. NMR spectroscopy also helped to demonstrate that the stoichiometry of the calixarene-thallium complex is 1:1, which becomes very useful in the calculations of the complex formation constant with sandwich membrane techniques in ISEs. Overall, NMR provided some interesting observations and useful data for the complexing abilities of the synthesized calixarenes, which further enhanced their application as ionophores in ISEs.

Once it had been demonstrated by NMR that the calixarenes acted as receptors for the thallium(I) ion, the four calixarene molecules were then incorporated into plasticized PVC together with an anion exchanger. Unfortunately, the calixarene

which was expected to show the most promise with respect to selectivity (Calixarene (2)), crystallized out in the membrane rendering it useless. Calibration graphs and selectivities were carried out on Calixarenes (1), (3) and (4) but as a consequence of Calixarene (3) also eventually crystallising out in the membrane, thus only Calixarenes (1) and (4) were tested further.

Calibration of the various electrodes was undertaken with solutions of increasing thallium(I) activity, and it was found that all electrodes exhibited Nernstian behaviour with slopes of around 59 mV decade^{-1}. This shows that the synthesized molecules could be incorporated into polymeric membranes and used to determine an unknown sample concentration from a calibration graph.

One of the major goals of this work was to improve the selectivity compared to previously studied thallium(I) ionophores. The selectivity of the three calixarenes were subsequently tested via the separate solution method where the membranes that had not been previously exposed to thallium(I) ions were examined from the most discriminated to least discriminated ions. The electrodes were conditioned appropriately with an highly discriminatory ion, and also contained the same ion in the inner filling solution, which permitted determinations of the optimum selectivity coefficients. By removing the outward flux, lower selectivity coefficients have been determined [183, 205]. All three calixarenes (1), (3) and (4) showed similar selectivity trends, with thallium being the primary ion in all cases and Nernstian behaviour exhibited by all ions tested. A membrane without ionophore was also tested to determine the selectivity of thallium(I) based purely on its lipophilicity. The trend of the ionophore free electrodes is similar to the calixarene incorporated membranes, but the magnitude of selectivities in the ionophore containing membranes is significantly larger. Even though the ionophore free membrane showed half a level of magnitude difference in the selectivity of silver with thallium based purely on lipophilicity, it is safe to assume that the silver to thallium selectivity shown in the membranes with ionophore is due to more than just lipophilicity. This is also expressed in the NMR complexation studies as thallium showed full complexation with minimal free ligand remaining whereas silver showed an equal mix of complex and free ligand in the spectra. All membranes with ionophore showed a moderate interference from silver, which would only be problematic if

samples contain a high concentration of silver. As most of the desired applications should have low silver concentrations, this should not be a problem. The calixarenes exhibited good-to-excellent selectivity over the alkali and alkaline earth metals; however, calixarene (4) appears to be slightly less selective than the other two calixarenes. Calixarene (4) experiences lower selectivities with cesium and potassium, which may be a consequence of the more open cavity and closeness to the inverted oxygen atoms available for binding.

Overall, the selectivity exhibited by the three calixarenes is relatively good in comparison to other thallium(I) ionophores; however, the improvement in selectivity through making the calixarene cavity more parallel in nature has not been fruitful. It should be noted that, the calixarene that was expected to provide the best selectivity could not be used since it was insoluble in the membrane.

Another objective of the work carried out in this thesis was to reduce the current limit of detection of the calixarene based thallium(I) selective electrodes. The current limits of detection experienced by all of the previously reported thallium(I) ionophores fall within the micro-molar region, which is mediocre in analytical chemistry, especially in the monitoring of heavy metals. This is heightened by the fact that thallium poisoning can occur below this concentration, and that a monitoring of thallium in blood and urine in patients also occurs around or below this region [56, 71]. In order to reduce the limit of detection of ISEs, ion fluxes through the membrane need to be controlled to prevent the release of primary ions into the Nernst layer. Of the variety of techniques that can be used to control ion fluxes, it was decided that the manipulation of the inner filling solution was the most appropriate to explore. Therefore, the thallium concentration in the inner side of the membrane can be controlled so that ion fluxes are not present or minimal at best. Two techniques were employed to control the inner solution: 1) the use of an EDTA buffered inner solution at elevated pH; and 2) the use of an exchangeable ion in the inner solution. The EDTA buffered inner filling solution was successful in reducing the limits of detection, with the lowest level achieved for calixarene (1) with a concentration limit of 8.3 nM (I.U.P.A.C.). Unfortunately, lower values could not be achieved for a variety of reasons, one being that thallium(I) does not bind strongly to EDTA and therefore preventing low concentrations of thallium on the inner side of

the membrane, another being the interference from H^+ ions in the sample and lastly, a possible interference from the interaction of the calixarene with organic components in the membrane. The lowering of the detection limits was successful; however, even lower limits are desired. To try and lower the limit of detection further it was decided to try and increase the pH of the sample solutions therefore minimizing interferences from H^+. The addition of lithium hydroxide and tris(hydroxymethyl)amino methane did not reduce the limit of detection further as desired, and as a consequence further optimization is required. A method for increasing the pH without introducing extra species is desired if the current limit of detection is to be reduced further. However, the detection limit may not be able to be reduced any further as the limits obtained in the solid-contact ISEs (SC-ISEs) were similar to those of the buffered inner-filling solution counterparts. Factors such as interfering interactions in the membrane phase between the ionophore and organic molecules may be influencing the lower detection limit of this series of thallium(I) selective ionophores, and may prevent it from being reduced further as these factors are beyond our present control.

An alternative to using EDTA to buffer the thallium(I) concentration on the inner side of the membrane is to incorporate an ion that is partially exchanged on the inner side of the membrane to prevent the outward flux of primary ions. This technique has the advantage of providing a stable response over longer periods of time. The limit of detection for this technique is better than the initial values with high primary ion concentrations in the inner solution but is inferior to the limits achievable through the use of EDTA. More testing should be carried out to ensure that the optimum level of exchange has been reached. However, future testing may be in vain if the minimum detection limit has already been reached for these ionophores.

The main objective of reducing detection limits has been achieved but further testing is required to ensure that the system has been optimized and to better understand the reason the detection limit may not be reduced further. With the proper control of ion fluxes, a reduction in the interfering H^+ ion and the possible elimination of other interfering mechanisms, a thallium(I) ISE with nanomolar detection limits may be possible. This thesis has demonstrated that the detection limit can be reduced from

the current literature values and are currently the lowest detection limits shown for a thallium(I) ISE.

The trend in ISEs in recent years has been the development and understanding of solid-contact ISEs, which would aid in the manufacture of miniaturized systems with low cost, robustness and mechanical flexibility [257]. It was decided to pursue this trend with the current series of thallium(I) selective ionophores, as lab-on-a-chip technology is the future in this field. In saying this, not all aspects of SC-ISEs are well understood and a significant amount of research is still required to develop these sensors sufficiently. The work conducted in this thesis attempted to incorporate the synthesized calixarenes to develop a thallium(I) sensitive SC-ISEs, and to also alleviate some of the problems associated with their design.

Four different electrode designs were trialled. One consisted of a graphite rod with a redox active conductive ink between the membrane and the solid graphite and the other three were gold substrate electrodes with different systems between the solid conducting support and the ion-selective membrane. Of the gold electrodes one had no intermediate layer between the membrane and the gold, the other two had polypyrrole and poly(3-octylthiophene) respectively. Only one of the calixarenes was chosen, as the results in Chapter 4 showed them to behave similarly. Calixarene (4) was successfully incorporated into all four electrodes with each producing Nernstian responses over a broad concentration range. The best detection limit (30.2 nM) was observed with the solid gold contact that used POT as the intermediate layer between the conducting substrate and the methyl methacrylate-decyl methacrylate (MMA-DMA) plasticizer free co-polymer membrane. The worst detection limit was exhibited by the graphite electrode which produced a limit of 0.31 μM, which is similar to the values obtained with the traditional inner filling solution method.

One of the biggest problems associated with solid contact electrodes is the formation of a water layer or droplets between the membrane and the solid substrate. When a water layer is present, ions can congregate at significantly high concentrations to perturb the electrodes response in low primary ion samples [261]. The water layer also established a half-cell required for the ion-to-electron transduction, but suffered

from substantial drifts. Various tests were carried out to show why the gold electrode with the POT and MMA-DMA co-polymer was the most successful.

The potential tests performed on the Plain-Au-SC when the solution was changed from the primary ion to an interfering ion over several hours, then back to the primary ion again demonstrated a water layer present. This is characteristic of SC-ISEs with this setup as water penetrates the membrane and establishes itself between the membrane and the solid substrate. The results of this test demonstrate why the detection limits of SC-ISE lie in the same region as an inner filling solution electrode with a higher concentration of primary ion on the inner side of the membrane. The Plain-Au-SC also suffered from potential drift, which is also characteristic of a water layer and an oxygen half-cell acting as the ion-to-electron transducer. The other three electrodes showed steady potentials over the test indicating no water layers present.

Electrochemical Impedance Spectroscopy (EIS) was also used as a new technique to try and determine the presence of a water layer between the solid substrate and the membrane. EIS has previously been used to test ISEs, and has been useful in gaining a fundamental understanding of the electrode working mechanism; however, this technique is an in-situ monitoring of the electrode from its initial contact with an aqueous solution until 48 hours after submersion in the solution. The test was aimed at identifying the presence of water between the layers by observing the changes in contact resistance in the complex plane plots.

The changes in contact resistance indicative of a water layer, were not observed in these four electrodes as has been previously observed for other systems where water layers/droplets are present. However, other changes in the data were observed between the four electrodes. The most significant difference occurs with the low-frequency semicircle, which is indicative of charge transfer occurring at the substrate/membrane interface. The electrode without an intermediate system between the substrate and the membrane (Plain-Au-SC) had to develop a charge transfer system once the water started to enter the interface, whereas the others had well defined systems and easily observable semicircles at the initial point of contact with the solution, demonstrating the effectiveness of the La-DCPI/electrodag, polypyrrole

and poly(3-octylthiophene) intermediate layers as ion-to-electron transducers. Without the well established ion-to-electron transducer, the electrode has to create one of its own, which is done through the established water layer and an oxygen half cell [255, 261, 264]. EIS has provided a useful technique for analysing SC-ISE, but more work is required to establish the parameters and conditions for an optimized water layer test. The electrode preparation may be a decisive element in the prevention of water layers, and more work is required to demonstrate the effectiveness of EIS in determining water layers.

It was also demonstrated by the redox test that the most stable response occurs when a well defined redox-capable intermediate layer is used between the membrane and the solid substrate. The best responses were observed for the graphite electrode and the gold electrode with POT and the MMA-DMA co-polymer. These two electrodes showed minimal changes in EMF when the redox nature of the sample was changed. The worst drift was observed for the solid contact electrode without an intermediate layer (Plain-Au-SC), which was to be expected as the system suffers from an ill defined interface.

One of the fundamental components of ISE's is the inert polymer which holds the active ingredients. It was decided to test the polymer membranes with small-angle neutron scattering to understand the microstructure of this crucial part of the sensor. The most interesting finding to come out of these experiments was that the new MMA-DMA co-polymer does not contain any microstructure with enough contrast to scatter neutrons. This is vastly different to the plasticized PVC membranes which show micro-spheres within the membrane, which were thought to be crystalline PVC. The plasticized PVC was also affected by water with the formation of a water phase developing with time, as evidenced by changes in membrane SANS curves over time. The same change was absent when water was exposed to the MMA-DMA co-polymer suggesting that water does not freely enter the polymer and establish itself as a new phase. The SANS testing demonstrates some of the benefits of using the new MMA-DMA copolymer in SC-ISEs, which may help prevent the formation of water layers, thereby producing better sensors.

Overall, the research was successful in synthesising several new ionophores, characterising them and incorporating them into ISEs that are useful in thallium detection. The electrodes showed good selectivity towards thallium and the best observed detection limits for a thallium(I) ISE. One of the ionophores was also successfully incorporated into a SC-ISEs which was used to determine thallium(I) at sub-micro molar concentrations.

6.1.   Future Work

This thesis has shown the development of five new calixarenes, three incorporated into liquid-contact ISEs, and one into a solid-contact ISEs for the application as a thallium sensor capable of determining free thallium(I) concentrations in a variety of samples. The work was successful on many fronts; however, some future work is required on different aspects. Calixarene (2) was synthesized to improve the thallium selectivity over other ions, but crystallised out in the membrane. The solubility of calixarene (2) can be improved by the attachment of more lipophilic ligands to the base structure. One place which may not affect the binding kinetics with thallium is the addition of longer hydrocarbon chains to the iso-propyl groups on the lower rim.

Further NMR complexation studies with the calixarenes and thallium would be beneficial, and may help to explain the splitting patterns when the ion is complexed with the molecule.

More work is required to optimize and better understand the lower detection limit of the current thallium(I) sensors for both the liquid-contact and the solid-contact. While this thesis showed that the current limit for thallium(I) ISEs could be reduced down to levels which would make them more applicable to trace level analysis, lower limits are desirable. This may be achieved by further optimizing the inner filling solution concentrations, or by reducing the impact of H^+ in the sample solutions, or by trying to increase the binding strength of either the ionophore or the buffering agent with thallium.

Even though it was demonstrated that the synthesized calixarenes could be incorporated into a SC-ISEs and used to determine thallium(I), more research is required into the working mechanisms of these types of sensors, so that eventually lab-on-a-chip technology and microelectrodes can be used in mainstream analytical chemistry. The optimization of the EIS test used in the prediction of water layers should be undertaken so that the correct parameters are established and can be used for any SC-ISE. The presence of water layers has been shown by this method, but the results demonstrated in this thesis indicate that slight changes to the electrode preparation may prevent water layers forming that are detectable through EIS, or that external interferences on the electrode system may be enough to hinder the technique from accurately determining if water layers are present. It may also be beneficial to further characterize the MMA-DMA co-polymer by SANS with a broader q-range and longer hydrating times to determine if any micro-structure is present.

Testing the response of the developed thallium(I) ISEs in natural samples that have been spiked with different concentrations of thallium(I) would also be of interest. This would allow for the direct evaluation of the capabilities of the electrodes for the monitoring of thallium(I) in the environment

References

1.   Gutsche, C.D., *Calixarenes*. 1989: The Royal Society of Chemistry. 223.

2.   Ungaro, R., *Introduction*, in *Calixarenes in Action*, L. Mandolini and Ungaro, R., Editors. 2000, Imperial College Press: London. p. 271.

3.   *Calixarenes 50th Anniversary: Commemorative Issue*, ed. J. Vicens, Asfari, Z., and Harrowfield, J. 1994, London: Kluwer academic publishers. 415.

4.   Bakker, E. and Pretsch, E., *A new wave of ion-selective electrodes*. Analytical Chemistry, 2002. **A**: p. 420-426.

5.   Morf, W.E., *The Principles of ion-selective electrodes and of membrane transport*. Studies in Analytical Chemistry, ed. E. Pungor, Simon, W., and Inczedy, J. Vol. 2. 1981, Amsterdam-Oxford-New York: Elsevier Scientific Publishing Company. 431.

6.   Lakahminarayanaiah, N., *Membrane Electrodes*. 1 ed. 1976, New York, San Francisco, London: Academic Press. 368.

7.   Tendeloo, H.J.C., *A new and easy method for the potentiometric determination of calcium concentrations in solutions*. Journal of Biological Chemistry, 1936. **113**: p. 333-339.

8.   Tendeloo, H.J.C., *Adsorption electrodes. II. Mineral electrodes*. Proc. Acad. Sci. Amsterdam, 1935. **38**: p. 434-441.

9.   Kolthoff, I.M. and Sanders, H.L., *Electric potentials at crystal surfaces and at silver halide surfaces in particular*. Journal of the American Chemical Society, 1937. **59**: p. 416-420.

10.   Sanders, H.L. and Kolthoff, I.M., *Photovoltaic behavior of pure silver bromide*. Journal of Physical Chemistry, 1940. **44**: p. 936-943.

11.   Pungor, E. and Hollos-Rokosinyi, E., *The use of membrane electrodes in the ananlysis of ionic concentrations*. Acta Chimica Academiae Scientiarum Hungaricae, 1961. **27**: p. 63-68.

12.   Frant, M.S. and Ross, J.W., *Electrode for sensing fluoride ion activity in solution*. Science, 1966. **154**(3756): p. 1553-1555.

13.   Brand, M.J.D. and Rechnitz, G.A., *Mechanistic studies on crystal-membrane ion-selective electrodes*. Analytical Chemistry, 1970. **42**(4): p. 478-483.

14.   Warner, T.B., *Lanthanum fluoride electrode response in water and in 1M sodium chloride*. 1969, Nav. Res. Lab.: Washington. p. 10.

15. Harrell, J.B., Jones, A.D., and Choppin, G.R., *Liquid ion-exchange membrane electrodes for polyvalent cations.* Analytical Chemistry, 1969. **41**(11): p. 1459-1462.

16. Butler, J.N. and Huston, R., *Activity measurements using a potassium-selective liquid ion-exchange electrode.* Analytical Chemistry, 1970. **42**(6): p. 676-679.

17. Lal, S. and Christian, G.D., *Potentiometric studies with a liquid ion-exchanger lead-selective electrode.* Analytica Chimica Acta, 1970. **52**(1): p. 41-46.

18. Wise, W.M., Kurey, M.J., and Baum, G., *Direct potentiometric measurement of potassium in blood serum with liquid ion-exchange electrode.* Clinical Chemistry, 1970. **16**(2): p. 103-106.

19. Hildebrandt, W.A. and Pool, K.H., *Liquid ion-exchange membrane electrode for lithium.* Talanta, 1976. **23**(6): p. 469-472.

20. Levins, R.J., *Barium ion-selective electrode based on a neutral carrier complex.* Analytical Chemistry, 1971. **43**(8): p. 1045-1047.

21. Ammann, D., Pretsch, E., and Simon, W., *Calcium ion-selective electrode based on a neutral carrier.* Analytical Letters, 1972. **5**(11): p. 843-850.

22. Stefanac, Z. and Simon, W., *Ion specific electrochemical behavior of macrotetrolides in membranes.* Microchemical Journal, 1967. **12**(1): p. 125-132.

23. Pioda, L.A.R., Stankova, V., and Simon, W., *Highly selective potassium ion responsive liquid-membrane electrode.* Analytical Letters, 1969. **2**(12): p. 665-674.

24. Moody, G.J., Oke, R.B., and Thomas, J.D.R., *Calcium-sensitive electrode based on a liquid ion exchanger in a poly(vinyl chloride) matrix.* Analyst, 1970. **95**(1136): p. 910-918.

25. Johnson, R.D. and Bachas, L.G., *Ionophore-based ion-selective potentiometric and optical sensors.* Analytical and Bioanalytical Chemistry, 2003. **376**(3): p. 328-341.

26. Bochenska, M., *Structural aspects of host molecules acting as ionophores in ion-selective electrodes.* Journal of Molecular Structure, 1998. **450**: p. 107-115.

27. Steed, J.W. and Atwood, J.L., *Supramolecular Chemistry.* 2000, Chichester: John Wiley & Sons. 745.

28. Qin, Y., Peper, S., and Bakker, E., *Plasticizer-free polymer membrane ion-selective electrodes containing a methacrylic copolymer matrix.* Electroanalysis, 2002. **14**(19-20): p. 1375-1381.

29. Ross, J.W., *Calcium-selective electrode with liquid ion exchanger.* Science, 1967. **156**: p. 1378-1379.

30. Diamond, D. and McKervey, A.M., *Calixarene-based sensing agents.* Chemical Society Reviews, 1996. **25**: p. 15-23.

31. Buhlmann, P., Pretsch, E., and Bakker, E., *Carrier-Based Ion-Selective Electrodes and Bulk Optodes. 2 Ionophores for Potentiometric and Optical Sensors.* Chemical Reviews, 1998. **98**: p. 1593-1687.

32. Tohda, K., Umezawa, Y., Yoshiyagawa, S., Hashimoto, S., and Kawasaki, M., *Cation permselectivity at the phase boundary of ionohore-incorporated solvent polymeric membranes as studied by optical second harmonic generation.* Analytical Chemistry, 1995. **67**(3): p. 570-577.

33. Diamond, D., *Calixarene-Based Sensing Agents*, in *Calixarenes 50th Anniversary: Commemorative Issue*, J. Vicens, Asfari, Z., and Harrowfield, J., Editors. 1994, Kluwer Academic Publishers: London. p. 415.

34. Kamata, S., Bhale, A., Fukunaga, Y., and Murata, H., *Copper(II)-Selective Electrode Using Thiuram Disulfide Neutral Carriers.* Analytical Chemistry, 1988. **60**: p. 2464-2467.

35. Wroblewski, W. and Brzozka, Z., Ag^+-selective electrodes based on lipophilic thioethers. Sensors and Actuators B, 1995. **24-25**: p. 183-187.

36. Sureshan, K.M., Shashidhar, M.S., and Varma, A., J., *Cyclitol-based metal-complexing agents. Effect of the relative orientation of oxygen atoms in the ionophoric ring on the cation-binding ability of myo-inositol-based crown ethers.* The Journal of Organic Chemistry, 2002. **67**(20): p. 6884-6888.

37. Lindner, E., Toth, K., Horvath, M., Pungor, E., Agai, B., Bitter, I., Toke, L., and Hell, Z., *Bis-crown ether derivatives as ionophores for potassium selective electrodes.* Fresenius' Zeitschrift fuer Analytische Chemie, 1985. **322**(2): p. 157-163.

38. Attiyat, A.S., Christian, G.D., and Bartsch, R.A., *Potentiometric selectivity study of crown ethers containing four ring oxygen atoms and bezoxymethyl or carboxylic acid side chains as ionophores for lithium and potassium.* Electroanalysis, 1989. **1**(1): p. 63-67.

39. Allen, J.R., Cynkowski, T., Desai, J., and Bachas, L.G., *Crown ether derivatives of anthraquinone as ionophores in ion-selective electrodes.* Electroanalysis, 1992. **4**(5): p. 533-537.

40. Siswanta, D., Nagatsuka, K., Yamanda, H., Kumakura, K., Hisamoto, H., Shichi, Y., Toshima, K., and Suzuki, K., *Structural ion selectivity of thia crown ether compounds with bulky block subunit and their application as an ion-sensing component for an ion-selective electrode.* Analytical Chemistry, 1996. **68**(23): p. 4166-4172.

41. Moriarty, R.M., Rao, M., Suresh, C., Tuladhar, S.M., D'Silva, C., Williams, G., and Richard, G., *Crown ether ionophores. Construction of neutral carrier ion-selective electrodes.* Journal of the American Chemical Society, 1993. **115**(3): p. 1194-1196.

42. Moriuchi-Kawakami, T., Nakazawa, S., Ota, M., Nishihira, M., Hayashi, H., Shibutani, Y., and Shono, T., *Pyrazole-containing crown ethers as ionophore for NH_4^+-selective electrodes.* Analytical Sciences, 1998. **14**(6): p. 1065-1068.

43. Forster, R.J., Cadogan, A., Diaz, M.T., and Diamond, D., *Calixarenes as active agents for chemical sensors.* Sensors and Actuators B, 1991. **4**: p. 325-331.

44. Bochenska, M., Hoffmann, M., and Lesinska, U., *Lower Rim Substituted tert-Butylcalix[4]arenes (Part VI). Synthesis and Ionophoric Properties of 5,11,17,23-Tetra-tert-Butyl-25,26,27,28-Tetrakis(3-Diethoxyphosphorylpropoxy)Calix[4]arene.* Journal of Inclusion Phenomena and Macrocyclic Chemistry, 2004. **49**(1 - 2): p. 57-60.

45. O'Connor, K.M. and Svehla, G., *Calixarene-based potentiometric ion-selective elctrodes for silver.* Talanta, 1992. **39**(1): p. 1549-1554.

46. Oh, H., Choi, E.M., Jeong, H., Nam, K.C., and Jeon, S., *Poly(vinyl chloride) membrane cesium ion-selective electrodes based on lipophilic calix[6]arene tetraester derivatives.* Talanta, 2000. **53**(3): p. 535-542.

47. Bakker, E., Buhlmann, P., and Pretsch, E., *Carrier-Based Ion-Selective Electrodes and Bulk Optodes. 1. General Characteristics.* Chemical Reviews, 1997. **97**(8): p. 3083-3132.

48. Beer, P.D., Gale, P.A., and Smith, D.K., *Supramolecular Chemistry.* Oxford Chemistry Primers. 1999, New York: Oxford University Press. 93.

49. Fiedler, U., *Influence of the dielectric constant of the medium on the selectivities of neutral carrier ligands in electrods membrane.* Analytica Chimica Acta, 1977. **89**: p. 111-118.

50. Bakker, E. and Qin, Y., *Electrochemical Sensors.* Analytical Chemistry, 2006. **78**(12): p. 3965-3984.

51. Eugster, R., Gehrig, P.M., Morf, W.E., Spichiger, U.E., and Simon, W., *Selectivity-modifying influence of anionic sites in neutral-carrier-based membrane electrodes.* Analytical Chemistry, 1991. **63**(20): p. 2285-2289.

52.   Ceresa, A., Bakker, E., Hattendorf, B., Gunther, D., and Pretsch, E., *Potentiometric polymeric membrane electrodes for measurement of environmental samples at trace levels: New requirements for selectivities and measuring protocols, and comparison with ICPMS.* Analytical Chemistry, 2001. **73**: p. 343-351.

53.   Telting-Diaz, M. and Bakker, E., *Effect of lipophilic ion-exchanger leaching on the detection limit of carrier-based ion-selective electrodes.* Analytical Chemistry, 2001. **73**(22): p. 5582-5589.

54.   Ammann, D., Pretsch, E., Simon, W., Lindner, E., Bezegh, A., and Pungor, E., *Lipophilic salts as membrane additives and their influence on the properties of macro- and micro-electrodes based on neutral carriers.* Analytica Chimica Acta, 1985. **171**: p. 119-129.

55.   Nagele, M., Mi, Y., Bakker, E., and Pretsch, E., *Influence of Lipophilic Inert Electrolytes on the Selectivity of Polymer Membrane Electrodes.* Analytical Chemistry, 1998. **70**(9): p. 1686-1691.

56.   Lis, J., Pasieczna, A., Karbowska, B., Zembrzuski, W., and Lukaszewski, Z., *Thallium in soils and stream sediments of a Zn-Pb mining and smelting area.* Environmental Science and Technology, 2003. **37**: p. 4569-4572.

57.   Nriagu, J.O., *Thallium in the Environment.* Advances in Environmental Science and Technology, ed. J.O. Nriagu. Vol. 29. 1998, New York: John Wiley and Sons. 284.

58.   Peter, A.L.J. and Viraiaghavan, T., *Thallium: a review of public health and environmental concerns.* Environment International, 2005. **31**: p. 493-501.

59.   Lenntech. *Thallium.* [Website] 2006 [cited 2006]; Available from: www.lenntech.com/Periodic-chart-elements/Tl-en.htm.

60.   Korenman, I.M., *Analytical Chemistry of Thallium.* Analytical Chemistry of Elements. 1969, London: Ann Arbor-Humphrey. 166.

61.   Pavlickova, J., Zbiral, J., Smatanova, M., Houserova, P., Cizmarova, E., Havlikova, S., and Kuban, V., *Uptake of thallium from artificially and naturally contaminated soils into rape (Brassica napus L.).* Journal of Agricultural and Food Chemistry, 2005. **53**: p. 2867-2871.

62.   Smith, I.C. and Carson, B.L., *Thallium.* Trace Metals in the Environment. Vol. 1. 1977, Michigan: Ann Arbor. 394.

63.   Cheam, V., *Thallium contamination of water in Canada.* Water Quality Research Journal of Canada, 2001. **36**(4): p. 851-877.

64.   Xiao, T., Guha, J., and Boyle, D., *High thallium content in rocks associated with Au-As-Hg-Tl and coal mineralization and its adverse environmental*

potential in SW Guizhou, China. Geochemistry: Exploration, Environment, Analysis, 2004. **4**: p. 243-252.

65. *Thallium*. [Webstie] 2006 [cited 2006]; Available from: http://en.wikipedia.org/wiki/Thallium.

66. *Thallium*. [Website] 1995 [cited 2006]; Available from: http://www.atsdr.cdc.gov/tfacts54.html.

67. *Consumer Factsheet on: Thallium*. [Website] 2006 [cited; Website]. Available from: http://www.epa.gov/safewater/contaminants/dw_contamfs/thallium.html.

68. Soriano, M.A. and Fereres, E., *Use of crops for in situ phytoremediation of polluted soils following a toxic flood from a mine spill.* Plant and Soil, 2003. **256**: p. 253-264.

69. Simon, M., Martin, F., Ortiz, I., Garcia, I., Fernandez, J., Fernandez, E., Dorronsoro, C., and Aguilar, J., *Soil pollution by oxidation of tailings from toxic spill of a pyrite mine.* Science of the Total Environment, 2001. **279**(1-3): p. 63-74.

70. Lin, T.S., Nriagu, J.O., and Wang, X.Q., *Thallium concentration in Lake trout from lake Michigan.* Bulletin of Environmental Contamination and Toxicology, 2001. **67**: p. 921-925.

71. Das, A.K., Dutta, M., Cervera, M.L., and de la Guardia, M., *Determination of thallium in water samples.* Microchemical Journal, 2007. **86**(1): p. 2-8.

72. Tsai, Y.-T., Huang, C.-C., Kuo, H.-C., Wang, H.-M., Shen, W.-S., Shih, T.-S., and Chu, N.-S., *Central nervous system effects in acute thallium poisoning.* NeuroToxicology, 2006. **27**(2): p. 291-295.

73. Dong, H., Zheng, H., Lin, L., and Ye, B., *Determination of thallium and cadmium on a chemically modified electrode with Langmuir-Blodgett film of p-allylcalix[4]arene.* Sensors and Actuators B: Chemical, 2006. **115**(1): p. 303-308.

74. Roper, E.D., Talanov, V.S., Gorbunova, M.G., Bartsch, R.A., and Talanova, G.G., *Optical Determination of Thallium(I) and Cesium(I) with a Fluorogenic Calix[4]arenebis(crown-6 ether) Containing One Pendent Dansyl Group.* Anal. Chem., 2007. **79**(5): p. 1983-1989.

75. Konishi, H., Takahashi, K., Nakamura, M., Sakamoto, H., and Kimura, K., *Investigation of metal ion complexation of pie-coordinate calixarene derivatives by electrospray-ionization mass spectrometry.* Journal of Inclusion Phenomena and Macrocyclic Chemistry, 2006. **54**(3-4): p. 147-152.

76. Coetzee, C.J. and Basson, A.J., *Potentiometric studies with thallium(I)-heteropoly acid salt-epoxy resin membranes.* Analytica Chimica Acta, 1973. **64**: p. 300-304.

77. Tamura, H., Kimura, K., and Shono, T., *Thallium(I)-Selective PVC Membrane Electrodes Based on Bis(crown ether)s.* Journal of Electroanalytical Chemistry, 1980. **115**: p. 115-121.

78. Yamashoji, Y., Tanaka, M., Nagamune, S., Ouchi, M., Hakushi, T., and Shono, T., *Polymer membrane thallium(I)-selective electrodes based on dibenzo-crown -6 ethers.* Analytical Sciences, 1991. **7**(3): p. 485-486.

79. Malik, W.U., Srivastava, S.K., Razdan, P., and Kumar, S., *Tungstoarsenates as ion-selective membranes for cesium and thallium(I) ions.* Journal of Electroanalytical Chemistry and Interfacial Electrochemistry, 1976. **72**(1): p. 111-116.

80. Szczepaniak, W. and Ren, K., *A Thallium(I)-Selective Electrode Based on a Liquid Ion-Exchanger Containing O,O'-Didecyldithiophosphoric acid.* Analytica Chimica Acta, 1976. **82**: p. 37-44.

81. Fogg, A.G., Al-Sibaai, A.A., and Burgess, C., *Ion-selective electrodes for the determination of antimony and thallium based on water-insoluble basic dye salts.* Analytical Letters, 1975. **8**(2): p. 129-137.

82. Coetzee, C.J. and Basson, A.J., *Cesium- and Thallium(I)-Sensitive Liquid Membranes Electrodes Based on Cesium- and Thallium Tetrakis(m-trifluoromethylphenyl)borates.* Analytica Chimica Acta, 1977. **92**: p. 399-403.

83. Coetzee, C.J., *Properties and analytical application of a thallium(I) ion-selective electrode.* Talanta, 1985. **32**(8, Part 2): p. 821-823.

84. Tamura, H., Kimura, K., and Shono, T., *Coated wire sodium- and potassium-selective electrodes based on Bis(crown ether) compounds.* Analytical Chemistry, 1982. **54**(1224-1227).

85. Tamura, H., Kimura, K., and Shono, T., *Effect of plasticizer on the selectivity of potassium-selective PVC membrane electrodes based on Bis(crown ether)s.* Bulletin of the Chemical Society of Japan, 1980. **53**(2): p. 547-548.

86. Kimura, K., Maeda, T., Tamura, H., and Shono, T., *Potassium-selective PVC membrane electrodes based on bis- and poly(crown ether)s.* Journal of Electroanalytical Chemistry, 1979. **95**(1): p. 91-101.

87. Masuda, Y., Yakabe, K., Shibutani, Y., and Shono, T., *Thallium(I) Ion-Selective Electrode Based on Polythiamacrocycles.* Analytical Sciences, 1994. **10**: p. 491-495.

88. Kimura, K., Tatsumi, K., Yokoyama, M., Ouchi, M., Mocerino, M.,, *Remarkable thallium(I) selectivity for ion sensors based on pie-coordination of calix[4]arene neutral carriers.* Analytical Communications, 1999. **36**: p. 229-230.

89. Park, K.S., Jung, S.O., Lee, S.S., and Kim, J.S., *Thallium(I)-selective electrodes based on calix[4]pyrroles.* Bulletin of the Korean Chemical Society, 2000. **21**(9): p. 909-912.

90. Khayatian, G., Shariati, S., and Abdollah, S., *Thallium(I)-selective membrane potentiometric sensor based on dibenzyldiaza-18-crown-6.* Bulletin of the Korean Chemical Society, 2003. **24**(4): p. 421-425.

91. Katsu, T., Ido, K., Takaishi, K., and Yokosu, H., *Thallium(I)-selective membrane electrodes based on calix[6]arene or calix[5]arene derivatives.* Sensors and Actuators B: Chemical, 2002. **87**(2): p. 331-335.

92. Gaber, A.A.A., *New thallium(I) ion selective electrode based on indeno pyran compound.* Sensors and Actuators B: Chemical, 2003. **96**(3): p. 615-620.

93. Ganjali, M.R., Pourjavid, M.R., Mouradzadegun, A., Hosseini, M., and Mizani, F., *Novel thallium(I)-selective membrane electrode based on a podal ligand.* Bulletin of the Korean Chemical Society, 2003. **24**(11): p. 1585-1589.

94. Park, K.M., Lee, Y.H., Jin, Y., Seo, J., Yoon, I., Lee, S.C., Park, S.B., Gong, M.S., Seo, M.L., and Lee, S.S., *Tetrathiaoxa Macrocycles with Dibenzo-subunits: A search for New Tl(I)- and Ag(I)-Selective Ionophores.* Supramolecular Chemistry, 2004. **16**(1): p. 51-58.

95. Singh, A.K. and Saxena, P., *A highly selective thallium(I) electrode based on a thia substituted macrocyclic ionophore.* Talanta, 2005. **66**: p. 993-998.

96. Ouchi, M. and Hakushi, T., *Cation binding by thallium(I) selective crown ethers.* Coordination Chemistry Reviews, 1996. **148**: p. 171-181.

97. Gholamreza, K., Satar, S., and Abdollah, S., *Thallium(I)-selective membrane potentiometric sensor based on dibenzyldiaza-18-crown-6.* Bulletin of the Korean Chemical Society, 2003. **24**(4): p. 421-425.

98. Saleh, M.B., *A Novel PVC membrane sensor for potentiometric determination of thallium(I).* Journal of Electroanalytical Chemistry, 1998. **448**: p. 33-39.

99. Yajima, S., Yoshioka, N., Tanaka, M., and Kimura, K., *Soft Metal Ion-Selective Electrodes Based on pie-Coordinate Calixarene Derivatives.* Electroanalysis, 2003. **15**(15-16): p. 1319-1326.

100. Beer, P.D. and Cooper, J.B., *Calixarene Based Anion Receptors*, in *Calixarenes in Action*, L. Mandolini and Ungaro, R., Editors. 2000, Imperial College Press: London. p. 271.

101. Gutsche, C.D., *Part One: History and Synthesis of Calixarenes - Single Step Synthesis and Properties of Calixarenes*, in *Calixarenes: A Versatile Class of Macrocyclic Compounds*, J. Vicens and Bohmer, V., Editors. 1991, Kluwer Academic: London. p. 264.

102. Gutsche, C.D., Dhawan, B., Levine, J.A., No, K.H., and Bauer, J., *Calixarenes 9. Conformational isomers of the ethers and esters of calix[4]arene.* Tetrahedron, 1983. **39**(3): p. 409-426.

103. Casnati, A., Sansone, F., and Ungaro, R., *Calixarene receptors in ion recognition and sensing.* Advances in Supramolecular Chemistry, ed. G.W. Gokel. Vol. 9. 2003: Cerberus Press Inc.

104. Iwamoto, K., Araki, K., and Shinkai, S., *Conformations and structures of tetra-O-alkyl-p-tert-butylcalix[4]arenes. How is the conformation of calix[4]arenes immobilized?* Journal of Organic Chemistry, 1991. **56**: p. 4955-4962.

105. Gutsche, C.D., Levine, J.A., and Sujeeth, P.K., *Calixarenes. 17. Functionalized calixarenes: The Claisen rearrangement route.* Journal of Organic Chemistry, 1985. **50**: p. 5802-5806.

106. Consoli, G.M.L., Granata, G., Galante, E., Cunsolo, F., and Geraci, C., *Novel nucleotide-calixarene conjugates via phosphoester linkage.* Tetrahedron Letters, 2006. **47**(19): p. 3245-3249.

107. Lynch, A., Eckhard, K., McMahon, G., Wall, R., Kane, P., Nolan, K., Schuhmann, W., and Diamond, D., *Cation Binding Selectivity of Partially Substituted Calix[4]arene Esters.* Electroanalysis, 2002. **14**(19-20): p. 1397-1404.

108. Oueslati, F., Dumazet-Bonnamour, I., and Lamartine, R., *New Azothiacalix[4]arenes Containing Biheterocyclic Subunits: Extraction and Complexation Properties.* Supramolecular Chemistry, 2005. **17**(3): p. 227-232.

109. Klenke, B., Nather, C., and Friedrichsen, W., *Selective side-chain functionalization of a calix[4]arene - 2,8,14,20-tetrabromo-25,26,27,28-tetramethoxycalix[4]arene.* Tetrahedron Letters, 1998. **39**(49): p. 8967-8968.

110. Bartlett, M.J., Mocerino, M., Ogden, M.I., Oliveira, A., Parkinson, G.M., Petterson, J.K., and Reyhani, M.M., *Amino Acid Modified Calixarenes as Crystal Growth Modifiers.* Journal of Material Science and Technology, 2005. **21**(Supp. 1): p. 1-5.

111.   Jones, F., Mocerino, M., Ogden, M.I., Oliveira, A., and Parkinson, G.M., *Bio-Inspired Calix[4]arene Additives for Crystal Growth.* Crystal Growth and Design, 2005. **5**: p. 2336-2343.

112.   Gutsche, C.D., *Calixarenes Revisited.* Monographs in Supramolecular Chemistry, ed. J.F. Stoddart. 1998, Cambridge: The Royal Society of Chemistry.

113.   Van Loon, J.D., Arduini, A., Coppi, L., Verboom, W., Pochini, A., Ungaro, R., Harkema, S., and Reinhoudt, D.N., *Selective functionalization of calix[4]arenes at the upper rim.* Journal of Organic Chemistry, 1990. **55**(21): p. 5639-5646.

114.   Shu, C.-M., Chung, W.-S., Wu, S.-H., Ho, Z.-C., and Lin, L.-G., *Synthesis of Calix[4]arenes with Four Different "Lower Rim" Substituents.* Journal of Organic Chemistry, 1999. **64**(8): p. 2673-2679.

115.   Ferguson, G., Gallagher, J.F., Lough, A.J., Notti, A., Pappalardo, S., and Parisi, M.F., *1,3-Calix[4]arene Crown Ether Conformers with a 3-Thienyl Pendant Functionality at the Lower Rim.* Journal of Organic Chemistry, 1999. **64**(16): p. 5876-5885.

116.   Ferguson, G., Gallagher, J.F., Giunta, L., Neri, P., Pappalardo, S., and Parisi, M., *Synthetic strategies to inherently chiral calix[4]arenes with mixed ligating functionalities at the lower rim.* Journal of Organic Chemistry, 1994. **59**(1): p. 42-53.

117.   Yan, C., An, L., and Sun, J., *Novel Synthesis of p-tert-Butylcalix[n]arenes Bearing Ethylene Glycol Ether Chains.* Synthetic Communications, 2004. **34**(24): p. 4493-4497.

118.   Arduini, A. and Casnati, A., *Calixarenes*, in *Macrocycle Synthesis - A Practical Approach*, D. Parker, Editor. 1996, Oxford University Press: New York. p. 251.

119.   Bohmer, V. and Vicens, J., *Part One: History and Synthesis of Calixarenes - Special Calixarenes, Synthesis and Properties*, in *Calixarenes: A Versatile Class of Macrocyclic Compounds*, J. Vicens and Bohmer, V., Editors. 1991, Kluwer Academic: London. p. 264.

120.   Gutsche, C.D. and Lin, L.-G., *Calixarenes 12: The Synthesis of Functionalized Calixarenes.* Tetrahedron, 1986. **42**(6): p. 1633-1640.

121.   Takayuki Sakurai, Y.T., *Synthesis of calix[4]arenes modified with germanium-containing side chains on the upper rim.* Applied Organometallic Chemistry, 2004. **18**(1): p. 23-27.

122.   Dermody, D.L., Lee, Y., Kim, T., and Crooks, R.M., *Synthesis, Characterization, and Chemical Sensitivity of Self-Assembled Bilayers*

Composed of Polydiacetylenes and Calix[4]arenes Chemically Modified on the Upper Rim. Langmuir, 1999. **15**(24): p. 8435-8440.

123. St'astny, V., Stibor, I., Petrickova, H., Sykora, J., and Lhotak, P., *Thiacalix[4]arene derivatives with proximally bridged lower rim.* Tetrahedron, 2005. **61**(42): p. 9990-9995.

124. Matthews, S.E., Rees, N.H., Felix, V., Drew, M.G.B., and Beer, P.D., *Thallium pie-cation complexation by calix[4]tubes: ^{205}Tl NMR and X-ray evidence.* Inorganic Chemistry, 2003. **42**: p. 729-734.

125. Nabeshima, T., Saiki, T., Sumitomo, K., and Akine, S., *Doubly bridged biscalix[4]arene for homotropic and heterotropic allosteric effects on ion recognition.* Tetrahedron Letters, 2004. **45**(24): p. 4719-4722.

126. Kraft, D., Loon, J.-D.V., Owens, M., Verboom, W., Vogt, W., McKervey, A.M., Bohmer, V., and Reinhoudt, D.N., *Double and triple calix[4]arenis connected via oxygen functions.* Tetrahedron Letters, 1990. **31**(34): p. 4941-4944.

127. Felix, V., Matthews, S., Beer, P.D., and Drew, M.G.B., *Selectivity of calix[4]tubes towards metal ions: A molecular dynamics study.* Physical Chemistry Chemical Physics, 2002. **4**: p. 3849-3858.

128. Aleksiuk, O., Grynszpan, F., and Biali, S.E., *Spirodienone route for aminodehydroxylation: monoaminotrihydroxy-p-tert-butylcalix[4]arene.* Journal of Organic Chemistry, 1993. **58**(8): p. 1994-1996.

129. Aleksiuk, O., Cohen, S., and Biali, S.E., *Selective hydroxyl replacement in calixarenes: Amino-, Azo-, and Xanthenocalixarene Derivatives.* Journal of the American Chemical Society, 1995. **117**(38): p. 9645-9652.

130. Delaigue, X. and Wais Hosseini, Mir, *Synthesis of a 1,3-alternate tetramercapto [1.1.1.1]metacyclophane.* Tetrahedron Letters, 1993. **34**(50): p. 8111-8112.

131. Gibbs, C.G. and Gutsche, C.D., *Calixarenes. 31. Synthesis and conformation of p-tert-butyltetramercaptocalix[4]arene.* Journal of the American Chemical Society, 1993. **115**(12): p. 5338-5339.

132. Delaigue, X., Harrowfield, J., Hosseini, M., Cian, A.D., Fischer, J., and Kyritsakas, N., *Exoditopic Receptors: Synthesis and structural studies on p-tert-butyltetramercaptocalix[4]arene and its Mercury Complexes.* Journal of the Chemical Society, Chemical Communications, 1994: p. 1579.

133. Perrin, R. and Harris, S., *Part Four: Industrial Applications*, in *Calixarenes: A Versatile Class of Macrocyclic Compounds*, J. Vicens and Bohmer, V., Editors. 1991, Kluwer Academic: London. p. 264.

134. Casnati, A., Della Ca', N., Fontanella, M., Sansone, F., Ugozzoli, F., Ungaro, R., Liger, K., and Dozol, J.-F., *Calixarene-Based Picolinamide Extractants for Selective An/Ln Separation from Radioactive Waste.* European Journal of Organic Chemistry, 2005. **2005**(11): p. 2338-2348.

135. Yordanov, A.T. and Max Roundhill, D., *Extraction of platinum from aqueous solution into chloroform using a 2-pyridylthio-N-oxide derivatized calix[4]arene as phase transfer reagent.* Inorganica Chimica Acta, 1997. **264**(1-2): p. 309-311.

136. Izatt, R.M., Lamb, J.D., Hawkins, R.T., Brown, P.R., Izatt, S.R., and Christensen, J.J., *Selective M^+-H^+ coupled transport of cations through a liquid membrane by macrocyclic calixarene ligands.* Journal of the American Chemical Society, 1983. **105**(7): p. 1782-1785.

137. Duncan, D.M. and Cockayne, J.S., *Application of calixarene ionophores in PVC based ISEs for uranium detection.* Sensors and Actuators B, 2001. **73**: p. 228-235.

138. Telting-Diaz, M., Regan, F., Diamond, D., and Smyth, M.R., *Comparison of a calixarene-based ion-selective electrode with two automated analyzers for the clinical determination of sodium in blood plasma*.* Journal of Pharmaceutical & Biomedical Analysis, 1990. **8**(8-12): p. 695-700.

139. Ungaro, R. and Pochini, A., *Part Three: Inclusion Properties of Calixarenes and their Derivatives - Calixarene-Based Cation Receptors and Carriers*, in *Calixarenes: A Versatile Class of Macrocyclic Compounds*, J. Vicens and Bohmer, V., Editors. 1991, Kluwer Academic: London. p. 264.

140. Schwing, M.J. and McKervey, A.M., *Part Three: Inclusion Properties of Calixarenes and Their Derivatives - Chemically modified Calixarenes as New Selective Receptors for Monovalent Cations*, in *Calixarenes: A Versatile Class of Macrocyclic Compounds*, J. Vicens and Bohmer, V., Editors. 1991, Kluwer Academic: London. p. 264.

141. Kumar, M., Mahajan, R.K., Sharma, V., Singh, H., Sharma, N., and Kaur, I., *Synthesis of new bis-calix[4]arenes with imine linkages. A search for new silver-selective sensors.* Tetrahedron Letters, 2001. **42**: p. 5315-5318.

142. Zeng, X., Weng, L., Chen, L., Xu, F., Li, Q., Leng, X., He, X., and Zhang, Z.Z., *The syntheses and Ag^+-selective electrode properties of benzothiazoylthiaalkoxy functionalized calix[4]arenes: an investigation of the structure-selectivity relationship in the ionophore-based ISEs.* Tetrahedron, 2002. **58**: p. 2647-2658.

143. Lu, J.-Q., Pang, D.W., Zeng, X., and He, X., *A new solid-state silver ion-selective electrode based on a novel tweezer-type calixarene derivative.* Journal of Electroanalytical Chemistry, 2004. **568**: p. 37-43.

144. Chen, L., Zeng, X., He, X., and Zhang, Z., *Selective electrodes for silver based on oplymeric membranes containing calix[4]arene derivatives.* Fresenius' Journal of Analytical Chemistry, 2000. **367**: p. 535-538.

145. Chen, L., Zhang, J., Zhao, W., He, X., and Liu, Y., *Double-armed calix[4]arene amide derivatives as ionophores for lead ion-selective electrodes.* Journal of Electroanalytical Chemistry, 2006. **589**(1): p. 106-111.

146. Lu, J., Chen, R., and He, X., *A lead ion-selective electrode based on a calixarene carboxyphenyl azo derivative.* Journal of Electroanalytical Chemistry, 2002. **528**: p. 33-38.

147. Szigeti, Z., Malon, A., Vigassy, T., Csokai, V., Grun, A., Wygladacz, K., Ye, N., Xu, C., Chebny, V.J., and Bitter, I., *Novel potentiometric and optical silver ion-selective sensors with subnanomolar detection limits.* Analytica Chimica Acta, 2006. **572**(1): p. 1-10.

148. Gupta, V.K., Ludwig, R., and Agarwal, S., *Anion recognition through modified calixarenes: a highly selective sensor for monohydrogen phosphate.* Analytica Chimica Acta, 2005. **538**(1-2): p. 213-218.

149. Matthews, S. and Beer, P.D., *Calixarene-based Anion Receptors.* Supramolecular Chemistry, 2005. **V17**(6): p. 411-435.

150. Cafeo, G., Kohnke, F.H., La Torre, G.I., Parisi, M.F., Nascone, R.P., White, A.J.P., and Williams, D.J., *Calix[6]pyrrole and hybrid Calix[n]furan[m]pyrroles (n+m = 6): Synthesis and host-guest chemistry.* Chemistry: A European Journal, 2002. **8**(14): p. 3148-3156.

151. Kral, V., Sessler, J.L., Shishkanova, T.V., Gale, P.A., and Volf, R., *Molecular Recognition at an Organic-Aqueous Interface: Heterocalixarenes as Anion Binding Agents in Liquid Polymeric Membrane Ion-Selective Electrodes.* Journal of the American Chemical Society, 1999. **121**(38): p. 8771-8775.

152. Kao, T.L., Wang, C.C., Pan, Y.T., Shiao, Y.J., Yen, J.Y., Shu, C.M., Lee, G.H., Peng, S.M., and Chung, W.S., *Upper rim allyl- and arylazo-coupled calix[4]arenes as highly sensitive chromogenic sensors for Hg^{2+} ion.* Journal of Organic Chemistry, 2005. **70**: p. 2912-2920.

153. Verboom, W., Datta, S., Asfari, Z., Harkema, S., and Reinhoudt, D.N., *Tetra-O-alkylated calix[4]arenes in the 1,3-alternate conformation.* J. Org. Chem., 1992. **57**(20): p. 5394-5398.

154. Gutsche, C.D. and Ibqal, M., *p-tert-Butylcalix[4]arene.* Journal of Organic Synthesis, 1990. **68**: p. 243.

155. Couton, D., Mocerino, M., Rapley, C., Kitammura, C., Yoneda, A., and Ouchi, M., *Silver and Thallium Ion Complexation with*

Allyloxycalix[4]arenes. Australian Journal of Chemistry, 1999. **52**: p. 227-229.

156. Lobler, R., *Synthesis and application of 1,3-alternate calix[4]arenes in the extraction of heavy metals*, Honours, 2002, Curtin University, 44

157. *Calixarenes: A versatile class of macrocyclic compounds.* Topics in inclusion science, ed. J.E.D. Davies. Vol. 3. 1991, London: Kluwer. 263.

158. Andreetti, G.D., Ungaro, R., and Pochini, A., *Crystal and molecular structure of cyclo{quater[(5-t-butyl-2-hydroxy-1,3-phenylene)methylene Toluene (1:1) clathrate.* Journal of the Chemical Society, Chemical Communications, 1979: p. 1005-1007.

159. *Calixarenes 2001*, ed. Z. Asfari, Bohmer, V., Harrowfield, J., and Vicens, J. 2001: Kluwer Academic Publishers. 683.

160. Nassimbeni, L.R., *Physicochemical Aspects of Host-Guest Compounds.* Accounts of Chemical Research, 2003. **36**(8): p. 631-637.

161. Ananchenko, G.S., Udachin, K.A., Dubes, A., Ripmeester, J.A., Perrier, T., and Coleman, A.W., *Guest Exchange in Single Crystals of van der Waals Nanocapsules.* Angewandte Chemie International Edition, 2006. **45**(10): p. 1585-1588.

162. Atwood, J.L., Barbour, L.J., and Jerga, A., *Polymorphism of pure p-tert-butylcalix[4]arene: conclusive identification of the phase obtained by desolvation.* Chemical Communications, 2002(24): p. 2952-2953.

163. Atwood, J.L., Barbour, L.J., and Jerga, A., *Storage of methane and freon by interstitial van der Waals confinement.* Science, 2002. **296**: p. 2367-2369.

164. Cecillon, S., Lazar, A., Danylyuk, O., Suwinska, K., Rather, B., Zaworotko, M.J., and Coleman, A.W., *Head-to-tail self-assembly of a calix[4]arene inclusion polymer controlled by a pendant arm.* Chemical Communications, 2005(19): p. 2442-2444.

165. Gibb, B.C., *A Solid-State Supramolecular Sweet Spot.* Angewandte Chemie International Edition, 2003. **42**(15): p. 1686-1687.

166. Rudkevich, D.M. and Leontiev, A.V., *Molecular Encapsulation of Gases.* Australian Journal of Chemistry, 2004. **57**(8): p. 713-722

167. Thallapally, P.K., Dobrzanska, L., Gingrich, T.R., Wirsig, T.B., Barbour, L.J., and Atwood, J.L., *Acetylene absorption and binding in a nonporous crystal lattice.* Angewandte Chemie International Edition, 2006. **45**: p. 6506-6509.

168.	Atwood, J.L., Barbour, L.J., Thallapally, P.K., and Wirsig, T.B., *A crystalline organic substrate absorbs methane under STP conditions.* Chemical Communications, 2005(1): p. 51-53.

169.	Thallapally, P.K., Wirsig, T.B., Barbour, L.J., and Atwood, J.L., *Crystal engineering of nonporous organic solids for methane sorption.* Chemical Communications, 2005(35): p. 4420-4422.

170.	Atwood, J.L., Barbour, L.J., Jerga, A., and Schottel, B.L., *Guest transport in a nonporous organic solid via dynamic van der Waals cooperativity.* Science, 2002. **298**: p. 1000-1002.

171.	Thallapally, P.K., Lloyd, G.O., Wirsig, T.B., Bredenkamp, M.W., Atwood, J.L., and Barbour, L.J., *Organic crystals absorb hydrogen gas under mild conditions.* Chemical Communications, 2005(42): p. 5272-5274.

172.	Atwood, J.L., Barbour, L.J., Lloyd, G.O., and Thallapally, P.K., *Polymorphism of pure p-tert-butylcalix[4]arene: subtle thermally-induced modifications.* Chemical Communications, 2004(8): p. 922-923.

173.	Enright, G.D., Udachin, K.A., Moudrakovski, I.L., and Ripmeester, J.A., *Thermally Programmable Gas Storage and Release in Single Crystals of an Organic van der Waals Host.* Journal of the American Chemical Society, 2003. **125**(33): p. 9896-9897.

174.	Barbour, L.J., *Crystal porosity and the burden of proof.* Chemical Communications, 2006(11): p. 1163-1168.

175.	Olmstead, M.M., Sigel, G., Hope, H., Xu, X., and Power, P.P., *Metallocalixarenes: syntheses and z-ray structures of titanium(IV), iron(III) and cobalt(II) complexes of p-tert-butylcalix[4]arene.* Journal of the American Chemical Society, 1985. **107**: p. 8087-8091.

176.	Izatt, S.R., Hawkins, R.T., Christensen, J.J., and Izatt, R.M., *Cation transport from multiple alkali cation mistures using a liquid membrane system containing a series of calixarene carriers.* Journal of the American Chemical Society, 1985. **107**: p. 63-66.

177.	Harrowfield, J., Ogden, M., and White, A., *Lanthanide Ion Complexes of Calixarenes. VII. Bimetallic Lanthanide Complexes of p-t-Butylcalix[8]arene From Dimethyl Sulfoxide Solutions.* Australian Journal of Chemistry, 1991. **44**(9): p. 1237-1247.

178.	Harrowfield, J., Ogden, M., and White, A., *Lanthanide Ion Complexes of Calixarenes. VIII. Bimetallic Lanthanide Complexes of p-t-Butylcalix[8]arene From Dimethylformamide Solutions.* Australian Journal of Chemistry, 1991. **44**(9): p. 1249-1262.

179.   Bernardino, R.J. and Costa Cabral, B.J., *Complexatin of calix[4]arene with alkali metal cations: Conformational binding selectivity and cation-pie driven inclusion.* Supramolecular Chemistry, 2002. **14**(1): p. 57-66.

180.   Ma, J.C. and Dougherty, D.A., *The Cation-pie Interaction.* Chem. Rev., 1997. **97**(5): p. 1303-1324.

181.   Casnati, A., Pochini, A., Ungaro, R., Ugozzoli, F., Arnaud-Neu, F., Fanni, S., Schwing, M.J., Egberink, R.J.M., Jong, F., and Reinhoudt, D.N., *Synthesis, complexation, and membrane transport studies of 1,3-alternate calix[4]arene-crown-6 Conformers: A new class of cesium selective ionophores.* Journal of the American Chemical Society, 1995. **117**(10): p. 2767-2777.

182.   Casnati, A., Pochini, A., Ungaro, R., Bocchi, C., Ugozzoli, F., Egberink, R.J.M., Struijk, H., Lugtenberg, R., Jong, F.D., and Reinhoudt, D.N., *1,3-Alternate Calix[4]arenecrown-5 Conformers: New Synthetic Ionophores with Better K^+/Na^+ Selectivity than Valinomycin.* Chemistry - A European Journal, 1996. **2**(4): p. 436-445.

183.   Bakker, E., *Determination of unbiased selectivity coefficients of neutral carrier-based cation-selective electrodes.* Analytical Chemistry, 1997. **69**: p. 1061-1069.

184.   Ikeda, A. and Shinkai, S., *On the Origin of High Ionophoricity of 1,3-alternate Calix[4]arenes: p-Donor Participation in Complexation of Cations and Evidence for Metal-Tunneling through the Calix[4]arene Cavity.* Journal of the American Chemical Society, 1994. **116**: p. 3102-3110.

185.   Ghidini, E., Ugozzoli, F., Ungaro, R., Harkema, S., El-Fadl, A.A., and Reinhoudt, D.N., *Complexation of alkali metal cations by conformationally rigid, stereoisomeric calix[4]arene crown ethers: A quantitative evaluation of preorganization.* Journal of the American Chemical Society, 1990. **112**(19): p. 6979-6985.

186.   Seneque, O., Campion, M., Giorgi, M., Mest, Y.L., and Reinaud, O., *Funnel Complexes with Co(II) and Ni(II): New Probes into the biomimetic coordination ability of the calix[6]arene-based tris(imidazole) system.* European Journal of Inorganic Chemistry, 2004: p. 1817-1826.

187.   Ceresa, A., Sokalski, T., and Pretsch, E., *Influence of key parameters on the lower detection limit and response function of solvent polymeric membrane ion-selective electrodes.* Journal of Electroanalytical Chemistry, 2001. **501**: p. 70-76.

188.   McKittrick, T., Diamond, D., Marrs, D.J., O'Hagan, P., and Anthony McKervey, M., *Calcium-selective electrode based on a calix[4]arene tetraphosphine oxide.* Talanta, 1996. **43**(7): p. 1145-1148.

189. Bochenska, M., Hoffmann, M., Lesinska, U., Luks, E., and Radecka-Paryzek, W., *Lower rim substituted tert-butylcalix[4]arenes. Part 8: Calix[4]arenes with dialkoxyphosphoryl functions. Synthesis and complexing properties.* Tetrahedron, 2005. **61**(52): p. 12307-12313.

190. Mudring, A.-V. and Rieger, F., *Lone pair effect in thallium(I) macrocyclic compounds.* Inorganic Chemistry, 2005. **44**: p. 6240-6243.

191. Speck, A.L., 2007, PLATON, a multipurpose crystallographic tool, Utrecht University, Utrecht, Netherlands

192. Evens, D.R., Huang, M., Fettinger, F.C., and Williams, T.L., *Synthesis and Characterisation of Diametrically Substituted Tetra-O-n-butylcalix[4]arene Ligands and their Chelated Complexes of Titanium, Molybdenum, and Palladium.* Inorganic Chemistry, 2002. **41**(23): p. 5986-6000.

193. Marcus, Y., *A simple empirical model describing the thermodynamics of hydration of ions of widely varying charges, sizes and shapes.* Biophysical Chemistry, 1994. **51**: p. 111-127.

194. Fielding, L., *Determination of Association Constants (Ka) from Solution NMR Data.* Tetrahedron, 2000. **56**: p. 6151-6170.

195. Beer, P.D., Drew, M.G.B., Gale, P.A., Leeson, P.B., and Ogden, M.I., *Structures of Potassium encapsulated within the 1,3-alternate conformation of calix[4]arenes.* Journal of the Chemical Society, Dalton Transactions, 1994: p. 3479-3485.

196. Koryta, J., *Ion -Selective Electrodes.* 1975, Cambridge: Cambridge University Press. 207.

197. Mikhelson, K.N., Lewenstam, A., and Didina, S.E., *Contribution of the Diffusion Potential to the Membrane Potential and to the Ion-Selective Electrode Response.* Electroanalysis, 1999. **11**(10-11): p. 793-798.

198. Umezawa, K., Ming Lin, X., Nishizawa, S., Sugawara, M., and Umezawa, Y., *Cation permselectivity in the phase boundary of ionophore-incorporated solvent polymeric membranes as studied by Fourier transform infrared attenuated total reflection spectrometry.* Analytica Chimica Acta, 1993. **282**(2): p. 247-257.

199. Pungor, E., *Ion-selective electrodes - history and conclusions.* Fresenius' Journal of Analytical Chemistry, 1997. **357**(2): p. 184-188.

200. Bakker, E., Buhlmann, P., and Pretsch, E., *The phase-boundary potential model.* Talanta, 2004. **63**: p. 3-20.

201. Bakker, E., Buhlmann, P., and Pretsch, E., *Polymer membrane ion-selective electrodes - What are the limits?* Electroanalysis, 1999. **11**(13): p. 915-933.

202.   Sokalski, T. and Lewenstam, A., *Application of Nernst-Planck and Poisson equations for interpretation of liquid-junction and membrane potentials in real-time and space domains.* Electrochemistry Communications, 2001. **3**(3): p. 107-112.

203.   Sokalski, T., Lingenfelter, P., and Lewenstam, A., *Numerical Solution of the Coupled Nernst-Planck and Poisson Equations for Liquid Junction and Ion Selective Membrane Potentials.* Journal of Physical Chemistry B, 2003. **107**(11): p. 2443-2452.

204.   Morf, W.E., *Calculation of liquid-junction potentials and membrane potentials on the basis of the Planck Theory.* Analytical Chemistry, 1977. **49**(6): p. 810-813.

205.   Bakker, E., Pretsch, E., and Buhlmann, P., *Selectivity of Potentiometric ion sensors.* Analytical Chemistry, 2000. **72**: p. 1127-1133.

206.   Nagele, M., Bakker, E., and Pretsch, E., *General description of the simultaneous response of potentiometric ionophore-based sensors to ions of different charge.* Analytical Chemistry, 1999. **71**: p. 1041-1048.

207.   IUPAC. *Compendium of Analytical Nomenclature: Definitive Rules.* [Website] 1997 [cited; Available from: http://www.iupac.org/publications/analytical_compendium.

208.   Sokalski, T., Zwickl, T., Bakker, E., and Pretsch, E., *Lowering the detection limit of solvent polymeric ion-selective electrodes. 1.Modeling the influence of steady-state ion fluxes.* Analytical Chemistry, 1999. **71**: p. 1204-1209.

209.   Buhlmann, P., Amemiya, S., Yajima, S., and Umezawa, Y., *Co-Ion Interference for Ion-Selective Electrodes Based on Charged and Neutral Ionophores: A Comparison.* Analytical Chemistry, 1998. **70**(20): p. 4291-4303.

210.   Yajima, S., Tohda, K., Buhlmann, P., and Umezawa, Y., *Donnan Exclusion Failure of Neutral Ionophore-Based Ion-Selective Electrodes Studied by Optical Second-Harmonic Generation.* Analytical Chemistry, 1997. **69**(10): p. 1919-1924.

211.   Buck, R.P., Toth, K., Graf, E., Horvai, G., and Pungor, E., *Donnan exclusion failure in low anion site density membranes containing valinomycin.* Journal of Electroanalytical Chemistry, 1987. **223**(1-2): p. 51-66.

212.   Ion, A.C., Bakker, E., and Pretsch, E., *Potentiometric Cd^{2+}-selective electrode with detection limit in the low ppt range.* Analytica Chimica Acta, 2001. **440**: p. 71-79.

213.   Bakker, E. and Pretsch, E., *Potentiometric sensors for trace-level analysis.* Trends in Analytical Chemistry, 2005. **24**(3): p. 199-207.

214. Bakker, E. and Pretsch, E., *Potentiometry at trace levels.* Trends in Analytical Chemistry, 2001. **20**(1): p. 11-19.

215. Lerchi, M., Bakker, E., Rusterholz, B., and Simon, W., *Lead-Selective bulk optodes based on neutral ionophores with subnanomolar detection limits.* Analytical Chemistry, 1992. **64**(14): p. 1534-1545.

216. Lerchi, M., Reitter, E., Simon, W., Pretsch, E., Chowdhury, A., and Kamata, S., *Bulk optodes based on neutral dithiocarbamate ionophores with high selectivity and sensitivity for silver and mercury cations.* Analytical Chemistry, 1994. **66**(10): p. 1713-1717.

217. Bakker, E., Willer, M., and Pretsch, E., *Detection limit of ion-selective bulk optodes and corresponding electrodes.* Analytica Chimica Acta, 1993. **282**(2): p. 265-271.

218. Schefer, U., Ammann, D., Pretsch, E., Oesch, U., and Simon, W., *Neutral carrier based calcium(2+)-selective electrode with detection limit in the sub-nanomolar range.* Analytical Chemistry, 1986. **58**(11): p. 2282-2285.

219. Qin, W., Zwickl, T., and Pretsch, E., *Improved detection limits and unbiased selectivity coefficients obtained by using ion-exchange resins in the inner reference solution of ion-selective polymeric membrane electrodes.* Analytical Chemistry, 2000. **72**: p. 3236-3240.

220. Ceresa, A., Radu, A., Peper, S., Bakker, E., and Pretsch, E., *Rational design of potentiometric trace level ion sensors. A Ag^+-selective electrode with a 100 ppt detection limit.* Analytical Chemistry, 2002. **74**: p. 4027-4036.

221. Szigeti, Z., *Optimisation of Ion-Selective Electrodes for Trace Metal Analysis*, PhD (Doctorate of Natural Sciences), 2005, Swiss Federal Institute of Technology, 162

222. Schneider, B., Zwickl, T., Federer, B., Pretsch, E., and Lindner, E., *Spectropotentiometry: A New Method for in Situ Imaging of Concentration Profiles in Ion-Selective Membranes with Simultaneous Recording of Potential-Time Transients.* Analytical Chemistry, 1996. **68**(24): p. 4342-4350.

223. Mi, Y., Mathison, S., Goines, R., Logue, A., and Bakker, E., *Detection limit of polymeric membrane potentiometric ion sensors: how can we go down to trace levels?* Analytica Chimica Acta, 1999. **397**: p. 103-111.

224. Sokalski, T., Ceresa, A., Fibbioli, M., Zwickl, T., Bakker, E., and Pretsch, E., *Lower the detection limit of solvent polymeric ion-selective membrane electrodes. 2. Influence of composition of sample and internal electrolyte solution.* Analytical Chemistry, 1999. **71**(6): p. 1210-1214.

225. Mathison, S. and Bakker, E., *Effect of transmembrane electrolyte diffusion on the detection limit of carrier-based potentiometric ion sensors.* Analytical Chemistry, 1998. **70**(2): p. 303-309.

226. Iglehart, M.L., Buck, R.P., and Pungor, E., *Plasticized poly(vinyl chloride) properties and characteristics of valinomycin electrodes. The d.c. current-voltage curves.* Analytical Chemistry, 1988. **60**(4): p. 290-295.

227. Long, R. and Bakker, E., *Optical determination of ionophore diffusion coefficients in plasticized poly(vinyl chloride) sensing films.* Analytica Chimica Acta, 2004. **511**(1): p. 91-95.

228. Radu, A., Meir, A.J., and Bakker, E., *Dynamic Diffusion Model for Tracing the Real-Time Potential Response of Polymeric Membrane Ion-Selective Electrodes.* Analytical Chemistry, 2004. **76**(21): p. 6402-6409.

229. Heng, L.Y. and Hall, E.A.H., *Methacrylate-acrylate based polymers of low plasticiser content for potassium ion-selective membranes.* Analytica Chimica Acta, 1996. **324**(1): p. 47-56.

230. Heng, L.H., Toth, K., and Hall, E.A.H., *Ion-transport and diffusion coefficients of non-plasticised methacrylic-acrylic ion-selective membranes.* Talanta, 2004. **63**: p. 73-87.

231. Puntener, M., Vigassy, T., Baier, E., Ceresa, A., and Pretsch, E., *Improving the lower detection limit of potentiometric sensors by covalently binding the ionophore to a polymer backbone.* Analytica Chimica Acta, 2004. **503**: p. 187-194.

232. Qin, Y., Peper, S., Radu, A., Ceresa, A., and Bakker, E., *Plasticizer-Free Polymer Containing a Covalently Immobilized Ca^{2+}-Selective Ionophore for Potentiometric and Optical Sensors.* Analytical Chemistry, 2003. **75**(13): p. 3038-3045.

233. Vigassy, T., Gyurcsanyi, R.E., and Pretsch, E., *Influence of incorporated lipophilic particles on ion fluxes through polymeric ion-selective membranes.* Electroanalysis, 2003. **15**(5-6): p. 375-382.

234. Vigassy, T., Gyurcsányi, Robert E., and Pretsch, E., *Rotating Ion-Selective Membrane Electrodes for Trace-Level Measurements.* Electroanalysis, 2003. **15**(15-16): p. 1270-1275.

235. Radu, A., Telting-Diaz, M., and Bakker, E., *Rotating Disk Potentiometry for Inner Solution Optimization of Low-Detection-Limit Ion-Selective Electrodes.* Analytical Chemistry, 2003. **75**(24): p. 6922-6931.

236. Lindner, E., Gyurcsányi, R.E., and Buck, R.P., *Tailored Transport Through Ion-Selective Membranes for Improved Detection Limits and Selectivity Coefficients.* Electroanalysis, 1999. **11**(10-11): p. 695-702.

237. Pergel, E., Gyurcsanyi, R.E., Toth, K., and Lindner, E., *Picomolar detection limits with current-polarized Pb^{2+} ion-selective membranes.* Analytical Chemistry, 2001. **73**: p. 4249-4253.

238. Shvarev, A. and Bakker, E., *Pulsed Galvanostatic Control of Ionophore-Based Polymeric Ion Sensors.* Analytical Chemistry, 2003. **75**: p. 4541-4550.

239. Sutter, J., Morf, W.E., de Rooij, N.F., and Pretsch, E., *Current response of ion-selective solvent polymeric membranes at controlled potential.* Journal of Electroanalytical Chemistry, 2004. **571**: p. 27-35.

240. Bedlechowicz, I., Sokalski, T., Lewenstam, A., and Maj-zurawska, M., *Calcium ion-selective electrodes under galvanostatic current control.* Sensors and Actuators B: Chemical Proceedings of the Tenth International Meeting on Chemical Sensors, 2005. **108**(1-2): p. 836-839.

241. Morf, W.E., Badertscher, M., Zwickl, T., de Rooij, N.F., and Pretsch, E., *Effects of controlled current on the response behavior of polymeric membrane ion-selective electrodes.* Journal of Electroanalytical Chemistry, 2002. **526**(1-2): p. 19-28.

242. Vigassy, T., Morf, W.E., Badertscher, M., Ceresa, A., de Rooij, N.F., and Pretsch, E., *Making use of ion fluxes through potentiometric sensor membranes: ISEs with step responses at critical ion activities.* Sensors and Actuators B: Chemical, 2001. **76**(1-3): p. 477-482.

243. Zwickl, T., Sokalski, T., and Pretsch, E., *Steady-State Model Calculations Predicting the Influence of Key Parameters on the Lower Detection Limit and Ruggedness of Solvent Polymeric Membrane Ion-Selective Electrodes.* Electroanalysis, 1999. **11**(10-11): p. 673-680.

244. Regal, W.R. *Toxicity, Thallium*. 2006 [cited 2006; Available from: http://www.emedicine.com/EMERG/topic926.htm.

245. Mi, Y. and Bakker, E., *Determination of complex formation constants of lipophilic neutral ionophores in solvent polymeric membranes with segmented sandwich membranes.* Analytical Chemistry, 1999. **71**(23): p. 5279-5287.

246. Kimura, K., Yajima, S., Tatsumi, K., Yokoyama, M., and Oue, M., *Silver Ion-Selective Electrodes Using pie-coordinate Calix[4]arene Derivatives as Soft Neutral Carriers.* Analytical Chemistry, 2000. **72**: p. 5290-5294.

247. *Silver*. Trace metals in the environment, ed. I.C. Smith and Carson, B.C. Vol. 2. 1977, Michigan: Ann Arbor Science.

248. Dan, D. and Dong, Y., *A PVC-coated carbon rod ion-selective electrode for thallium and its application to the analysis of rocks and minerals.* Talanta, 1988. **35**(7): p. 589-590.

249.   Bakker, E. and Meyerhoff, M.E., *Ionophore-based membrane electrodes: new analytical concepts and non-classical response mechanisms.* Analytica Chimica Acta, 2000. **416**(2): p. 121-137.

250.   Sokalski, T., Ceresa, A., Zwickl, T., and Pretsch, E., *Large Improvement of the Lower Detection Limit of Ion-Selective Polymer Membrane Electrodes.* Journal of the American Chemical Society, 1997. **119**(46): p. 11347-11348.

251.   Szigeti, Z., Bitter, I., Toth, K., Latkoczy, D.J., Fliegel, D., Gunther, D., and Pretsch, E., *A novel polymeric membrane electrode for the potentiometric analysis of Cu^{2+} in drinking water.* Analytica Chimica Acta, 2005. **532**: p. 129-136.

252.   *Critically Selected Stability Constants of Metal Complexes Database*, in *Scientific Databases and Online Systems*, R.M. Smith and Martel, A.E., Editors. 2001, National Institute of Standards and Technology: Texas.

253.   Das, A. and Changdar, S.N., *Measurement of diffusion coefficients of thallium ion in H_2O and D_2O systems at different concentrations.* J. Phys., 1992. **39**(4): p. 317-321.

254.   Cattrall, R.W. and Freiser., H., *Coated wire ion selective electrodes.* Analytical Chemistry, 1971. **43**(13): p. 1905-1906.

255.   Cattrall, R.W., Drew, D.M., and Hamilton, I.C., *Some alkylphosphoric acid esters for use in coated-wire calxium-selective electrodes. Part 1. Response characteristics.* Analytica Chimica Acta, 1975. **76**: p. 269-277.

256.   Hulanicki, A. and Trojanowicz, M., *Calcium-selective electrodes with PVC membrnaes and solid internal contacts.* Analytica Chimica Acta, 1976. **87**: p. 411-417.

257.   Cadogan, A., Gao, Z., Lewenstam, A., Ivaska, A., and Diamond, D., *All-solid-state sodium-selective electrode based on a calixarene ionophore in a poly(vinyl chloride) membrane with a polypyrrole solid contact.* Analytical Chemistry, 1992. **64**: p. 2496-2501.

258.   Komaba, S., Arakawa, J., Seyama, M., Osaka, T., Satoh, I., and Nakamura, S., *Flow injection analysis of potassium using an all-solid-state potassium-selective electrode as a detector.* Talanta, 1998. **46**: p. 1293-1297.

259.   Bhat, V.S., Ijeri, V.S., and Srivastava, A.K., *Coated wire lead(II) selective potentiometric sensor based on 4-tert-butylcalix[6]arene.* Sensors and Actuators B, 2004. **99**: p. 98-105.

260.   Gyurcsanyi, R.E., Rangisetty, N., Clifton, S., Pendley, B.D., and Lindner, E., *Microfabricated ISEs: critical comparison of inherently conducting polymer and hydrogel based inner contacts.* Talanta:Molecular Recognition and Chemical Sensors, 2004. **63**(1): p. 89-99.

261. Fibbioli, M., Morf, W.E., Badertscher, M., Rooij, N.F.d., and Pretsch, E., *Potential drifts of solid-contact ion-selective electrodes due to zero-current ion fluxes through the sensor membrane.* Electroanalysis, 2000. **12**(16): p. 1286-1292.

262. Schnierle, P., Kappes, T., and Hauser, P.C., *Capillary Electrophoretic Determination of Different Classes of Organic Ions by Potentiometric Detection with Coated-Wire Ion-Selective Electrodes.* Analytical Chemistry, 1998. **70**(17): p. 3585-3589.

263. Fibbioli, M., Bandyopadhyay, K., Liu, S.G., Echegoyen, L., Enger, O., Diederich, F., Gingery, D., Buhlmann, P., Persson, H., Suter, U.W., and Pretsch, E., *Redox-active self-assembled monolayers for solid-contact polymeric membrane ion-selective electrodes.* Chemistry Materials, 2002. **14**: p. 1721-1729.

264. Hauser, P.C., Chiang, D.W.L., and Wright, G.A., *A potassium-ion selective electrode iwth valinomycin based poly(vinyl chloride) membrane and a poly(vinyl ferrocene) solid contact.* Analytica Chimica Acta, 1995. **302**: p. 241-248.

265. Lynch, A., Diamond, D., Lemonie, P., McLaughlin, J., and Leader, M., *Solid-state ion-selective electrode arrays.* Electroanalysis, 1998. **10**(16): p. 1096-1100.

266. Walsh, S., Diamond, D., McLaughlin, J., McAdams, E., Woolfson, D., Jones, D., and Bonner, M., *Solid-state sodium-selective sensors based on screen-printed Ag/AgCl reference electrodes.* Electroanalysis, 1997. **9**(17): p. 1318-1324.

267. Fibbioli, M., Bandyopadhyay, K., Liu, S.G., Echegoyen, L., Enger, O., Diederich, F., Buhlmann, P., and Pretsch, E., *Redox-active self-assembled monolayers as novel solid contacts for ion-selective electrods.* Chemical Communications, 2000: p. 339-340.

268. Lui, D., Meruva, R.K., Brown, R.B., and Meyerhoff, M.E., *Enhancing EMF stability of solid-state ion-selective sensors by incorporating silver-ligand complexes within polymeric films.* Analytica Chimica Acta, 1996. **321**: p. 173-183.

269. *Conductive polymers: Synthesis and electrical properties.* Handbook of organic conducting molecules and polymers, ed. H.S. Nalwa. Vol. Volume 2. 1997, New York: John Wiley & Sons. 865.

270. Heeger, A., *Semiconducting and metallic polymers: the fourth generation of polymeric materials.* Synthetic metals, 2002. **125**: p. 23-42.

271. Aldissi, M., *Inherently conducting polymers: Processing, Fabrication, Application, Limitations.* 1989, New Jersey: Noyes Data Corporation. 96.

272.   MacDiarmid, A.G., *Synthetic metals: a novel role for organic polymers.* Synthetic Metals, 2002. **125**: p. 11-22.

273.   Bobacka, J., Ivaska, A., and Lewenstam, A., *Potentiometric ion sensors based on conducting polymers.* Electroanalysis, 2003. **15**(5-6): p. 366-374.

274.   Heimo, J., Berthold, M., and Kaden, H., *Functional layers for chemical sensors based on conducting polypyrrole.* Macromolecular Symposium, 2001. **164**: p. 181-186.

275.   Kaden, H., Jahn, H., Berthold, M., Juttner, K., Mangold, K.-M., and Schafer, S., *Polypyrrole as the active material for potentiometric sensors.* Chemical Engineering & Technology, 2001. **24**(11): p. 1120-1124.

276.   Dong, S., Zhisheng, S., and Ziling, L., *Chloride chemical sensor based on an organic conducting polypyrrole polymer.* Analyst, 1988. **113**(10): p. 1525-1528.

277.   Wallace, G.G., Spinks, G.S., and Teasdale, P.R., *Conductive electroactive polymers: Intelligent materials systems.* 1997, Lancaster: Technomic.

278.   Michalska, A.J., Appaih-Kusi, C., Heng, L.H., Walkiewicz, S., and Hall, E.A.H., *An experimental study of membrane materials and inner contacting layers for ion-selective K^+ electrodes with a stable response and good dynamic range.* Analytical Chemistry, 2004. **76**: p. 2031-2039.

279.   Michalska, A.J. and Hall, E.A.H., *Inducing a cationic response in poly(pyrrole) films.* Electroanalysis, 1999. **11**(10-11): p. 756-762.

280.   Migdalski, J., Blaz, T., and Lewenstam, A., *Conducting polymer-based ion-selective electrodes.* Analytica Chimica Acta, 1996. **322**(3): p. 141-149.

281.   Lindfors, T. and Ivaska, A., *Calcium-selective electrode based on polyaniline functionalized with bis[4-(1,1,3,3-tetramethylbutyl)phenyl]phosphate.* Analytica Chimica Acta, 2001. **437**(2): p. 171-182.

282.   Bobacka, J., Ivaska, A., and Lewenstam, A., *Plasticizer-free all-solid-state potassium-selective electrode based on poly(3-octylthiophene) and valinomycin.* Analytica Chimica Acta, 1999. **385**(1-3): p. 195-202.

283.   Kankare, J. and Vinokurov, I.A., *Potentiometric Response of Conducting Polymer Electrodes for Oxygen in Neutral Aqueous Solutions.* Analytical Chemistry, 1997. **69**(13): p. 2337-2342.

284.   Vinokurov, I.A., *A new kind of redox sensor based on conducting polymer films.* Sensors and Actuators B: Chemical, 1992. **10**(1): p. 31-35.

285.   Shim, Y.-B., Stilwell, D.E., and Park, S.-M., *Electrochemistry of conductive polymer X: Polyaniline-based potentiometric sensor for dissolved oxygen.* Electroanalysis, 1991. **3**(1): p. 31-36.

286. Trojanowicz, M., Krawczyk, A.L.T.K.V., Lähdesmäki, I., and Szczepek, W., *Flow injection amperometric detection of ammonia using a polypyrrole-modified electrode and its application in urea and creatinine biosensors.* Electroanalysis, 1996. **8**(3): p. 233-243.

287. Lahdesmaki, I., Lewenstam, A., and Ivaska, A., *A polypyrrole-based amperometric ammonia sensor.* Talanta, 1996. **43**(1): p. 125-134.

288. Lahdesmaki, I., Kubiak, W.W., Lewenstam, A., and Ivaska, A., *Interferences in a polypyrrole-based amperometric ammonia sensor.* Talanta, 2000. **52**(2): p. 269-275.

289. Bobacka, J., *Conducting polymer-based solid-state ion-selective electrodes.* Electroanalysis, 2006. **18**(1): p. 7-18.

290. Tourillon, G. and Garnier, F., *New electrochemically generated organic conducting polymers.* Journal of Electroanalytical Chemistry, 1982. **135**: p. 173-178.

291. *Handbook of Conducting Polymers.* 2nd ed, ed. T.A. Skotheim, Elsenbaumer, R.L., and Reynolds, J.R. 1998, New York: Marcel Dekker.

292. Dumanska, J. and Maksymiuk, K., *Studies on spontaneous charging/discharging processes of polypyrrole in aqueous electrolyte solutions.* Electroanalysis, 2001. **13**(7): p. 567-573.

293. Michalska, A. and Maksymiuk, K., *The influence of spontaneous charging/discharging of conducting polymer ion-to-electron transducer on potentiometric responses of all-solid-state calcium-selective electrodes.* Journal of Electroanalytical Chemistry, 2005. **576**: p. 339-352.

294. Liu, D., Meruva, R.K., Brown, R.B., and Meyerhoff, M.E., *Enhancing EMF stability of soli-state ion-selective sensors by incorporating lipophilitc silver-ligand complexes within polymeric films.* Analytica Chimica Acta, 1996. **321**: p. 173-183.

295. Florou, A.B., Prodromidis, M.I., Tzouwara-Karayanni, S.M., and Karayannis, M.I., *Fabrication and voltammetric study of lanthanum 2,6-dichlorophenolindophenol chemically modified screen printed electrodes. Application for the determination of ascorbic acid.* Analytica Chimica Acta, 2000. **423**: p. 107-114.

296. Veltsistas, P.G., Prodromidis, M.I., and Efstathiou, C.E., *All-solid-state potentiometric sensors for ascorbic acid by using a screen-printed compatible solid contact.* Analytica Chimica Acta, 2004. **502**(1): p. 15-22.

297. Sutter, J., Radu, A., Peper, S., Bakker, E., and Pretsch, E., *Solid-contact polymeric membrane electrodes with detection limits in the subnanomolar range.* Analytica Chimica Acta, 2004. **523**: p. 53-59.

298. Kucza, W., Danielewski, M., and Lewenstam, A., *EIS simulations for ion-selective site-based membranes by a numerical solution of the coupled Nernst-Planck-Poisson equations.* Electrochemistry Communications, 2006. **8**(3): p. 416-420.

299. Pejcic, B.B., *Mechanistic studies of several chalcogenide based potentiometric chemical sensors in marine water*, Doctor of Philosophy, 2003, Curtin University of Technology, 242

300. Pejcic, B.B. and De Marco, R., *Impedance spectroscopy: Over 35 years of electrochemical sensor optimization.* Electrochimica Acta, 2006. **Article In Press**.

301. Covington, A.K. and Zhou, D.-M., *ac impedance properties of ETH1001-based calcium ion selective membranes.* Electrochimica Acta, 1992. **37**(15): p. 2691-2694.

302. Horvai, G., Graf, E., Toth, K., Pungor, E., and Buck, R.P., *Plasticized poly(vinyl chloride) properties and characteristics of valinomycin electrodes. 1. High-frequency resistances and dielectric properties.* Analytical Chemistry, 1986. **58**: p. 2735-2740.

303. Toth, K., Graf, E., Horvai, G., Pungor, E., and Buck, R.P., *Plasticized poly(vinyl chloride) properties and characteristics of valinomycin electrodes. 2. Low-frequency, surface-rate and warburg impedance characteristics.* Analytical Chemistry, 1986. **58**: p. 2741-2744.

304. Nahir, T.M. and Buck, R.P., *Steady-state-current impedance spectroscopy of plasticized PVC membranes containing neutral ion carriers.* Electrochimica Acta, 1993. **38**(18): p. 2691-2697.

305. Konopka, A., Sokalski, T., Michalska, A., Lewenstam, A., and Maj-Zurawska, M., *Factors Affecting the Potentiometric Response of All-Solid-State Solvent Polymeric Membrane Calcium-Selective Electrode for Low-Level Measurements.* Analytical Chemistry, 2004. **76**(21): p. 6410-6418.

306. Gamry-Instruments. *Electrochemical Impedance Spectroscopy Theory: A Primer*. [Website] 2006 [cited 2006; Available from: http://www.gamry.com/App_Notes/EIS_Primer/EIS_Primer.htm.

307. Vazquez, M., *Potentiometric Ion Sensors Based on Conducting Polymers*, Doctorate of Philosophy, 2005, Abo Akademi University, 64

308. Macdonald, D.D., *Application of Electrochemical Impedance Spectroscopy in Electrochemistry and Corrosion Science,*, in *Techniques for Characterization of Electrodes and Electrochemical Processes*, R. Varma and Selman, J.R., Editors. 1991, John Wiley and Sons.

309. Macdonald, J.R., ed., *Impedance Spectroscopy Emphasizing Solid Materials and Systems*. 1987: John Wiley & Sons.

310. Mansfeld, F. and Lorenz, W.J., *Electrochemical Impedance Spectroscopy (EIS): Application in Corrosion Science and Technology*, in *Techniques for Characterization of Electrodes and Electrochemical Processes*, R. Varma and Selman, J.R., Editors. 1991, John Wiley & Sons.

311. Bard, A.J. and Faulkner, L.R., *Electrochemical Methods: Fundamentals and Applications*. 2 ed. 2001, New York: John Wiley & Sons.

312. Gabrielli, C., Hemery, P., Letellier, P., Masure, M., Perrot, H., Rahmi, M.I., and Turmine, M., *Investigation of ion-selective electrodes with neutral ionophores and ionic sites by EIS. II. Application to K^+ detection*. Journal of Electroanalytical Chemistry, 2004. **570**: p. 291-304.

313. Han, W.-S., Park, M.-Y., Chung, K.-C., Cho, D.-H., and Hong, T.-K., *Potentiometric sensor for hydrogen ion based on N,N'-dialkylbenzylethylenediamine neutral carrier in a poly(vinyl chloride) membrane with polyaniline solid contact*. Talanta, 2001. **54**(1): p. 153-159.

314. Legin, A., Makarychev-Mikhailov, S., Kirsanov, D., Mortensen, J., and Vlasov, Y., *Solvent polymeric membranes based on tridodecylmethylammonium chloride studied by potentiometry and electrochemical impedance spectroscopy*. Analytica Chimica Acta, 2004. **514**: p. 107-113.

315. Ehrenbeck, C. and Juttner, K., *Ion conductivity and permselectivity measurements of polypyrrole membranes at variable states of oxidation*. Electrochimica Acta: Electrochemistry of Electroactive Polymer Films, 1996. **41**(11-12): p. 1815-1823.

316. Lindfors, T., Sjoberg, P., Bobacka, J., Lewenstam, A., and Ivaska, A., *Characterization of a single-piece all-solid-state lithium-selective electrode based on soluble conducting polyaniline*. Analytica Chimica Acta, 1999. **385**(1-3): p. 163-173.

317. Momma, T., Yamamoto, M., Komaba, S., and Osaka, T., *Analysis of the long-term potential stability of an all-solid-state potassium-selective electrode with electroactive polypyrrole film*. Journal of Electroanalytical Chemistry, 1996. **407**: p. 91-96.

318. Bobacka, J., *Potential Stability of All-Solid-State Ion-Selective Electrodes Using Conducting Polymers as Ion-to-Electron Transducers*. Analytical Chemistry, 1999. **71**(21): p. 4932-4937.

319. Jimenez-Morales, A., Galvan, J.C., and Aranda, P., *A new silver-ion selective sensor based on a polythiacrown-ether entrapped by sol-gel*. Electrochimica Acta, 2002. **47**: p. 2281-2287.

320. Heng, L.H. and Hall, E.A.H., *Methacrylaic-acrylic polymers in ion-selective membranes: achieving the right polymer recipe.* Analytica Chimica Acta, 2000. **403**: p. 77-89.

321. E. Lindner, V.V.C., S. Ufer, R. P. Buck, W. J. Kao, M. R. Neuman, J. M. Anderson,, *Ion-selective membranes with low plasticizer content: Electroanalytical characterization and biocompatibility studies.* Journal of Biomedical Materials Research, 1994. **28**(5): p. 591-601.

322. Lindner, E., Cosofret, V.V., Buck, R.P., Johnson, T.A., Ash, R.B., Neuman, M.R., Kao, W.J., and Anderson, J.M., *Electroanalytical and biocompatibility studies on microfabricated array sensors.* Electroanalysis, 1995. **7**(9): p. 864-870.

323. Heng, L.H. and Hall, E.A.H., *Producing "self-plasticizing" ion-selective membranes.* Analytical Chemistry, 2000. **72**: p. 42-51.

324. Heng, L.H. and Hall, E.A.H., *One-Step synthesis of K^+-Selective Methacrylic-Acrylic copolymers containing grafted ionophores and requiring no plasticizer.* Electroanalysis, 2000. **12**(3): p. 178-186.

325. Malinowska, E., Gawart, L., Parzuchowski, P., Rokicki, G., and Brzozka, Z., *Novel approach of immobilization of calix[4]arene type ionophore in 'self plasticized' polymeric membrane.* Analytica Chimica Acta, 2000. **421**: p. 93-101.

326. Sutter, J., Lindner, E., Gyurcsanyi, R.E., and Pretsch, E., *A polypyrrole-based solid-contact Pb^{2+}-selective PVC-membrane electrode with a nanomolar detection limit.* Analytical and Bioanalytical Chemistry, 2004. **380**: p. 7-14.

327. Michalska, A., Konopka, A., and Maj-Zurawska, M., *All-Solid-State Calcium Solvent Polymeric Membrane Electrode for Low-Level Concentration Measurements.* Analytical Chemistry, 2003. **75**(1): p. 141-144.

328. Sutter, J. and Pretsch, E., *Response Behavior of Poly(vinyl chloride)- and Polyurethane-Based Ca^{2+}-Selective Membrane Electrodes with Polypyrrole- and Poly(3-octylthiophene)-Mediated Internal Solid Contact.* Electroanalysis, 2006. **18**(1): p. 19-25.

329. Michalska, A. and Maksymiuk, K., *Conducting polymer membranes for low activity potentiometric ion sensing.* Talanta: Molecular Recognition and Chemical Sensors, 2004. **63**(1): p. 109-117.

330. Sutter, J. and Pretsch, E., *Response behaviou of poly(vinyl chloride)- and polyurethane-Based Ca^{2+}-selective membrane electrodes with polypyrrole- and poly(3-octylthiophene)-Mediated Internal solid contact.* Electroanalysis, 2006. **18**(1): p. 19-25.

331.   Qin, Y. and Bakker, E., *Quantification of the Concentration of Ionic Impurities in Polymeric Sensing Membranes with the Segmented Sandwich Technique.* Analytical Chemistry, 2001. **73**(17): p. 4262-4267.

332.   Gilbert, E., *Applications of Small-Angle Neutron Scattering.* 2004, Bragg Institute, ANSTO in Partnership: Sydney.

333.   Ye, Q., Borbely, S., and Horvai, G., *Microstructure of ion-selective plasticised PVC membranes studied by small angle neutron scattering.* Analytical Chemistry, 1999. **71**: p. 4313-4320.
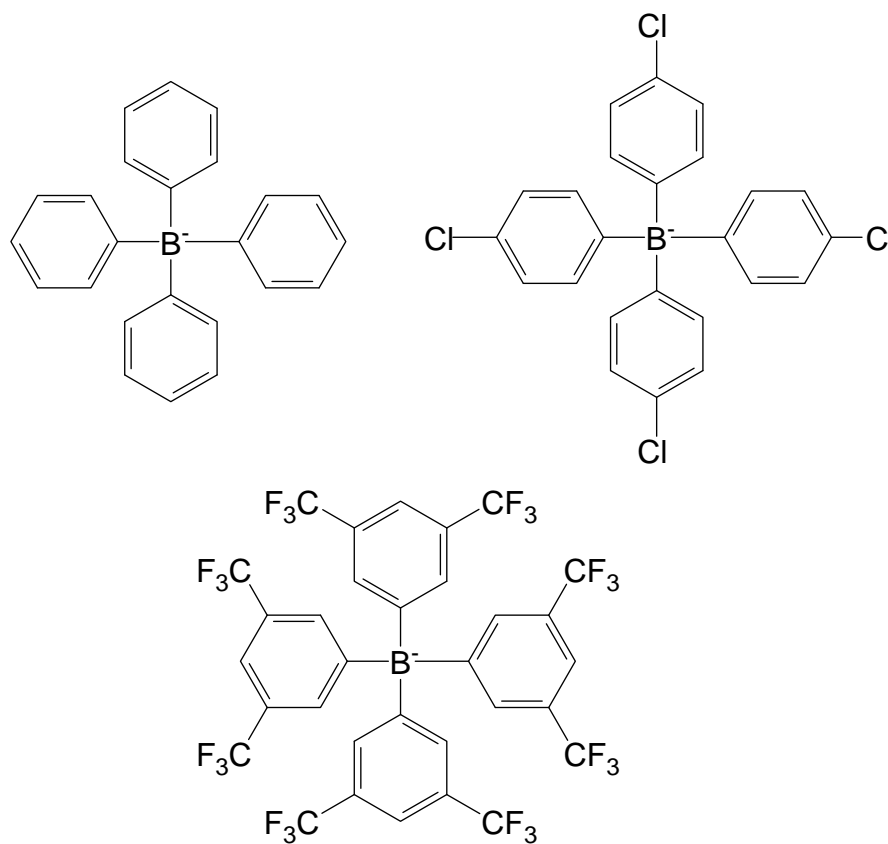
Appendix I

Figure I: Structures of three ion-exchangers used in ISEs. The counter ion of the phenyl borate derivatives are typically K^+ of Na^+.
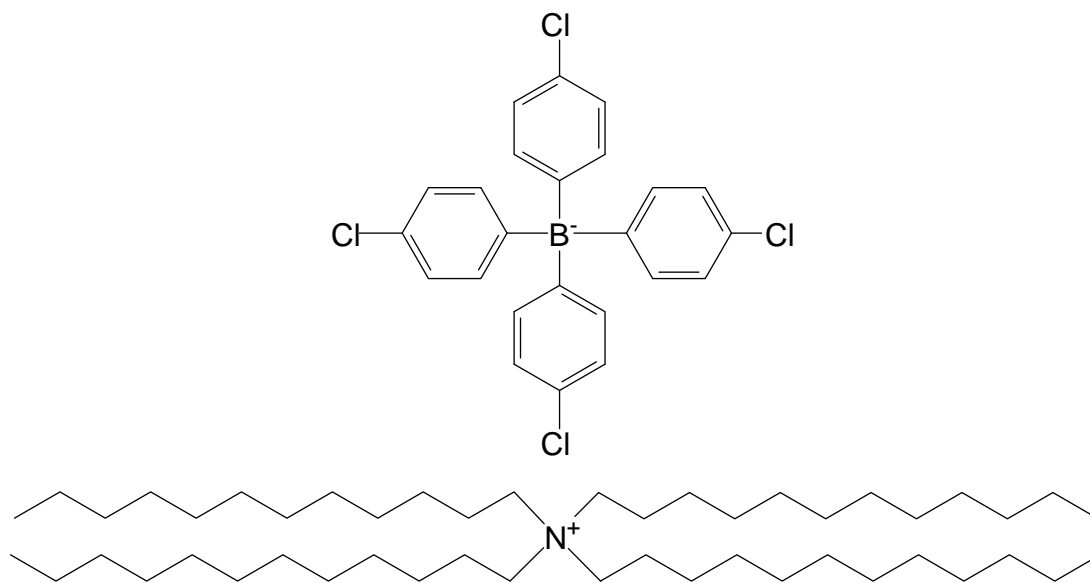
Appendix II

Figure II: The structure of a lipophilic salt used in ISEs (common name: ETH 500).

Appendix III

Tetrathia-dibenzo macrocycle
(a)

(b)
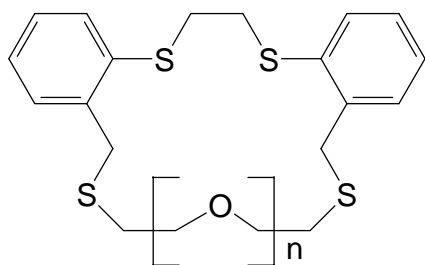
n = 1 or 2
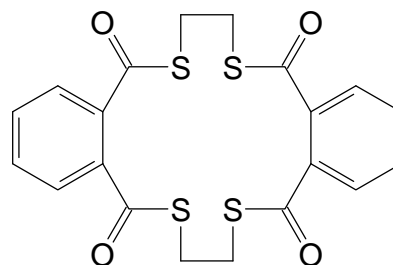
Quinoline-carbonitrile Compound
(c)
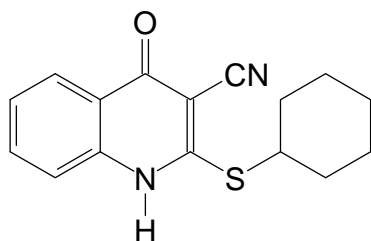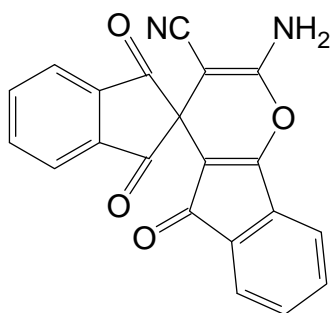
Calixarene Derivatives
(d)
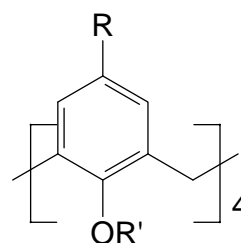
1 : R = H   R' = -CH$_2$CH$_2$CH$_3$
2 : R = H   R' = -CH$_2$CH=CH$_2$
3 : R = t-Bu R' = -CH$_2$CH$_2$CH$_3$
4 : R = t-Bu R' = -CH$_2$CH=CH$_2$

Indeno-pyrand
(e)

Bis(crown ether)
(f)
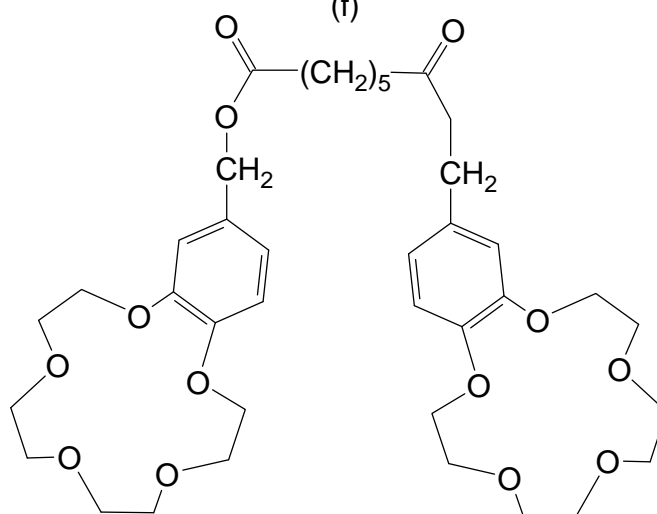
Figure III: Structures of organic molecules used as thallium(I) ionophores in ISEs.
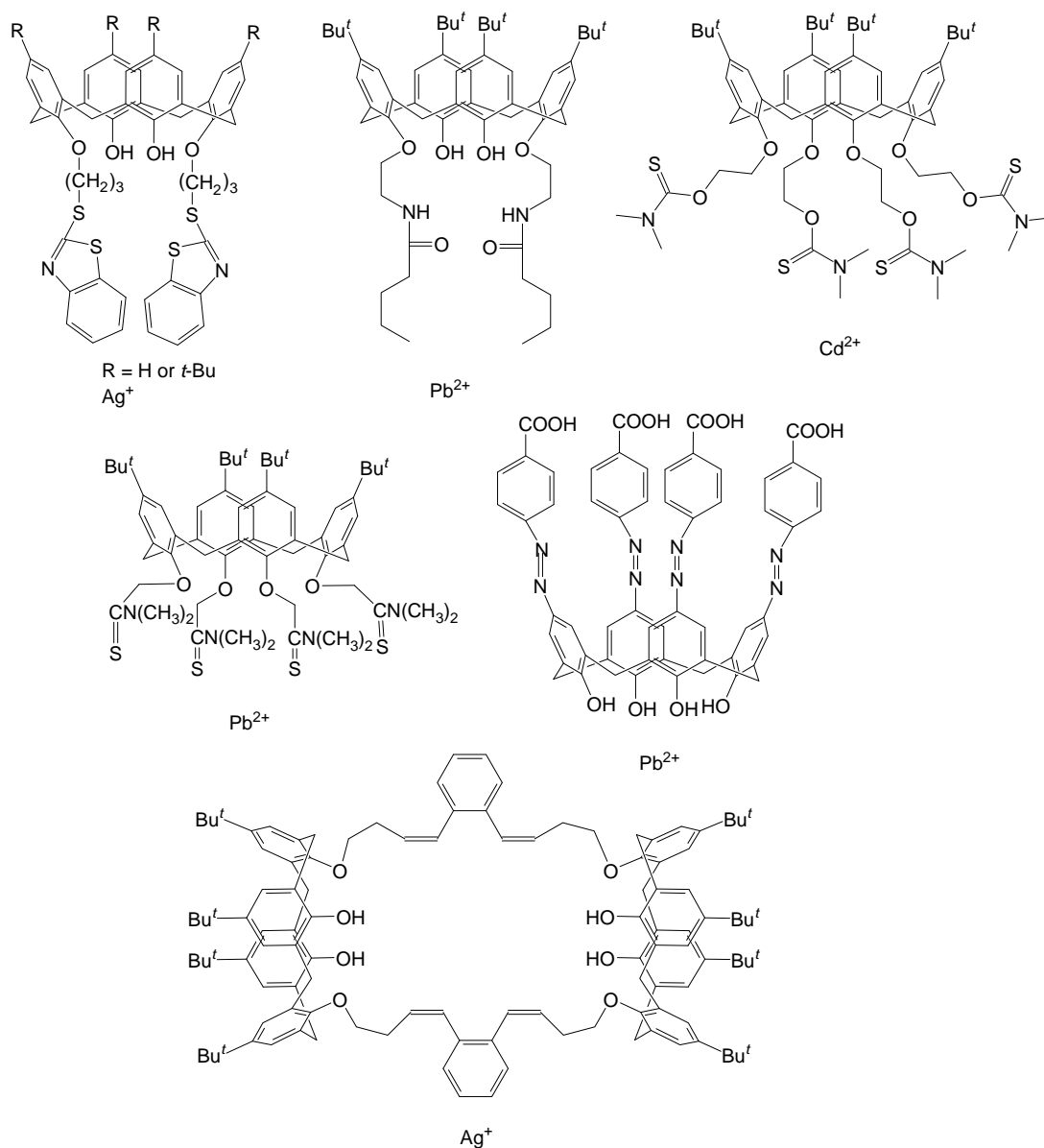(a) , (b) , (c) , (d) , (e) , (f)

Appendix IV

Figure IV: Structures of selected examples of several calixarenes uses as ionophores for heavy metals.

Appendix V: Crystal and Refinement Information

The structure determinations were carried out by Prof. Allan H. White and Dr Brian W. Skelton, at the University of Western Australia.

| Compound.S	Calixarene (1)	Calixarene (1).CHCl$_3$	Calixarene (2)	Calixarene (2).0.5 CHCl$_3$
	C$_{56}$H$_{80}$O$_4$	C$_{57}$H$_{81}$Cl$_3$O$_4$	C$_{40}$H$_{48}$O$_4$	C$_{40.5}$H$_{48.5}$Cl$_{1.5}$O$_4$
M_r Dalton	817.36	936.63	592.82	652.51
Crystal system	Monoclinic	Monoclinic	Tetragonal	Tetragonal
Space group	$P2_1/c$	$C2/c$	$I4_1/a$	$P4/ncc$
a, Å	10.901(5)	17.425(1)	19.627(3)	19.268(3)
b, Å	22.919(10)	21.365(2)		
c, Å	41.74(2)	15.461(1)	17.867(3)	19.225(3)
α, deg.				
β, deg,	97.068(8)	102.620(2)		
γ, deg.				
V, Å	10349	5617	6883	7136
D_c	1.04$_9$	1.10$_7$	1.14$_4$	1.21$_5$
Z	8	4	8	8
μ, mm^{-1}	0.064	0.20	0.07	0.184
specimen, mm	0.15 x 0.06 x 0.06	0.24 x 0.13 x 0.09	0.17 x 0.13 x 0.07	0.75 x 0.18 x 0.09
'$T'_{min,max}$	0.81/1	0.81, 0.91	0.94/1	0.76, 0.96
$2\theta_{max}$, deg.	50	65	53	53
N_t	78765	57761	31581	68517
$N(R_{int})$	18145(0.093)	9927(0.023)	3522(0.031)	3643(0.029)
N_o	4719	6533	2030	2872
R, R_w	0.12, 0.13	0.057, 0.079	0.056, 0.075	0.047, 0.078

Appendix VI
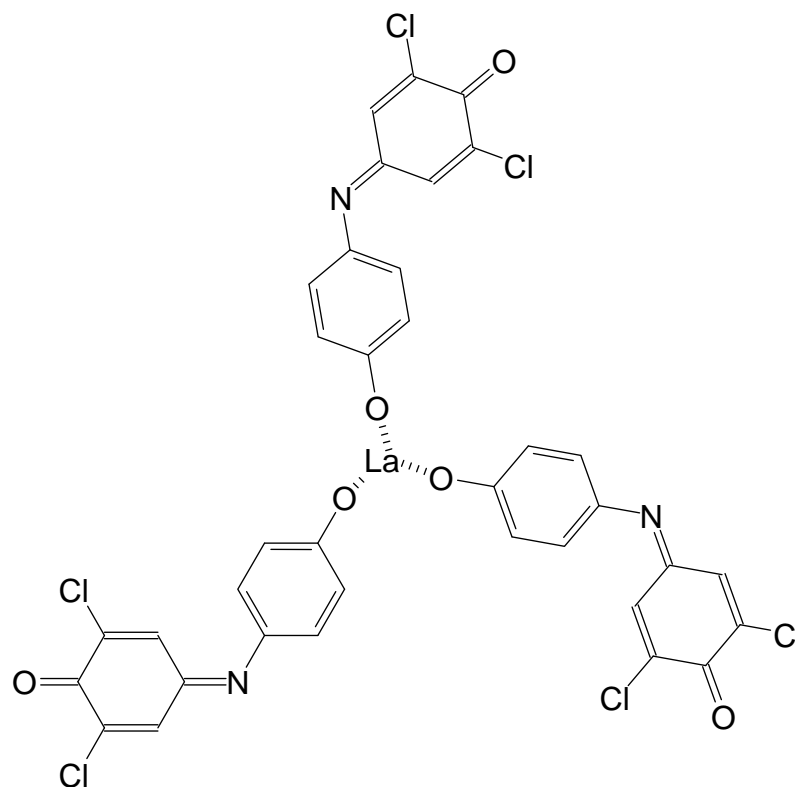
Figure V: Structure of the La-2,6-dichlorophenolindophenol La(DCPI)$_3$ redox active water insoluble salt.
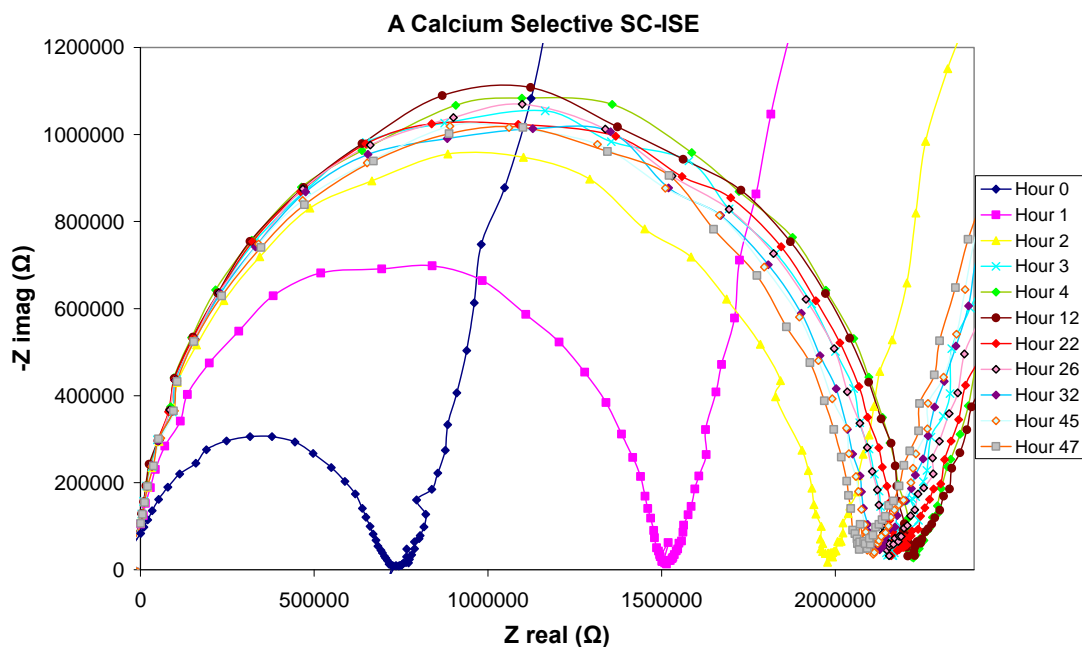
Appendix VII

Figure VI: Complex plane plot of a calcium selective SC-ISE showing a positive water layer test. The impedance initially increases over four hours then stabilises till 22 hours where it then starts to fall over a period of 10 hours and finally stabilises at this lower impedance. The decrease in impedance after 22 hours is attributed to water reaching the interface between the membrane and the solid substrate, which lowers the contact resistance.